THE EXPERIMENTAL CAMPAIGN AND NUMERICAL SIMULATIONS OF THE CONSTRAIN PROJECT

TECHNICAL REPORT – PART 2

DEVELOPMENT OF ANALYTICAL MODELS TO DESIGN THE REINFORCEMENTS NUMERICAL SIMULATION OF THE SEISMIC PERFORMANCE ACHIEVED WITH THE REINFORCEMENT

N. Gattesco[a], I. Boem[a], E. Rizzi[a], A. Bez[a], M. Gams[b], M. Farič[b], V. Pučnik[b], A. Dudine[c]

[a]*University of Trieste, Department of Engineering and Architecture, Via Alfonso Valerio 6/1, 34127 Trieste, Italy*
[b]*University of Ljubljana, Faculty of Civil and Geodetic Engineering, Jamova cesta 2, 1000 Ljubljana, Slovenia*
[c]*Fibre Net S.p.a., Via Jacopo Stellini, 3 – Z.I.U., 33050 Pavia di Udine (UD), Italy*

PROJECT PARTNERS

LP: Università degli Studi di Trieste (a)
Dipartimento di Ingegneria e Architettura,
via Alfonso Valerio 6/1, 34127 Trieste, Italia
segreteria@dia.units.it

PP2: Fibre Net S.p.A. (c)
via Jacopo Stellini, ZIU, Pavia di Udine (UD), Italia
info@fibrenet.info

PP3: Veneziana Restauri Costruzioni Srl,
via dell'Industria 9, Gruaro (VE), Italia
info@venezianarestauri.it

PP4: Univerza v Ljubljani (b)
Fakulteta za Gradbenitsvo in Geodezijo,
Kongesni trg 12, Ljubljana, Slovenija
euprojekti@uni-lj.si

PP5: IGMAT d.d., Institut za gradbene materiale,
Polje 351C, Ljubljana, Slovenija
info@igmat.eu

PP6: Kolektor CPG d.o.o., Cestno podjetje Nova Gorica,
Industrijska cesta 2, Kromberk, SI-5000 Nova Gorica,
Slovenija
cpg@kolektor.com

CONTENTS

1 Introduction

Assessing the structural behaviour of existing masonry structures under seismic excitation is a complex engineering problem, and planning and estimating the effect of an intervention to improve the seismic response is even more complicated. The problem includes engineering issues, such as how to improve the response of structures built of weak and flexible old masonry with new materials, which are much stronger and stiffer. But the problems encountered when planning an intervention are not only engineering ones. Owners may wonder, does the intervention require that the residents move out temporarily? For how long do they have to move out? If there is an extensive intervention inside the building, how will it affect existing installations? Finally, the direct and indirect costs of interventions to improve the seismic response of masonry structures are not cheap. All these factors make it difficult for owners to decide for such interventions. Therefore, they often keep the buildings in their existing state, which is vulnerable to earthquakes. The impact of this risk on society is significant because of a large share of such buildings in building stock. Alternatively, they may choose a demolition and brand new construction, which requires a lot of resources and, by extension, produces many emissions.

The CONSTRAIN project aims to develop new methods of strengthening that are less invasive and more comfortable for the residents. This is achieved mainly by limiting the interventions to one side of the structure. The proposed strengthening technology is based on coating the walls with composite (GFRP mesh) reinforced mortars (CRM system) and advanced anchors on only one side.

One of the problems with proposing a strengthening intervention only on one side of the wall is that the confidence of the professional community in such interventions is low. In the case of seismic loads with many load reversals and potentially large compressive stresses in the wall, the coating can lose the bond to the wall and detach. If this happens, the composite action of the wall and the coating is lost, and the coating becomes ineffective. In the case of coating on both sides of the wall, the situation is much better. Coatings on both sides can be connected by anchors, which confine the wall in the middle, connect all leaves of the wall and increase the compatibility with the (weak) masonry wall. The structural engineer will prefer two-sided coating and consider one-sided coating only if there are enough proofs that it works.

Due to scepticism of the professional community about one-sided coatings, the experimental campaign in the project was extensive (Table 1 of the first part of the report). It consists of eight full-scale in-plane cyclic shear compression tests on piers, three full-scale out-of-plane cyclic tests on piers, eight full-scale cyclic tests on spandrels, strengthened with the CRM system; moreover, two tests on the strengthened tie-beams, with GFRP mesh in bed mortar joints, and two tests on mid storey tie-beams made by using strips of a carbon fibre reinforced polymer (CFRP).

Three types of masonry were considered in the tests: two-leaf rubble stone masonry and single and double-leaf brick masonry. The strengthening intervention was specially designed for each of the masonry types.

A test setup had to be designed, manufactured, and assembled for each type of test. Furthermore, a sample had to be constructed for each individual test, equipped with instruments, tested, and the results processed. After each test, the sample had to be demolished and the rubble disposed of.

Finally, a full-scale pilot building was tested in reference and strengthened state to demonstrate the efficiency of the proposed strengthening technique (CRM system) in real-life conditions and in a systematic way. The results of the tests conclusively show that the proposed strengthening works well, improves structural response, is cost-effective and quick and easy to apply.

The first part of this report presents the results of all the tests performed within the project, while this second part includes the results of many numerical simulations. Some numerical simulations were performed to derive crucial material parameters required for design, and these parameters are calculated and presented in the report next to each test. Other numerical simulations were done to evaluate the performance of existing mathematical models by comparing them to the experimental results. These comparisons were successful, which shows that the developed strengthening intervention can be designed using existing design software and mathematical models. Furthermore, the abovementioned material parameters obtained from the tests can be used in the design.

The last numerical analysis is a case study on an actual five-storey building to compare the costs of a standard intervention using coating on both sides and the newly developed method with coating on only one side. The results overwhelmingly show that the newly developed method is more cost-efficient. Crucially, when the new method is used, the residents can stay in the building, and the business is not interrupted.

2 Numerical modelling

2.1 FEA Modelling

Some of the specimens that were tested during the project have been modelled with the FEM software Abaqus v. 6.12. In particular in this Section, the results of the numerical modelling of shear-compression tests on piers and shear-bending tests on spandrels is presented. At the end of each sub-section involving one of the models, a direct comparison between the experimental and numerical behaviour is reported. The modelling considered only the monotonical behaviour of the samples and the numerical curves were compared to the experimental ones.

2.2 Material properties calibration

Careful consideration was paid on the mechanical characterization of the masonry and reinforcement materials.

Concrete, which constitute the material of the top and bottom RC elements, was assumed as an indefinitely elastic and isotropic material.

The mechanical characteristics of materials are summarized in Table 1.

Table 1: Mechanical properties of the materials used in the models

Material	Elasticity modulus [MPa]	Density [kg/m^3]	Poisson modulus ν [-]
Reinforced concrete	40000	2500	0.2
Stone masonry	1074	2100	0.43
Single leaf brick masonry	2183	1800	0.43
Two leaf brick masonry	2183	1800	0.43
Reinforcement plaster	9000	1800	0.43

2.2.1 Post-failure behaviour

The masonry and the reinforcement were described in the form of an equivalent, homogeneous and isotropic material having a linear elastic behaviour up to failure, based on the test results and on what reported in scientific literature (Gattesco *et al*. 2015 and 2017). The post-cracked behaviour was based on an appropriate calibration of the "concrete damaged plasticity" (CDP) mechanical model. This mechanical model, developed by Lubliner et al. 1989 for RC components and further elaborated by Lee and Fenves (1998), well applies to materials with a quasi-brittle behaviour such as masonry. Recent examples for masonry structural systems can be found in Pandey *et al*. and Xiong *et al*. (2014). In the CDP model, the yield surface function considers different evolution of strength under tensile and compressive stresses (Fig. 1). In this research, the main input parameters were defined in accordance with Gattesco *et al*. 2015. The dilation angle φ and the ratio f_{b0}/f_{c0} between the equibiaxial compressive failure stress to the uniaxial compressive one, specifically, were assumed equal to 40° and 1.16 respectively. The ratio of the second stress invariant on the tensile meridian (K) was

assumed equal to 1, while the eccentricity parameter, that defines the rate at which the function approaches the asymptote was assumed equal to 0.1. Tension stiffening effects and post-cracked compressive behaviour for the masonry were described in the form of stress-strain post-failure relationships in Table 2.

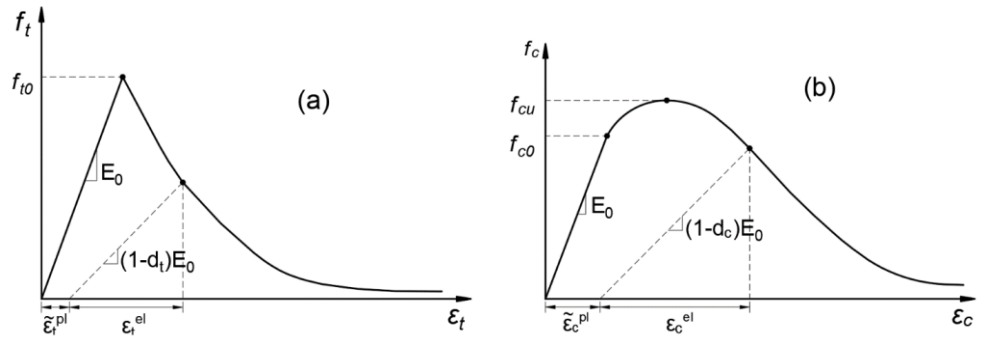

Fig. 1: Mechanical behaviour of masonry under uniaxial (a) tension and (b) compression (Abaqus)

Table 2: Tension stiffening stress-strain multilinear relationships for the masonry

Post-failure behaviour (masonry)			
Stone masonry			
Tensile behaviour		Compressive behaviour	
f_t (MPa)	$\varepsilon_{t,pl}$(-)	f_c (MPa)	$\varepsilon_{c,pl}$(-)
0.13	0	2.5	0
0.13	0.0042	3.5	0.0035
0.0013	0.01	3.5	0.005
Single leaf brick masonry			
Tensile behaviour		Compressive behaviour	
f_t (MPa)	$\varepsilon_{t,pl}$(-)	f_c (MPa)	$\varepsilon_{c,pl}$(-)
0.15	0	2	0
0.15	0.005	4	0.002
0.08	0.015	5	0.0035
		6.25	0.0069
		6.86	0.0105
		6	0.011
		1	0.014
Two leaf brick masonry			
Tensile behaviour		Compressive behaviour	
f_t (MPa)	$\varepsilon_{t,pl}$(-)	f_c (MPa)	$\varepsilon_{c,pl}$(-)
0.12	0	2	0
0.12	0.001	4	0.002
0.01	0.01	5	0.0035
		6.25	0.0069
		6.86	0.0105
		6	0.011
		1	0.014

2.2.2 Reinforcement

In order to represent the reinforcement, several modelling approaches were considered to reduce the computational complexity of the model. In particular, these approaches were used to model the CRM tensile tests presented in Gattesco *et al*. (2017) (Fig. 2). A first model was constituted by 4 nodes shell elements (S4R), representing the mortar, with the GFRP mesh acting as a rebar layer embedded in the middle of the shell ply as a reinforcement. A second model was realized with an equivalent homogeneous material, constituted by 3D solid, 8-node brick elements (C3D8R). The post-cracked behaviour was based on an appropriate calibration of the concrete damaged plasticity mechanical model.

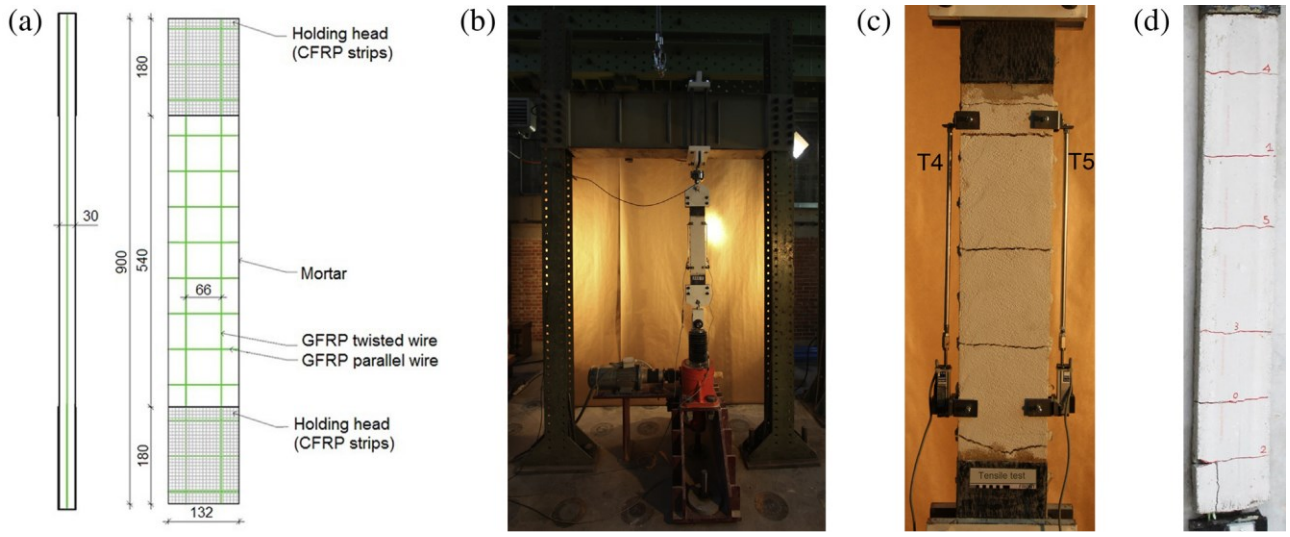

Fig. 2: Tensile test: (a) GFRP reinforced mortar layer samples, (b) test setup and view of samples (c) and (d) crack pattern at the end of the tests

Considering the results given by the two different approaches and the computational costs, the equivalent homogeneous material proved to be a better solution. The comparison between the numerical result obtained with the latter model and the experimental curves is reported in Fig. 3.

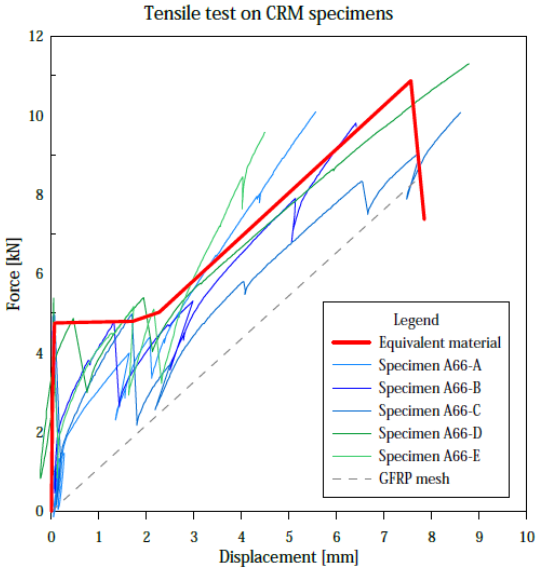

Fig. 3: Comparison between the numerical and the experimental curves of the CRM tensile tests

The comparison shows a good correlation between the model and the experimental behaviour; thus, this type of modelling was adopted for all the reinforced specimens. The brick elements representing the reinforcement were connected to the masonry elements with a tie constrain (Fig. 4b and c), which connects two separate surfaces together so that there is no relative motion between them. The mesh defined for the reinforced plaster was compatible with the masonry mesh, with prismatic elements having a square section and a side of $l_{mesh} = 0.066$ m, by the thickness of the coating, equal to 0.035 m for the rubblestone masonry specimens and equal to 0.03 m for the brick masonry ones.

Tension stiffening effects and post-cracked compressive behaviour of the reinforcement were described in the form of stress-strain post-failure relationships in Table 3.

Table 3: Tension stiffening stress-strain multilinear relationships for the reinforcement

Post-failure behaviour (reinforcement)			
Stone masonry			
Tensile behaviour		Compressive behaviour	
f_t (MPa)	$\varepsilon_{t,pl}$(-)	f_c (MPa)	$\varepsilon_{c,pl}$(-)
1.30	0	18	0
1.30	0.005	20	0.0005
2.30	0.02	20	0.002
0.1	0.021		
Single leaf brick masonry			
Tensile behaviour		Compressive behaviour	
f_t (MPa)	$\varepsilon_{t,pl}$(-)	f_c (MPa)	$\varepsilon_{c,pl}$(-)
2.26	0	22	0
2.26	0.005	30	0.0004
3.2	0.0187	30	0.004
0.1	0.02		
Two leaf brick masonry			
Tensile behaviour		Compressive behaviour	
f_t (MPa)	$\varepsilon_{t,pl}$(-)	f_c (MPa)	$\varepsilon_{c,pl}$(-)
2.26	0	22	0
2.26	0.005	30	0.0004
3.2	0.0187	30	0.004
0.1	0.02		

2.3 Shear-compression numerical models

In accordance with the test setup presented in Section 6 of the first part of the report, the numerical models of the shear-compression test piers consisted of two concrete beams, the masonry wall and the reinforcement were derived. Concrete, masonry, and reinforcement elements were described in the form of 3D solid, 8-node brick elements available in the ABAQUS/Standard element library (C3D8R). A regular mesh pattern with a constant mesh size of l_{mesh} = 0.066 m was used. The interaction between the elements constituting the masonry and the concrete components, having coincident mesh nodes at the contact surfaces, was guaranteed by means of merged nodes on the boundary of the adjacent elements.

The upper stiff steel element was described in the form of a rigid body constraint about a reference node. The latter acted on the nodes of the elements of the top concrete beam, lying on a X-Z plane, restraining the out of plane translations in the Z-axis direction, and the rotations about the three axes ($u_z = ur_x = ur_y = ur_z = 0$).

To account for the deformations of the steel base plate that were observed during the experimental tests, in the numerical model a series of springs, directed in the Y direction, rigidly connected to the ground, were modelled. Their stiffness was determined considering a simplified static scheme, with the steel plate performing as a fixed beam, in correspondence of the anchor bolts and loaded by two concentrated forces located at the points where the RC beam brackets are welded to the plate.

The nodes located at the base of the model were constrained to prevent translations in the X an Z directions ($u_x = u_z = 0$), as displayed in Fig. 4;

A quasi-static dynamic implicit analysis, considering geometric nonlinearities, in displacement control was carried out to overcome convergence problems due to the formation of cracks. An appropriate loading time history was defined to avoid dynamic effects, thus maintaining a static behaviour. The analysis was performed in two steps. In the first step, uniformly distributed vertical loads were applied on the upper nodes of the elements of the top concrete beam, acting as an equivalent vertical pressure ($\sigma_0 = 0.5\ MPa$). Gravity loads were also considered. In the second step, the static loads from the previous analysis were maintained and a horizontal lateral displacements u_x, with a monotonic linear rising time history, was imposed to the nodes of the top concrete element, as presented in Fig. 4. For the stone masonry, the thickness of each element was equal to 0.0875 m.

2.3.1 Stone masonry specimens

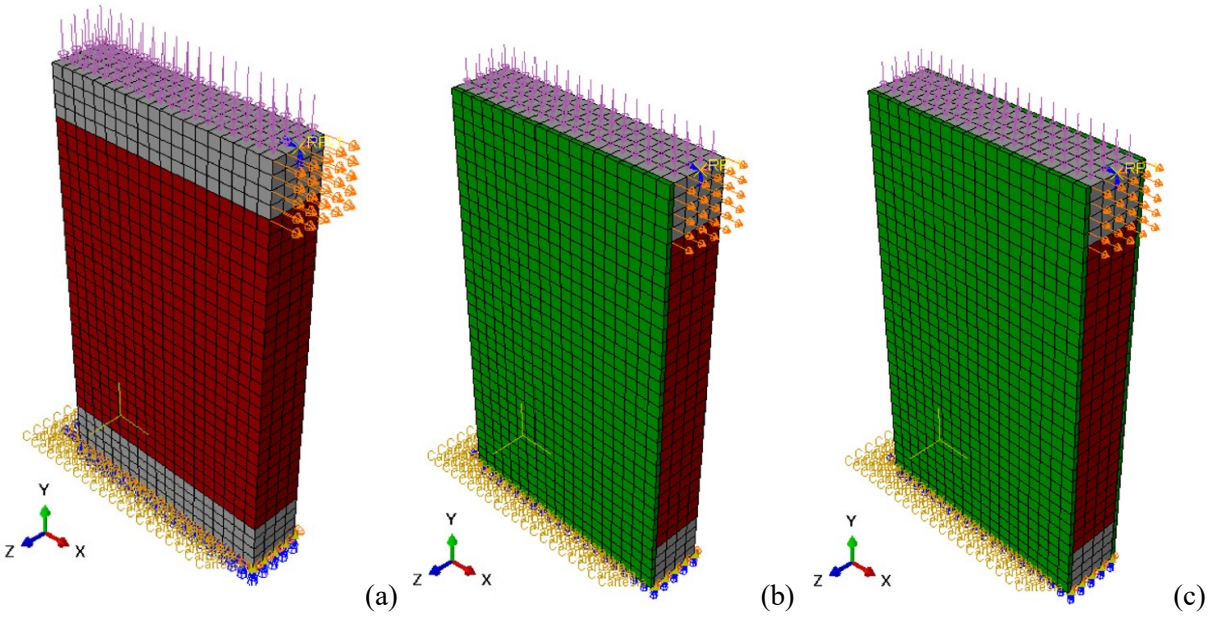

Fig. 4: Numerical model FE-P-R2U (a); FE-P-R2R-1 (b) and FE-P-R2R-2 (c)

2.3.1.1 Unreinforced FEM

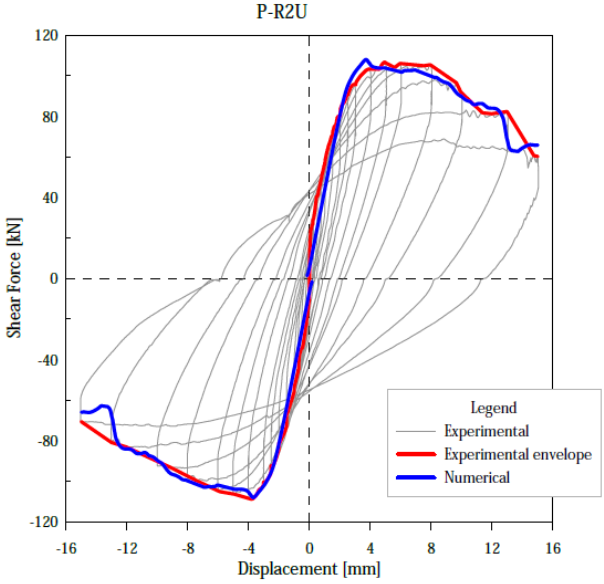

Fig. 5: Model FE-P-R2U: comparison between numerical and experimental curves of shear force – top displacement

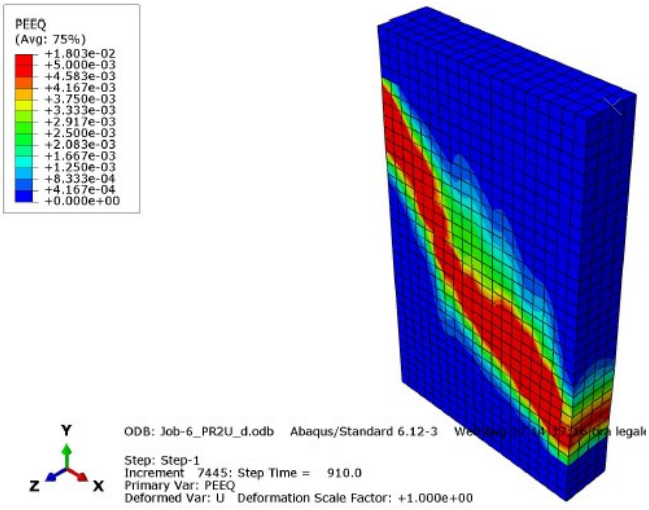

Fig. 6: Model FE-P-R2U: damage distribution at the end of the simulation

Imposed Displacement	Observation
2.5 mm	First vertical crack at the middle of the wall
4 mm	Peak resistance
5 mm	The crack became diagonal, indicating a shear response
15 mm	Failure due to diagonal shear cracking. Damage is concentrated in a principal crack.

From the diagram reported in Fig. 5 a good agreement between the numerical results and the experimental measures can be observed.

Considering the experimental trend, a good calibration of the masonry parameters was obtained. The numerical model well fits the shear force peak, and quite well the descending branch in positive and negative loading directions. It has to be considered that the equivalent homogenous material used for the masonry cannot take into account for the interaction between the stone elements and the mortar, thus the distribution of the crack is linear and perpendicular to the main tensile direction.

It can also be noted that there are some shear force drops at numerical level. These occurred at significant crack propagation during the analysis.

2.3.1.2 One side reinforced FEM

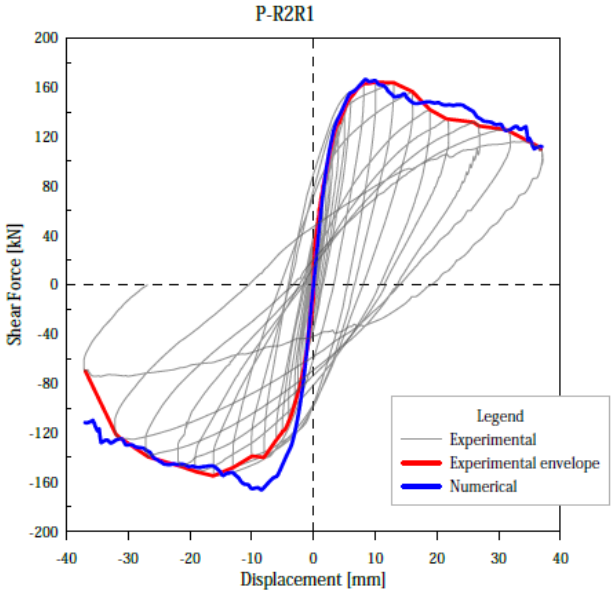

Fig. 7: Model FE-P-R2R-1: comparison between numerical and experimental curves of shear force – top displacement

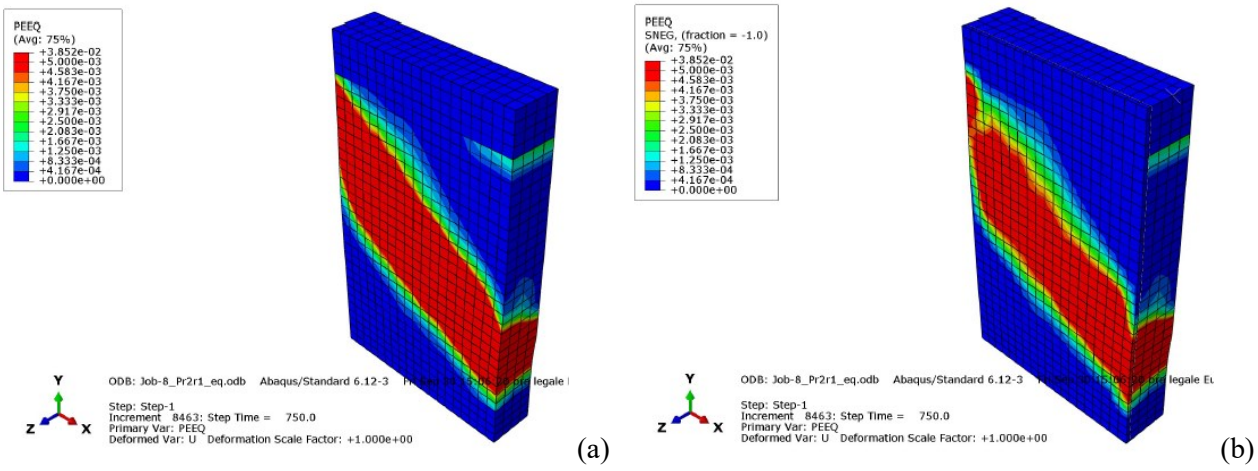

Fig. 8: Model FE-P-R2R-1: damage distribution at the end of the simulation on the masonry side (a) and on the reinforced side (b)

Imposed Displacement	Observation
2.6 mm	First vertical crack at the middle of the wall on the coating and the unstrengthened side.
2.6 mm – 6 mm	The vertical crack propagates.
6 mm – 14 mm	Peak resistance is reached. The main vertical crack in the masonry became diagonal. The damage is more distributed in the reinforcement, but still with a diagonal pattern.
14 mm – 33 mm	The diagonal shear crack propagates untill failure. Damage is more distributed than in the unreinforced specimen.

As can be noted in Fig. 7, a good agreement between experimental and numerical trends was reached. A good calibration of the reinforced parameters was obtained, maintaining the masonry behaviour of the unreinforced specimen. The numerical model well fits the shear force peak and the descending branch in positive direction. The descending branch in the negative direction fits well the experimental trend, in terms of shear force peak, and quite well the trend after the peak. It has to be considered that the analysis was monotonic and could not consider the accumulation of damage that occurred in the cyclic test.

2.3.1.3 Two side reinforced FEM

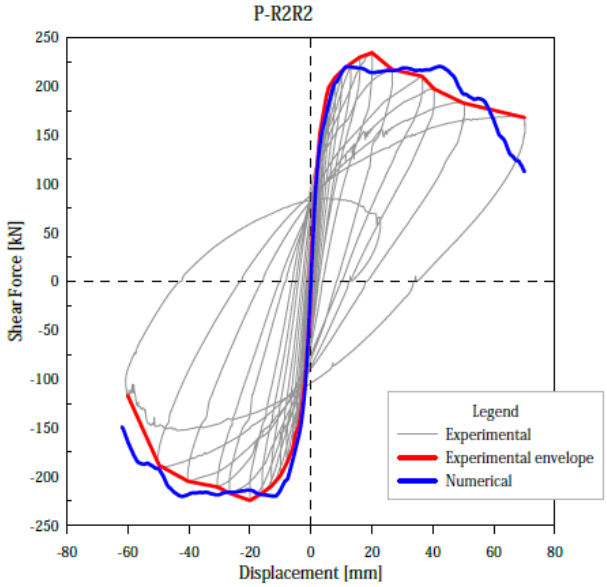

Fig. 9: Model FE-P-R2R-2: comparison between numerical and experimental curves of shear force – top displacement

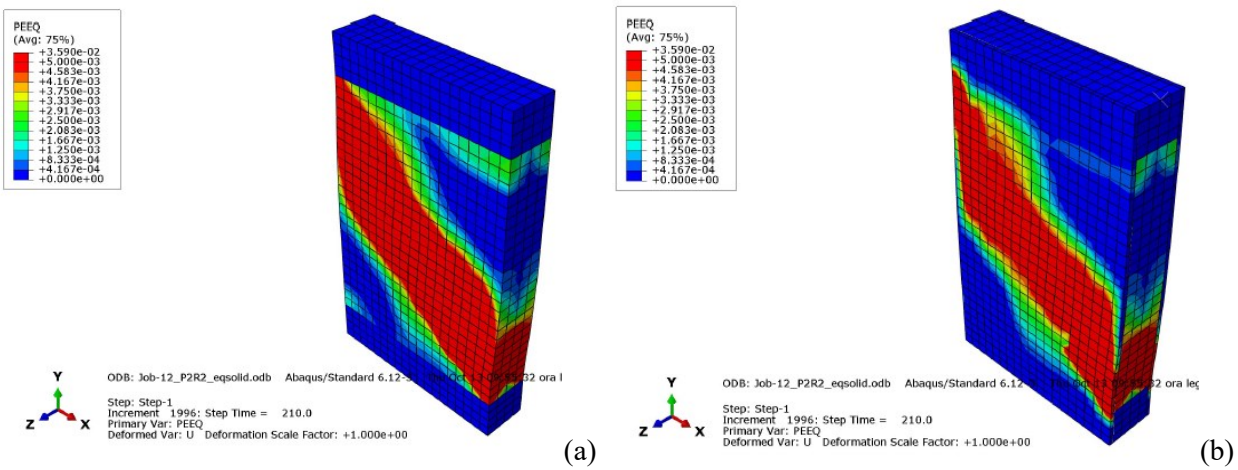

Fig. 10: Model FE-P-R2R-2: damage distribution at the end of the simulation on the masonry side (a) and on the reinforced side (b)

Imposed Displacement	Observation
4 mm	First horizontal crack appeared at the top corner between masonry and RC top beam.
8 mm	From the horizontal crack, an inclined propagation caused the appearing of a diagonal crack which interest the whole high of the masonry elements.
10 mm – 18 mm	Peak resistance is reached. The vertical crack and the horizontal ones (at the top and at the base of the masonry) propagation indicates a combinate shear and flexural failure.
18 mm – 40 mm	The diagonal cracks propagates vertically, causing a spread of damage in the specimen. As seen in the experimental trend, a combination of shear and flexural mechanisms can be observed.
40 mm – 70 mm	Damage continued untile failure

As can be noted in Fig. 9, a good agreement between experimental and numerical trends was reached. Material behaviours remained the same as previous simulations. The shear force peak is slightly underestimated compared to the experimental one (-5.9%), but the numerical descending branch fits quite well the trend obtained experimentally. It is important to note that, particularly in the negative direction, it is well estimated the moment and the drop in resistance that occurs after the breakage of the GFRP mesh.

2.3.2 Single leaf brick masonry specimens

To resemble the experimental test, the concrete beams used in the unreinforced model had a width of 0.35 m, while the reinforced sample's concrete beams had a width of 0.25 m (Fig. 11). The width of the masonry has been modified to 0.25 m and the thickness of each element is equal to 0.0625 m.

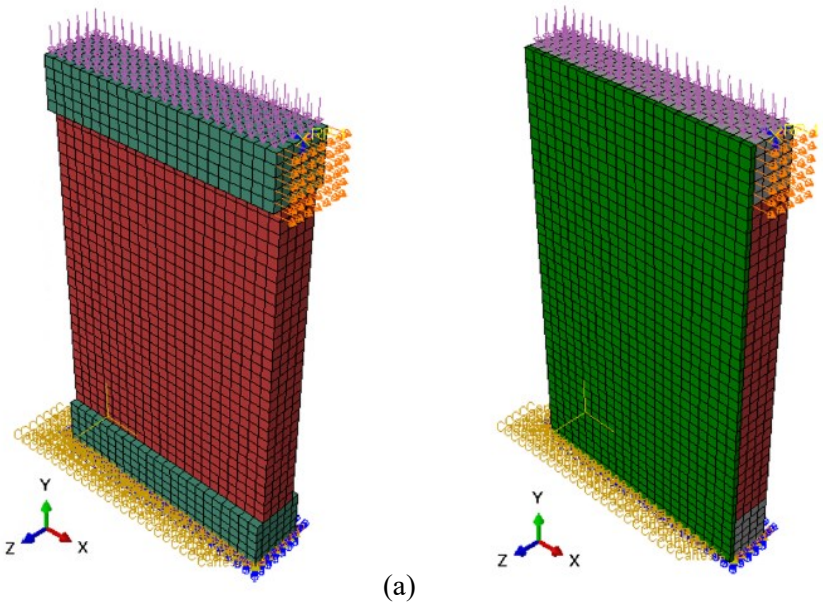

(a) (b)

Fig. 11: Numerical model FE-P-B1U (a); FE-P-B1R (b)

2.3.2.1 Unreinforced FEM

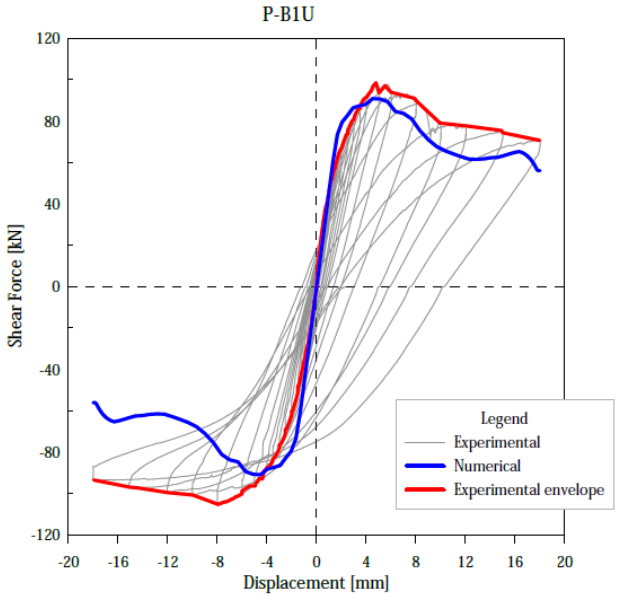

Fig. 12: Model FE-P-B1U: comparison between numerical and experimental curves of shear force – top displacement

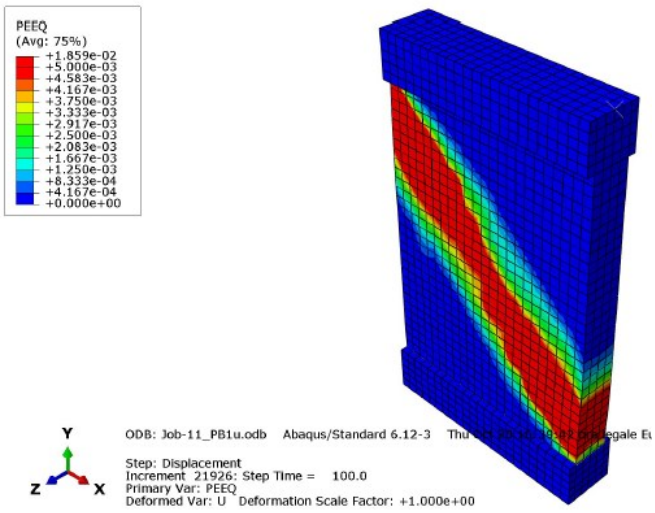

Fig. 13: Model FE-P-B1U: damage distribution at the end of the simulation

Imposed Displacement	Observation
1.5 mm	First horizontal crack appeared at the top left corner.
2 mm	A central vertical crack formed at the centre of the specimen, while the horizontal cracks grew.
3.5 mm	The vertical crack propagates diagonally, indicating a shear failure.
4 mm – 6 mm	Peak force is reached.
6 mm – 18 mm	The diagonal crack continued propagating until the end of the test.

As can be noted in Fig. 12, a quite good agreement between experimental and numerical trends was reached. The shear force peak is fairly underestimated compared to the experimental one (-7.7% in the positive side and -13.6% in the negative one), but the numerical descending branch fits quite well the trend obtained experimentally, particularly for the positive direction. The homogenization of the material allows only a partial capture of the crack pattern, which experimentally occurs in the mortar joints, but it is adequate to identify the failure mechanism as early as the first crack appears.

2.3.2.2 One side reinforced FEM

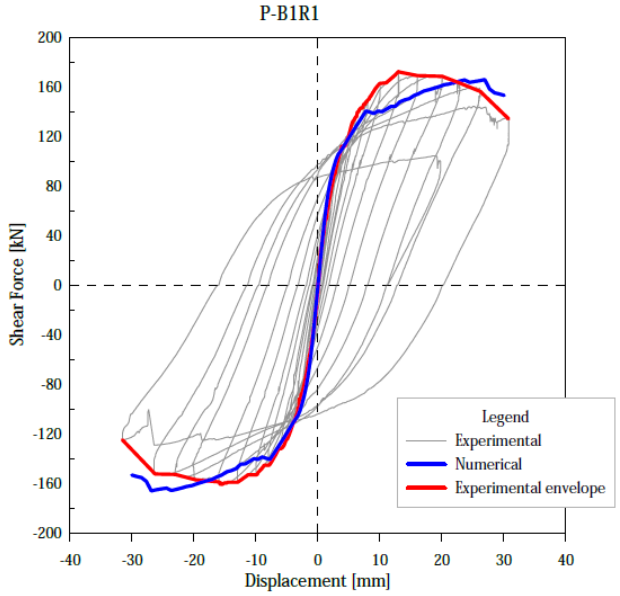

Fig. 14: Model FE-P-B1R: comparison between numerical and experimental curves of shear force – top displacement

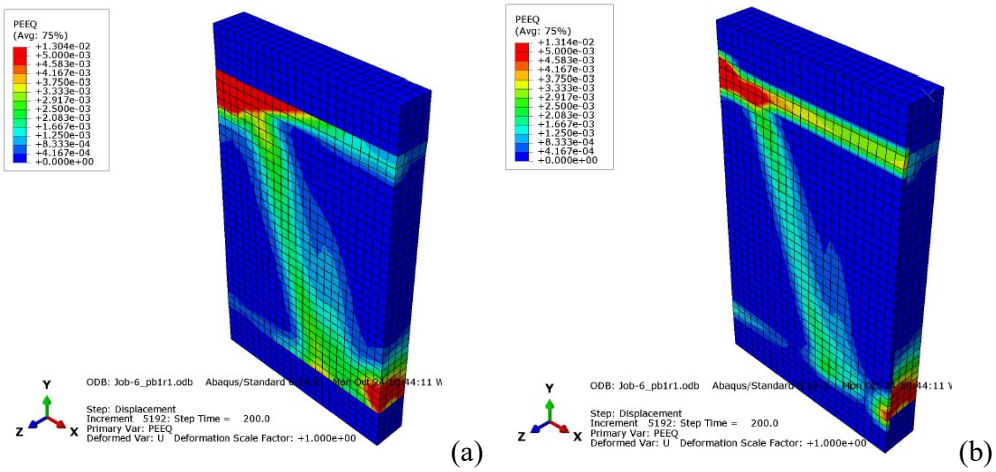

Fig. 15: Model FE-P-B1R: damage distribution at the end of the simulation on the masonry side (a) and on the reinforced side (b)

Imposed Displacement	Observation
3 mm	First horizontal crack appeared at the top left corner both in the reinforcement and in the masonry.
3 mm – 14 mm	The horizontal crack propagates horizontally, with a pure bending failure behaviour.
14 mm – 33 mm	The horizontal cracks propagate both in the top and in the bottom area of the specimen, in addition a diagonal damage is present.

As can be noted in Fig. 14, a good agreement between experimental and numerical trends was reached. The shear force peak fits the experimental one, but not at the same displacements. The initial stiffness drop fits well the experimental behaviour and the numerical descending branch happens at the same time as the experimental

one, which occurs when the GFRP mesh tears. Through the analysis of the crack pattern, the first failure mechanism that occurs is of a flexural type.

2.3.3 Two leaf brick masonry specimens

The dimensions used in these models are the same as the FE-P-B1 models.

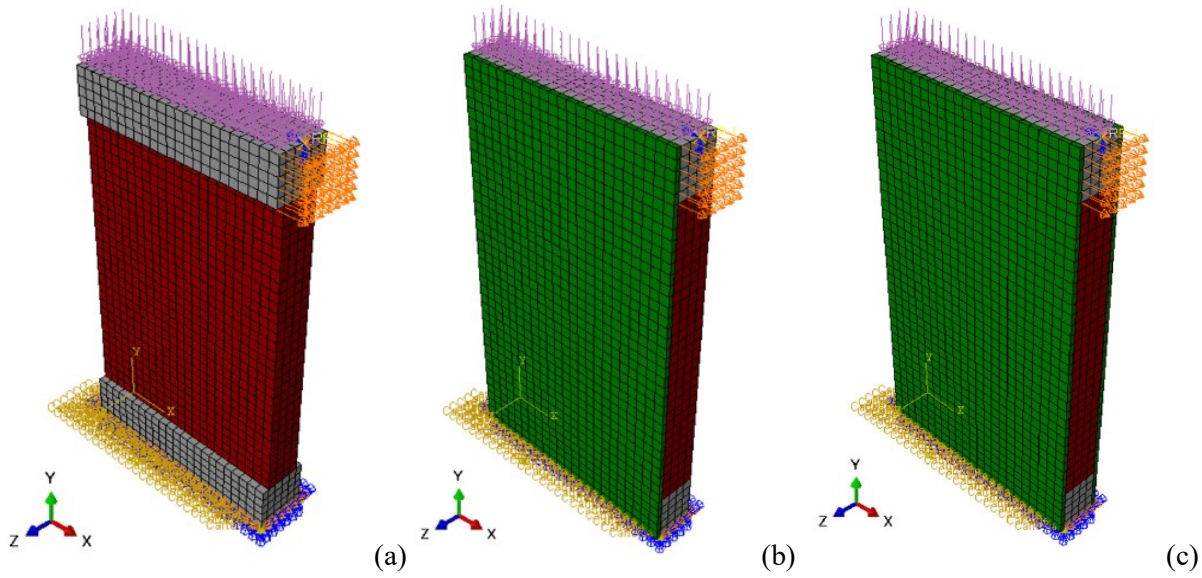

Fig. 16: Numerical model FE-P-B2U (a); FE-P-B2R-1 (b) and FE-P-B2R-2 (c)

2.3.3.1 Unreinforced FEM

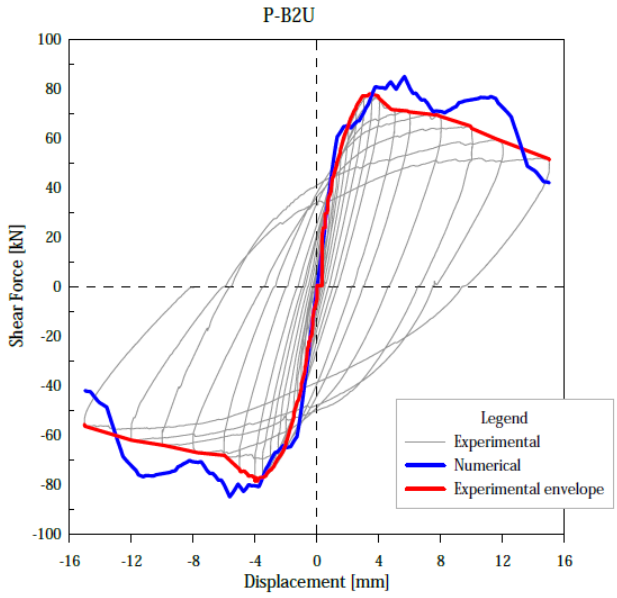

Fig. 17: Model FE-P-B2U: comparison between numerical and experimental curves of shear force – top displacement

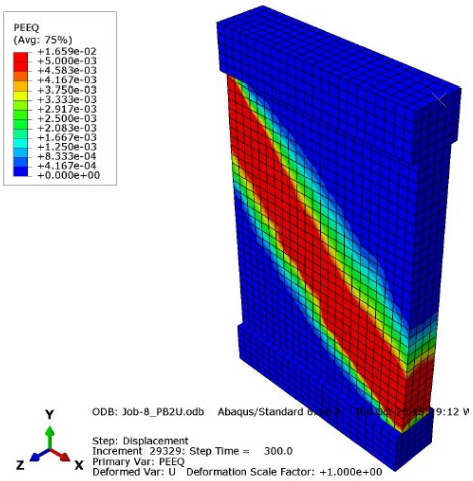

Fig. 18: Model FE-P-B2U: damage distribution at the end of the simulation

Imposed Displacement	Observation
2 mm	The first diagonal crack started creating at the centre of the specimen.
4 mm – 6 mm	Peak resistance is reached.
6 mm – 15 mm	The diagonal crack propagates until failure, indicating a shear failure mechanism.

As can be noted in Fig. 17, a fairly good agreement between experimental and numerical trends was reached. Tha masonry behaviour is the same used for the single-leaf specimen, scaled on the experimental resistance obtained for the double-leaf masonry. The shear force peak fits the experimental one, with a slight overestimation (+8.2%). The numerical descending branch fits well the trend obtained experimentally, both for the positive and the negative direction.

2.3.3.2 One side reinforced FEM

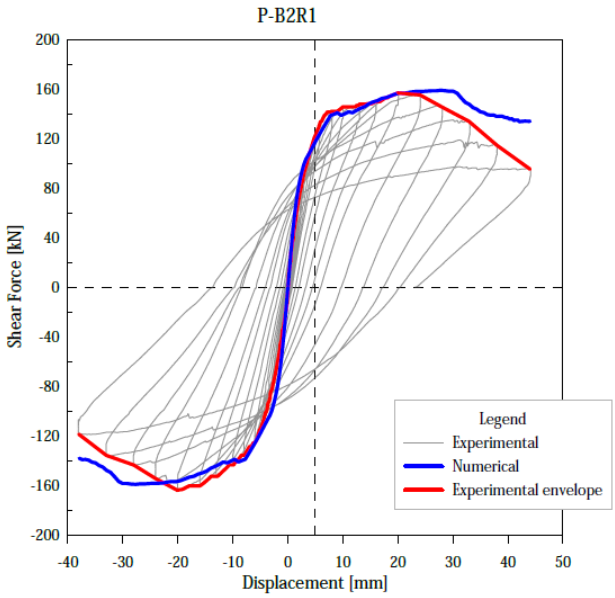

Fig. 19: Model FE-P-B2R-1: comparison between numerical and experimental curves of shear force – top displacement

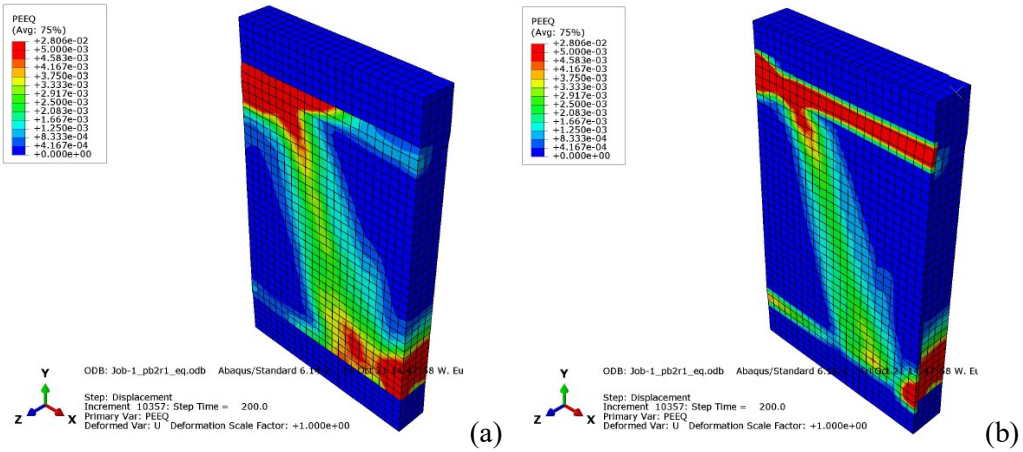

Fig. 20: Model FE-P-B2R-1: damage distribution at the end of the simulation on the masonry side (a) and on the reinforced side (b)

Imposed Displacement	Observation
2 mm	The first horizontal crack started creating at the top of the specimen.
2 mm – 8 mm	Propagation of horizontal cracks.
8 mm – 30 mm	The peak force is reached, the horizontal cracks propagated and a diagonal damage is observed, starting from the top corner. Flexural failure is dominant.
30 mm – 40 mm	The cracks propagated further, with reduce stiffness in shear-displacement trend.

As can be noted in Fig. 19, a good agreement between experimental and numerical trends was reached. The masonry behaviour is the same used for the unreinforced specimen, the reinforcement behaviour remains the same as the previous analysis. The shear force peak fits the experimental one, although the descending branch is slightly underestimated and it happens at a higher displacement value. The flexural failure mode is correctltly evaluated with the numerical model.

2.3.3.3 Two side reinforced FEM

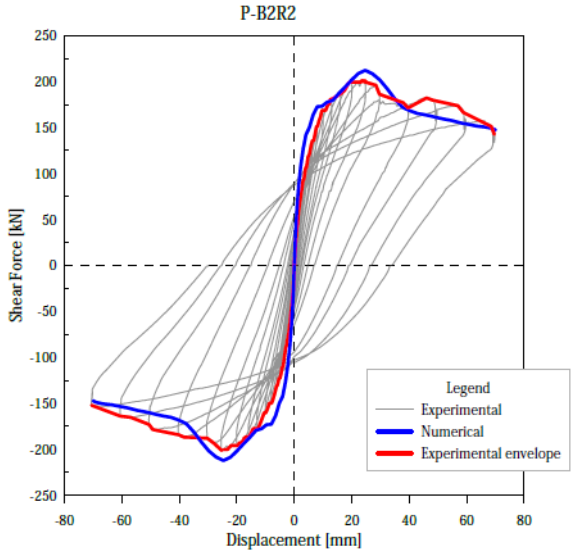

Fig. 21: Model FE-P-B2R-2: comparison between numerical and experimental curves of shear force – top displacement

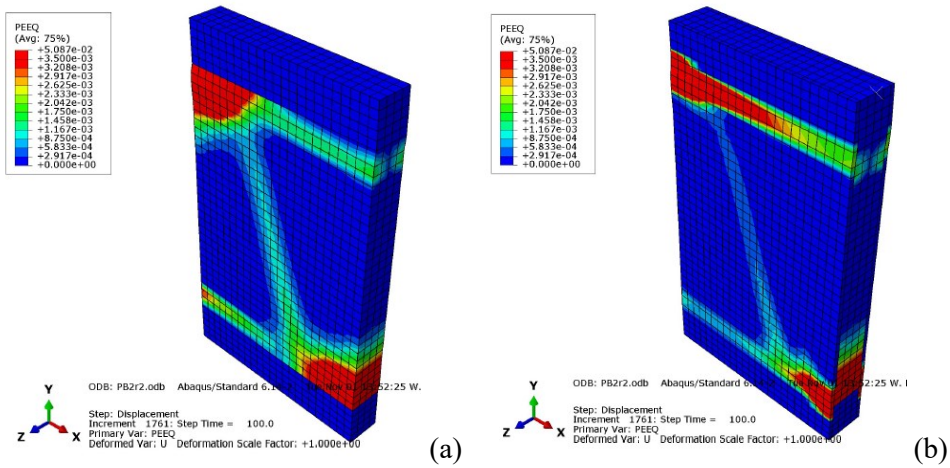

Fig. 22: Model FE-P-B2R-2: damage distribution at the end of the simulation on the masonry side (a) and on the reinforced side (b)

Imposed Displacement	Observation
2 mm	The first horizontal crack started creating in the reinforcement at the top of the specimen.
2 mm – 10 mm	The horizontal crack propagated, affecting the entire width of the sample .
25 mm	Peak resistance is reached. A horizontal crack at the base of the specimen started propagating. Flexural failure is dominant.
30 mm	A diagonal damage started propagating in the specimen.
30 mm – 70 mm	Cracks continue to propagate both in the corner of the specimen and in diagonal, until the final displacement is reached.

As can be noted in Fig. 21, a good agreement between experimental and numerical trends was reached. The masonry behaviour is the same used for the unreinforced specimen and the reinforcement behaviour remains the same as previous analysis. The shear force peak fits the experimental one, as well as the descending branch. The flexural failure mode is corrrectly evaluated with the numerical model.

2.4 Shear-bending numerical models

In accordance with the test setup presented in Section 8 of the first part of the report, the numerical models of the shear-bending test spandrels consisted of two masonry piers, modelled from mid-height of the lower opening to mid-height of the upper one, the masonry spandrel, four concrete beams, two steel beams and the reinforcement. Concrete, masonry, steel and the reinforcement were described in the form of 3D solid, 8-node brick elements available in the ABAQUS/Standard element library (C3D8R). A regular mesh pattern with a constant mesh size of l_{mesh} = 0.066 m was used. The structural interaction between elements constituting the masonry and the concrete components, having coinciding mesh nodes at the contact surfaces, was guaranteed by means of merged nodes on the boundary of the elements.

The specimen was restrained by two rotational hinges, the first one allowed rotation and sliding and the latter one allowed only rotation. In the numerical model these conditions were represent by restraining the steel beam nodes located in the points where the hinges were positioned in the experimental specimen.

For the stone specimens, the wooden lintel was modelled with an orthotropic material, considering average mechanical properties of spruce timber. The connection with the masonry was assured by rigid connectors at the top of the lintel, which guaranteed solidary displacements between the elements. The other lintel surfaces were modelled in contact with the masonry, so that there was no interpenetration. For the brick specimens, the lintel was modelled with the same behaviour as the masonry.

A quasi-static dynamic implicit analysis, considering geometric nonlinearities, in displacement control was carried out to overcome convergence problems due to the formation of cracks. An appropriate loading time history was defined to avoid dynamic effects, thus maintaining a static behaviour. The analysis was performed in two steps. In the first step, uniformly distributed vertical loads were applied on both piers on the upper nodes of the top concrete beams, acting as an equivalent vertical pressure ($\sigma_0 = 0.33$ MPa). Gravity loads were also considered.

In the second step, the static loads from the previous analysis were maintained and a vertical lateral displacement u_y, with a monotonic linear rising time history, was imposed to the nodes at the ends of the steel beams located under the lintel. The results obtained in this way are equivalent to the ones obtained by applying the forces, experimentally measured and applied with the two actuators, at the steel beam ends (as it has been done in the experimental test). The applied displacements are derived from the experimentally measured ones, corresponding on the effects given by applying the external forces from the two actuators.

The spandrel drift was evaluated by considering the vertical displacements of the nodes at base of the two steel beams under the lintel, and dividing the difference between these two displacements by the spandrel span. The shear force was evaluated at the mid-section of the spandrel, with the Free Body Cut feature provided by the software.

2.4.1 Stone masonry specimens

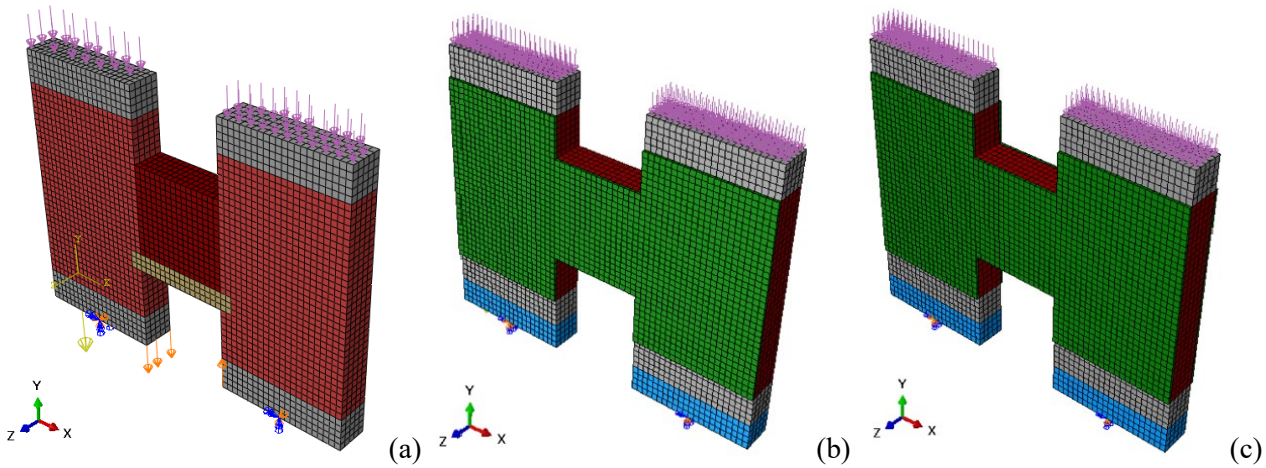

(a) (b) (c)

Fig. 23: Numerical model FE-S-R2U (a); FE-S-R2R-1 (b) and FE-S-R2R-2 (c)

2.4.1.1 Unreinforced FEM

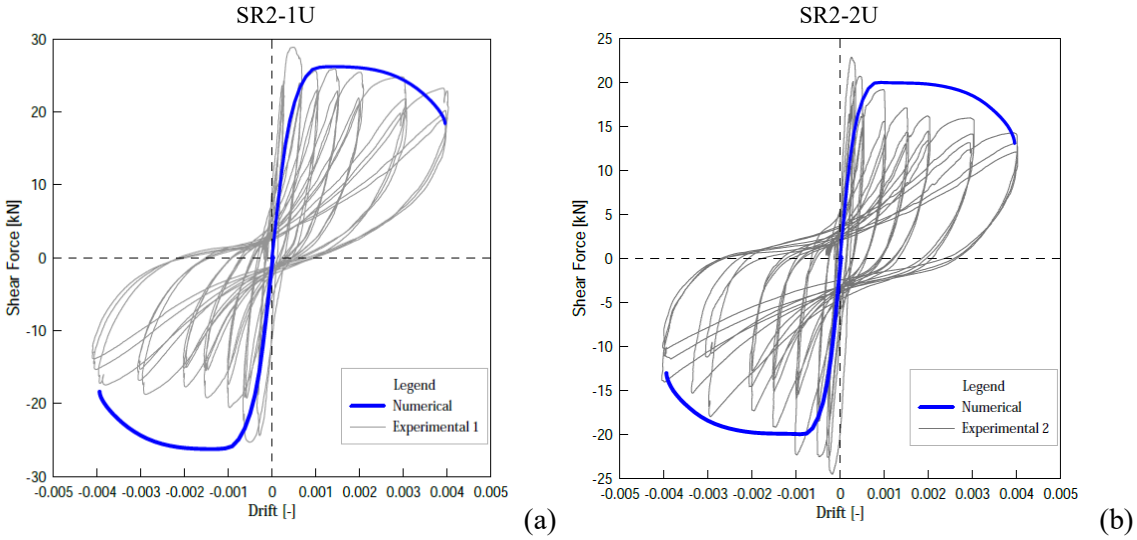

Fig. 24: Model FE-S-R2U: comparison between numerical and experimental curves of shear force – spandrel drift for the first specimen SR2-1U (a) and the second one SR2-2U(b)

The SR2-1U specimen is the spandrel that, after the unreinforced test, has been reinforced on one side, while the SR2-2U specimen has been reinforced on both sides.

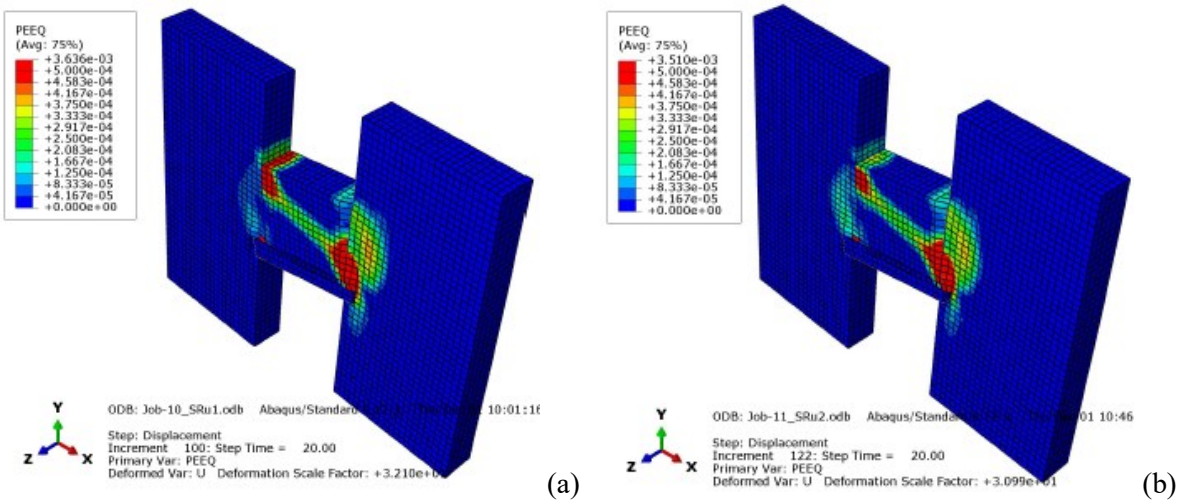

Fig. 25: Model FE-S-R2U: damage distribution at the end of the simulation for the specimen 1 (a) and the specimen 2 (b)

Drift	Observation
0.03%	A first vertical crack compared at the top angle of the spandrel
0.08%	The diagonal crack formed in the spandrel.
0.1%	The peak shear force is reached. In this moment both the vertical and the diagonal cracks are wider.
0.4%	The cracks grew until the end of the test, a damage is also observed on the interface between the masonry and the wood lintel

From the diagrams reported in Fig. 24 a good agreement between the numerical results and the experimental measures can be observed. The two specimens differ in tensile strength by about 20%, in fact the second one has lower experimental force peak (80% lower than the sample 1 shear force peak).

Considering the experimental trends, a good calibration of the masonry parameters was obtained. The numerical model fits the descending branch in positive and negative loading directions, while a slight under-estimation is observed for the shear force peak (about -10%). It can be noted an underestimation of the stiffness in the initial elastic phase, despite a higher elastic modulus considered compared to the experimental results in the compression test on masonry. This can be explained considering the experimental trend of the compression tests, bearing in mind that the spandrel is subjected to low compressions, and noted that in the first phase (with low compression) the behaviour is stiffer. It has to be considered that the equivalent homogenous material used for the masonry cannot take into account for the interaction between the stone elements and the mortar, thus the distribution of the crack is linear and perpendicular to the main tensile direction.

The numerical descending branch of the negative curve of specimen SR2-1U and of that of the positive curve of specimen SR2-2U evidence an overestimation over the experimental results, probably due to damage accumulated at the formation of the first cracks.

2.4.1.2 One side reinforced FEM

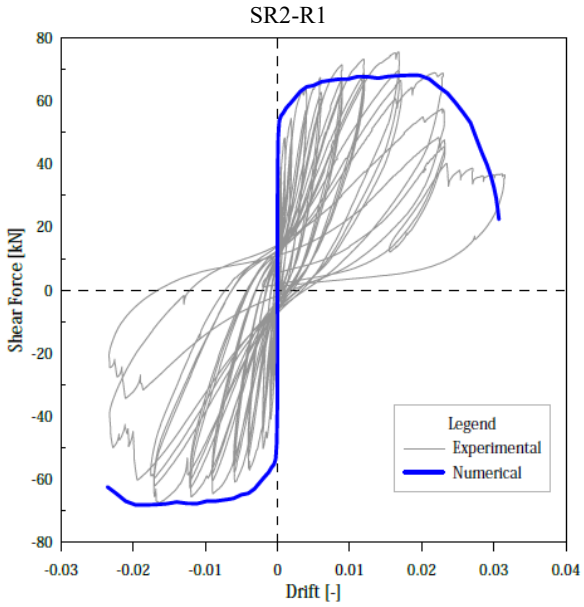

Fig. 26: Model FE-S-R2R-1: comparison between numerical and experimental curves of shear force – spandrel drift

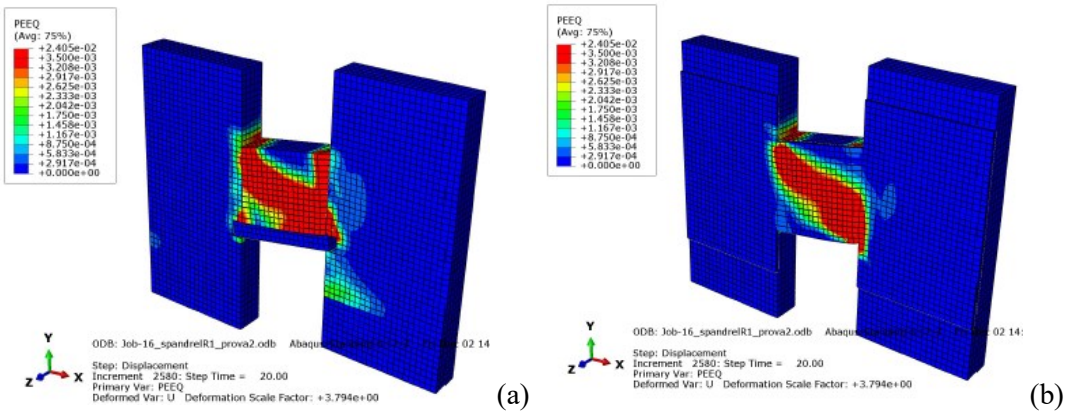

Fig. 27: Model FE-S-R2R-1: damage distribution at the end of the simulation on the masonry side (a) and on the reinforced side (b)

Drift	Observation
0.10%	Two cracks formed at the top corner and on the bottom corner of the spandrel, more significantly on the masony elements.
0.15%	A diagonal crack started forming both on the masonry and on the reinforcement
0.15% - 0.70%	The cracks grew and spread over the entire area of the spandrel
0.70% - 3%	Progressive damage until failure of the GFRP mesh.

As can be noted in Fig. 26, a good agreement between experimental and numerical trends was reached. The masonry behaviour is the same used for piers, the reinforcement behaviour remains the same as previous analysis. The shear force peak fits well the experimental one, in this case the evaluation of the stiffness is better. The positive peak is slightly underestimated (-9.8%), but the negative one is evalued correctly. The numerical descending branches fit well the experimental ones, as well as the resistance drop occurred at the mesh rupture.

2.4.1.3 Two side reinforced FEM

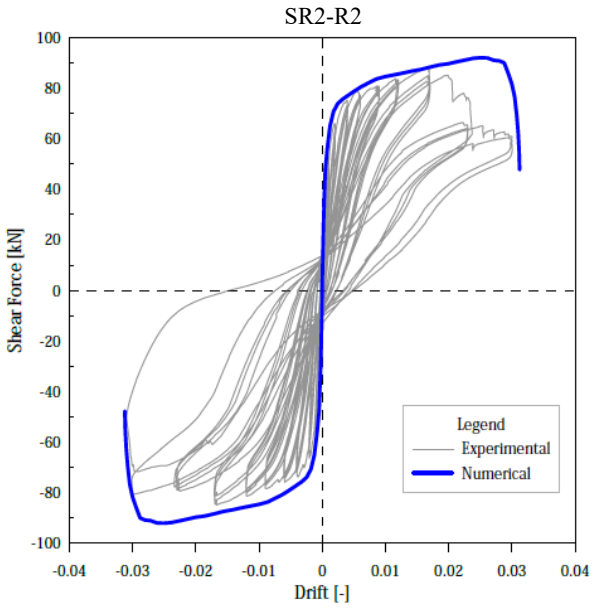

Fig. 28: Model FE-S-R2R-2: comparison between numerical and experimental curves of shear force – spandrel drift

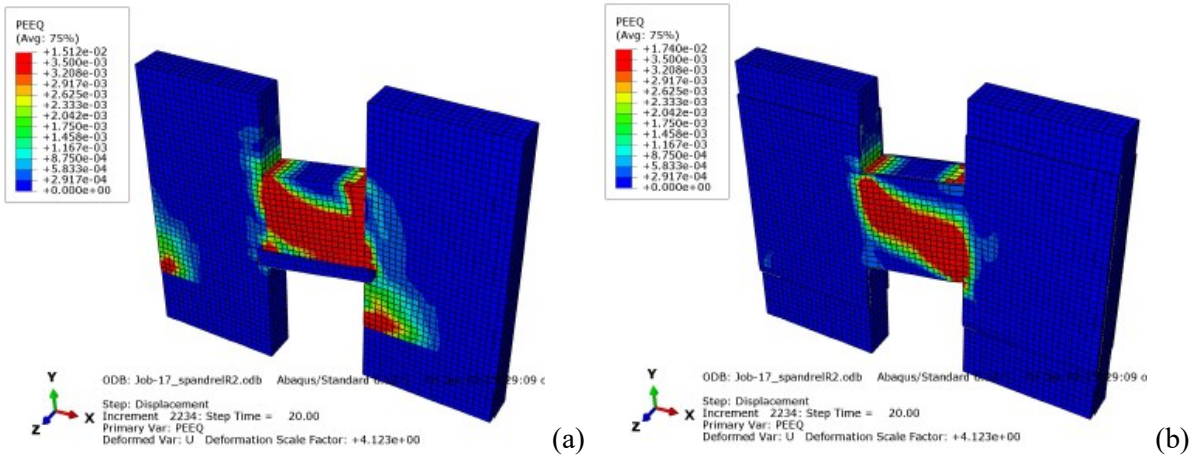

Fig. 29: Model FE-S-R2R-2: damage distribution at the end of the simulation on the masonry side (a) and on the reinforced side (b)

Drift	Observation
0.15%	The first vertical crack formed at the top corner of the spandrel.
0.25%	A diagonal crack started forming both on the masonry and on the reinforcement.
0.25% - 0.80%	The cracks grew and reach the entire height of the spandrel.
0.80% - 3%	The vertical crack grew significantly and a concentrated damage can be noted in the corners of the spandrel. The flexural failure can be clearly individuated.

As can be noted in Fig. 28, a good agreement between experimental and numerical trends was reached. The masonry behaviour is the same used for the piers and the reinforcement behaviour remains the same as previous analysis. The shear force peak is in good agreement with the experimental one, considering an average between positive and negative directions. Also in this case the stiffness is properly evaluated. The numerical descending branch fits the experimental one in the negative direction, identifying correctly also the stiffness drop. The positive trend is slightly more resisntant than the experimental one (+4.2%), and the stiffness drop is slightly shifted in terms of drift.

2.4.2 Single leaf brick masonry specimens

To resemble the experimental test, the concrete beams used in the unreinforced model had a width of 0.35 m, while the reinforced sample's concrete beams had a width of 0.25 m. The width of the masonry has been modified to 0.25 m and the thickness of each element is equal to 0.0625 m.

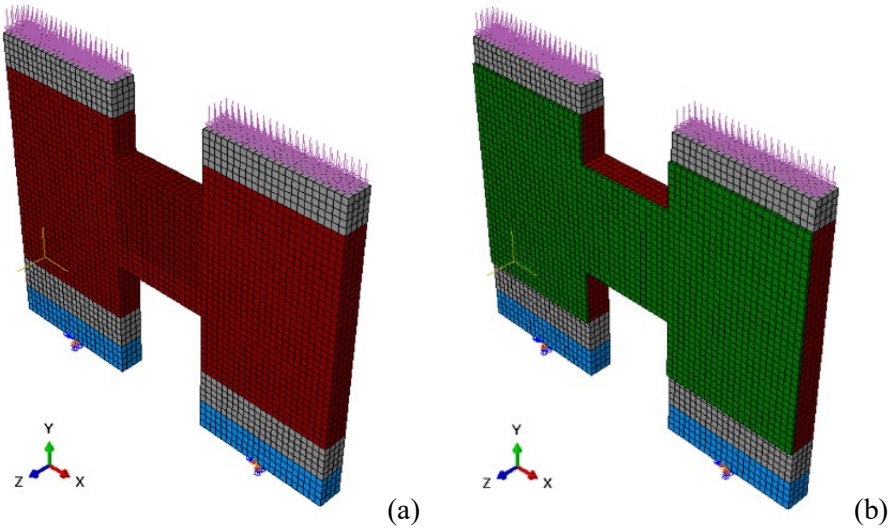

Fig. 30: Numerical model FE-S-B1U (a); FE-S-B1R (b)

2.4.2.1 Unreinforced FEM

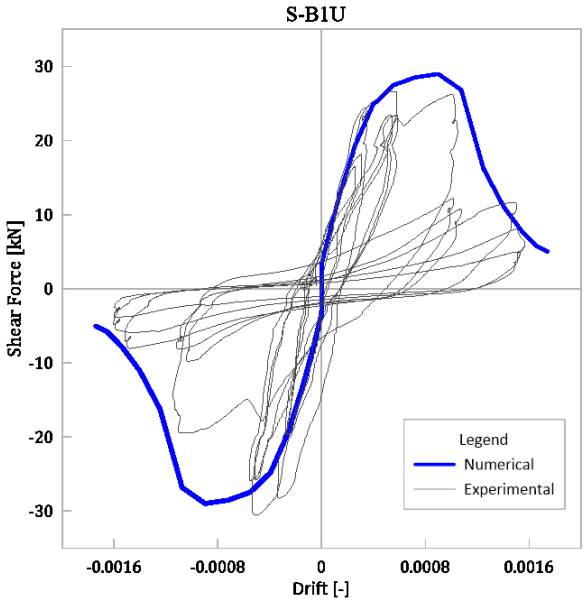

Fig. 31: Model FE-S-B1U: comparison between numerical and experimental curves of shear force – spandrel drift

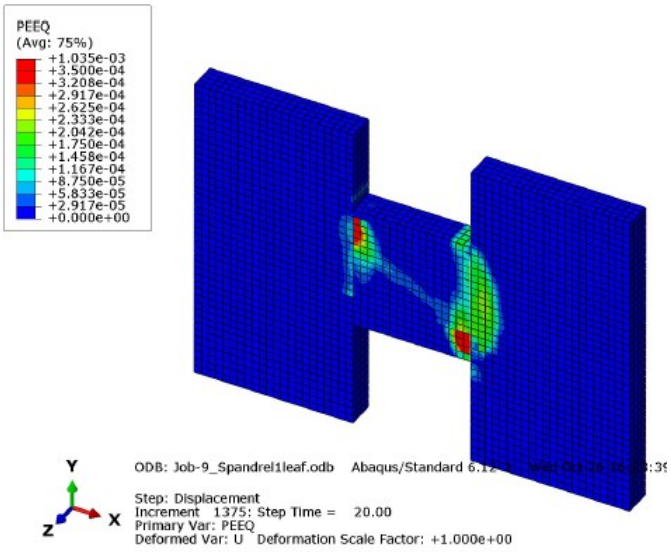

Fig. 32: Model FE-S-B1U: damage distribution at the end of the simulation

Drift	Observation
0.014%	The first damage can be noted in the lintel. A first vertical crack compared at the top angle of the spandrel
0.02% - 0.08%	The peak resistance is reached. The vertical crack propagated and a diagonal crack formed in the spandrel.
0.15%	End of the test, damage is consistent at lintel level and on the diagonal crack formed in the spandrel.

As can be noted in Fig. 31, a good agreement between experimental and numerical trends was reached. The masonry behaviour is the same used for the piers. Considering what observed in the experimental test, a particular attention was paid to the lintel behaviour. In fact, the lintel was defined as the masonry material, but with a reduced tensile strength due to its orientation. The calibration was considered reasonable, since numerically the first damage of the lintel was well fitted. The shear force peak was averagely slightly underestimated (-1.8%), but the numerical descending branch fits the experimental curve both in the positive and negative directions.

2.4.2.2 One side reinforced FEM

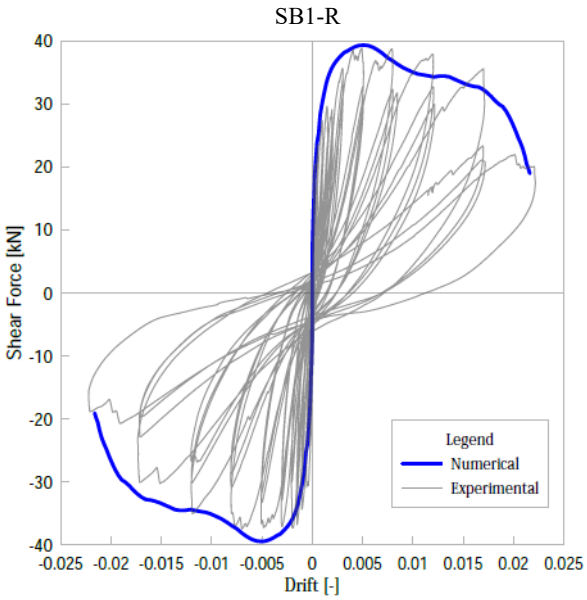

Fig. 33: Model FE-S-B1R: comparison between numerical and experimental curves of shear force – spandrel drift

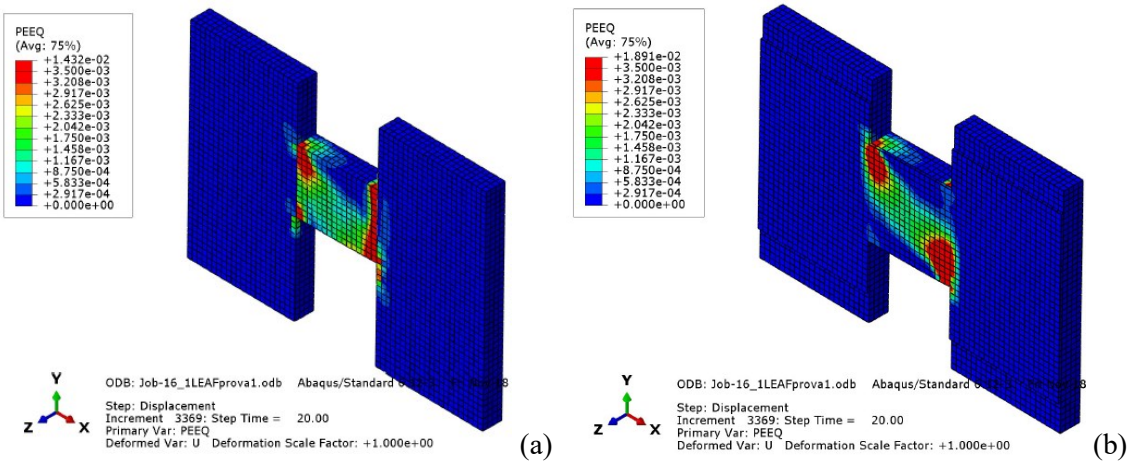

Fig. 34: Model FE-S-B1R: damage distribution at the end of the simulation on the masonry side (a) and on the reinforced side (b)

Drift	Observation
0.045%	The first vertical crack appeared in the spandrel, at the interface with the pier.
0.05% - 0.3%	The vertical crack propagated and a diagonal crack started to form in the masonry at spandrel level.
0.3% - 0.56%	After reaching the maximum resistance, the cracks propagated further and affected the entire dimension of the spandrel.
0.56% - 2.2%	Cracks continue to spread over the spandrel vertically and diagonally till the end of the test.

As can be noted in Fig. 33, a good agreement between experimental and numerical trends was reached. The masonry behaviour is the same used for the unreinforced model and the reinforcement has the same behaviour

of the previous analysis. Considering the high level of damage reached in the unreinforced test, the following considerations were taken into account in the numerical modelling:

- after the test the lintel was completely detached from the spandrel, for this reason it was neglected in the model;
- the vertical cracks at the interface between spandrel and piers were significant. For this reason spandrel and piers were not considered to be perfectly adherent, but a friction value of 0.30 has been considered at the interface. This allow to consider the interlocking provided at the already formed crack level;
- a reduction of 30% of the masonry tensile strength has to be taken into account.

Neglecting these considerations in the analysis means a non-negligible overestimation of the maximum resistance of the specimen.

It can be noted that the shear force peak fits the experimental one, with a slight overestimation (averagely +3.3%), and the descending branches fit well the trends obtained in the test.

2.4.3 Two leaf brick masonry specimens

The dimensions used in these models are the same as the FE-S-B1 models.

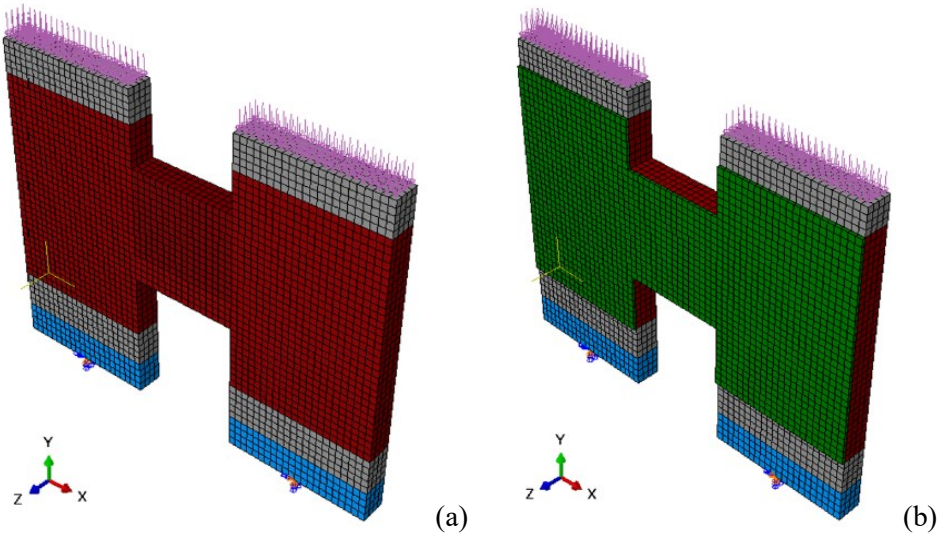

Fig. 35: Numerical model FE-S-B2U (a) and FE-S-B2R-1 (b)

2.4.3.1 Unreinforced FEM

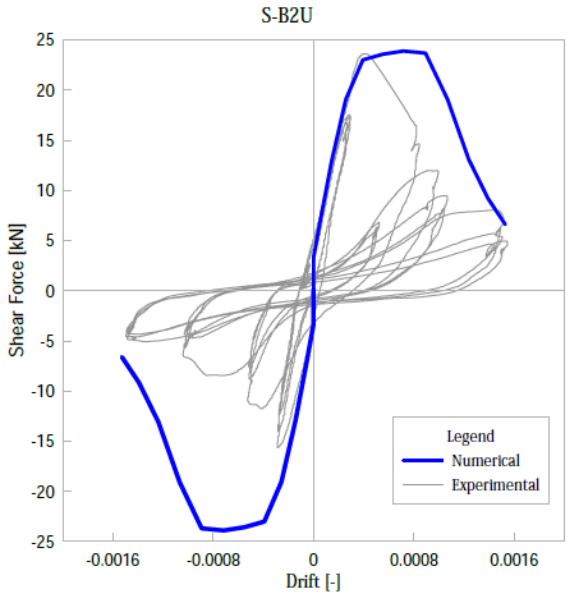

Fig. 36: Model FE-S-B2U: comparison between numerical and experimental curves of shear force – spandrel drift

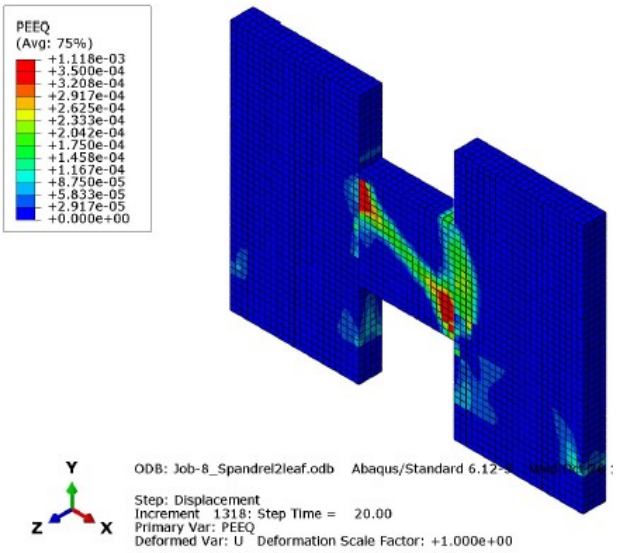

Fig. 37: Model FE-S-B2U: damage distribution at the end of the simulation

Drift	Observation
0.02%	The first damage can be noted in the lintel.
0.05%	A first vertical crack compared at the top angle of the spandrel. The peak force is reached.
0.08%	A diagonal crack started propagating in the centre of the spandrel.
0.08% - 0.16%	Both the vertical and the diagonal cracks propagated through the entire dimension of the spandrel. An important damage was also present on the lintel corner.

As can be noted in Fig. 36, a good agreement between experimental and numerical trends was reached. The masonry behaviour is the same used for the piers. As done for the single-leaf specimen, the lintel was defined as the masonry material but considering a reduced tensile strength, because of the different tensile direction. The behaviour considered was the same as the previous one. The first stiffness degradation due to the damage accumulated in the lintel was well fitted. Also, the shear force peak fits well the experimental one in the positive direction, while the negative direction was not considered due to the problems occurred during the experimental test. The descending branch fits the experimental one both in the positive and in the negative direction, with a slight overestimation of the softening.

2.4.3.2 One side reinforced FEM

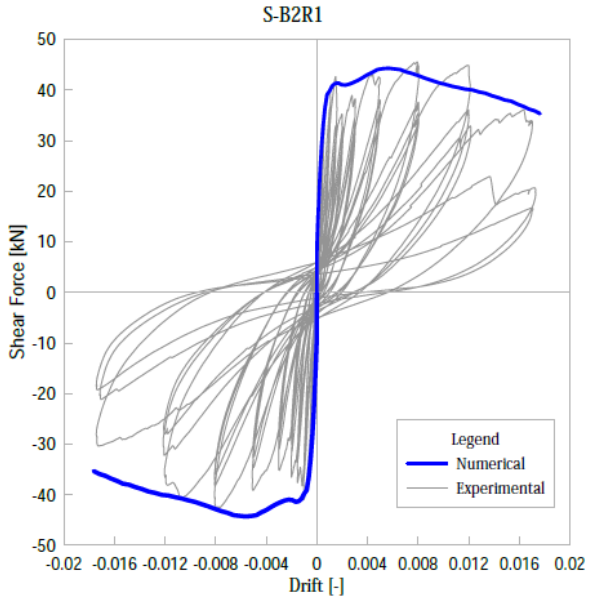

Fig. 38: Model FE-S-B2R-1: comparison between numerical and experimental curves of shear force – spandrel drift

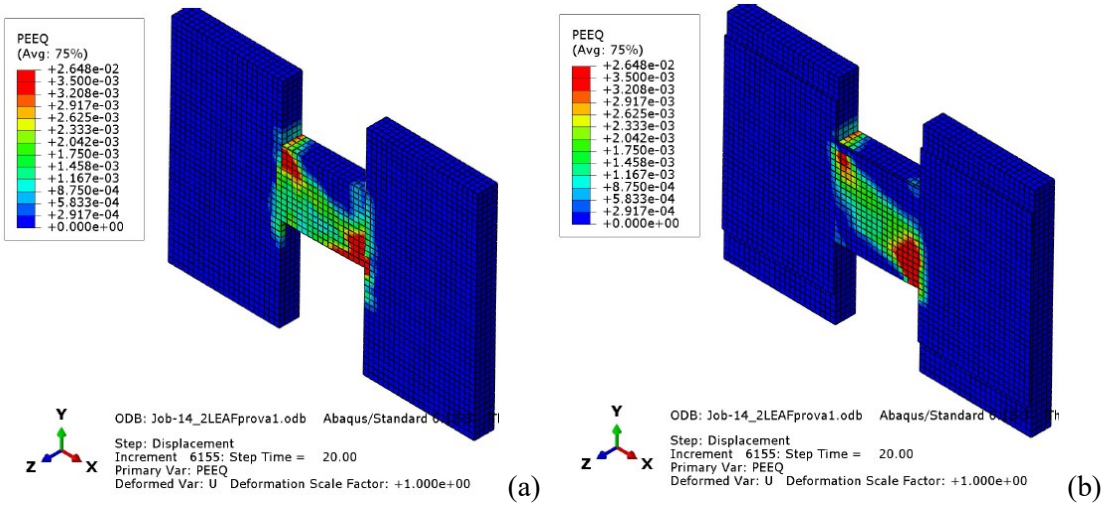

Fig. 39: Model FE-S-B2R-1: damage distribution at the end of the simulation on the masonry side (a) and on the reinforced side (b)

Drift	Observation
0.05%	The first vertical crack appeared in the spandrel, at the interface with the pier.
0.15%	The vertical crack propagated in the masonry and in addition a diagonal crack started forming in the spandrel. Damage started appearing also in the reinforcement.
0.50%	The maximum resistance is reached. Vertical cracks interested both the masonry and the reinforcement, while a diagonal crack created in the masonry propagated.
0.50% - 1.72%	Cracks continue to spread over the spandrel vertically and horizontally till the end of the test, interesting the entire dimension of the spandrel both in the masonry and in the reinforcement.

As can be noted in Fig. 38, a good agreement between experimental and numerical trends was reached. The masonry behaviour and the reinforcement one is the same used for previous analysis. Also, in this case, considering the high level of damage reached in the unreinforced test, the following considerations were taken into account in the numerical modelling:

- after the test the lintel was completely detached from the spandrel, for this reason it has been neglected in the model;
- a reduction of 30% of the masonry tensile strength has to be taken into account.

Neglecting these considerations in the analysis means a non-negligible overestimation of the maximum resistance of the specimen.

The shear force peak fits the experimental one (with less than 1% overestimation), and the descending branches fit well the trends obtained in the test.

2.5 Analytical modelling

2.5.1 Equivalent frame model and plastic hinges

In the equivalent frame approach, a wall (Fig. 40a) is divided into deformable parts (piers and spandrels) and rigid parts (Fig. 40b); each part is schematically represented with a segment and assumed as a beam/column. The piers and spandrels are deformable beams/columns which can perform elastically and inelastically. The rigid parts representing the intersections among piers and spandrels (nodal areas) are so stiff that their deformations are negligible; their actual length may be considered with rigid segments connecting the extremities of deformable elements to the nodes (Fig. 40c). The elastic response of beams/columns is modelled by their flexibility, and the inelastic response is lumped in rotational and shear plastic hinges, as shown in Fig. 40d. The rotational plastic hinges at the ends of the beam/column simulate the inelastic bending response, and the shear plastic hinge at mid-length models the inelastic shear response.

With this approach, the entire structure is modelled by many connected beams, i.e. frames. Hence the name, equivalent frame method.

The plastic hinges contain information about inelastic response and consider all properties of the wall, presence of coating, etc. The equations (models) for plastic hinges are presented in detail in the following sections.

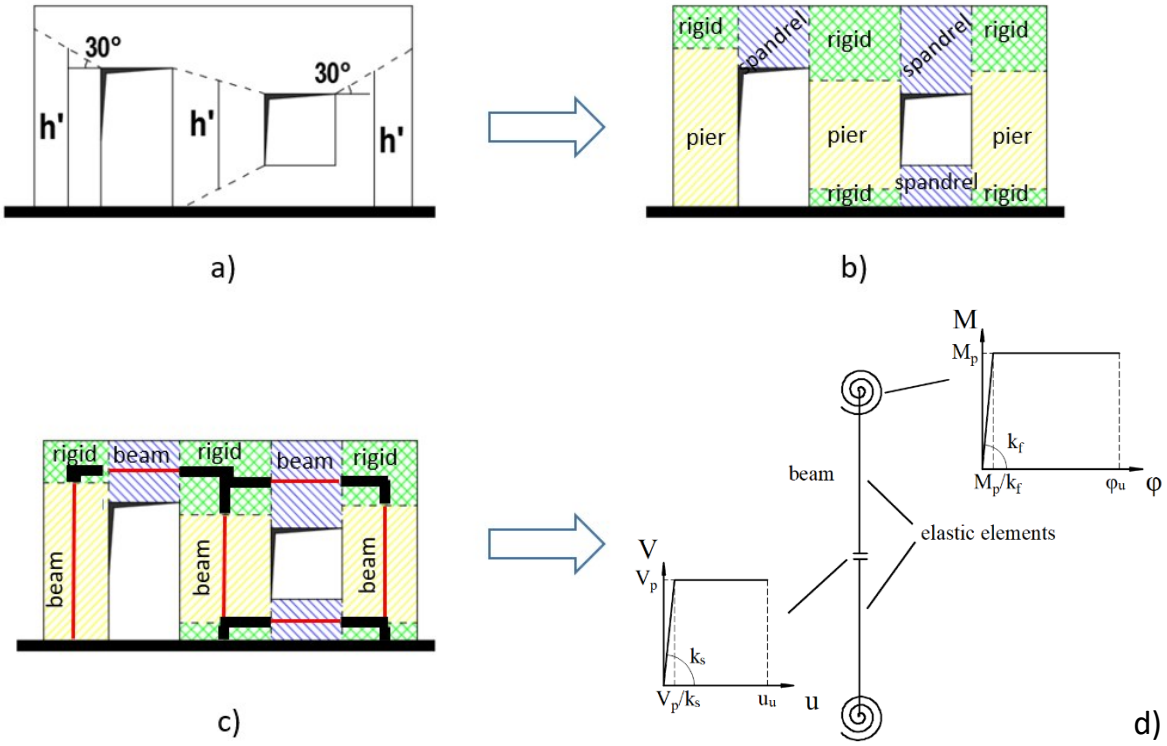

Fig. 40: The concept of equivalent frame modelling

2.5.2 URM elements

2.5.2.1 Resistance of masonry piers to bending

$$M_{Rd,b(U)} = \frac{\sigma_0 \cdot b^2 \cdot t}{2}\left(1 - \frac{\sigma_0}{0.85 \cdot f_m}\right)$$

$$V_{Rd,b(U)} = \frac{2 \cdot M_{Rd,b(U)}}{h} = \frac{\sigma_0 \cdot b^2 \cdot t}{h}\left(1 - \frac{\sigma_0}{0.85 \cdot f_m}\right)$$

With:

h = height of the masonry wall;

b = width of the masonry wall;

t = thickness of the masonry;

σ_0 = average normal stress (compression - σ_0 =N/(b t));

f_m = compressive strength of masonry;

N = axial force in the element.

2.5.2.2 Resistance of piers to shear with diagonal cracking

$$V_{Rd,dc(U)} = \frac{1.5 \cdot \tau_{0(U)} \cdot b \cdot t}{\alpha} \cdot \sqrt{\left(1 + \frac{\sigma_0}{1.5 \cdot \tau_{0(U)}}\right)}$$

With:

$\tau_{0(U)}$ = average shear strength of unreinforced masonry in the absence of axial forces;

$\alpha = h/b$ = form factor (values are between 1.1 and 1.5).

2.5.2.3 The ultimate drift of the flexural hinges of the masonry piers

The ultimate displacement of piers in bending is 1.0% of their height (§7.8.2.2.1 of NTC 2018). The displacement can be larger in the case of rigid body movements (rocking). The hinge is assumed to be elastic-perfectly plastic until collapsing.

2.5.2.4 The ultimate drift of the shear hinges of the masonry walls

The ultimate displacement of piers at full resistance in diagonal shear is 0.5 % of their height (§7.8.2.2.2 of NTC 2018). The displacement can be larger in the case of rigid body movements (rocking).

After reaching 0.5%, resistance drops to 50 % and the diagram is extended to 0.8% drift. The residual resistance observed in the experimental tests (Section 6 of the frst part of the report) is more than 50% in stone masonry and 60% in brick.

2.5.2.5 Flexural strength of the spandrels

$$M_{R1} = \frac{2}{3} \cdot f_{t,eq} \cdot t_s \cdot \frac{h^2}{4}$$

$$V_{R1} = \frac{2M_{R1}}{L}$$

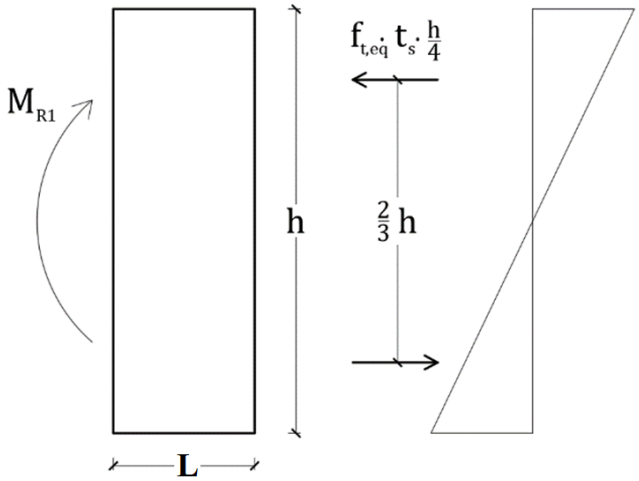

Fig. 41: Simple flexural strength of the non-cracked section

With:

$$f_{t,eq} = \frac{(\tau_{0_{(U)}} + 0.65\ \sigma_p) \cdot b_{eff}}{b_h}$$

$f_{t,eq}$ = equivalent tensile strength. Tensile strength is due to the initial shear strength and friction. Friction is due to the normal stress in the piers and is calculated with a 0.65 coefficient of friction;

t_s = thickness of the wall;

h = height of the wall;

L = length of the wall;

σ_p = normal stress in adjacent piers;

b_{eff} = effective overlapping length of masonry unit (stone, brick);

b_h = total thickness of a wall.

2.5.2.6 Diagonal shear resistance of spandrels

$$V_{R2} = \frac{f_{tm} \cdot h \cdot t_s}{\alpha} \cdot \sqrt{1 + \frac{\sigma_h}{f_{tm}}}$$

With:

$\alpha = \frac{L}{h}$ where $1.0 \leq \alpha \leq 1.5$

σ_h is the horizontal axial stress in the spandrel (positive if compression). Usually, it is zero.

$f_{tm} = 1.5 \cdot \tau_{0_{(U)}}$, according to C8.7.1.16 of the Circular.

2.5.2.7 The ultimate drift of the spandrels in bending

In §C8.7.1.3.1.1 of the Circular, it is indicated that the limit threshold for the ultimate displacement at the near collapse is equal to 1.5% of the length of the spandrel. The hinge is assumed to be elastic perfectly plastic.

2.5.2.8 The ultimate drift of spandrels in shear

§C8.7.1.3.1.1 of the Circular states that the ultimate drift is 0.5%. However, residual strength can be maintained up to 1.5 % drift if there is an effective lintel. A residual strength value equals 40% in the case of a well-clamped wooden lintel. A multilinear constitutive model can be adopted, which considers these aspects.

2.5.3 Strengthened elements

2.5.3.1 Resistance of strengthened masonry piers in bending

The procedure for calculating strengthened pier in bending presented below follows the CNR 215/2018. The CNR recognizes that the peak resistance of mesh strands depends on strengthening intervention. In some cases, the failure can occur due to delamination between the coating and the wall; in other cases, the fibres might slip from the mortar. Only in the best case are the fibres fully utilized, and the failure mechanism is due to tensile fracture of the mesh strands.

If no better test is available, the lap shear test is used to check the collapse mechanism and determine the peak resistance of the mesh. An example of the test is shown in Fig. 42. In the present project, more representative tests, such as cyclic shear compression tests, were performed. These have shown conclusively that in the present intervention method, the fibres of the mesh fracture in tension.

Fig. 42: Shear lap test

The calculation of flexural resistance of a strengthened masonry pier is based on the following assumptions:

- Planar cross-sections remain planar after deformation (Bernoulli's hypothesis)
- Perfect adhesion between masonry and FRP bars
- Bilinear stress-strain law for masonry in compression (Fig. 43, right)
- Zero tensile strength of masonry and mortar coating
- Linear stress distribution in GFRP mesh in tension (Fig. 43, left)
- Zero compressive strength of GFRP mesh
- The effect of the eccentricity of the coating is neglected

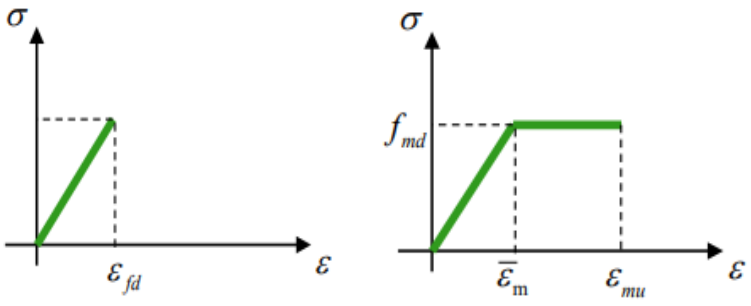

Fig. 43: Material laws of FRP mesh in tension (left) and masonry in compression (right)

The pier geometry is shown in Fig. 44.

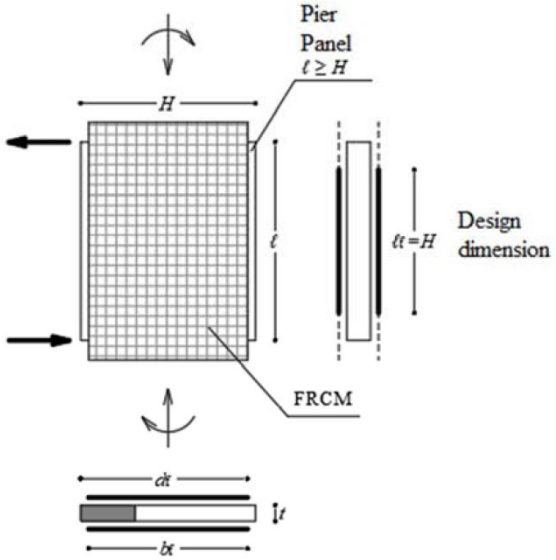

Fig. 44: The scheme of a pier and the mesh according to CNR 2018

A general-purpose software for calculating a cross-section that considers the above assumptions can be used. However, analytical expressions can be derived due to the linear stress distributions, and the CNR 215/2018 provides such analytical expressions in Appendix 1. In the expressions, the tensile mesh strands are transformed into a layer of thickness t_{2f}.

Three cases are considered: i) compressive crushing on the compressive edge ($\varepsilon_m = \varepsilon_{mu}$), ii) tensile fracture of mesh ($\varepsilon_f = \varepsilon_{fd}$) and non-linear stress distribution in compression ($\bar{\varepsilon}_m \leq \varepsilon_m \leq \varepsilon_{mu}$), and iii) tensile fracture of mesh ($\varepsilon_f = \varepsilon_{fd}$) and linear stress distribution in compression ($\varepsilon_m \leq \overline{\varepsilon_m}$). The solution is the lowest of the three cases.

For the case i), failure due to compressive crushing of masonry, the equations are:

$$M_{Rd}(N_{Sd}) = f_{md} \cdot \frac{t \cdot y_n}{2} \cdot \left[H \cdot (1-k) - y_n \cdot (1-k)^2 + k \cdot \left(\frac{H}{2} - y_n + \frac{2}{3} \cdot k \cdot y_n\right)\right] + \frac{\varepsilon_{mu}}{y_n}$$

$$\cdot E_f \cdot t_{2f} \frac{\left(d_f - y_n\right)^2}{12} \cdot \left(2 \cdot y_n + 4 \cdot d_f - 3 \cdot H\right)$$

$$k = \frac{\bar{\varepsilon}_m}{\varepsilon_{mu}}$$

$$y_n = \frac{N_{Sd} - E_f \cdot t_{2f} \cdot d_f \cdot \varepsilon_{mu} + \sqrt{{N_{Sd}}^2 + E_f \cdot t_{2f} \cdot d_f \cdot \varepsilon_{mu}\left[(2-k)t \cdot d_f \cdot f_{md} - 2N_{Sd}\right]}}{t \cdot f_{md}(2-k) - E_f \cdot t_{2f} \cdot \varepsilon_{mu}}$$

For case ii), failure due to tensile fracture of mesh ($\varepsilon_f = \varepsilon_{fd}$) and non-linear stress distribution in compression ($\bar{\varepsilon}_m \leq \varepsilon_m \leq \varepsilon_{mu}$) the equations are:

$$M_{Rd}(N_{Sd}) = f_{md} \cdot \frac{t}{12} \cdot \left[2 \cdot d_f \cdot y_n \cdot \xi \cdot (2 \cdot \xi + 3) + 3 \cdot H \cdot [y_n \cdot (2 + \xi) - \xi \cdot d_f] - 2 \cdot {y_n}^2 \cdot (\xi^2 + 3 + 3 \cdot \xi) - 3 \cdot \xi^2 \cdot {d_f}^2\right] + \varepsilon_{fd} \cdot E_f \cdot t_{2f} \frac{d_f - y_n}{12}\left(2 \cdot y_n + 4 \cdot d_f - 3H\right)$$

$$\xi = \bar{\varepsilon}_m / \varepsilon_{fd}$$

$$y_n = \frac{2 \cdot N_{Sd} + t \cdot \xi \cdot f_{md} \cdot d_f + E_f \cdot t_{2f} \cdot d_f \cdot \varepsilon_{fd}}{t \cdot f_{md}(2 + \xi) + E_f \cdot t_{2f} \cdot \varepsilon_{fd}}$$

Finally, for case iii), tensile fracture of mesh ($\varepsilon_f = \varepsilon_{fd}$) and linear stress distribution in compression ($\varepsilon_m \leq \overline{\varepsilon_m}$) the equations are:

$$M_{Rd}(N_{Sd}) = \frac{t \cdot E_m \cdot \varepsilon_{fd}}{12} \cdot \frac{{y_n}^2}{d_f - y_n}(3 \cdot H - 2 \cdot y_n) + \varepsilon_{fd} \cdot E_f \cdot t_{2f} \frac{d_f - y_n}{12}(2 \cdot y_n + 4 \cdot d_f - 3 \cdot H)$$

$$y_n = \frac{N_{Sd} + E_f \cdot t_{2f} \cdot d_f \cdot \varepsilon_{fd} - \sqrt{{N_{Sd}}^2 + E_m \cdot \varepsilon_{fd} \cdot d_f \cdot t \cdot \left(E_f \cdot t_{2f} \cdot d_f \cdot \varepsilon_{fd} + 2N_{Sd}\right)}}{\varepsilon_{fd} \cdot (E_f \cdot t_{2f} - t \cdot E_m)}$$

ε_{fd} = effective mesh strain (equal to ultimate strain in the present case)

M_{Rd} =design bending moment resistance

N_{Sd}=design axial (compressive) force

$\bar{\varepsilon}_m$=masonry compressive strain at plastic limit

ε_{mu}=ultimate masonry compressive strain

y_n =depth of neutral axis

H=height of the pier

t=thickness of masonry

E_m=elastic modulus of masonry

d_f=distance between extreme tension in FCRM and extreme compression in masonry

f_{md}=compressive strength of masonry

t_{2f}=equivalent thickness of the tensile layer

E_f=elastic modulus of the reinforcing mesh

Alternatively, to the analytical expressions of CNR 215/2018, a general-purpose program for cross-section calculation can be used. Both calculations give the same result.

2.5.3.2 Resistance of reinforced masonry piers to diagonal shear

Formulas for diagonal shear strength (Turnšek - Čačovič) can be used:

$$V_{Rd(CRM)} = \frac{1.5 \cdot \tau_{0_{(R)}} \cdot b \cdot t}{\alpha} \cdot \sqrt{\left(1 + \frac{\sigma_0}{1.5 \cdot \tau_{0_{(R)}}}\right)}$$

assuming for $\tau_{0_{(R)}}$ the equivalent resistance value that takes into account also the reinforced coating. The value is obtained from experimental studies (*Boem and Gattesco, 2021*):

$$\tau_{0_{(R)}} = \beta \cdot \left(\tau_{0_{(U)}} + m \cdot \frac{t_c}{t} \cdot \frac{f_{t,c}}{1.5}\right)$$

Where $\tau_{0\,(U)}$ is the shear strength in the absence of axial forces for URM masonry;

$\alpha = \frac{h}{b}$ where $1 \leq \alpha \leq 1.5$;

t_c = thickness of the coating (reinforced plaster);

$f_{t,c}$ = tensile strength of the mortar for coating, which is assumed to be equal to $\frac{1}{10}$ of its compressive strength;

β is a coefficient that considers the effectiveness of the reinforcement. It is 0.8 for brick masonry and 1.0 for stone masonry;

m = number of reinforced sides of the masonry.

2.5.3.3 The ultimate drift of strengthened piers in bending

According to §7.8.3.2.1 of the NTC 2018, the ultimate displacement for non-linear static analysis can be assumed 1.6 % of the panel's height. In the case of reinforcement on one side only, the hinge is assumed elastic - perfectly plastic until collapse.

In the case of stone masonry reinforced on both sides, experiments showed that the ultimate drift at 80 % residual strength was equal to 2.5%.

2.5.3.4 The ultimate drift of strengthened piers in shear

The ultimate displacement for reinforced masonry, according to §7.8.3.2.2 of the NTC 2018, is 0.8% of the panel's height.

Experimentally, the drifts at 80 % residual strength were:

1.4% for single-sided reinforced stone masonry (see Section 6.5.2 of the first part of the report);

1.6% for single-sided reinforced brick masonry (see Section 6.5.5 of the first part of the report);

2.5% for stone and brick masonry strengthened on both sides (see Sections 6.5.3 and 6.5.8 of the first part of the report).

2.5.3.5 Flexural strength of strengthened spandrels

The calculation of flexural resistance of strengthened spandrels according to CNR 215/2018 is essentially the same as the calculation for piers. The only difference is that the load is now vertical, H and l are swapped, there is no compressive force (Fig. 45) and E_m, f_{md} and ε_m refer to the horizontal direction of the masonry.

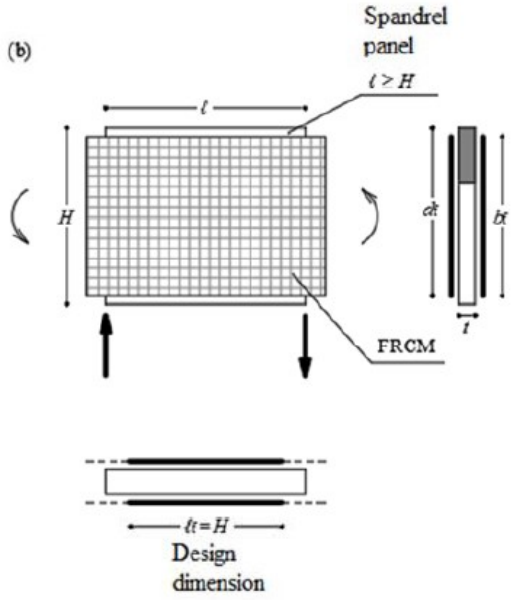

Fig. 45: The scheme of a spandrel and the mesh according to CNR 215/2018

2.5.3.6 Resistance of strengthened spandrels to diagonal shear

$$V_t = min\left(V_{t,M} + V_{t,S}; V_{t,max}\right)$$

with:

$$V_{t,M} = d \cdot t \cdot f_{vd}$$

$$V_{t,S} = \frac{z \cdot m \cdot T_w}{s}$$

$$V_{t,max} = 0.25 \cdot f_m \cdot t \cdot d$$

$V_{t,M}$ = resistance of masonry;

$V_{t,S}$ = resistance of the coating;

d = the distance between the compressed edge and the centre of gravity of all tensile strands;

z = arm of the internal force couple assumed equal to $0.9 \cdot d$;

s = pitch of the mesh strands;

T_w = tensile strength of the single wire of the network;

m = number of sides with coating.

2.5.3.7 The ultimate drift strengthened spandrels in bending

Experimentally observed drift in stone masonry spandrels strengthened on one side was 2.0 % (see Section 8.5.2 of the first part of the report).

2.5.3.8 The ultimate drift of strengthened spandrels in shear

Experimentally observed shear drift at the near collapse was 2.0% for the stone masonry strengthened on one side only (see Section 8.5.2 of the first part of the report). Stone masonry reinforced on both sides (Section 8.5.3 of the first part of the report) experienced a drop in resistance at 2.0% drift, which stabilized at 60 % residual resistance and remained until 3.0 % drift.

2.5.3.9 Constitutive law of plastic hinges

The force-displacement relationship, which describes the behaviour of plastic hinges in bending and shear, is shown schematically in Fig. 46. The limit states in the graph are: IO = immediate occupancy, LS = life safety, and CP = collapse prevention.

Tables 4 to 7 show the values for points B, C, D and E for unreinforced piers, unreinforced spandrels, strengthened piers and strengthened spandrels.

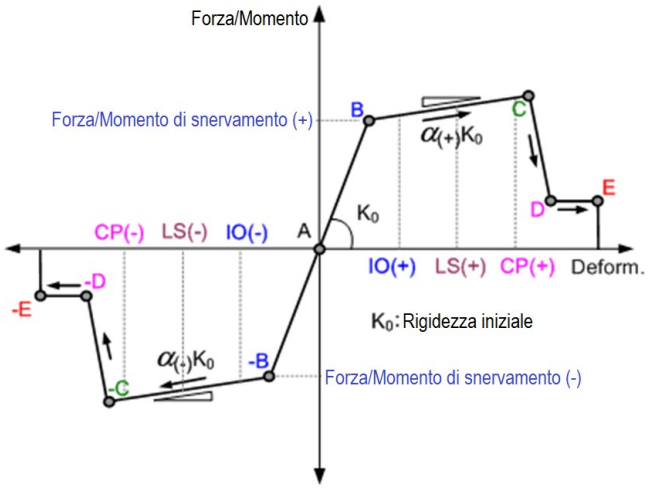

Fig. 46: Envelope of a generic plastic hinge in the MIDAS GEN program

Table 4: Plastic hinges for URM piers

URM pier				
Point	Flexural hinge		Shear hinge	
	Resistance	Drift	Resistance	Drift
A.	0	0	0	0
B.	$M_{Rd,b(U)}$	$\delta_{B(M)}$	$V_{Rd,dc(U)}$	$\delta_{B(V)}$
C.	$M_{Rd,b(U)}$	1.0%	$V_{Rd,dc(U)}$	0.5%
D.	$0.3 \cdot M_{Rd,b(U)}$	1.1 %	$0.5 \cdot V_{Rd,dc(U)}$	0.8%
E.	$0.3 \cdot M_{Rd,b(U)}$	2.0 %	$0.5 \cdot V_{Rd,dc(U)}$	0.9%

Table 5: Plastic hinges for URM spandrels

URM spandrel				
Point	Flexural hinge		Shear hinge	
	Resistance	Drift	Resistance	Drift
A.	0	0	0	0
B.	M_{R1}	$\delta_{B(M)}$	V_{R2}	$\delta_{B(V)}$
C.	M_{R1}	1.0%	V_{R2}	0.5%
D.	$0.3 \cdot M_{R1}$	1.3%	$0.4 \cdot V_{R2}$	0.5%
E.	$0.3 \cdot M_{R1}$	2.0%	$0.4 \cdot V_{R2}$	1.5%

Table 6: Plastic hinges for strengthened piers

Strengthened piers				
Point	Flexural hinge		Shear hinge	
	Resistance	Drift	Resistance	Drift
A.	0	0	0	0
B.	$M_{Rd,(R)}(N_{Ed})$	$\delta_{B(M)}$	$V_{Rd(CRM)}$	$\delta_{B(V)}$
C.	$M_{Rd,(R)}(N_{Ed})$	1.6%	$V_{Rd,(CRM)}$	0.8%
D.	$0.8 \cdot M_{Rd,(R)}(N_{Ed})$(2 sides only)	1.6%	$0.8 \cdot V_{Rd,(CRM)}$	0.8%
E.	$0.8 \cdot M_{Rd,(R)}(N_{Ed})$(2 sides only)	2.5%	$0.8 \cdot V_{Rd,(CRM)}$	1.4% stone (1 side) 1.6% bricks (1 side) 2.5% stone and brick (2 sides)

Table 7: Plastic hinges for strengthened spandrels

Strengthened spandrels				
Point	Flexural hinge		Shear hinge	
	Resistance	Drift	Resistance	Drift
A.	0	0	0	0
B.	$M_{Rd,(R)}(N_{Ed})$	$\delta_{B(M)}$	V_t	$\delta_{B(V)}$
C.	$M_{Rd,(R)}(N_{Ed})$	2.0%	V_t	2.0%
D.	-	-	$0.4 \cdot V_t$	2.0% (2 sides only)
E.	-	-	$0.4 \cdot V_t$	3.0% (2 sides only)

$\delta_{B(V)}$ and $\delta_{B(M)}$ in Tables 4 - 7 are the drifts for the shear and bending, which correspond to the yield point B (Fig. 46), calculated as:

$$\delta_{B(V)} = \frac{V_{Rd}}{\frac{K_p}{2} \cdot h} \quad e \quad \delta_{B(M)} = \frac{M_{Rd}}{\frac{K_p}{2} \cdot h^2}$$

Where K_p is the element stiffness, calculated as:

$$K_p = \frac{1}{\frac{1.2 \cdot h}{G \cdot b \cdot t} + \frac{l^3}{12 \cdot I_{m(G)} \cdot E}}$$

$$G = \frac{1}{3} \cdot E$$

$$I_{m(G)} = t \cdot \frac{l^3}{12}$$

With:

t = section thickness;

h = width of the pier wall or width of the wall;

l = height of the pier or length of the spandrel.

It should be emphasized that for the strengthened elements, it is necessary to take into account the additional contribution of the coating:

$$E_{eq} = \frac{E_m \cdot t + E_c \cdot t_c}{t}$$

$$G_{eq} = \frac{G_m \cdot t + G_c \cdot t_c}{t}$$

$$G_m = \frac{1}{3} \cdot E_m$$

$$G_c = \frac{E_c}{2 \cdot (1 + \nu_c)}$$

Here the subscript "m" indicates the masonry, and the subscript "c" indicates the coating.

2.6 URM pilot building by equivalent frame model

The building was analysed using an equivalent frame model in the Midas GEN software. The dimensions of the building are described in Section 11 of the first part of the report. The loading apparatus was also modelled to account for the distribution of forces between the two longitudinal walls. The loading apparatus was modelled by rigid elements, and the connections between it and the building were modelled so that they did not induce any additional unespected stiffness. The lengths of the piers and the rigid segments shown in Fig. 48 were calculated using Dolce's rule (*Dolce, 1989*).

2.6.1 Plastic hinges

The software automatically calculates the resistance of each hinge based on the analytical expressions presented in Section 2.5.2.

In the calibration process, the calculation of the spandrel hinges was somewhat adjusted. The (small) vertical stress of adjacent piers was neglected in the calculation of the flexural resistance of spandrels.

The stiffness of flexural and shear plastic hinges was calculated as:

$$K_f = \frac{6 \cdot E_m \cdot J}{h}$$

$$K_s = \frac{G_m \cdot A}{h \cdot \chi}$$

Where:

χ = shear factor of the section;

A = area of the cross-section;

J = second moment of area of the wall cross-section in the bending direction;

h = effective height of the pier or length of the spandrel.

The drifts used for the plastic hinges are reported in Table 8. The adopted values are very similar to those from the literature.

Table 8: Drifts used to model plastic hinges in the numerical model of the URM pilot building

URM pier				
Point	Flexural hinge		Shear hinge	
	Resistance	Drift	Resistance	Drift
A.	0	0	0	0
B.	$M_{Rd,b(U)}$	$\delta_{B(M)}$	$V_{Rd,dc(U)}$	$\delta_{B(V)}$
C.	$M_{Rd,b(U)}$	1.0%	$V_{Rd,dc(U)}$	0.5%
D.	$0.3 \cdot M_{Rd,b(U)}$	1.5 %	$0.5 \cdot V_{Rd,dc(U)}$	0.8%
E.	$0.3 \cdot M_{Rd,b(U)}$	2.0 %	$0.5 \cdot V_{Rd,dc(U)}$	0.85%
URM spandrel				
Point	Flexural hinge		Shear hinge	
	Resistance	Drift	Resistance	Drift
A.	0	0	0	0
B.	M_{R1}	$\delta_{B(M)}$	V_{R2}	$\delta_{B(V)}$
C.	M_{R1}	1.5%	$0.7 \cdot V_{R2}$	0.2%
D.	$0.3 \cdot M_{R1}$	1.5%	$0.3 \cdot V_{R2}$	0.5%
E.	$0.3 \cdot M_{R1}$	2.0%	$0.3 \cdot V_{R2}$	0.6%

2.6.2 Material properties of masonry

The mechanical characteristics of the masonry used in the analysis are based on the values presented in Section 3.3 of the first part of the report. The material properties are summarized in Table 9.

Table 9: Masonry mechanical parameters used to calculate the plastic hinge resistances

E_m [Mpa]	1050	Masonry Young's modulus
G_m [Mpa]	350	Masonry shear modulus
f_m [Mpa]	2.4	Masonry compressive reisistance in the vertical direction
f_{hm} [Mpa]	1.2	Masonry reisistance in the horizontal direction
τ_0 [Mpa]	0.08	Masonry shear reisstance in absence of normal tension
ρ [kN/m^3]	21.0	Masonry self weight
ε_{c2} [‰]	2.0	Limit strain at constant compressive resistance (Fig. 47)
ε_{cu} [‰]	10.0	Ultimate strain

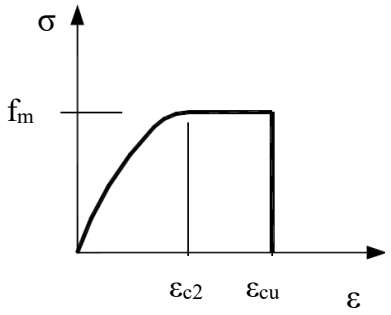

Fig. 47: Simplified constitutive law for masonry

2.6.3 Numerical analysis of the unreinforced pilot building

A pushover analysis was conducted by imposing lateral displacement on the middle node of the horizontal element connecting the two vertical elements of the loading apparatus. Supports to fix the translations and the rotation in the wall plane were applied at the base of the ground story beam elements (piers).

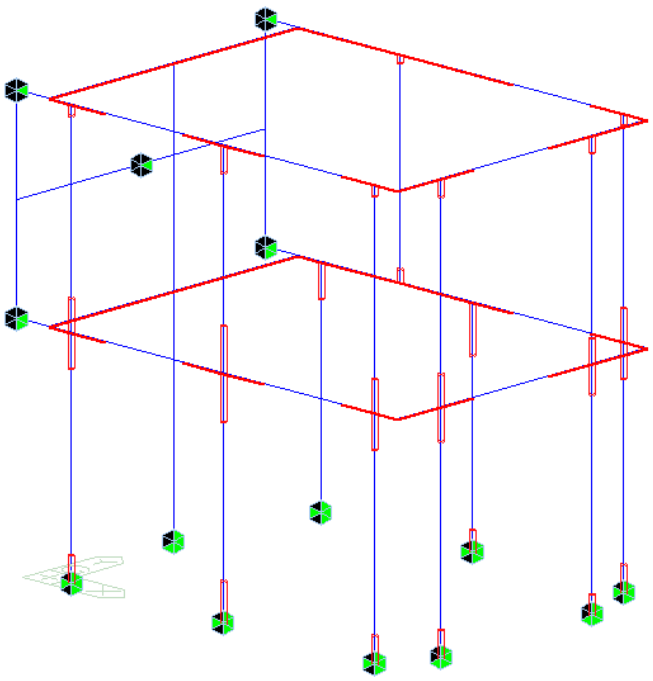

Fig. 48: Equivalent frame model of the pilot building (red segments are rigid)

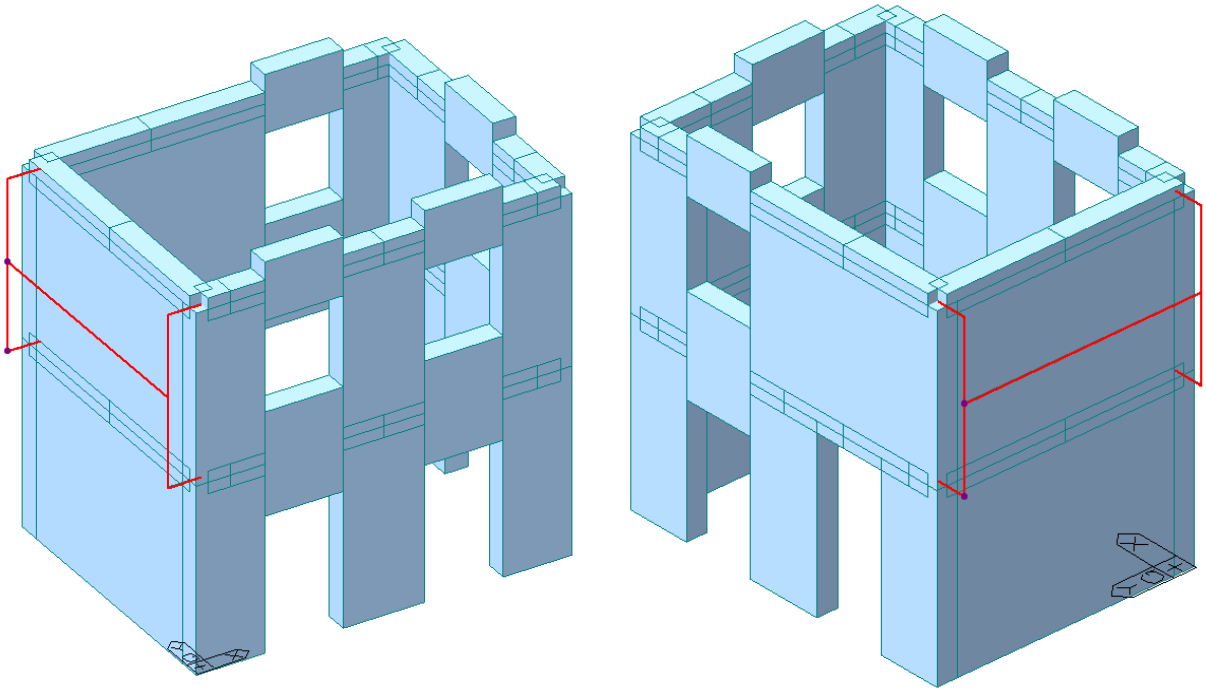

Fig. 49: Equivalent frame model of the pilot building (extruded view)

2.6.3.1 Modal analysis

The results of the modal analysis are presented in Table 10. The predominant X direction mode is shown in Fig. 50. The first mode of vibration is a translational mode in *Y* direction, while the second one is translational in *X* direction. Consequently, *X* direction will be referred to as the second mode of vibration, while *Y* direction will be referred as the first one. The participanting masses associated with the first and second vibration modes are 84.51% and 93.75%, respectively. The structure vibrates predominantly in the second mode. The periods of vibration in the *Y* and *X* directions are equal to 0.175 s and 0.161 s, respectively. It must be noted that the elastic modulus of the masonry was considered halved to account for the cracked state, as suggested by the NTC 2018 standard (in chapter 7.2.6).

Table 10: Results of modal analysis

EIGENVALUE ANALYSIS													
	Mode No	Frequency (rad/sec)		Frequency (cycle/sec)		Period (sec)		Tolerance					
	1	35.8769		5.7100		0.1751		5.6095e-49					
	2	38.9631		6.2012		0.1613		5.3118e-48					
MODAL PARTICIPATION MASSES PRINTOUT													
	Mode No	TRAN-X		TRAN-Y		TRAN-Z		ROTN-X		ROTN-Y		ROTN-Z	
		MASS(%)	SUM(%)	MASS(%)	SUM(%)	MASS(%)	SUM(%)	MASS(%)	SUM(%)	MASS(%)	SUM(%)	MASS(%)	SUM(%)
	1	0.5493	0.5493	84.5131	84.5131	0.0000	0.0000	0.0000	0.0000	0.0000	0.0000	7.9345	7.9345
	2	93.7511	94.3003	0.3517	84.8648	0.0000	0.0000	0.0000	0.0000	0.0000	0.0000	0.2653	8.1998

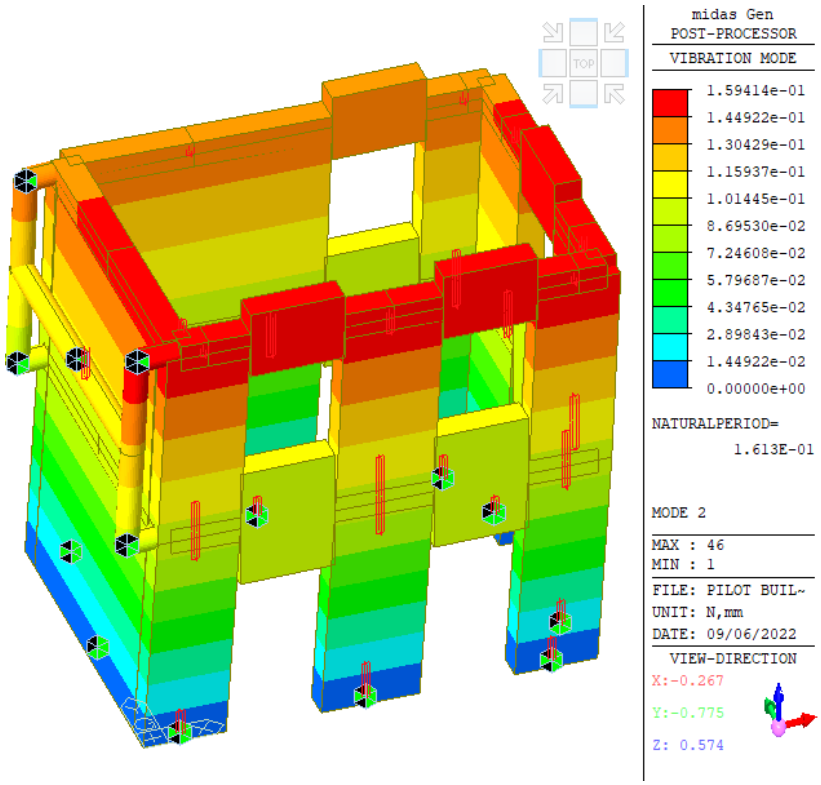

Fig. 50: Second vibration mode (first translational mode in X direction)

2.6.3.2 Pushover analysis

In the pushover analysis, the actual vertical loads acted on the structure, and the distribution of horizontal forces depended on the stiffness of the longitudinal walls. The model included the loading apparatus to simulate horizontal force distribution properly. The pushover analysis was performed up to a 2nd story displacement of 50 mm. The resulting pushover curve is presented in Fig. 51, and key observations of the model behaviour are presented in Table 11. The failure mechanism is shown in Fig. 52.

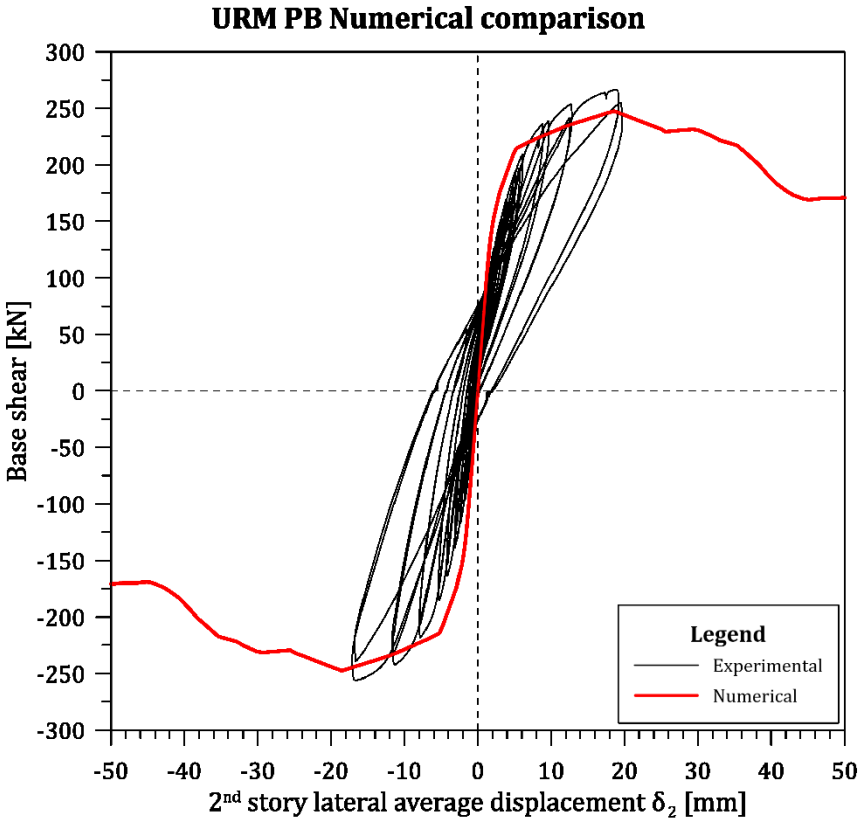

Fig. 51: Pilot building numerical comparison with the equivalent frame model

Table 11: Equivalent frame model behaviour

Top floor displacement [mm]	Observation
2.4	Flexural cracking (point B reached) in all spandrels of East and West walls and piers of the top floor.
5.6	Shear cracking (point B) of the middle pier of the West wall on the 1st story
27.0	Failure (point E) of the middle pier of the West wall on the 1st story
29.0	Cracking (point B) in the middle pier of the East wall on the 2nd story
32.8	Near collapse (point D) in the southern spandrel of the East wall.
35.2	Maximum resistance (point C) at the base of most of the 1st story piers.
40.0	Failure (point E) of the southern spandrel of the East wall.

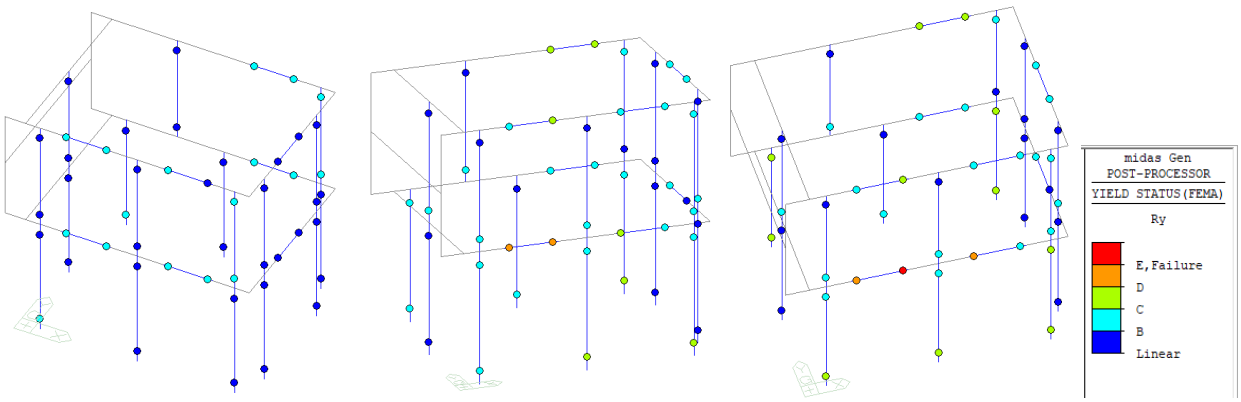

(a) (b) (c)

Fig. 52: Numerical model hinge status of yielding by FEMA, positive loading direction: Top story displacement equal to 2.4 mm (a); 32.8 mm (b); 40.0 mm (c)

Even though the numerical pushover curve reproduces the stiffness and resistance of the building quite well, the numerical model indicates a 1st story collapse mechanism (in the test, there was a 2nd story collapse). The difference can be attributed to the effect of corner piers, which interact with the cross walls. This interaction causes the middle pier on 2nd story to be the weakest of the three and the first to damage. In the test, the middle pier was damaged first too.

2.7 Strengthened pilot building by equivalent frame model

2.7.1 Properties of the masonry and materials for strengthening

The mechanical characteristics of materials for strengthening (GFRP mesh and mortar for coating) were obtained from technical data sheets and the manufacturers. The mortar for coating is FBNHL15MPa, and the GFRP mesh for reinforcing is FB-MESH66x66T96AR. Their mechanical properties are reported in Table 12.

Table 12: Material properties of materials for strengthening

FB-MESH66x66T96AR			FBNHL15MPa		
A_s	15.34	mm^2	f_c	15	MPa
f_{yk}	365	MPa	$f_{t,c}$	1.1	MPa
E_s	25000	MPa	E_c	5000	MPa
ε_{su}	14.5	‰			
Mesh pitch	66	mm			

The additional GFRP mesh installed at the corners was considered when calculating the bending resistance of side longitudinal piers. Ten vertical reinforcement mesh strands were considered in the most distant position from the compressed edge and double reinforcement bars up to 330 mm from the in tension edge were also considered.

The elastic and shear moduli were increased due to the coating, as described in Section 2.5.3.9. The stiffness of the plastic hinges was also increased to account for the effect of the coating. The thickness of the beam

element sections remained 350 mm, but an equivalent weight density was used to consider the added weight of the mortar coating.

2.7.2 Plastic hinges

At first, an elastic analysis was carried out to determine the compressive stress on each pier element. Then the plastic hinge's resistances were calculated as presented in Section 2.5.3.

The stiffness of flexural and shear plastic hinges was calculated as:

$$K_f = \frac{6 \cdot E_{eq} \cdot J}{h^3}$$

$$K_s = \frac{G_{eq} \cdot A}{h \cdot \chi}$$

Where:

χ = shear factor of the section;

A = area of the cross-section;

J = second moment of area of the wall cross-section in the bending direction;

h = effective height of the pier or length of the spandrel.

E_{eq} and G_{eq} take into account the additional contribution of the coating.

The drifts used for the plastic hinges were similar to those from literature and have been calibrated somewhat to reproduce the observed behaviour. The drifts used in the analysis are reported in Table 13.

Table 13: Drifts used to model plastic hinges in the numerical model of the strengthened pilot building

RM pier				
Point	Flexural hinge		Shear hinge	
	Resistance	Drift	Resistance	Drift
A.	0	0	0	0
B.	$M_{Rd,b(URM)}$	$\delta_{B(M)}$	$V_{Rd,dc(URM)}$	$\delta_{B(V)}$
C.	$M_{Rd,b(URM)}$	1.8%	$V_{Rd,dc(URM)}$	0.8%
D.	$0.5 \cdot M_{Rd,b(URM)}$	4.0 %	$0.6 \cdot V_{Rd,dc(URM)}$	1.6%
E.	$0.5 \cdot M_{Rd,b(URM)}$	4.2 %	$0.6 \cdot V_{Rd,dc(URM)}$	1.8%

RM Spandrel		
Point	Flexural hinge	
	Resistance	Drift
A.	0	0
B.	M_{R1}	$\delta_{B(M)}$
C.	M_{R1}	1.5%
D.	$0.3 \cdot M_{R1}$	1.5%
E.	$0.3 \cdot M_{R1}$	2.0%

The calculations show that all piers and spandrels fail in bending. The exception is the large pier in the West wall, which fails in shear.

2.7.3 Numerical analysis of the strengthened pilot building

The analysis was performed with displacement imposed on the middle node of the horizontal beam, connecting the two vertical beam elements of the loading apparatus. Plastic hinges were assigned to the pier and spandrel beam elements.

2.7.3.1 Modal analysis

The results of the modal analysis are presented in Table 14. The first mode of vibration is a translational mode in *Y* direction, while the second one is translational in *X* direction. The predominant mode of vibration in *X* direction is shown in Fig. 53. The participating masses associated with the first and second mode of vibration are 85.36% and 93.47%, respectively. The structure vibrates predominantly in the second mode. The periods of vibration in the *Y* and *X* directions are equal to 0.154 s and 0.142 s, respectively. That is a decrease of 12.3 % in *Y* and 11.7 % in *X* directions, which is caused by the global stiffness increase of the structure due to the coating. It must be noted that the elastic moduli of the materials were halved to account for the cracked cross-section, as suggested by the NTC 2018 standard in chapter 7.2.6.

Table 14: Results of modal analysis

Node	Mode	UX		UY		UZ		RX		RY		RZ	
EIGENVALUE ANALYSIS													
	Mode No	Frequency (rad/sec)		Frequency (cycle/sec)		Period (sec)		Tolerance					
	1	40.9249		6.5134		0.1535		1.5835e-47					
	2	44.2169		7.0373		0.1421		1.3619e-46					
MODAL PARTICIPATION MASSES PRINTOUT													
	Mode No	TRAN-X		TRAN-Y		TRAN-Z		ROTN-X		ROTN-Y		ROTN-Z	
		MASS(%)	SUM(%)	MASS(%)	SUM(%)	MASS(%)	SUM(%)	MASS(%)	SUM(%)	MASS(%)	SUM(%)	MASS(%)	SUM(%)
	1	0.5290	0.5290	85.3638	85.3638	0.0000	0.0000	0.0000	0.0000	0.0000	0.0000	7.0602	7.0602
	2	93.4709	93.9999	0.3614	85.7252	0.0000	0.0000	0.0000	0.0000	0.0000	0.0000	0.2060	7.2662

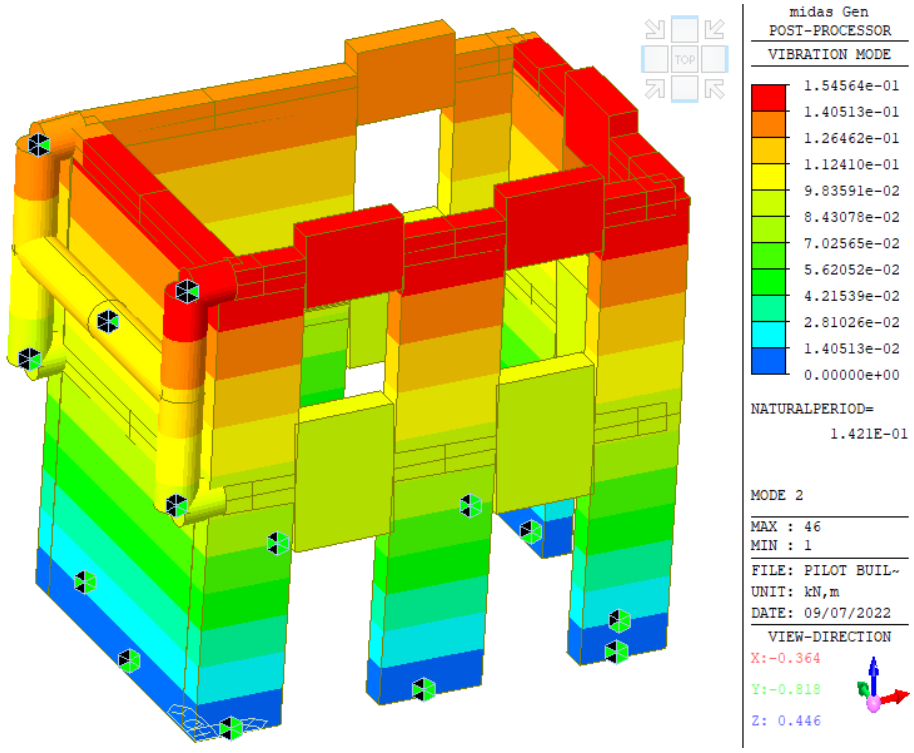

Fig. 53: Second vibration mode (translational in the X direction)

2.7.3.2 Pushover analysis

The pushover analysis considers nonlinear static behaviour. After applying vertical loads, the horizontal displacements are imposed until a 2nd story displacement reaches 100 mm in the *X* direction. The loads were

applied in positive and negative loading directions. Hence, there were two pushover analyses for the strengthened building. The resulting pushover curves are presented in Fig. 54. Key observations of the model behaviour are presented in Table 15. The collapse mechanism evolution is shown in Fig. 55.

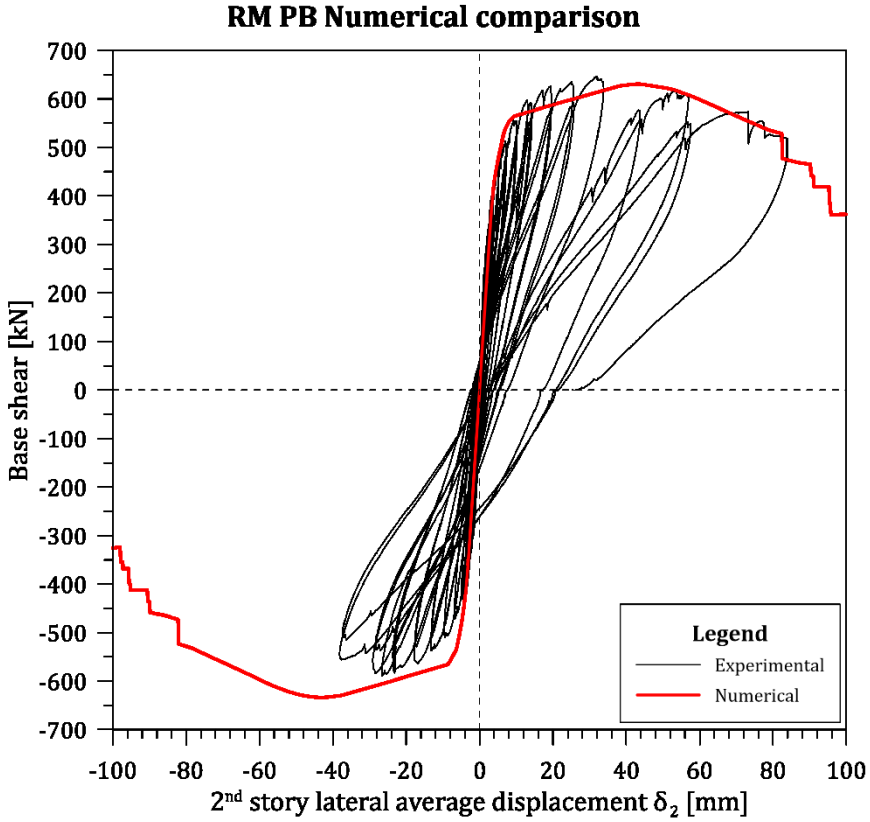

Fig. 54: Pilot building numerical comparison with the equivalent frame model

Table 15: Equivalent frame model behaviour

Top floor displacement [mm]	Observation
4.0	Flexural cracking (point B) in the 1st story piers of the longitudinal walls
5.2	Flexural cracking (point B) of the southernmost 1st story spandrel pier of the East wall
6.4	Flexural cracking (point B) of the 2nd story spandrel West wall
8.0	Flexural cracking (point B) of the 2nd story middle pier of the East wall
8.6	Flexural cracking (point B) of all the 1st story spandrels of the longitudinal walls and in the 2nd story northernmost spandrel of the East wall
13.2	Flexural cracking (point B) in the 2nd story northernmost piers of the longitudinal walls
36.0	Flexural cracking (point B) in the 2nd story southernmost spandrel of the East wall.
41.6	Maximum bending resistance (point C) in the middle piers of the 1st storey of the longitudinal walls
44.0	Maximum bending resistance (point C) in all of the 1st storey piers of the longitudinal walls, except for the corner pier adjacent to the door.
53.2	Maximum bending resistance (point C) in all of the 1st storey piers of the longitudinal walls.
79.0	Near collapse (point D) in the middle 1st story pier of the East wall
82.4	Failure (point E) of the middle pier on the 1st storey of the East wall
86.0	Near collapse (point D) of the middle pier on the 1st story of the West wall
90.2	Failure (point E) of the middle pier on 1st storey of the West wall
95.6	Failure (point E) of all the 1st story piers of the longitudinal walls

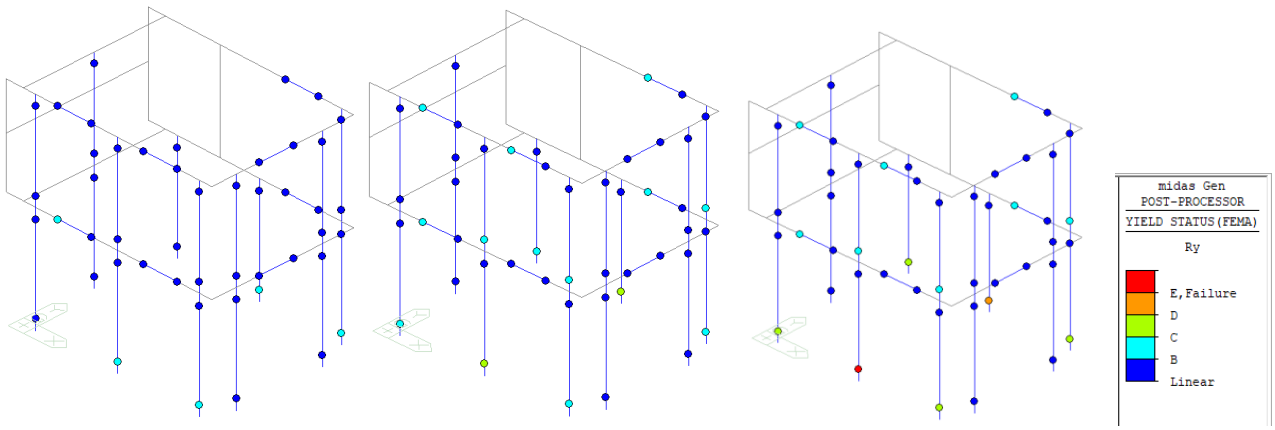

(a) (b) (c)

Fig. 55: Numerical model hinge status of yielding by FEMA, positive loading direction: Top story displacement equal to 5.2 mm (a); 41.6 mm (b); 86.0 mm (c)

The numerical pushover curve reproduces the stiffness and resistance of the building quite well. The match is better in the positive direction of loading. The resistance in the simulations was highly influenced by the additional reinforcement added in the corner piers of the longitudinal walls. The behaviour observed in the numerical model evidence a 1st story collapse mechanism characterized by the formation of flexural hinges at

the base and the top of the piers; the same mechanism was observed in the experimental test (Section 11.8 of the first part of the report).

2.8 Case study: cost analysis of one and two-side strengthening

This numerical analysis demonstrates the cost reduction if the coating is applied only on one side of the walls. The effect of strengthening on the seismic resistance and the intervention cost is analysed on an actual building for two types of intervention solutions called R1 and R2. In R1, the coating is applied only on the external side of perimetric walls, and in R2, the coating is applied on both sides of load-bearing structural walls.

2.8.1 The Grande albergo Terme di Comano building

The building "Grande hotel Terme di Comano" from the municipality of Stenico (TN), Italy, is shown in Fig. 56.

Fig. 56: Grande Albergo Terme di Comano

The bottom three floors of the building are made with stone masonry, and the top two floors are constructed with brick masonry. In total, the structure has five floors above the ground. The building dates back to the early 1900s; the top two floors are from the end of the 1920s. In the 1950s, the ground floor was extended, adding the porch to the west and south. Wooden balconies have also been added to the south wall.

The construction is isolated from other buindings andhas a mainly square plan with a small internal shaft. The floor structures of the first three floors are made of timber, while those on the top two floors are made of brick and concrete.

In the 1960s, an additional floor was added.

In the 1990s, the construction was abandoned.

The floor plan of the structure and the location of the coating is shown in, e.g. Fig. 57.

2.8.2 Intervention R1 (strengthening only on one side)

The R1 is based on one-sided strengthening as proposed in this project, i.e. a 3 cm thick mortar coating reinforced by GFRP mesh and anchored to the masonry using GFRP “L connectors” and artificial diatons. Only external load-bearing walls are considered for strengthening. The wooden floors are stiffened and tied to walls by steel tie rods.

The location of the coating is shown with red lines in the structure's floor plan in Fig. 57.

The procedure of strengthening is described in Section 4.6 of the first part of the report.

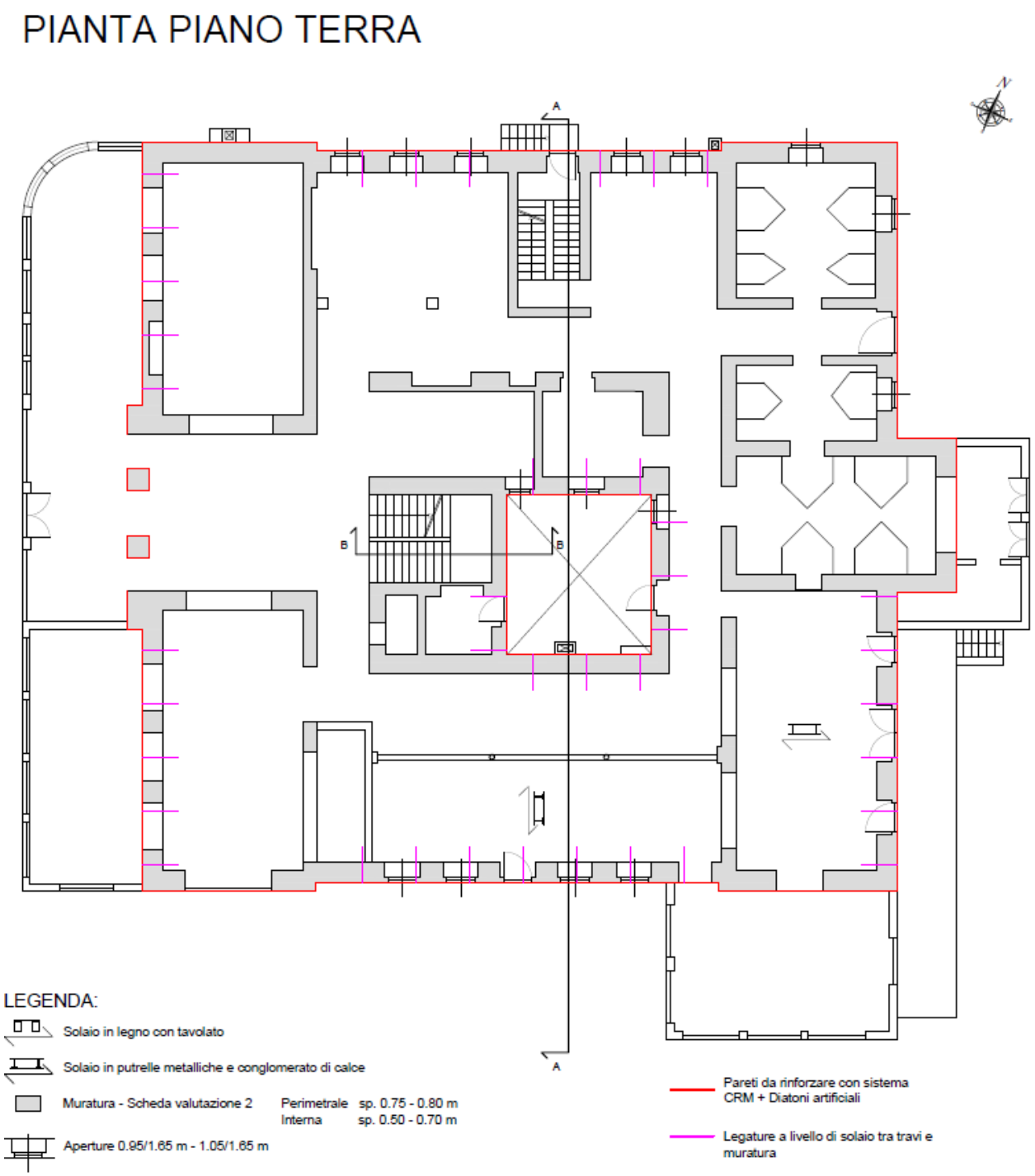

Fig. 57: Floor plan - intervention R1 (red lines depict coating)

2.8.3 Intervention R2 (strengthening on two sides)

The R2 is an intervention using mortar coating on both sides of the load-bearing walls and only “L connectors”. The wooden floors are stiffened and tied to walls by steel tie rods.

The location of the coating is shown with red lines in the structure's floor plan in Fig. 58.

The procedure of strengthening is described in Section 4.7 of the first part of the report.

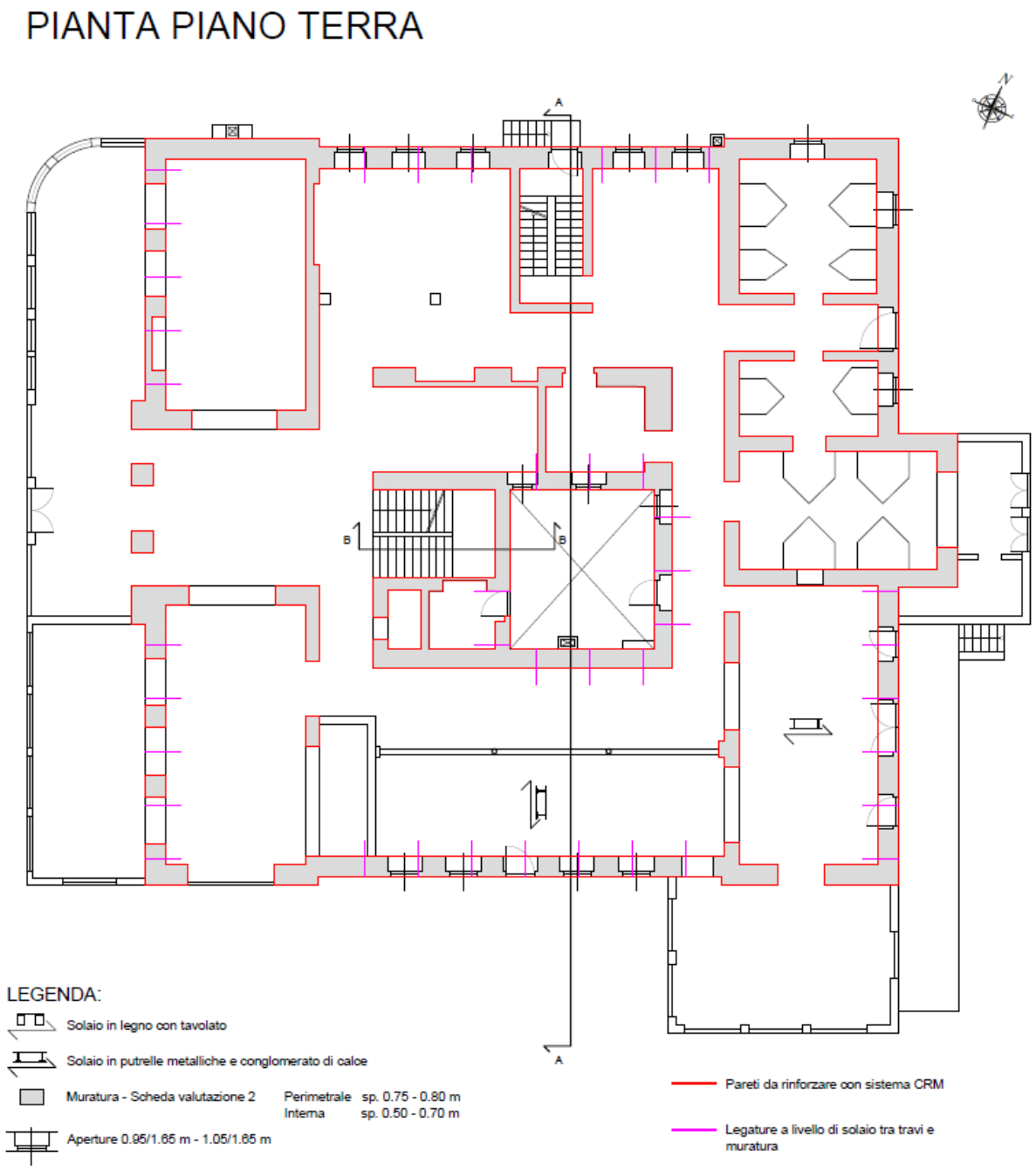

Fig. 58: Floor plan - intervention R2 (red lines depict coating)

2.8.4 Strengthening floor structures

Floors need to be strengthened for both R1 and R2 interventions. The purpose of strengthening is to connect joists with masonry and to tie walls on both sides of the joists.

The steps of the procedure are:

1. Removal of the plaster or false ceiling to expose the wooden beams.
2. Create holes in the masonry at the height of the floor beams.
3. Connect steel tie rods to the beams and anchor them to the masonry by steel plates or poles. The tie rods are arranged following the warping of the floors every third beam (about every 2.5m).
4. Restore the plaster or false ceiling.

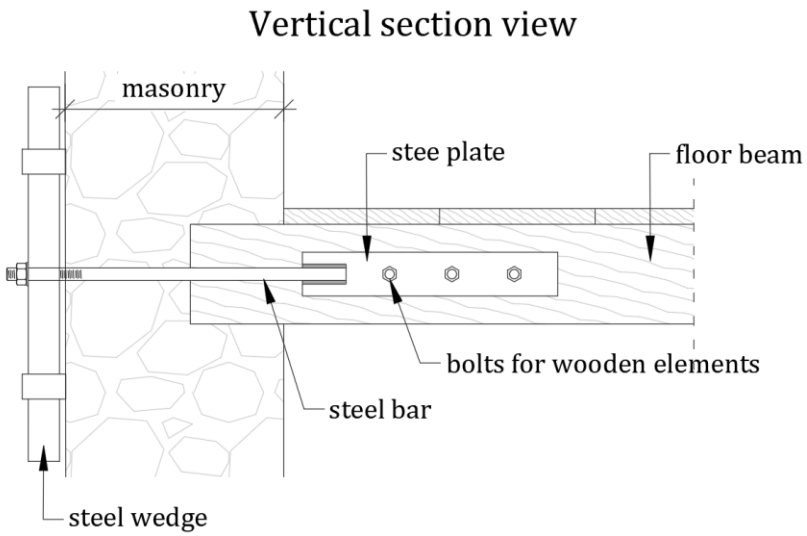

Fig. 59: Example of a steel post connector between the floor beams and the masonry

Additional steel ties should be installed to tie the walls together (perpendicular to the direction of wooden joists). The procedure of installation is:

1. Making holes in the masonry.
2. Insert steel ties (Fig. 59), two at each floor level, connected to the beams adjacent to the perpendicular wall.
3. Fill the holes with cement mortar.
4. Positioning of end steel plates and tightening.

2.8.5 Material properties of masonry

The mechanical characteristics of the masonry were taken as the average values from the intervals proposed in table C8.5.I of the Circular of the NTC 2018, except for the value of the stone masonry, which was assumed to be slightly higher than the average value, justified by the compression tests performed. The types of masonry considered are:

- Irregular soft stone masonry;

- Solid brick and lime mortar masonry.

The material properties are summarized in Table 16:

Table 16: Material properties of masonry

Properties of materials	f_m	τ_0	f_{hd}	f_{v0}	E	G	E_{cr}	G_{cr}
	[MPa]	[MPa]	[MPa]	[MPa]	[MPa]	[MPa]	[MPa]	[MPa]
Irregular soft stone masonry	1.8	0.040	0.9	-	1080	360	540	180
Solid brick and lime mortar masonry	3.45	0.09	1,725	0.2	1500	500	750	250

Where

E_{cr} = Young's modulus of the cracked section;

G_{cr} = Shear modulus of the cracked section.

2.8.6 Properties of materials for strengthening

The mechanical characteristics of materials for strengthening (GFRP mesh and mortar for coating) were obtained from technical data sheets and the manufacturer's tests. The mortar for coating is FBNHL15MPa, and the GFRP mesh for reinforcing it is FB-MESH66x66T96AR. The characteristics are reported in Table 17.

Table 17: Material properties of materials for strengthening

FB-MESH66x66T96AR			FBNHL15MPa		
$A_{s,WARP}$	8.9	mm^2	f_c	15	MPa
$A_{s,WEFT}$	11.6	mm^2	$f_{t,c}$	1.1	MPa
f_{yk}	365	MPa			
E_s	25000	MPa			
ε_{su}	14.5	‰			
Mesh pitch	66	mm			

2.8.7 Numerical analysis of the URM building

A non-linear static analysis (pushover) was carried out to evaluate the seismic response of the Comano building. The building was analyzed using an equivalent frame model created with the Midas GEN software. The analysis is performed according to the NTC 2018.

The view of the structural model, the equivalent frame model and the supports are shown in Figs. 60-62.

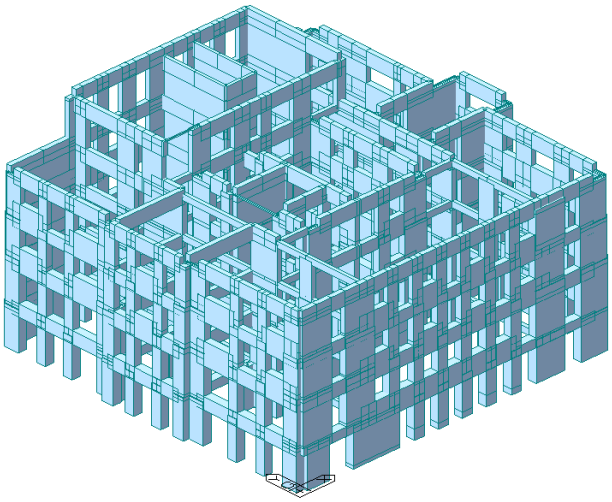

Fig. 60: Geometry of the "Comano" building

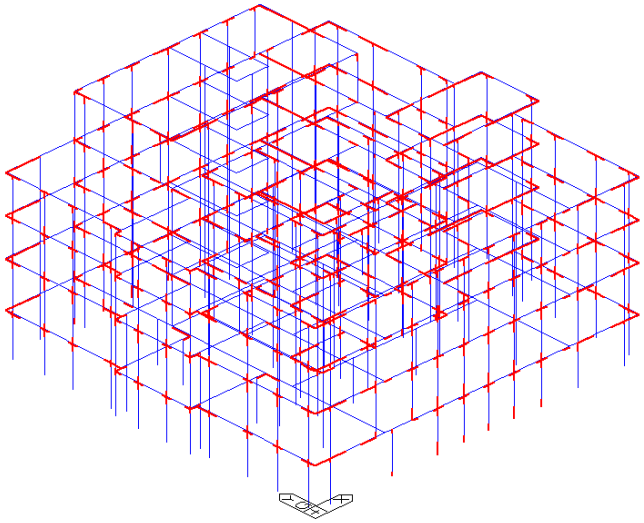

Fig. 61: Equivalent frame model of the structure

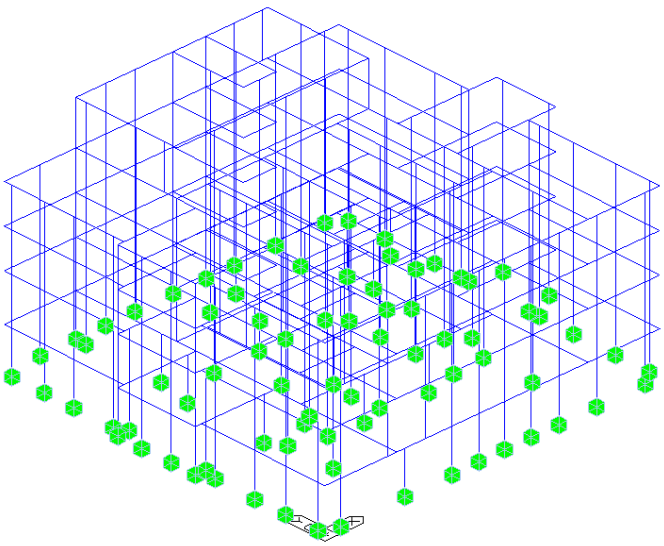

Fig. 62: Constraints (supports)

The structure has three types of floors (wooden, concrete and wooden roof) whose self-weight is calculated automatically by the software. Dead and live loads used in the calculation are shown in Table 18.

Table 18: Dead and live floor load

Loads considered for the different floors	G_2 [kN / m2]	Q_k [kN / m2]
Wooden floor	1.8	2
Brick-concrete floor	3	2
Roof covering	1.7	0.5

The seismic combination of actions for gravitational loads, according to §2.5.3 NTC 2018, is:

$$G_1 + G_2 + \sum_{i=1}^{n} (\psi_{2i} \cdot Q_{ki})$$

The floors were considered infinitely rigid.

2.8.7.1 Modal analysis

The results of the modal analysis are presented in Table 19. The first two modes of vibration are shown in Figs. 63 and 64. The first mode of vibration is a translational mode in *Y* direction, while the second one is translational in *X* direction. Consequently, *X* direction will be referred to as the second mode of vibration, while *Y* direction will be referred as the first one. The participanting masses associated with the first and second mode of vibration are 67.67% and 72.61%, respectively. The structure vibrates predominantly in the first (translational) mode, which is normal for masonry structures of low to medium height.

Table 19: Results of modal analysis

Mode	UX		UY		UZ		RX		RY		RZ	
EIGENVALUE ANALYSIS												
Mode No	Frequency (rad/sec)		Frequency (cycle/sec)		Period (sec)		Tolerance					
1	14.7969		2.3550		0.4246		2.3635e-27					
2	16.6752		2.6539		0.3768		2.3635e-27					
MODAL PARTICIPATION MASSES PRINTOUT												
Mode No	TRAN-X		TRAN-Y		TRAN-Z		ROTN-X		ROTN-Y		ROTN-Z	
	MASS(%)	SUM(%)	MASS(%)	SUM(%)	MASS(%)	SUM(%)	MASS(%)	SUM(%)	MASS(%)	SUM(%)	MASS(%)	SUM(%)
1	0.9667	0.9667	67.6668	67.6668	0.0013	0.0013	0.3335	0.3335	0.0005	0.0005	6.9406	6.9406
2	72.6116	73.5783	1.3109	68.9777	0.0008	0.0021	0.0035	0.3370	0.4266	0.4271	0.0777	7.0184

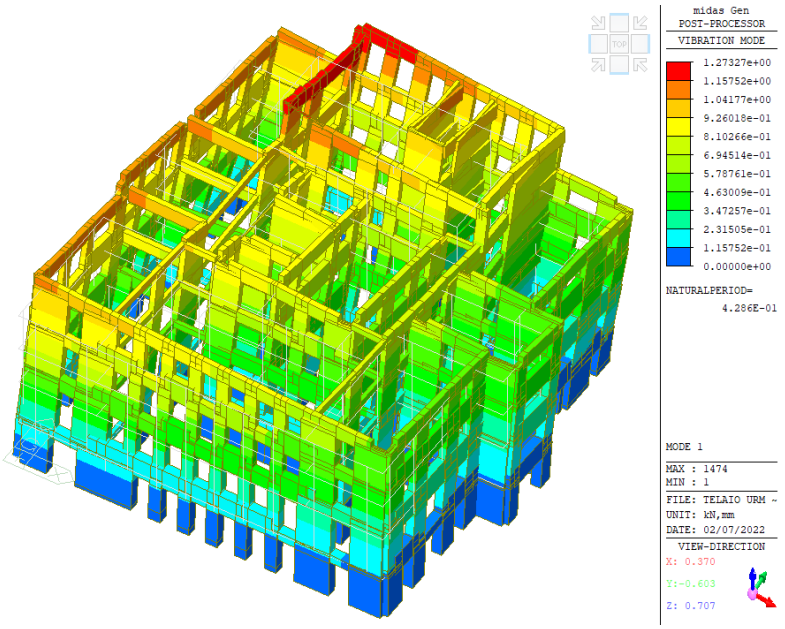

Fig. 63: First vibration mode (translational in dir. Y)

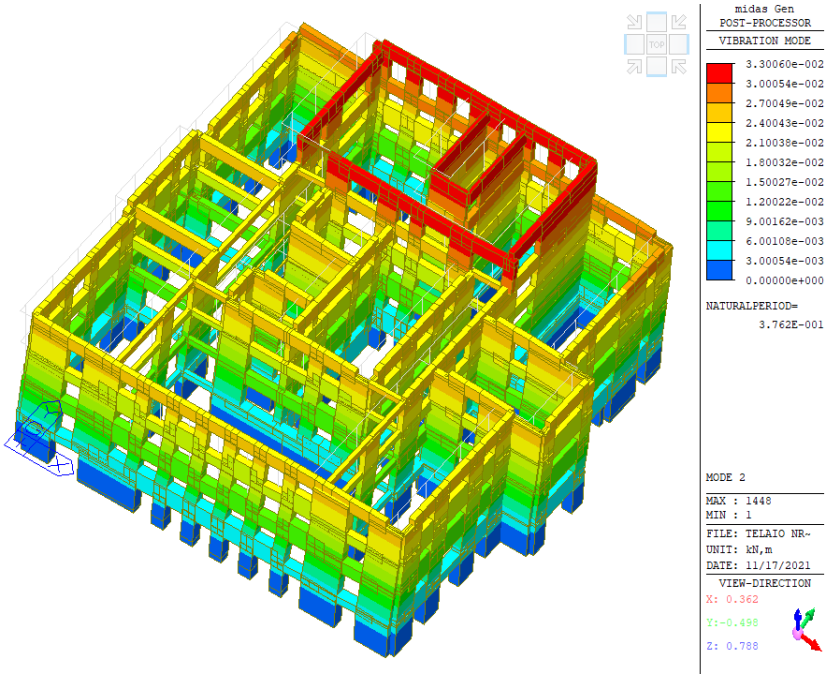

Fig. 64: Second vibration mode (translational in dir. X)

2.8.7.2 Pushover analysis

In the pushover analysis, the seismic combination of vertical loads was acting on the structure, and the distribution of horizontal forces was according to the dominant vibration mode. The pushover analysis was performed to a roof displacement of 50 mm. The loads were applied in both directions (X and Y) and positive and negative directions. Hence, there were four pushover analyses for the URM building.

The failure mechanism for both directions is shown in Figs 65 and 66. In the *Y* direction, the collapse is due to shear failure in spandrels of perimeter walls parallel to seismic loading on the second and third floors. Orange and red circles in Fig. 65 denote the locations of the failure.

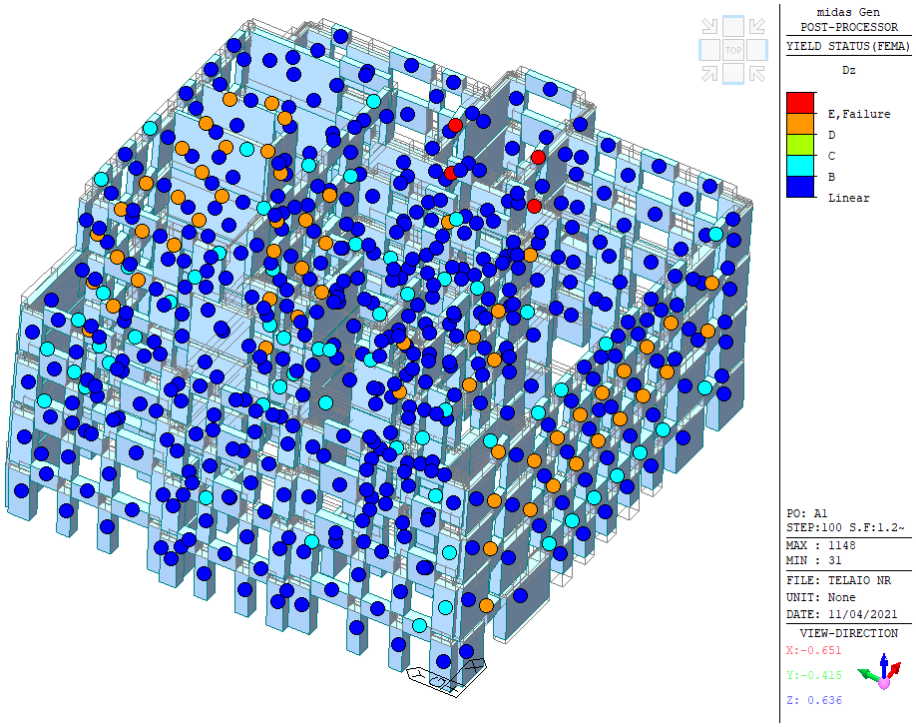

Fig. 65: Failure mechanism (URM building, Y direction). Circles denote the state of elements.

In the *X* direction, the failure mechanism again shows the high vulnerability of spandrels. The most critical damage is concentrated in spandrels of walls parallel to the direction of the loading. The second and third floors are critical, as shown in Fig. 66.

The pushover response curves are shown in Figs 69 and 70.

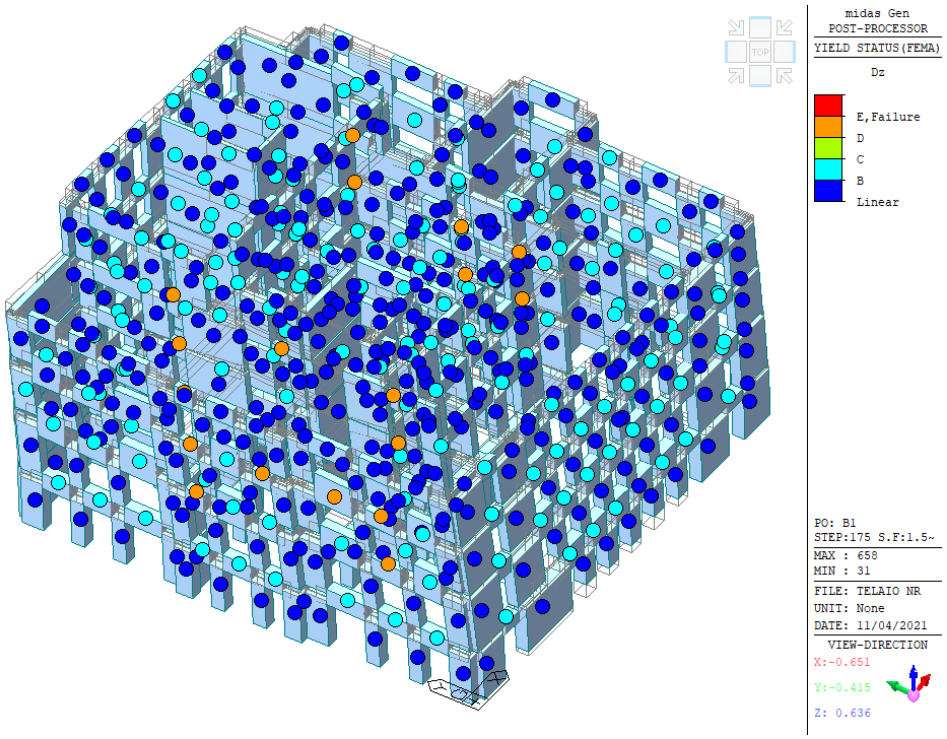

Fig. 66: Failure mechanism (URM building, X direction). Circles denote the state of elements.

2.8.8 Numerical analysis of the strengthened structure

The plastic hinge properties of all hinges had to be recalculated to analyse the strengthened structure. The recalculation was performed separately for cases of R1 and R2 interventions. The failure mechanisms of the strengthened structures are shown in Figs 67 and 68.

The presence of reinforced coatings significantly affects the failure mechanism, which is different for URM, R1 and R2 structures. Nevertheless, most damages were to the spandrels.

The pushover response curves are shown in Figs 69 and 70.

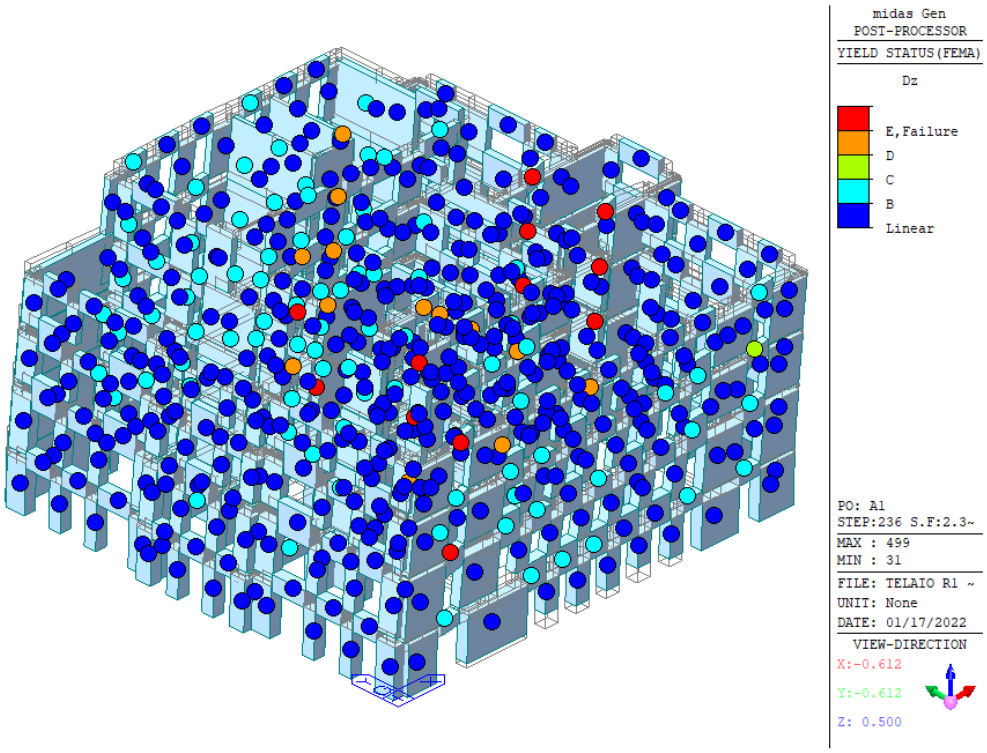

Fig. 67: Failure mechanism (R1 strengthened building, X direction). Circles denote the state of elements.

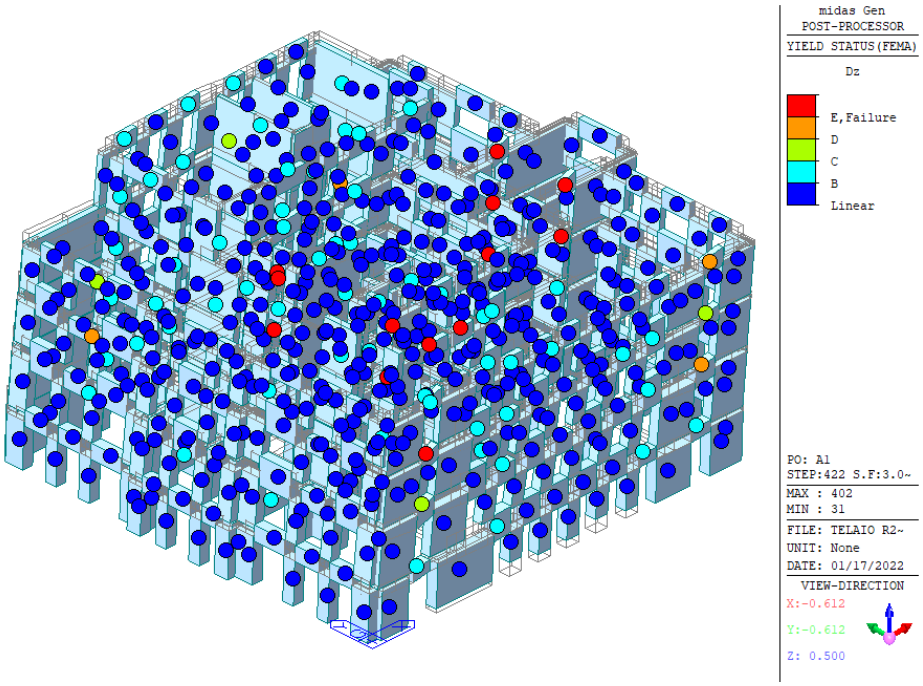

Fig. 68: Failure mechanism (R2 strengthened building, X direction). Circles denote the state of elements.

2.8.9 Comparison of pushover capacity curves

The pushover capacity curves are presented in Figs 69 and 70. As the figures show, the seismic behaviour is significantly improved by strengthening as both resistance and displacement capacity are increased.

In direction *X*, the resistance is increased compared to the URM state by 79 % and 128.9 % for R1 and R2, respectively. Additionally, the displacement capacity is increased by 53.6 % and 85.8 % for R1 and R2, respectively.

In direction *Y*, the resistance is increased compared to the URM state by 59.3 % and 124.2.9 % for R1 and R2, respectively. Additionally, the displacement capacity is increased by 116.6 % and 144.7 % for R1 and R2, respectively.

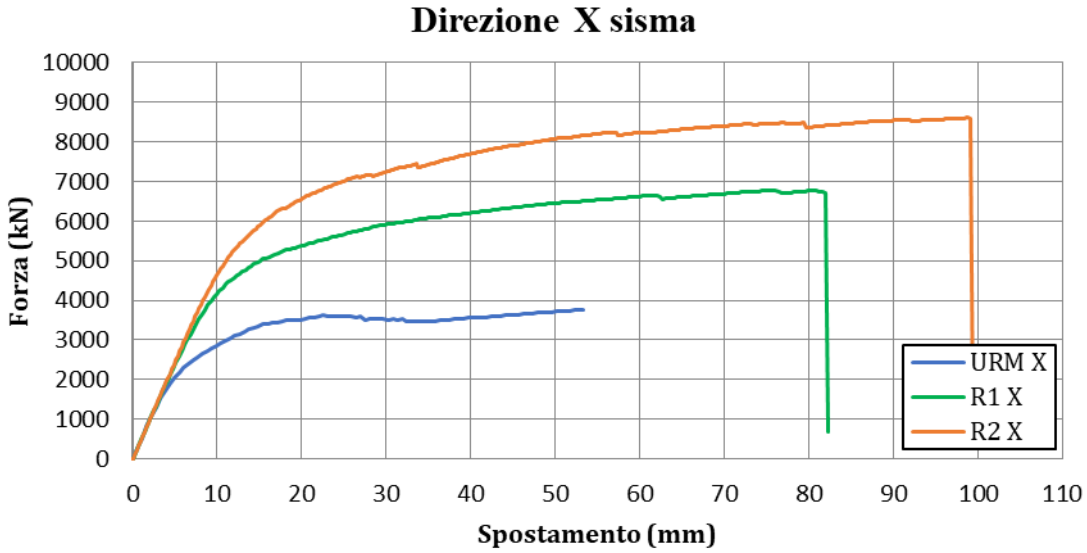

Fig. 69: Pushover capacity curves for URM, R1 and R2 structures. Direction X.

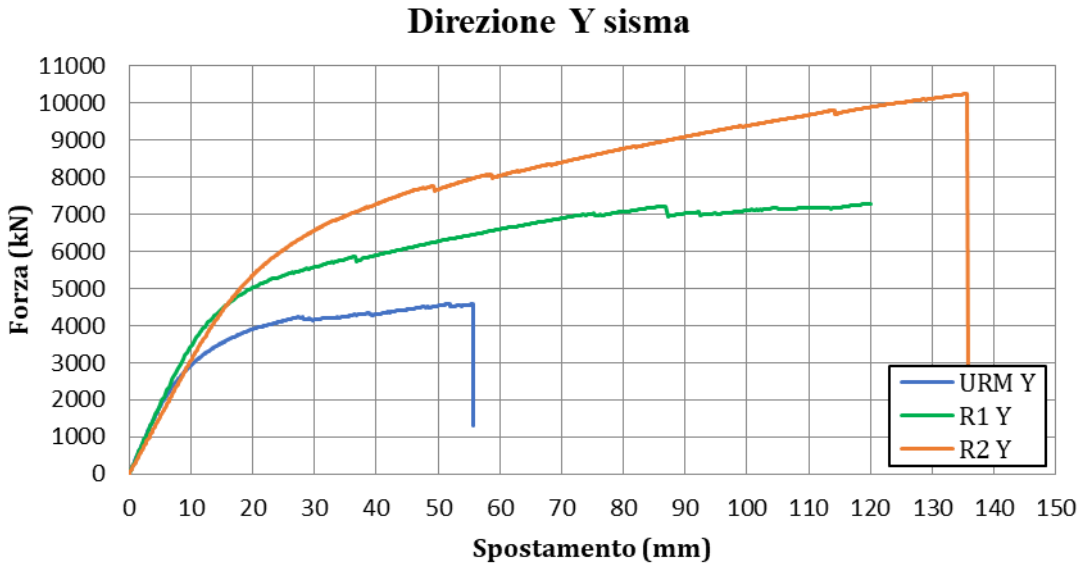

Fig. 70: Pushover capacity curves for URM, R1 and R2 structures. Direction X.

2.8.10 Design seismic capacity

The pushover capacity curves shown in the previous section can be used to calculate seismic demand using the «Capacity spectrum method» (Circular NTC 2018, §C7.3.4.2, method B). This gives seismic demand in

the form of the highest peak ground acceleration (a_g) for a specific location. Comparing the demand to the capacity indicates if a structure fulfils the resistance requirements at a particular location.

Three locations were considered in the calculations. The Stenico (TN) with a low seismic demand ($a_g = 0.094\ g$), Udine (UD) with medium seismic demand ($a_g = 0.274\ g$), and L'Aquila (AQ) with high seismic demand ($a_g = 0.334\ g$). The parameters of seismic demand for all considered locations are shown in Table 20.

For each location, all three configurations were considered (URM, R1 and R2) and both directions (X and Y). Life safety (SLV) and collapse (SLC) limit states are considered for all simulations.

Table 20: Seismic demand parameters

Seismic parameters	Stenico(soil type C)		L'Aquila(soil type C)		Udine(soil type B)	
	SLV	SLC	SLV	SLC	SLV	SLC
SS (-)	1.500	1.500	1.330	1.219	1.198	1.128
ST (-)	1.000	1.000	1.000	1.000	1.000	1.000
F0 (-)	2.631	2.665	2.364	2.400	2.447	2.486
ag (g)	0.074	0.094	0.261	0.334	0.206	0.274
Tc * (s)	0.304	0.320	0.347	0.364	0.332	0.346
Cc (-)	1.555	1.530	1.490	1.466	1.372	1.360
TB (s)	0.158	0.163	0.172	0.178	0.152	0.157
TC (s)	0.473	0.490	0.517	0.534	0.456	0.471
TD (s)	1.896	1.976	2.644	2.936	2.424	2.696

The results of the calculations are shown in Tables 21 and 22. The results show that the URM structure has sufficient seismic capacity only in the region with the lowest seismic demand (Stenico). If strengthened with R1 intervention, the capacity is adequate for an area with medium seismic demand (Udine) but not for high seismic demand (L'Aquila). If strengthened using R2 intervention, the capacity is larger than for R1 but still insufficient for high seismic demand (L'Aquila).

The improvement in capacity is illustrated in Table 23. It clearly shows that R2 intervention is superior to R1.

Table 21: Seismic demand and capacity for the life safety limit state (SLV)

Loc.	Case	Seismic demand ag [g]	Seismic capacity ag [g]	Safety index	Check
Stenico	URM X	0.074	0.104	1.40	✓
	URM Y	0.074	0.107	1.45	✓
	R1 X	0.074	0.166	2.25	✓
	R1 Y	0.074	0.202	2.73	✓
	R2 X	0.074	0.208	2.81	✓
	R2 Y	0.074	0.235	3.18	✓
Udine	URM X	0.206	0.145	0.70	✗
	URM Y	0.206	0.150	0.73	✗
	R1 X	0.206	0.233	1.13	✓
	R1 Y	0.206	0.282	1.37	✓
	R2 X	0.206	0.290	1.41	✓
	R2 Y	0.206	0.329	1.59	✓
L'Aquila	URM X	0.261	0.119	0.46	✗
	URM Y	0.261	0.123	0.47	✗
	R1 X	0.261	0.191	0.73	✗
	R1 Y	0.261	0.231	0.89	✗
	R2 X	0.261	0.239	0.91	✗
	R2 Y	0.261	0.270	1.03	✓

Table 22: Seismic demand and capacity for the collapse limit state (SLC)

Loc.	Case	Seismic demand ag [g]	Seismic capacity ag [g]	Safety index	Check
Stenico	URM X	0.094	0.116	1.23	✓
	URM Y	0.094	0.123	1.31	✓
	R1 X	0.094	0.191	2.03	✓
	R1 Y	0.094	0.232	2.47	✓
	R2 X	0.094	0.236	2.51	✓
	R2 Y	0.094	0.273	2.91	✓
Udine	URM X	0.274	0.172	0.63	✗
	URM Y	0.274	0.183	0.67	✗
	R1 X	0.274	0.283	1.03	✓
	R1 Y	0.274	0.344	1.25	✓
	R2 X	0.274	0.352	1.28	✓
	R2 Y	0.274	0.403	1.47	✓
L'Aquila	URM X	0.334	0.145	0.43	✗
	URM Y	0.334	0.155	0.46	✗
	R1 X	0.334	0.240	0.72	✗
	R1 Y	0.334	0.291	0.87	✗
	R2 X	0.334	0.296	0.89	✗
	R2 Y	0.334	0.342	1.03	✓

Table 23: Improvement of seismic capacity

		% improvement
SLV	URM - R1 X	60.4
	URM - R1 Y	87.8
	URM - R2 X	100.2
	URM - R2 Y	119.0
SLC	URM - R1 X	65.3
	URM - R1 Y	88.3
	URM - R2 X	104.5
	URM - R2 Y	121.5

2.8.11 Cost analysis

A detailed analysis of costs of materials and workmanship was performed for R1 and R2 interventions. However, it should be noted that the calculation *does not* include indirect costs such as lodging for occupants at an alternative location during construction works or stopping a business. Taking indirect costs into account would substantially increase the difference of costs of intervention R2 with respect to intervention R1.

The summary of the costs is shown in Table 24. The costs of interventions R1 and R2 are 804,090.00 € and 1,307,730.00 €, respectively.

Table 24: Detailed cost analysis

	Intervention R1	Intervention R2
Description	Amount	Amount
Structural reinforcement interventions		
Structural reinforcement works	€ 598.485	€ 851.445
Foundation works	€ 21,690	€ 72.315
Reinforcement of floors	€ 34.545	€ 34.545
Cantonal nailing	€ 33,470	€ 36.965
Demolition and restoration work	€ 81,100	€ 268.960
Subtotal	€ 769.290	€ 1,264.230
SAFETY CHARGES		
Security charges	€ 34,800	€ 43,500
TOTAL	804,090.00 €	1,307,730.00 €

Considering the case of Udine, the average improvement of seismic capacity by R1 intervention is 75.5 %. At the estimated total cost of 804.090,00 EUR, the cost for a one per cent improvement of seismic capacity is 10.660,00 EUR.

In the case of R2 intervention, on the other hand, the average improvement of seismic capacity by R2 intervention is 111.3 %. At the estimated total cost of 1.307.730,00 EUR, the cost for a one per cent improvement of seismic capacity is 11.752,00 EUR.

The R1 strengthening is about 10 % cheaper per one per cent improvement of seismic capacity.

In addition to the cost difference presented above, the time needed to complete the intervention also differs. The estimated construction times are shown in Table 25. In addition to shorter construction times, a business typically does not have to be stopped in case of R1 intervention, whereas for R2, it must be.

Table 25: Comparison of construction times

	Time		
Intervention	1 standard team	2 standard teams	3 standard teams
R1	14 months	7.5 months	5 months
R2	23 months	12 months	8 months

2.8.12 Conclusions

The case study has shown that one-sided strengthening is cheaper in relative terms (per increase of seismic capacity) by about 10 %. It is also sufficient for regions with moderate seismic demand. Additionally, the intervention does not require temporary alternative accommodation for residents or stopping business.

The two-sided strengthening achieves higher seismic capacity than the one-sided strengthening and may be required in case of high seismic demand.

3 Summary and conclusions

This report presents the results of the CONSTRAIN project, which deals with developing and testing a new, more convenient and cost-effective system for seismic strengthening existing masonry structures. The newly developed method of strengthening is based on mortar coating, reinforced by a GFRP mesh and anchored into the masonry by two types of anchors. Crucially, the coating is applied on one side only.

Because the coating is applied only on the outside of the building, residents can stay in the building during strengthening works. Or, in the case of commercial buildings, the operation of a business does not have to be interrupted. These reasons make it much more likely for property owners to strengthen existing buildings. The alternative to strengthening is either to continue living in buildings seismically vulnerable or to demolish the building and replace it with a new one. In the former case, the situation presents a clear danger to the residents and their economic well-being. In the latter case, the cost of replacing the building is considerable in terms of money, resource use, and, by extension, emissions.

As mentioned in the introduction, designing a seismic intervention with coating on one side of the walls only is challenging. For the developed system to be successful, the existing masonry and coating should work together as a composite material. Achieving the composite action of both materials is not simple, as the materials are quite different in terms of stiffness and non-linear behavior. Proper composite action of both materials is achieved only if the coating and the masonry walls are balanced and adequately anchored together. Furthermore, it is virtually impossible to know if an intervention is efficient without extensive experimental testing. In the present project, a new seismic strengthening intervention was designed combining and merging the knowledge of all partners and subsequently extensively tested to verify its efficiency.

Numerical simulations of the response of the unreinforced and strengthened structure by equivalent frame method and using standard models found in guidelines (e.g., CNR 2018) have shown that the new strengthening intervention can be successfully modelled using existing models and design software. As detailed in Sections 2.5.2 and 2.7, the successful modelling shows that the design procedures already exist, and that the new intervention can be implemented immediately.

To test how much one and two-sided strengthening increases seismic resistance and what is the difference in costs, a case study on a full-scale five-storey building was performed in Section 2.8. Strengthening by applying coating on both sides (as opposed to one side only) of the walls is stronger and can provide higher seismic capacity. The one-sided coating may not be enough in regions with high seismic demand, such as e.g., L'Aquila, with a peak ground acceleration of 0.334 g. However, the newly developed intervention could be successfully used for regions with moderate and low seismic risk.

A detailed cost analysis, which included only costs of workmanship and materials but not indirect costs of moving residents to a temporary location, has shown that one-sided strengthening is about 10 % cheaper per unit of seismic capacity increase. The time of construction work is also much less (about 40 %). If the costs of temporary moving out of residents were considered, a one-sided coating would be even more appealing.

Extensive experimental testing and thorough numerical simulations have shown that the newly developed intervention method for seismic strengthening is efficient, successful and financially appealing. It offers an alternative to expensive and inconvenient traditional methods, which could make many owners decide to strengthen their property. The efficient new intervention uses fewer resources and increases the safety of people living in strengthened buildings.

Acknowledgements

We thank the Interreg Italy-Slovenia Cooperation Programme 2014-2020 that funded the project CONSTRAIN.

We thank all the project partners that actively contributed to the experimental campaign. In particular we thank Kolektor CPG d.o.o. and Veneizna Restauri Costruzioni S.r.l. for building the samples that were tested; Fibrenet S.p.A. for the supply of materials for sample reinforcement, management of press communication in Italy, organization of seminars and their contribution to the research, testing and report production; Igmat d.d. for managing the press communication in Slovenia, organize the seminars and administrate the contract with the University of Brescia for the Pilot Building tests.

We thank Eng. Sara Verza and Dr. Matteo Barnaba for working for a period on the project at the University of Trieste and Dr. Franco Trevisan for helping in the preparation of the tests that were carried out at the University of Trieste. We thank Eng. Carlos R. Passerino and Eng. Salvatore Grassia for the help in the execution of the tests that were carried out at Fibre Net and at the University of Brescia. We thank Rok Harej, Marko Kovačič and Barbara Smole from Kolektor CPG d.o.o. for help with the organization of masons. We thank Aleš Kastelic from IGMAT d.d. for help with recording videos of the tests.

We also thank the staff of the laboratory of Civil Engineering of the University of Brescia, and particularly Professor Fausto Minelli, Dr. Luca Facconi and Dr. Sara Lucchini for providing support organizing and carrying out the pilot building tests.

References

M. Dolce, «Schematizzazione e modellazione per azioni nel piano delle pareti, Corso sul consolidamento degli edifici in muratura in zona sismica, Ordine degli Ingegneri, Potenza». 1989.

Federal Emergency Management Agency, *ATC FEMA 306: Evaluation of earthquake damaged concrete and masonry wall buildings – Basic Procedures Manual*, n. ATC FEMA 306. 1999.

midas Gen. MIDASoft, Inc., 2021.

V. Turnsek e F. Čačovič, «Some experimental results on the strength of brick masonry walls», *Proceedings of the 2nd international brick masonry conference, Stoke-on-trent*, pagg. 149–56, 1970.

I. Boem e N. Gattesco, «Rehabilitation of Masonry Buildings with Fibre Reinforced Mortar: Practical Design Considerations Concerning Seismic Resistance», *Key Eng. Mater.*, vol. 898, pagg. 1–7, ago. 2021, doi: 10.4028/www.scientific.net/KEM.898.1.

European Union, *EN 1996-1-1: Eurocode 6: Design of masonry structures - Part 1-1: General rules for reinforced and unreinforced masonry structures*. 2005.

European Union, *EN 1998-1: Eurocode 8: Design of structures for earthquake resistance – Part 1: General rules, seismic actions and rules for buildings*. 2004.

S. Cattari e S. Lagomarsino, «A Strength Criterion For The Flexural Behaviour Of Spandrels In Unreinforced Masonry Walls», 2008.

N. Gattesco, L. Macorini, e A. Dudine, «Experimental Response of Brick-Masonry Spandrels under In-Plane Cyclic Loading», *J. Struct. Eng.*, vol. 142, n. 2, Art. n. 2, feb. 2016, doi: 10.1061/(ASCE)ST.1943-541X.0001418.

Ministero delle Infrastrutture e dei Trasporti, *NTC 2018: Aggiornamento delle «Norme tecniche per le costruzioni».*

Ministero delle Infrastrutture e dei Trasporti, *CIRCOLARE 21 gennaio 2019, n. 7 C.S.LL.PP.: Istruzioni per l'applicazione dell'«Aggiornamento delle "Norme tecniche per le costruzioni"» di cui al decreto ministeriale 17 gennaio 2018*.

CNR DT 200 R1/2013 (2013) 'Instructions for the Design, Execution and Control of Static Consolidation Interventions through the use of Fiber-reinforced Composites'. National research Council, Rome, Italy.

CNR-DT 203/2006 (2007) 'Guide for the Design and Construction of Concrete Structures Reinforced with Fiber-Reinforced Polymer Bars'. National research Council, Rome, Italy.

N. Gattesco e I. Boem, «Experimental and analytical study to evaluate the effectiveness of an in-plane reinforcement for masonry walls using GFRP meshes», *Constr. Build. Mater.*, vol. 88, pagg. 94–104, lug. 2015, doi: 10.1016/j.conbuildmat.2015.04.014.

N. Gattesco e I. Boem, «Out-of-plane behavior of reinforced masonry walls: Experimental and numerical study», *Compos. Part B Eng.*, vol. 128, pagg. 39–52, nov. 2017, doi: 10.1016/j.compositesb.2017.07.006.

N. Gattesco e I. Boem, «Characterization tests of GFRM coating as a strengthening technique for masonry buildings», *Compos. Struct.*, vol. 165, pagg. 209–222, apr. 2017, doi: 10.1016/j.compstruct.2017.01.043.

Abaqus/CAE v.6.12 Documentation Collection, Dassault Systèmes, 2012.

N. Gattesco, C. Amadio, e C. Bedon, «Experimental and numerical study on the shear behavior of stone masonry walls strengthened with GFRP reinforced mortar coating and steel-cord reinforced repointing», *Eng. Struct.*, vol. 90, pagg. 143–157, mag. 2015, doi: 10.1016/j.engstruct.2015.02.024.

J. Lubliner, J. Oliver, S. Oller, e E. Oñate, «A plastic-damage model for concrete», *Int. J. Solids Struct.*, vol. 25, n. 3, pagg. 299–326, 1989, doi: 10.1016/0020-7683(89)90050-4.

J. Lee e G. L. Fenves, «Plastic-Damage Model for Cyclic Loading of Concrete Structures», *J. Eng. Mech.*, vol. 124, n. 8, pagg. 892–900, ago. 1998, doi: 10.1061/(ASCE)0733-9399(1998)124:8(892).

A. K. Pandey e R. S. Bisht, «Numerical Modelling of Infilled Clay Brick Masonry under Blast Loading», Adv. Struct. Eng., vol. 17, n. 4, pagg. 591–606, apr. 2014, doi: 10.1260/1369-4332.17.4.591

X. Y. Xiong, R. J. Xue, S. Zhang, e L. J. Wang, «The Finite Element Analysis on Seismic Performance of Ring Beam and Constructional Column with Different Storey in Masonry Building», *Adv. Mater. Res.*, vol. 919–921, pagg. 1016–1019, apr. 2014, doi: 10.4028/www.scientific.net/AMR.919-921.1016.

N. Gattesco, I. Boem. «Characterization tests of GFRM coating as a strengthening technique for masonry buildings», Composite Structures, 2017, doi: 10.1016/j.compstruct.2017.01.043

Appendix

TAV.
P1

SHEAR-COMPRESSION TESTS ON MASONRY PIERS
SAMPLE CHARACTERISTICS

Quotes in cm - Scale 1:50

UNREINFORCED MASONRY SAMPLES

SOLID BRICK MASONRY SINGLE LEAF P-B1U

Frontal view

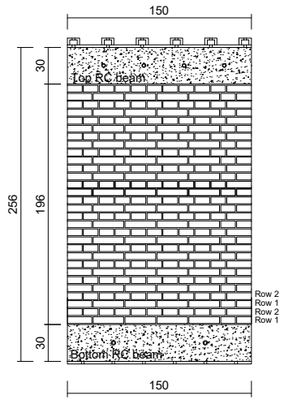

Horizontal section

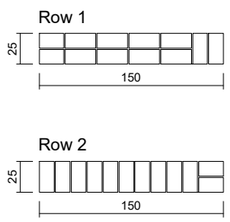

SOLID BRICK MASONRY DOUBLE LEAF P-B2U

Frontal view

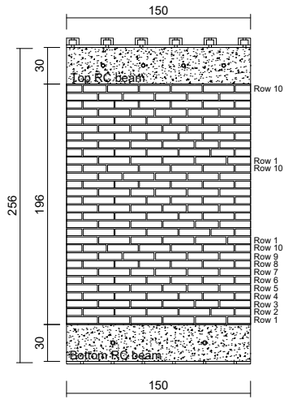

Horizontal section

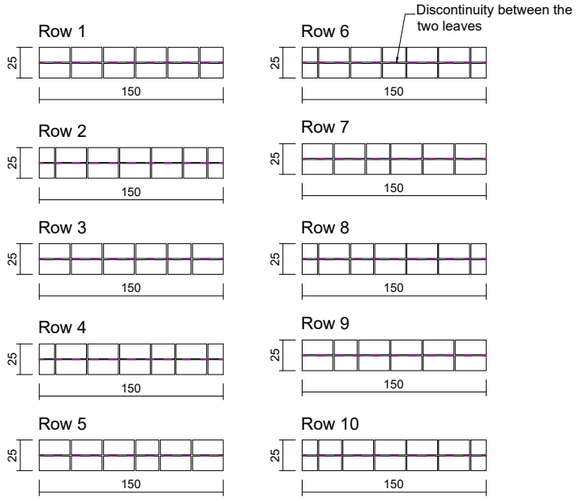

STONE MASONRY DOUBLE LEAF P-R2U

Frontal view

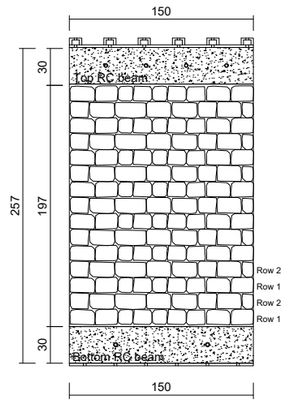

Horizontal section

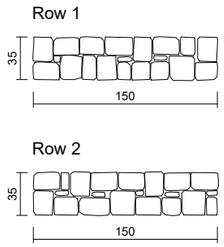

For the RC beam, use concrete C25/30 and steel B450C
Reinforcement: main bars 2Ø14, stirrups Ø8, 8 cm pitch

MATERIALS
- Solid bricks UNI 5.5x12x25 "San Marco Rosso Vivo - Terreal"
- Stones: sandstone, roughly squared, mean dimensions 12x15x20 cm³
- Hydraulic lime mortar: dosage lime-dry sand 1:5 (in volume)
  200 kg of lime and 1400 of kg dry sand for 1m³ of mortar
  Hydraulic lime "i.pro PLASTOCEM - Italcementi"
  Silica sand "Sabbia lavata 0/6 mm - Dal Zotto Srl"
  Add water so to obtain a plastic consistency for the mortar

NOTES:
Before installation, immerse the bricks in water until complete saturation and wet the stones with sprinkle water
In solid brick masonry, the mortar joints have a thickness of 1 cm
In stone masonry, the mortar joints have to be as thin as possible

TOT n° of sample type "P": 8
TOT n° of tests type "P": 8
PLACE OF CONSTRUCTION AND TESTING: Trieste University Laboratory

Masonry type	Leafs	Unreinforced	Reinforced
Solid brick	Single	X	X(I)
	Double	X	X(II) X(III)
Stone	Double	X	X(II) X(III)

(I) CRM on one side, GFRP L-shape connectors
(II) CRM on one side + diatones
(III) CRM on both sides, GFRP L-shape passing-through connectors

TAV.
P2

SHEAR-COMPRESSION TESTS ON MASONRY PIERS
SAMPLE CHARACTERISTICS

Quotes in cm - Scale 1:50

SOLID BRICK MASONRY - SINGLE LEAF (CRM on one side)
P-B1R

Back view
(unreinforced side)

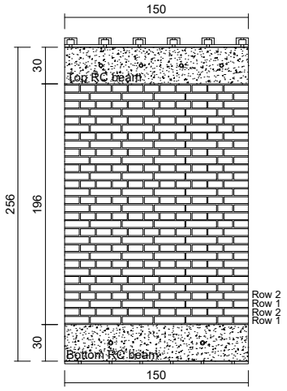

Front view
(reinforced side)

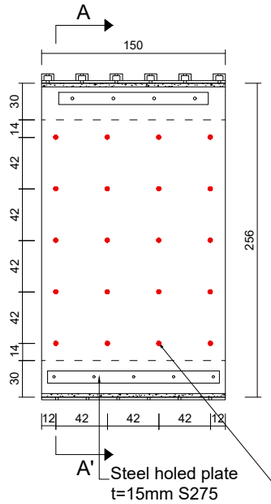

Section A-A'

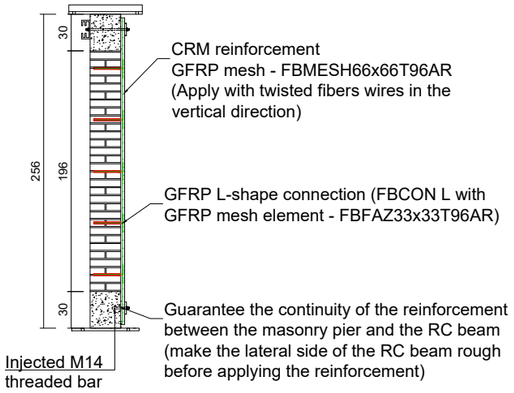

Horizontal section

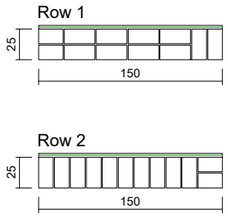

CRM reinforcement - Scale 1:25

Transversal section

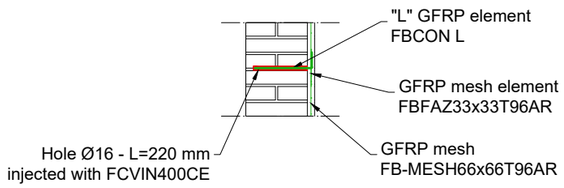

Frontal view

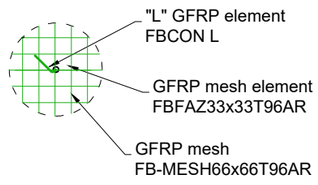

MATERIALS
For the masonry:
- Solid bricks UNI 5.5x12x25 "San Marco Rosso Vivo - Terreal"
- Hydraulic lime mortar: dosage lime-dry sand 1:5 (in volume)
  200 kg of lime and 1400 of kg dry sand for 1m³ of mortar
  Hydraulic lime "i.pro PLASTOCEM - Italcementi"
  Silica sand "Sabbia lavata 0/6 mm - Dal Zotto Srl"
  Add water so to obtain a plastic consistency for the mortar

NOTES:
-Before installation, immerse the bricks in water until complete saturation
-The mortar joints have a thickness of 1 cm
-Make the lateral sides of the RC beams rough before applying the rinforcement

For the reinforcement:
- GFRP Mesh: FBMESH66x66T96AR (minimum overlapping lenght: 132 mm, placed at the half thickness of the mortar coating)
- GFRP local device: FBFAZ66x66T96AR
- GFRP L-shape connection: FBCON L 200x100 for solid brick masonry
  FCVIN400CE vinylester chemical anchor
- Mortar coating: FBNHL 15 MPa - natural lime mortar

NOTE:
- Guarantee the continuity of the reinforcement between the masonry and the RC beams

For the RC beam:
- use concrete C25/30 and steel B450C
- reinforcement: main bars 2 Ø14, stirrups Ø8, 8 cm pitch

TOT n° of sample type "P": 8
TOT n° of tests type "P": 8
PLACE OF CONSTRUCTION AND TESTING: Trieste University Laboratory

Masonry type	Leafs	Unreinforced	Reinforced
Solid brick	Single	X	X(I)
	Double	X	X(II) X(III)
Stone	Double	X	X(II) X(III)

(I) CRM on one side, GFRP L-shape connectors
(II) CRM on one side + diatones
(III) CRM on both sides, GFRP L-shape passing-through connectors

TAV.
P3

SHEAR-COMPRESSION TESTS ON MASONRY PIERS
SAMPLE CHARACTERISTICS

Quotes in cm - Scale 1:50

SOLID BRICK MASONRY - DOUBLE LEAF (CRM on one side + Artificial Diatons)
P-B2R-1

Back view
(unreinforced side)

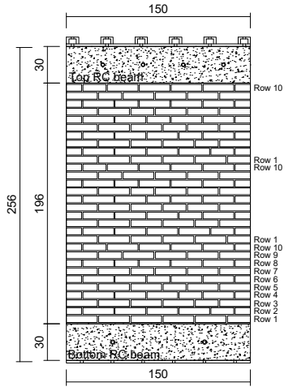

Front view
(reinforced side)

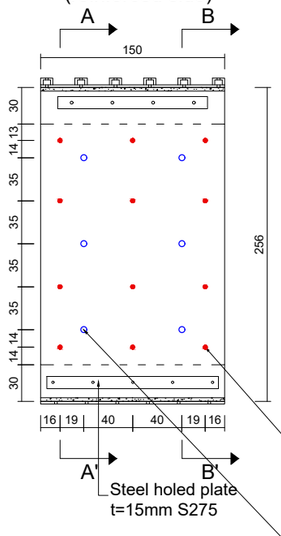

Section A-A'

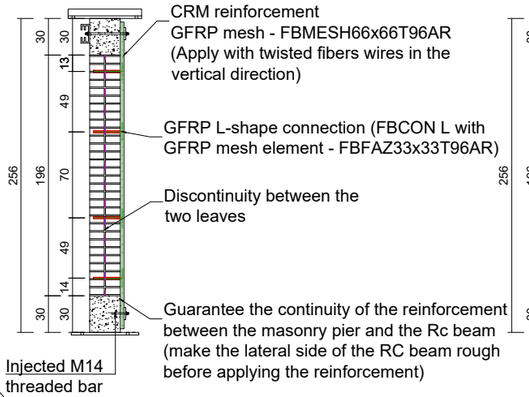

Section B-B'

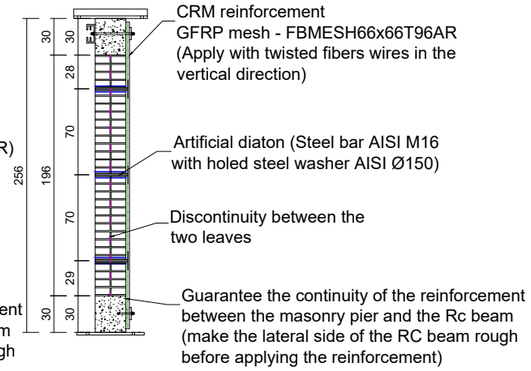

Horizontal section

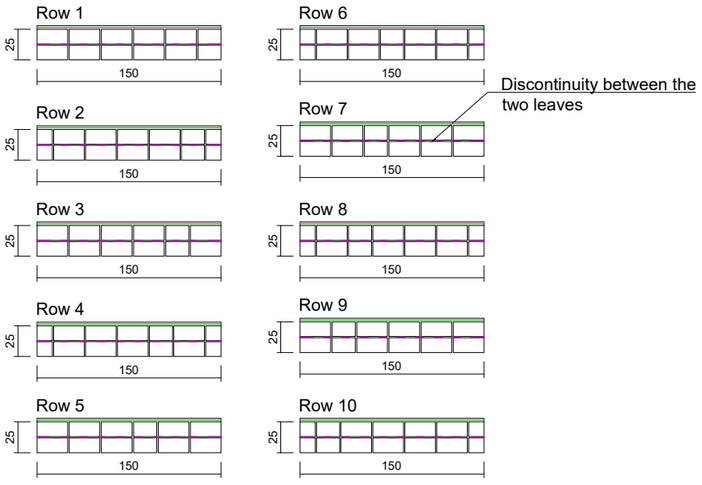

Hole Ø16mm - L=220 mm
Use coring machine with rotation system
(no percussion)

Hole Ø50mm - L=250 mm (passing through)
Use coring machine with rotation system (no
percussion)

MATERIALS
For the masonry:
- Solid bricks UNI 5.5x12x25 "San Marco Rosso Vivo - Terreal"
- Hydraulic lime mortar: dosage lime-dry sand 1:5 (in volume)
  200 kg of lime and 1400 of kg dry sand for 1m³ of mortar
  Hydraulic lime "i.pro PLASTOCEM - Italcementi"
  Silica sand "Sabbia lavata 0/6 mm - Dal Zotto Srl"
  Add water so to obtain a plastic consistency for the mortar

NOTES:
- Before installation, immerse the bricks in water till complete saturation
- The mortar joints have a thickness of 1 cm

For the reinforcement:
- GFRP Mesh: FBMESH66x66T96AR (minimum overlapping lenght: 132 mm, placed at the half thickness of the mortar coating)
- GFRP local device: FBFAZ66x66T96AR
- GFRP L-shape connection: FBCON L 200x100 for solid brick masonry
  FCVIN400CE vinylester chemical anchor
- Mortar coating: FBNHL 15 MPa - natural lime mortar
- Artificial diatones: steel bars AISI 304 (or 316) M16 l=350 mm for stone masonry, Struttura Tixo - TX 351 injection grout or equivalent cementitious based grout with inroganic grow and antishrink additives, minimum compressive strength 50 MPa
- Holed steel washer Ø150, AISI 304 (or 316) with central nut M16

NOTES:
- Make the lateral sides of the RC beams rough before applying the rinforcement

For the RC beam:
-use concrete C25/30 and steel B450C
-reinforcement: main bars 2 Ø14, stirrups Ø8, 8 cm pitch

CRM reinforcement - Scale 1:25

Transversal section

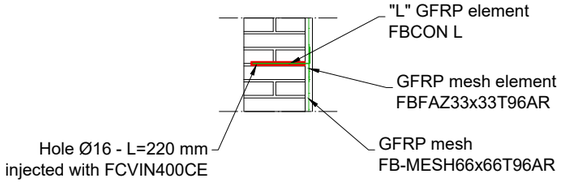

Frontal view

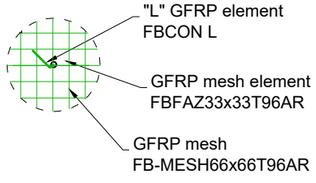

Artificial diaton - Scale 1:25

Transversal section

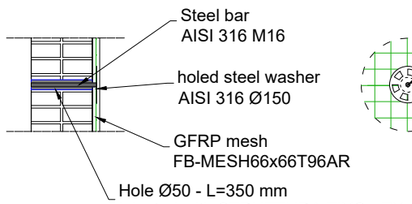

Frontal view

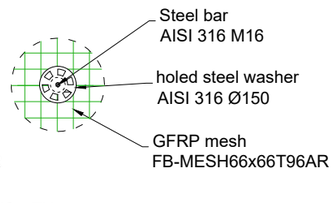

TOT n° of sample type "P": 8
TOT n° of tests type "P": 8
PLACE OF CONSTRUCTION AND TESTING: Trieste University Laboratory

Masonry type	Leafs	Unreinforced	Reinforced
Solid brick	Single	X	X(I)
	Double	X	X(II) X(III)
Stone	Double	X	X(II) X(III)

(I) CRM on one side, GFRP L-shape connectors
(II) CRM on one side + diatones
(III) CRM on both sides, GFRP L-shape passing-through connectors

TAV.
P4

SHEAR-COMPRESSION TESTS ON MASONRY PIERS
SAMPLE CHARACTERISTICS

Quotes in cm - Scale 1:50

SOLID BRICK MASONRY - DOUBLE LEAF (CRM on both sides)
P-B2R-2

Unreinforced view

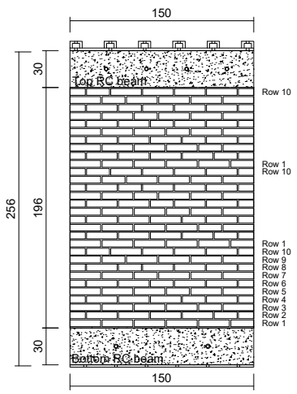

Reinforced view

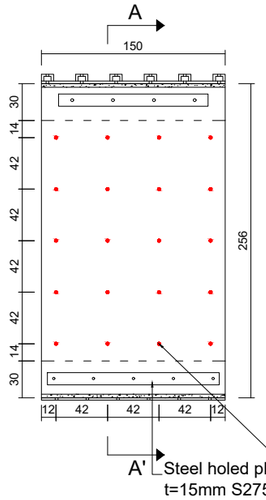

Section A-A'

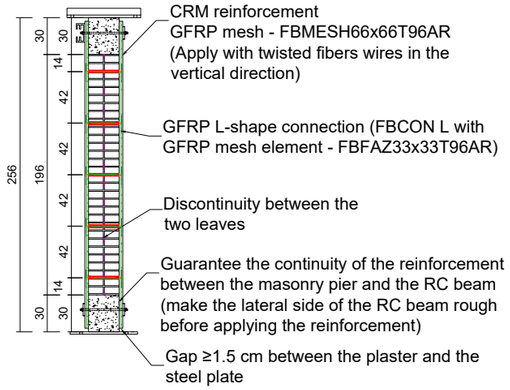

Hole Ø24mm - L=250 mm (passing through)
Use coring machine with rotation system (no percussion)

Horizontal section

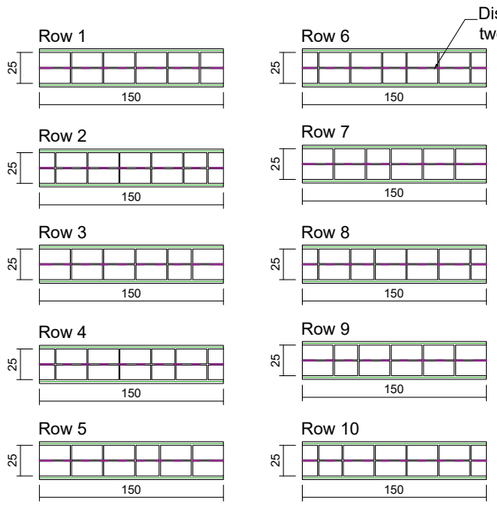

CRM reinforcement - Scale 1:25

Transversal section

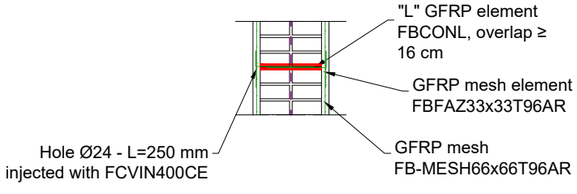

Frontal view

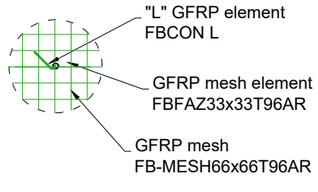

MATERIALS
For the masonry:
- Solid bricks UNI 5.5x12x25 "San Marco Rosso Vivo - Terreal"
- Hydraulic lime mortar: dosage lime-dry sand 1:5 (in volume)
  200 kg of lime and 1400 of kg dry sand for 1m³ of mortar
  Hydraulic lime "i.pro PLASTOCEM - Italcementi"
  Silica sand "Sabbia lavata 0/6 mm - Dal Zotto Srl"
  Add water so to obtain a plastic consistency for the mortar

NOTES:
- Before installation, immerse the bricks in water till complete saturation
- The mortar joints have a thickness of 1 cm

For the reinforcement:
- GFRP Mesh: FBMESH66x66T96AR (minimum overlapping lenght: 132 mm, placed at the half thickness of the mortar coating)
- GFRP local device: FBFAZ66x66T96AR
- GFRP L-shape connection: FBCON L 200x100 for solid brick masonry
  FCVIN400CE vinylester chemical anchor
- Mortar coating: FBNHL 15 MPa - natural lime mortar
- Artificial diatones: steel bars AISI 304 (or 316) M16 l=350 mm for stone masonry, Struttura Tixo - TX 351 injection grout or equivalent cementitious based grout with inroganic grow and antishrink additives, minimum compressive strength 50 MPa
- Holed steel washer Ø150, AISI 304 (or 316) with central nut M16

NOTES:
- Make the lateral sides of the RC beams rough before applying the rinforcement

For the RC beam:
- use concrete C25/30 and steel B450C
- reinforcement: main bars 2 Ø14, stirrups Ø8, 8 cm pitch

TOT n° of sample type "P": 8
TOT n° of tests type "P": 8
PLACE OF CONSTRUCTION AND TESTING: Trieste University Laboratory

Masonry type	Leafs	Unreinforced	Reinforced
Solid brick	Single	X	X(I)
	Double	X	X(II) X(III)
Stone	Double	X	X(II) X(III)

(I) CRM on one side, GFRP L-shape connectors
(II) CRM on one side + diatones
(III) CRM on both sides, GFRP L-shape passing-through connectors

TAV.
P5

SHEAR-COMPRESSION TESTS ON MASONRY PIERS
SAMPLE CHARACTERISTICS

Quotes in cm - Scale 1:50

STONE MASONRY - DOUBLE LEAF (CRM on one side + Artificial Diatons)
P-R2R-1

Back view
(unreinforced side)

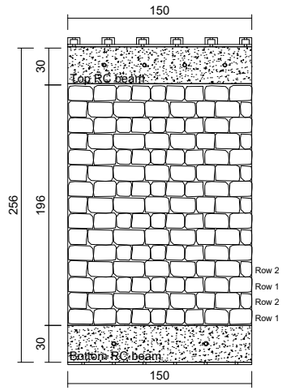

Front view
(reinforced side)

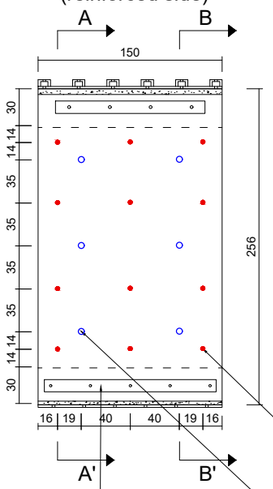

Section A-A'

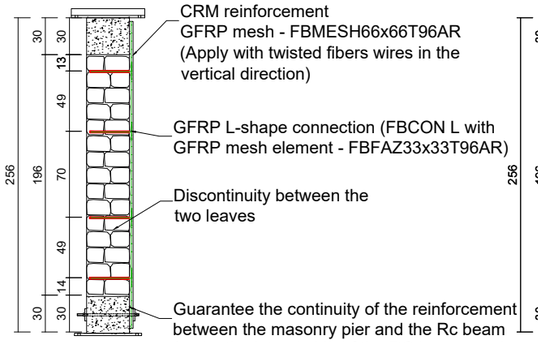

Section B-B'

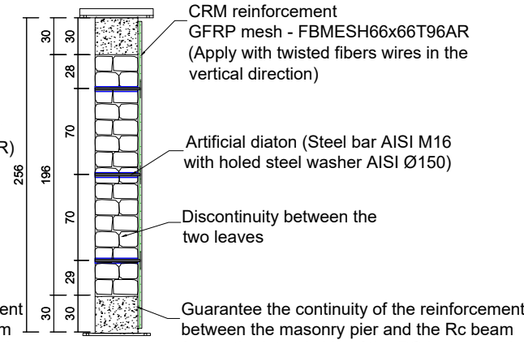

Horizontal section

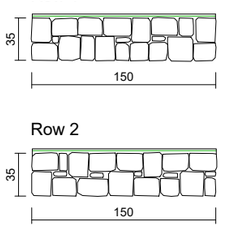

Steel holed plate
t=15mm S275

Hole Ø16mm - L=320 mm
Use coring machine with rotation system
(no percussion)

Hole Ø50mm - L=350 mm (passing through)
Use coring machine with rotation system (no percussion)

CRM reinforcement - Scale 1:25

Transversal section

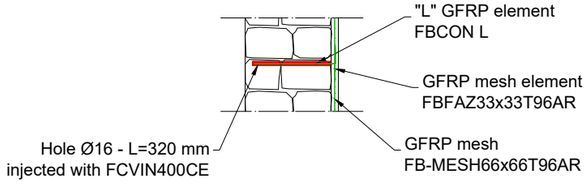

Frontal view

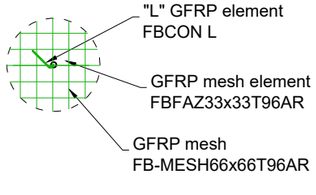

Artificial diaton - Scale 1:25

Transversal section

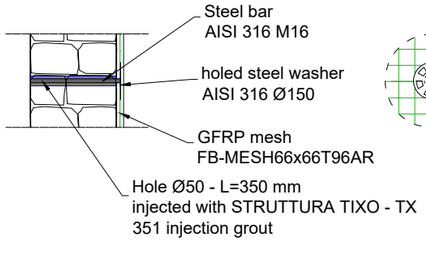

Frontal view

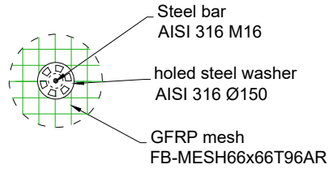

MATERIALS
For the masonry:
- Stones: sandstone, roughly squared, mean dimensions 12x15x20 cm³
- Hydraulic lime mortar: dosage lime-dry sand 1:5 (in volume)
  200 kg of lime and 1400 of kg dry sand for 1m³ of mortar
  Hydraulic lime "i.pro PLASTOCEM - Italcementi"
  Silica sand "Sabbia lavata 0/6 mm - Dal Zotto Srl"
  Add water so to obtain a plastic consistency for the mortar

NOTES:
-Before installation wet the stones with sprinkle water
-The mortar joints have to be as thin as possible

For the reinforcement:
- GFRP Mesh: FBMESH66x66T96AR (minimum overlapping lenght: 132 mm, placed at the half thickness of the mortar coating)
- GFRP local device: FBFAZ66x66T96AR
- GFRP L-shape connection: FBCON L 300x100 for stone masonry
  FCVIN400CE vinylester chemical anchor
- Mortar coating: FBNHL 15 MPa - natural lime mortar
- Artificial diatones: steel bars AISI 304 (or 316) M16 l=350 mm for stone masonry, Struttura Tixo - TX 351 injection grout or equivalent cementitious based grout with inroganic grow and antishrink additives, minimum compressive strength 50 MPa
- Holed steel washer Ø150, AISI 304 (or 316) with central nut M16

NOTES:
- Make the lateral sides of the RC beams rough before applying the rinforcement

For the RC beam:
- use concrete C25/30 and steel B450C
- reinforcement: main bars 2 Ø14, stirrups Ø8, 8 cm pitch

TOT n° of sample type "P": 8
TOT n° of tests type "P": 8
PLACE OF CONSTRUCTION AND TESTING: Trieste University Laboratory

Masonry type	Leafs	Unreinforced	Reinforced
Solid brick	Single	X	X(I)
	Double	X	X(II) X(III)
Stone	Double	X	X(II) X(III)

(I) CRM on one side, GFRP L-shape connectors
(II) CRM on one side + diatones
(III) CRM on both sides, GFRP L-shape passing-through connectors

TAV.
P6

SHEAR-COMPRESSION TESTS ON MASONRY PIERS
SAMPLE CHARACTERISTICS

Quotes in cm - Scale 1:50

STONE MASONRY - DOUBLE LEAF - REINFORCED SAMPLE (CRM on both sides)
P-R2R-2

Unreinforced view

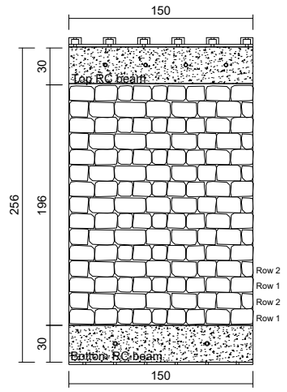

Reinforced view

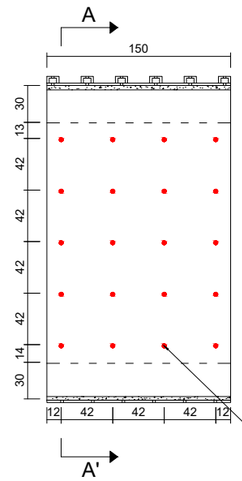

Section A-A'

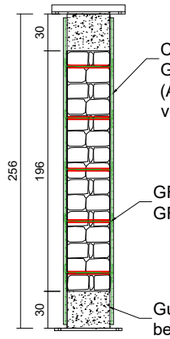

CRM reinforcement
GFRP mesh - FBMESH66x66T96AR
(Apply with twisted fibers wires in the vertical direction)

GFRP L-shape connection (FBCON L with GFRP mesh element - FBFAZ33x33T96AR)

Guarantee the continuity of the reinforcement between the masonry pier and the Rc beam (make the lateral side of the RC beam rough before applying the reinforcement)

Hole Ø24mm - L=350 mm (passing through)
Use coring machine with rotation system (no percussion)

Horizontal section

Row 1

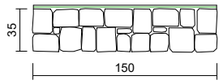

Row 2

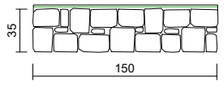

CRM reinforcement - Scale 1:25

Transversal section

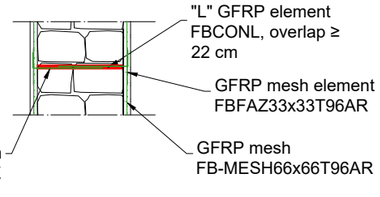

Frontal view

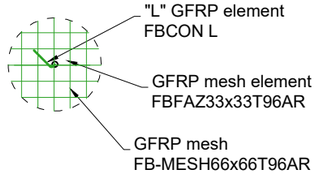

MATERIALS
For the masonry:
- Stones: sandstone, roughly squared, mean dimensions 12x15x20 cm³
- Hydraulic lime mortar: dosage lime-dry sand 1:5 (in volume)
  200 kg of lime and 1400 of kg dry sand for 1m³ of mortar
  Hydraulic lime "i.pro PLASTOCEM - Italcementi"
  Silica sand "Sabbia lavata 0/6 mm - Dal Zotto Srl"
  Add water so to obtain a plastic consistency for the mortar

NOTES:
- Before installation wet the stones with sprinkle water
- The mortar joints have to be as thin as possible

For the reinforcement:
- GFRP Mesh: FBMESH66x66T96AR (minimum overlapping lenght: 132 mm, placed at the half thickness of the mortar coating)
- GFRP local device: FBFAZ66x66T96AR
- GFRP L-shape connection: FBCON L 300x100 for stone masonry
  FCVIN400CE vinylester chemical anchor

NOTES:
- Make the lateral sides of the RC beams rough before applying the rinforcement

For the RC beam:
- use concrete C25/30 and steel B450C
- reinforcement: main bars 2 Ø14, stirrups Ø8, 8 cm pitch

TOT n° of sample type "P": 8
TOT n° of tests type "P": 8
PLACE OF CONSTRUCTION AND TESTING: Trieste University Laboratory

Masonry type	Leafs	Unreinforced	Reinforced
Solid brick	Single	X	X(I)
	Double	X	X(II) X(III)
Stone	Double	X	X(II) X(III)

(I) CRM on one side, GFRP L-shape connectors
(II) CRM on one side + diatones
(III) CRM on both sides, GFRP L-shape passing-through connectors

TAV.
P7

SHEAR-COMPRESSION TESTS ON MASONRY PIERS
CARPENTERY

Quotes in mm - Scale 1:25

MATERIALS

Steel S275
Welding: a = 4 mm

Test set-up - Scale 1:50

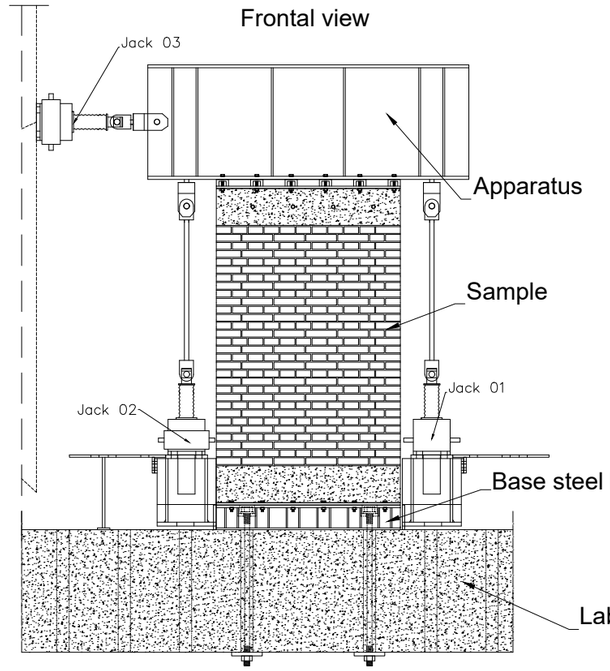

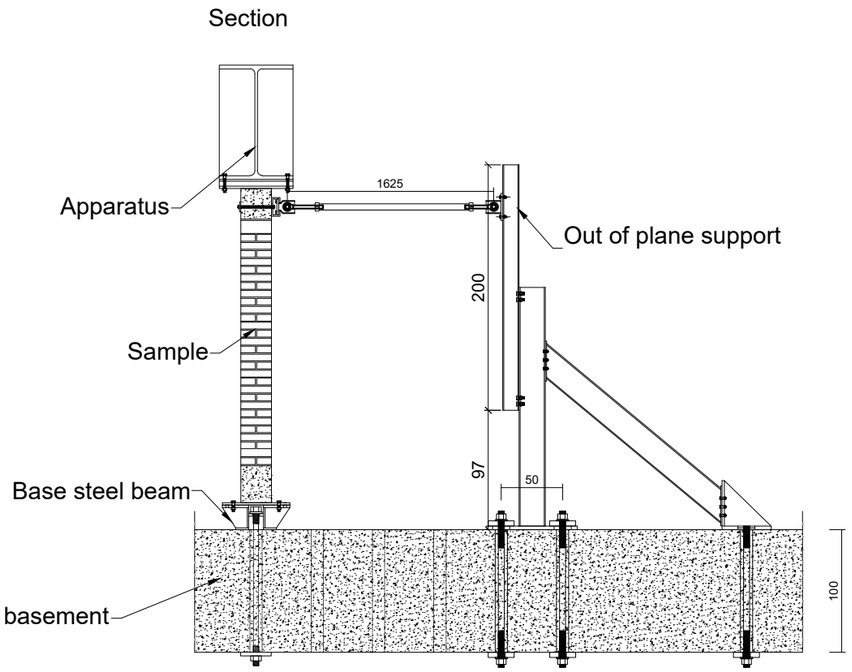

Base steel beam

Wireframe view

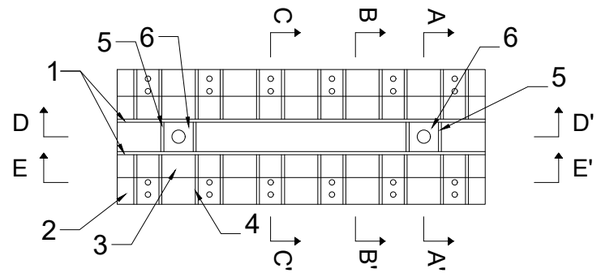

1 - Steel plate ≠12x165x1500 mm^3 (2x)

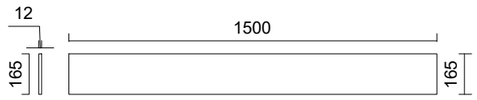

2 - Steel plate ≠550x1500x20 mm^3 (1x)

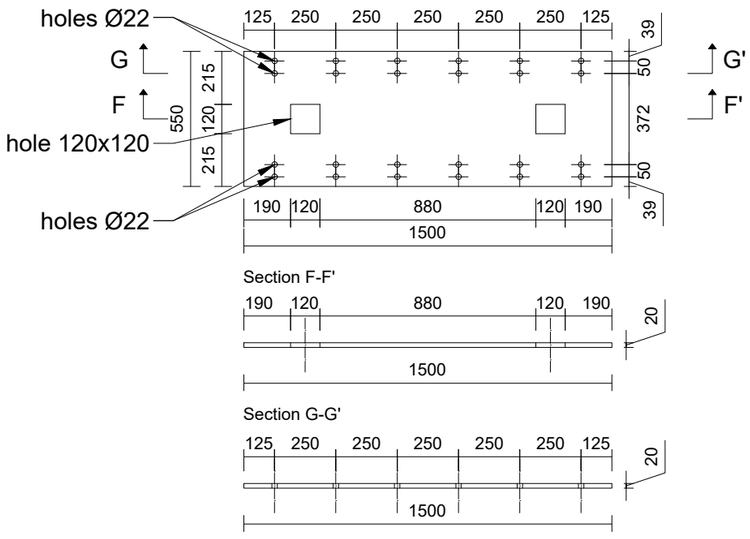

3 - Steel plate ≠106x1500x15 mm^3 (2x)

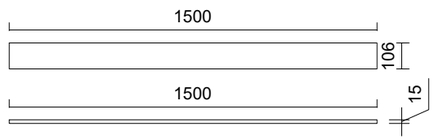

4 - Steel plate ≠165x203x198x94x12 mm^3 (24x)

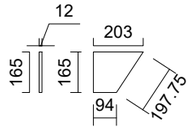

5 - Steel plate ≠120x12x50 mm^3 (4x)

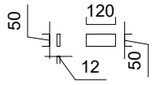

6 - Steel plate ≠120x144x20 mm^3 (2x)

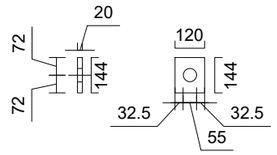

Section E-E'

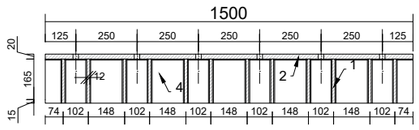

Section A-A'

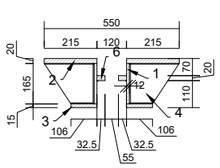

Section B-B'

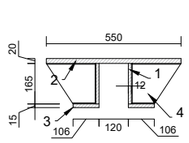

Section C-C'

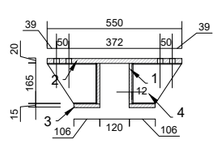

Section D-D'

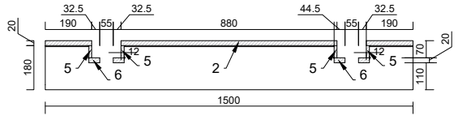

ASSEMBLY INSTRUCTION

- Weld elements "4" to "1"
- Weld elements "3" to "1" and "4"
- Weld elements "5" to "1"
- Weld elements "6" to "1" and "5"
- Weld element "2" to "1", "4" and "5"

TAV.
P8

SHEAR-COMPRESSION TESTS ON MASONRY PIERS
CARPENTERY

Quotes in mm - Scale 1:25

MATERIALS

For the RC beam, use concrete C25/30 and steel B450C
Reinforcement: main bars 2 Ø14, stirrups Ø8, 8 cm pitch

For steel elements, use Steel S275

Ribbed steel plate

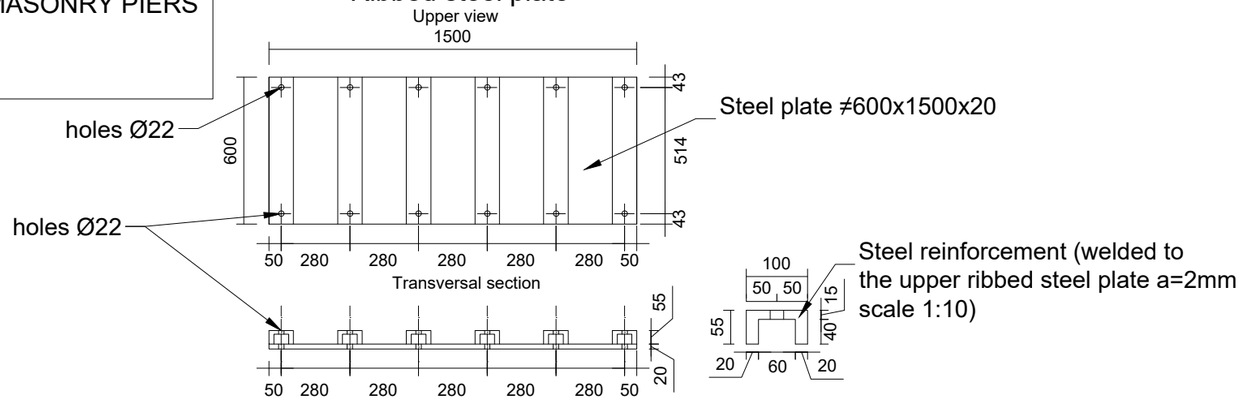

Bottom RC Beam 250x300x1500 mm^3 (2x)

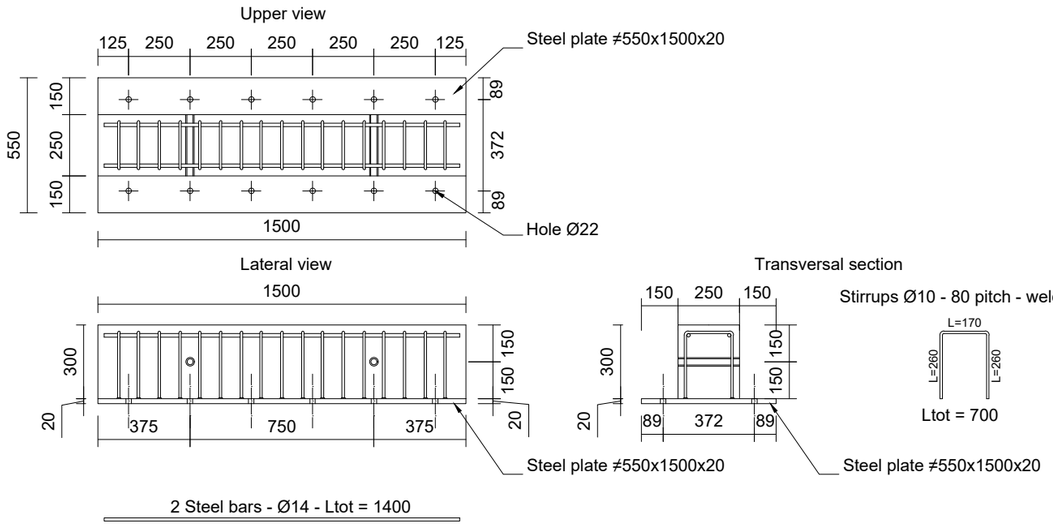

Top RC Beam 250x300x1500 mm^3 (2x)

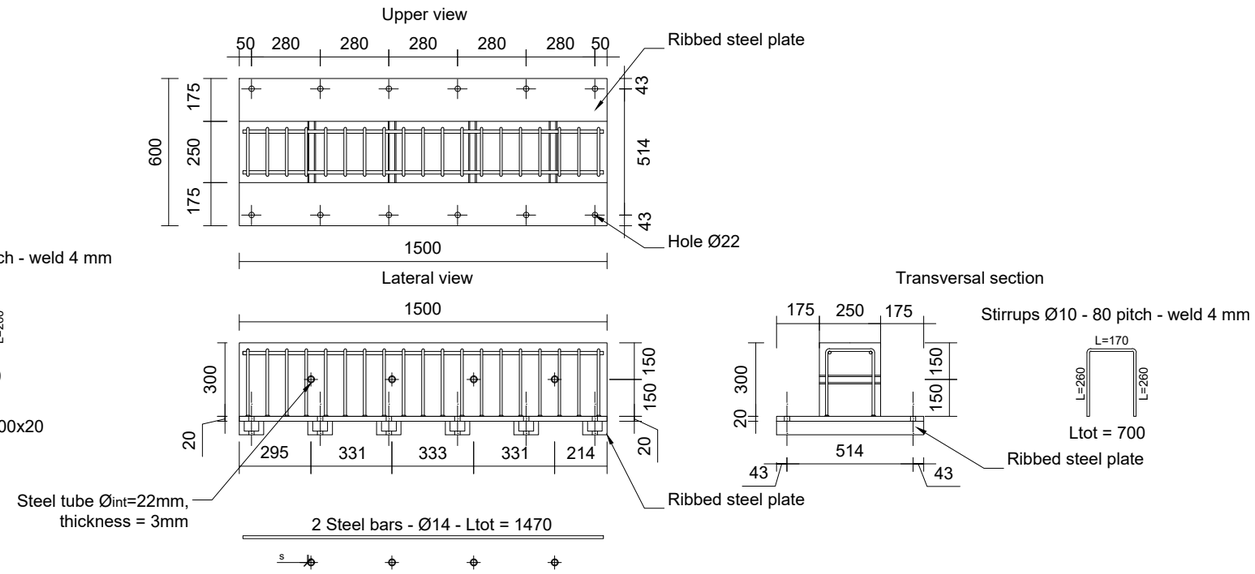

Bottom RC Beam 350x300x1500 mm^3 (3x)

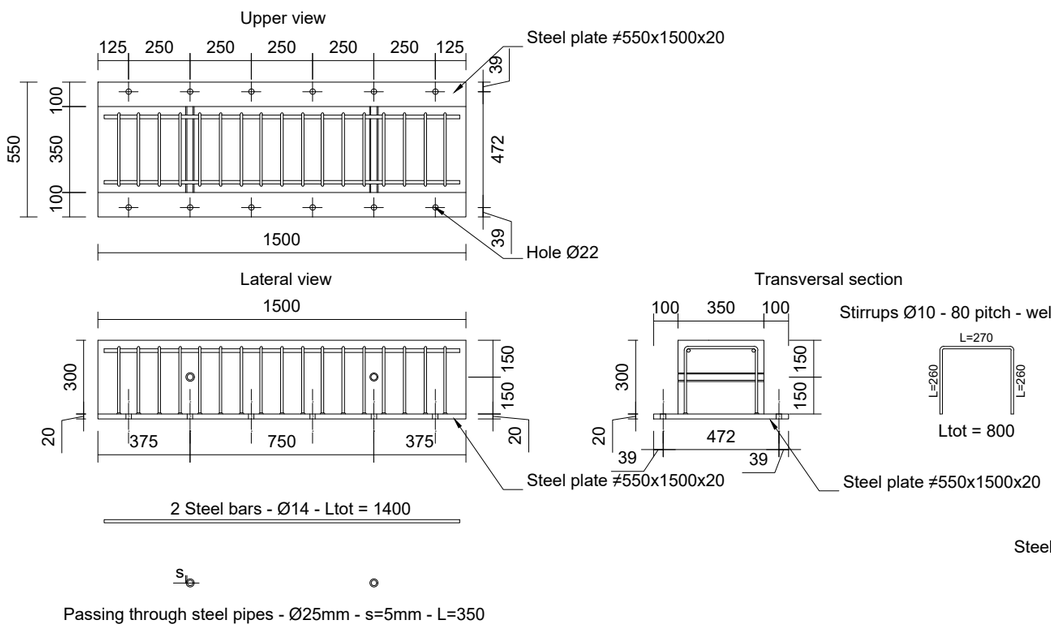

Top RC Beam 350x300x1500 mm^3 (3x)

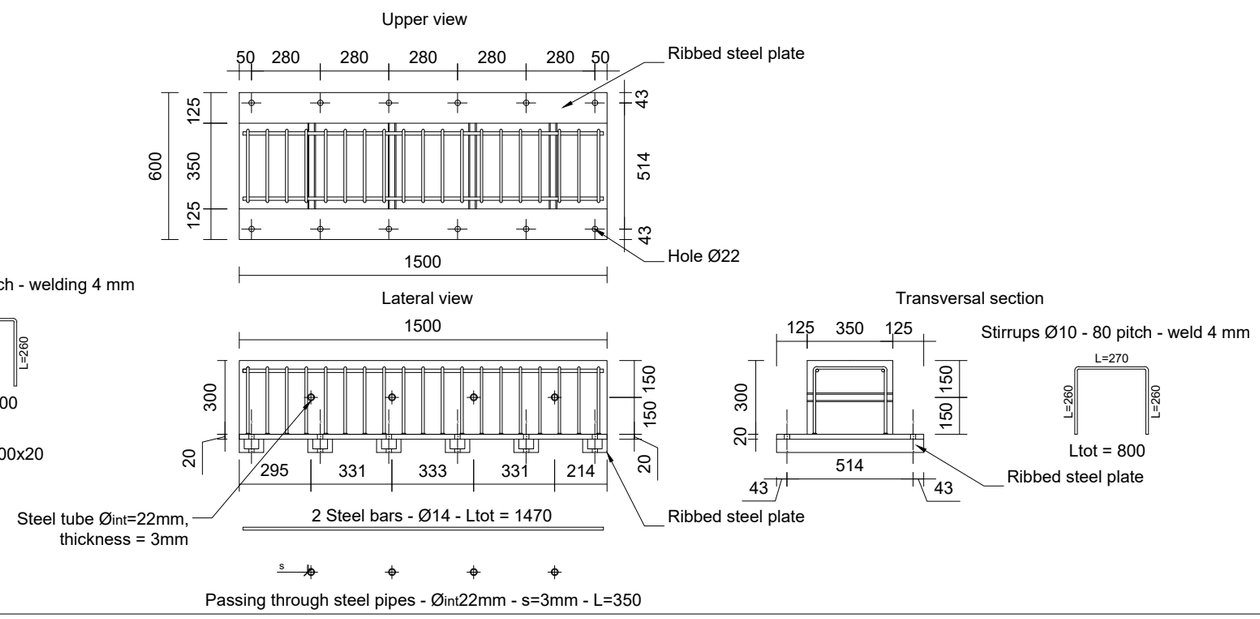

TAV.
P9

SHEAR-COMPRESSION TESTS ON MASONRY PIERS
CARPENTERY

Quotes in mm - Scale 1:5

FORK with Ø30 calibrated hole - steel S275 (2x)

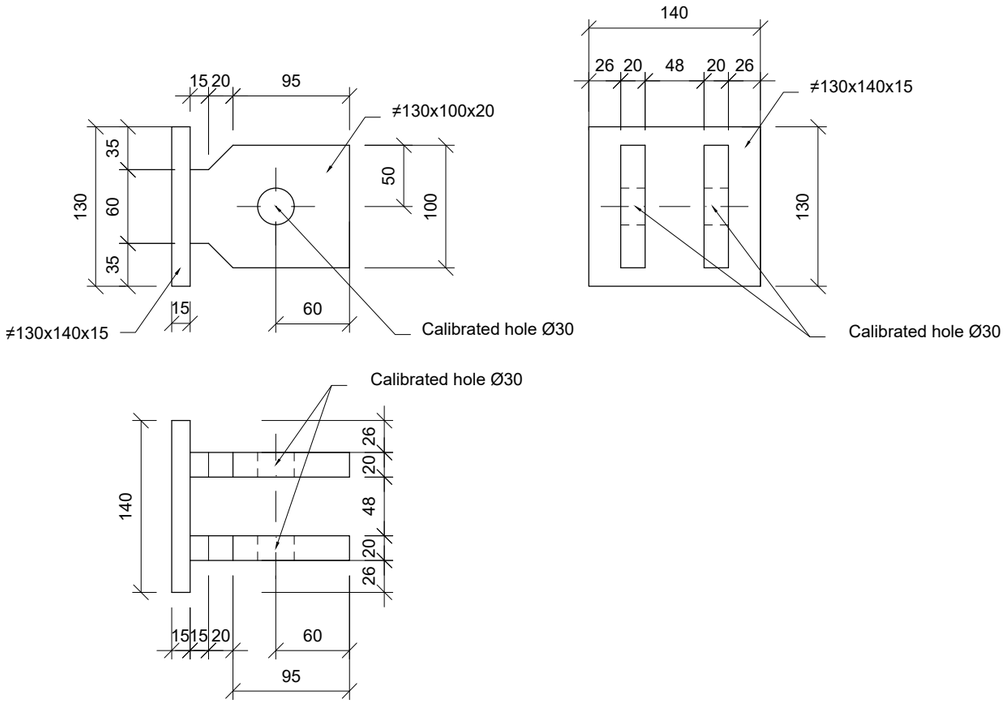

FORK with Ø30 calibrated hole - steel S275 (2x)

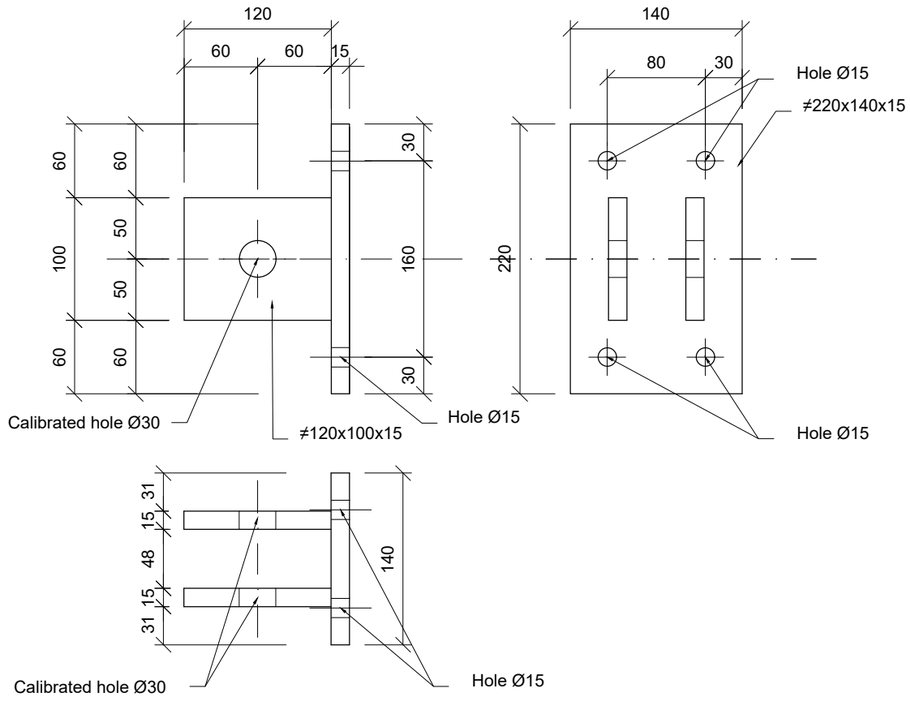

Sleeve - S275 (x2)

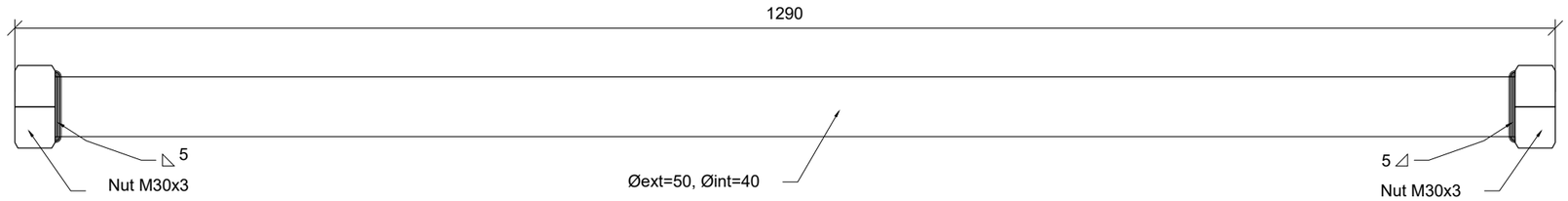

C beam - steel S275 (1x)

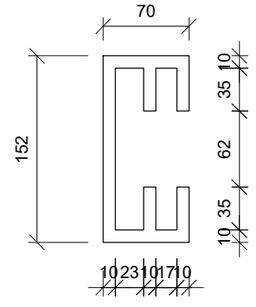

CALIBRATED DOWEL PINS C40 steel (2x)

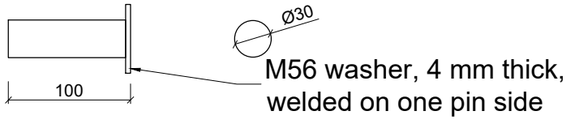

BALL JOINT MALE Ø30 - steel S275 (2x)

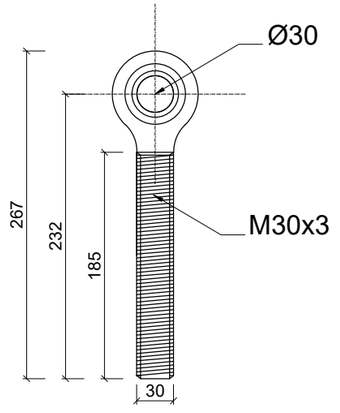

BALL JOINT MALE Ø30 - steel S275 (2x)

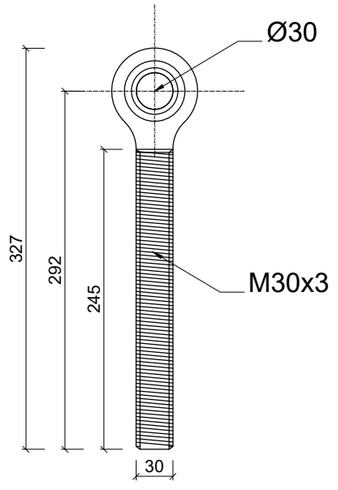

TAV.
P10

SHEAR-COMPRESSION TESTS ON MASONRY PIERS
CARPENTERY
Quotes in cm - Scale 1:5

HOLED PLATE - steel S275 (1x)

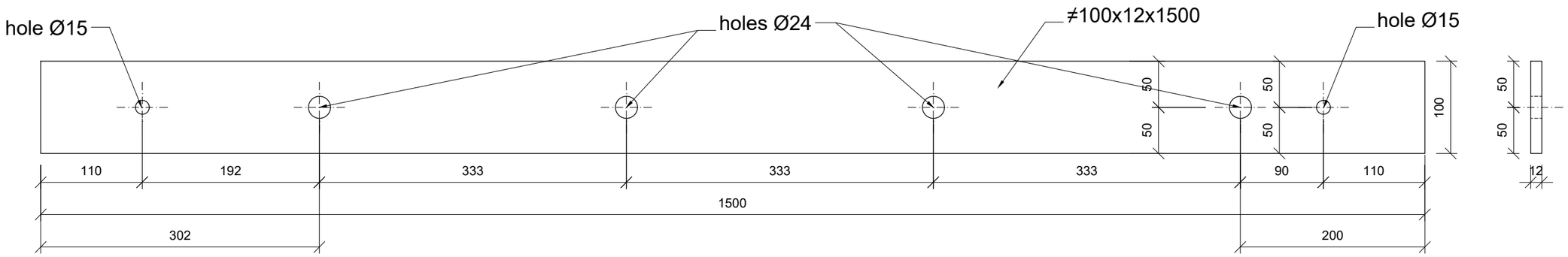

HOLED PLATE - steel S275 (2x)

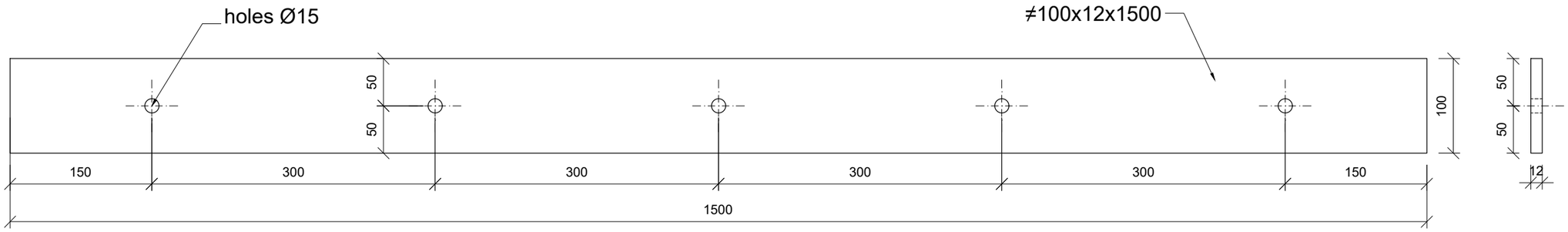

M14x2 THREADED STEEL BAR - Steel 8.8 (6x)

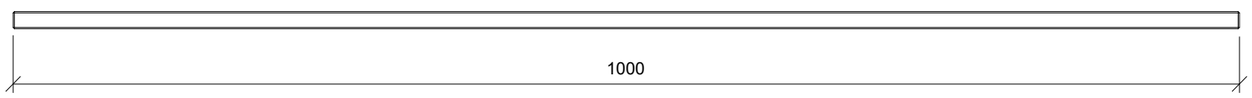

M14x2 NUT - Steel 8.8 UNI 5588 (20x)

M14 WASHER - UNI 6592 (20x)

TAV.
B1

BENDING TESTS ON MASONRY WALLS
SAMPLE CHARACTERISTICS

Quotes in cm - Scale 1:50

SOLID BRICK MASONRY - SINGLE LEAF (CRM on one side)
B-B1

Back view (unreinforced side)

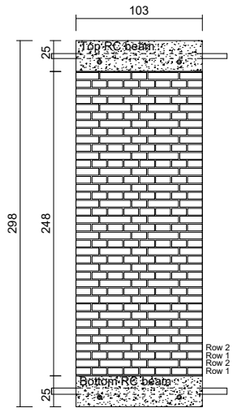

Front view (reinforced side)

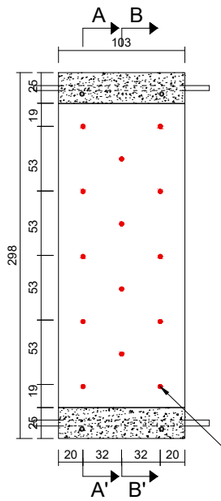

Section A-A'

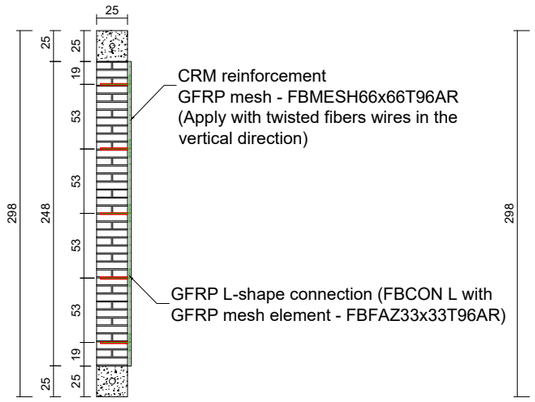

Section B-B'

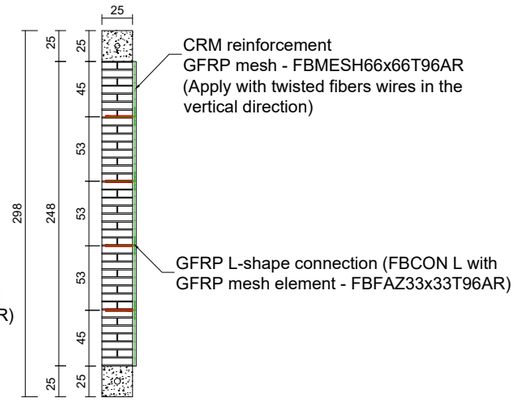

Hole Ø16mm - L=220 mm
Use coring machine with rotation system
(no percussion)

Horizontal section

Row 1

Row 2

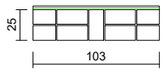

Top RC beam 25x25x103 cm^3

Frontal view

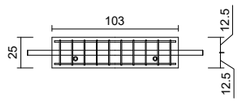

Transversal section

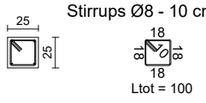

2 Steel bars sup - Ø14 - Ltot = 96

2 Steel bars inf - Ø14 - Ltot = 96

1 x Steel bar - Ø40 - Ltot = 143 (steel C40)

Steel pipes - Ø25mm - s=5mm - L=250

Bottom RC beam 25x25x103 cm^3

Frontal view

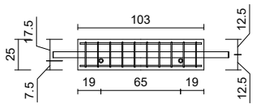

Transversal section

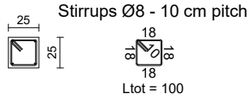

2 Steel bars sup - Ø14 - Ltot = 96

2 Steel bars inf - Ø14 - Ltot = 96

1 x Steel bar - Ø50 - Ltot = 143 (steel C40)

Steel pipes - Ø25mm - s=5mm - L=250

CRM reinforcement - Scale 1:25

Transversal section

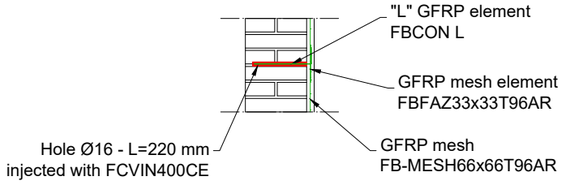

Frontal view

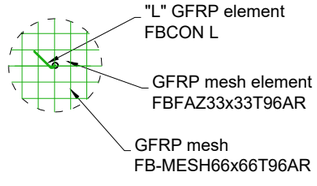

MATERIALS
For the masonry:
- Solid bricks UNI 5.5x12x25 "San Marco Rosso Vivo - Terreal"
- Hydraulic lime mortar: dosage lime-dry sand 1:5 (in volume)
  200 kg of lime and 1400 of kg dry sand for 1m³ of mortar
  Hydraulic lime "i.pro PLASTOCEM - Italcementi"
  Silica sand "Sabbia lavata 0/6 mm - Dal Zotto Srl"
  Add water so to obtain a plastic consistency for the mortar

NOTES:
Before installation, immerse the bricks in water till complete saturation
The mortar joints have a thickness of 1 cm

For the reinforcement:
- GFRP Mesh: FBMESH66x66T96AR (minimum overlapping lenght: 132 mm, placed at the half thickness of the mortar coating)
- GFRP local device: FBFAZ66x66T96AR
- GFRP L-shape connection: FBCON L 200x100 for solid brick masonry
  FCVIN400CE vinylester chemical anchor
- Mortar coating: FBNHL 15 MPa - natural lime mortar

For the RC beam:
- concrete C25/30 and steel B450C

For steel bars:
- cold drowe steel, c40

BENDING TESTS ON MASONRY WALLS (B)

TOT n° of sample type "B": 3
TOT n° of tests type "B": 3
PLACE OF CONSTRUCTION AND TESTING: Trieste University Laboratory

Masonry type	Leafs	Reinforced
Solid brick	Single	X(I)
	Double	X(II)
Stone	Double	X(II)

(I) CRM on one side, GFRP L-shape connectors
(II) CRM on one side + diatones

TAV.
B2

BENDING TESTS ON MASONRY WALLS
SAMPLE CHARACTERISTICS

Quotes in cm - Scale 1:50

SOLID BRICK MASONRY - DOUBLE LEAF (CRM on one side + diatons)

Back view
(unreinforced side)

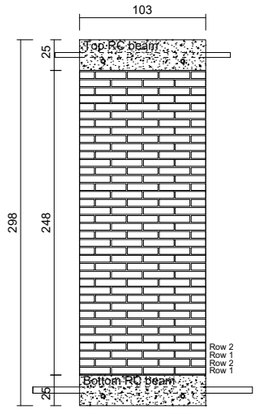

Front view
(reinforced side)

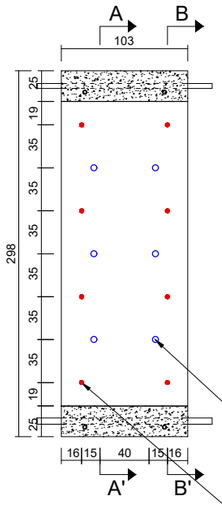

Section A-A'

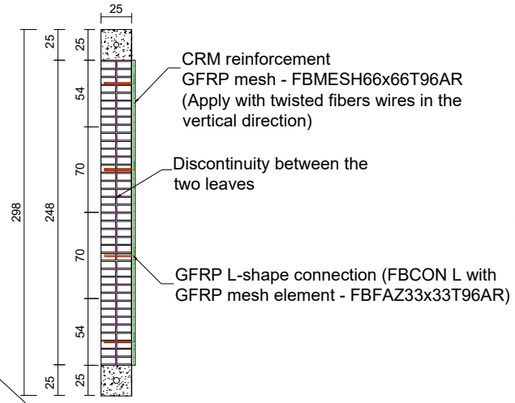

Section B-B'

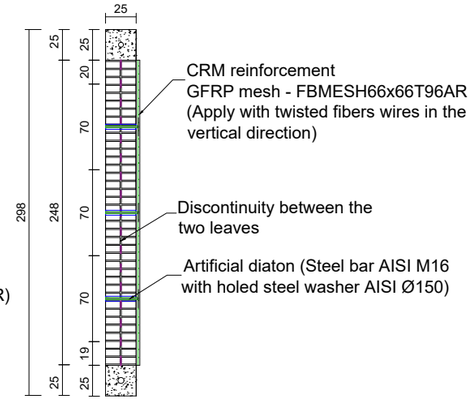

Hole Ø50mm - L=250 mm (passing through)
Use coring machine with rotation system (no percussion)

Hole Ø16mm - L=220 mm
Use coring machine with rotation system (no percussion)

Horizontal section

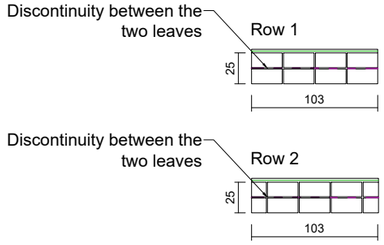

Top RC beam 25x25x103 cm^3

Frontal view

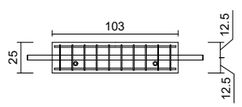

Transversal section

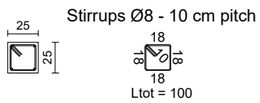

2 Steel bars sup - Ø14 - Ltot = 96

2 Steel bars inf - Ø14 - Ltot = 96

1 x Steel bar - Ø40 - Ltot = 143 (steel C40)

Steel pipes - Ø25mm - s=5mm - L=250

Bottom RC beam 25x25x103 cm^3

Frontal view

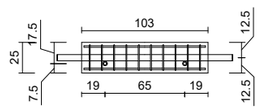

Transversal section

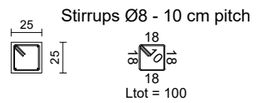

2 Steel bars sup - Ø14 - Ltot = 96

2 Steel bars inf - Ø14 - Ltot = 96

1 x Steel bar - Ø50 - Ltot = 143 (steel C40)

Steel pipes - Ø25mm - s=5mm - L=250

CRM reinforcement - Scale 1:25

Transversal section

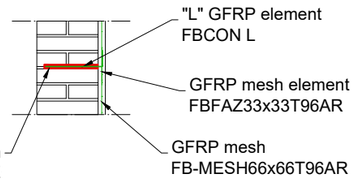

Frontal view

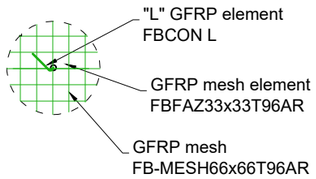

Artificial diaton - Scale 1:25

Transversal section

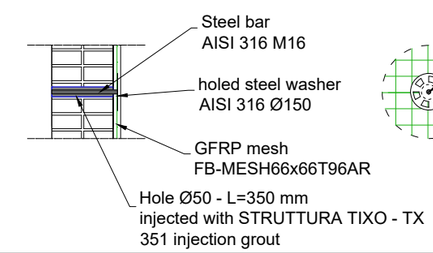

Frontal view

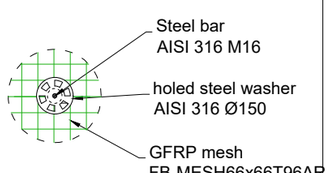

MATERIALS
For the masonry:
- Solid bricks UNI 5.5x12x25 "San Marco Rosso Vivo - Terreal"
- Hydraulic lime mortar: dosage lime-dry sand 1:5 (in volume)
  200 kg of lime and 1400 of kg dry sand for 1m³ of mortar
  Hydraulic lime "i.pro PLASTOCEM - Italcementi"
  Silica sand "Sabbia lavata 0/6 mm - Dal Zotto Srl"
  Add water so to obtain a plastic consistency for the mortar

NOTES:
Before installation, immerse the bricks in water till complete saturation
The mortar joints have a thickness of 1 cm

For the reinforcement:
- GFRP Mesh: FBMESH66x66T96AR (minimum overlapping lenght: 132 mm, placed at the half thickness of the mortar coating)
- GFRP local device: FBFAZ66x66T96AR
- GFRP L-shape connection: FBCON L 200x100 for solid brick masonry
  FCVIN400CE vinylester chemicalanchor
- Mortar coating: FBNHL 15 MPa - natural lime mortar
- Artificial diatones: steel bars AISI 304 (or 316) M16 l=350 mm for stone masonry, Struttura Tixo - TX 351 injection grout or equivalent cementitious based grout with inroganic grow and antishrink additives, minimum compressive strength 50 MPa
- Holed steel washer Ø150, AISI 304 (or 316) with central nut M16

For the RC beam:
-concrete C25/30 and steel B450C

For steel bars:
-cold drawn steel, c40

BENDING TESTS ON MASONRY WALLS (B)

TOT n° of sample type "B": 3
TOT n° of tests type "B": 3
PLACE OF CONSTRUCTION AND TESTING: Trieste University Laboratory

Masonry type	Leafs	Reinforced
Solid brick	Single	X(I)
	Double	X(II)
Stone	Double	X(II)

(I) CRM on one side, GFRP L-shape connectors
(II) CRM on one side + diatones

TAV. B3

BENDING TESTS ON MASONRY WALLS
SAMPLE CHARACTERISTICS

Quotes in cm - Scale 1:50

STONE MASONRY - DOUBLE LEAF (CRM on one side + diatons)
B-R2

Back view (unreinforced side)

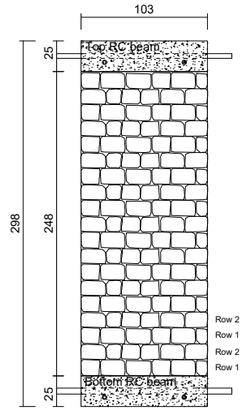

Front view (reinforced side)

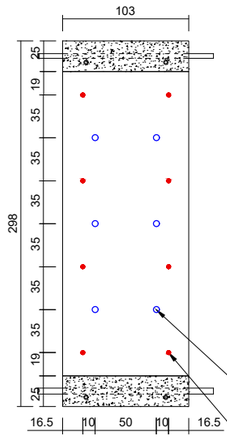

Section A-A'

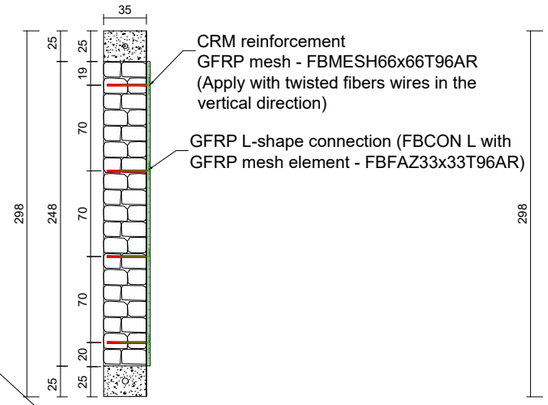

Section B-B'

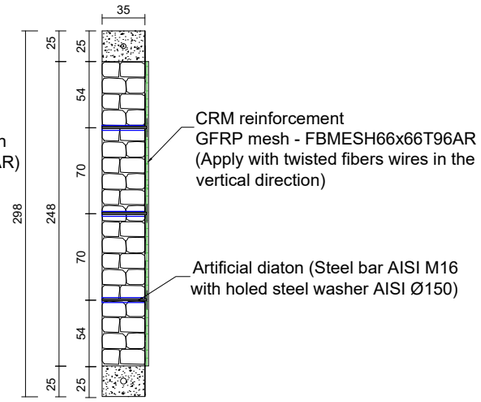

Hole Ø50mm - L=350 mm (passing through)
Use coring machine with rotation system (no percussion)

Hole Ø16mm - L=320 mm
Use coring machine with rotation system (no percussion)

Horizontal section

Row 1

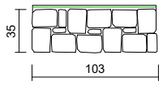

Row 2

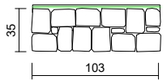

Top RC beam 35x25x103 cm^3

Frontal view

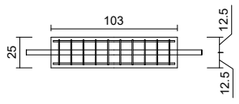

Transversal section

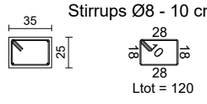

2 Steel bars sup - Ø14 - Ltot = 96

2 Steel bars inf - Ø14 - Ltot = 96

1 x Steel bar - Ø40 - Ltot = 143 (steel C40)

Steel pipes - Ø25mm - s=5mm - L=250

Bottom RC beam 35x25x103 cm^3

Frontal view

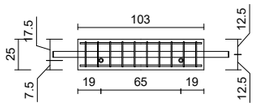

Transversal section

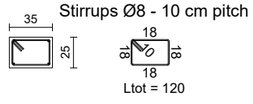

2 Steel bars sup - Ø14 - Ltot = 96

2 Steel bars inf - Ø14 - Ltot = 96

1 x Steel bar - Ø50 - Ltot = 143 (steel C40)

Steel pipes - Ø25mm - s=5mm - L=250

CRM reinforcement - Scale 1:25

Transversal section

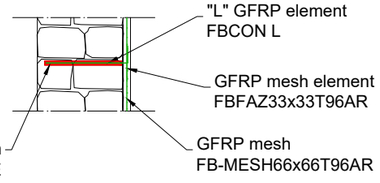

Frontal view

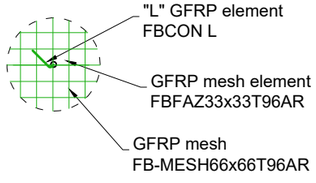

Artificial diaton - Scale 1:25

Transversal section

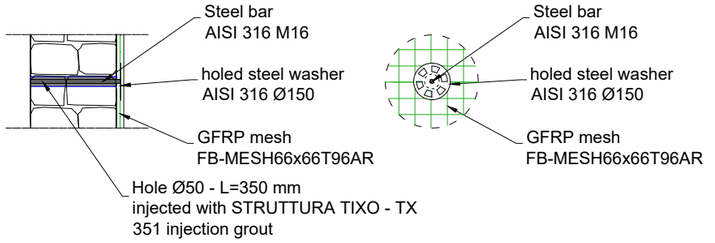

Frontal view

MATERIALS
For the masonry:
-Stones: sandstone, roughly squared, mean dimensions 12x15x20 cm³
-Hydraulic lime mortar: dosage lime-dry sand 1:5 (in volume)
200 kg of lime and 1400 of kg dry sand for 1m³ of mortar
Hydraulic lime "i.pro PLASTOCEM - Italcementi"
Silica sand "Sabbia lavata 0/6 mm - Dal Zotto Srl"
Add water so to obtain a plastic consistency for the mortar

NOTES:
Before installation wet the stones with sprinkle water
The mortar joints have to be as thin as possible

For the reinforcement:
- GFRP Mesh: FBMESH66x66T96AR (minimum overlapping lenght: 132 mm, placed at the half thickness of the mortar coating)
- GFRP local device: FBFAZ66x66T96AR
- GFRP L-shape connection: FBCON L 300x100 for stone masonry
  FCVIN400CE vinylester chemical anchor
- Mortar coating: FBNHL 15 MPa - natural lime mortar
- Artificial diatones: steel bars AISI 304 (or 316) M16 l=350 mm for stone masonry, Struttura Tixo - TX 351 injection grout or equivalent cementitious based grout with inroganic grow and antishrink additives, minimum compressive strength 50 MPa
- Holed steel washer Ø150, AISI 304 (or 316) with central nut M16

For the RC beam:
-concrete C25/30 and steel B450C

For steel bars:
-cold drawn steel, c40

BENDING TESTS ON MASONRY WALLS (B)

TOT n° of sample type "B": 3
TOT n° of tests type "B": 3
PLACE OF CONSTRUCTION AND TESTING: Trieste University Laboratory

Masonry type	Leafs	Reinforced
Solid brick	Single	X(I)
	Double	X(II)
Stone	Double	X(II)

(I) CRM on one side, GFRP L-shape connectors
(II) CRM on one side + diatones

Interreg ITALIA-SLOVENIJA | CONSTRAIN

TAV. **B.1**

BENDING TESTS ON MASONRY WALLS
TEST SET-UP
Quotes in cm - Scale 1:20

LATERAL VIEW (Scale 1:25)

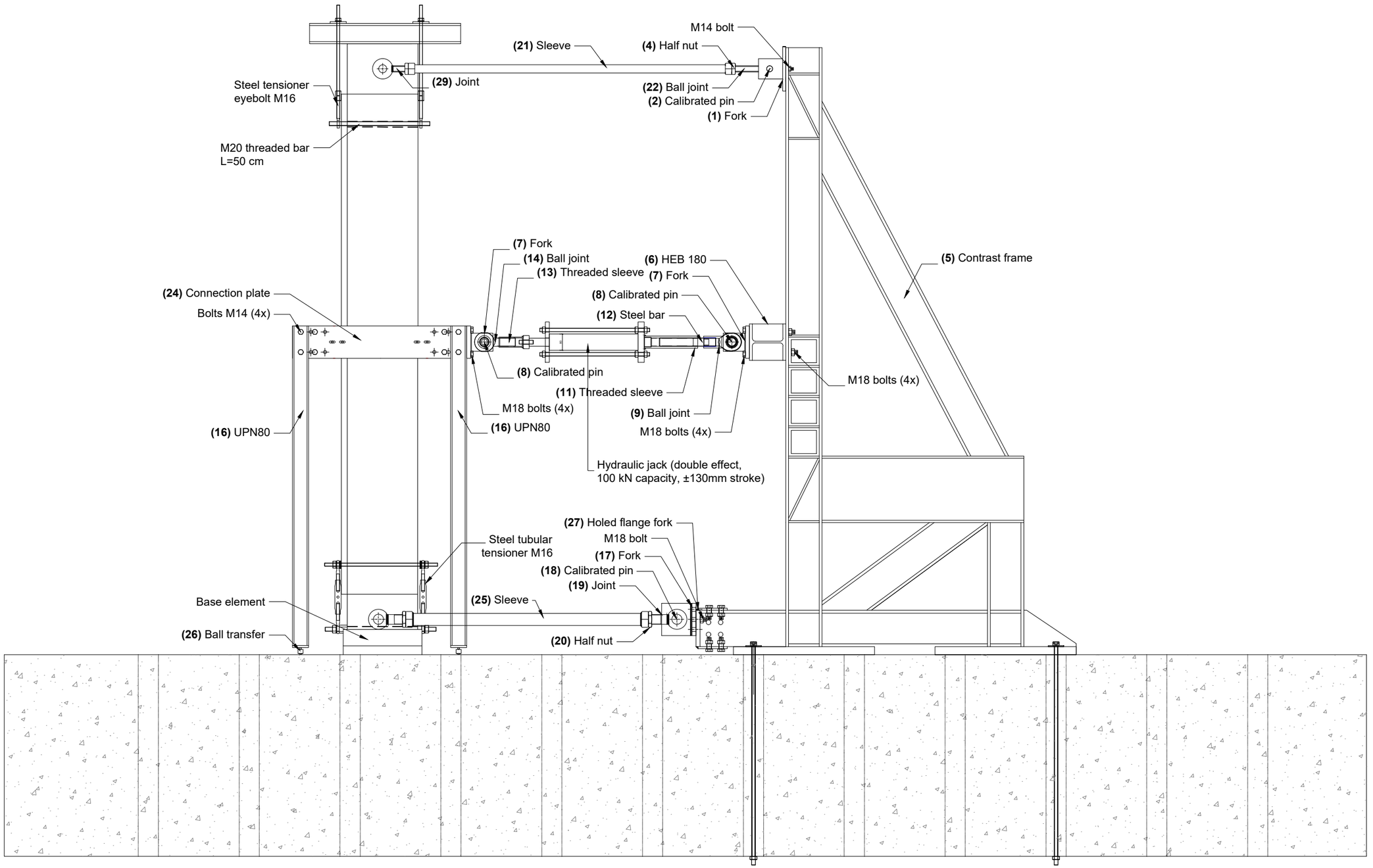

TAV.
B.2

BENDING TESTS ON MASONRY WALLS
TEST SET-UP
Quotes in cm - Scale 1:20

PLAN VIEW (Scale 1:25)

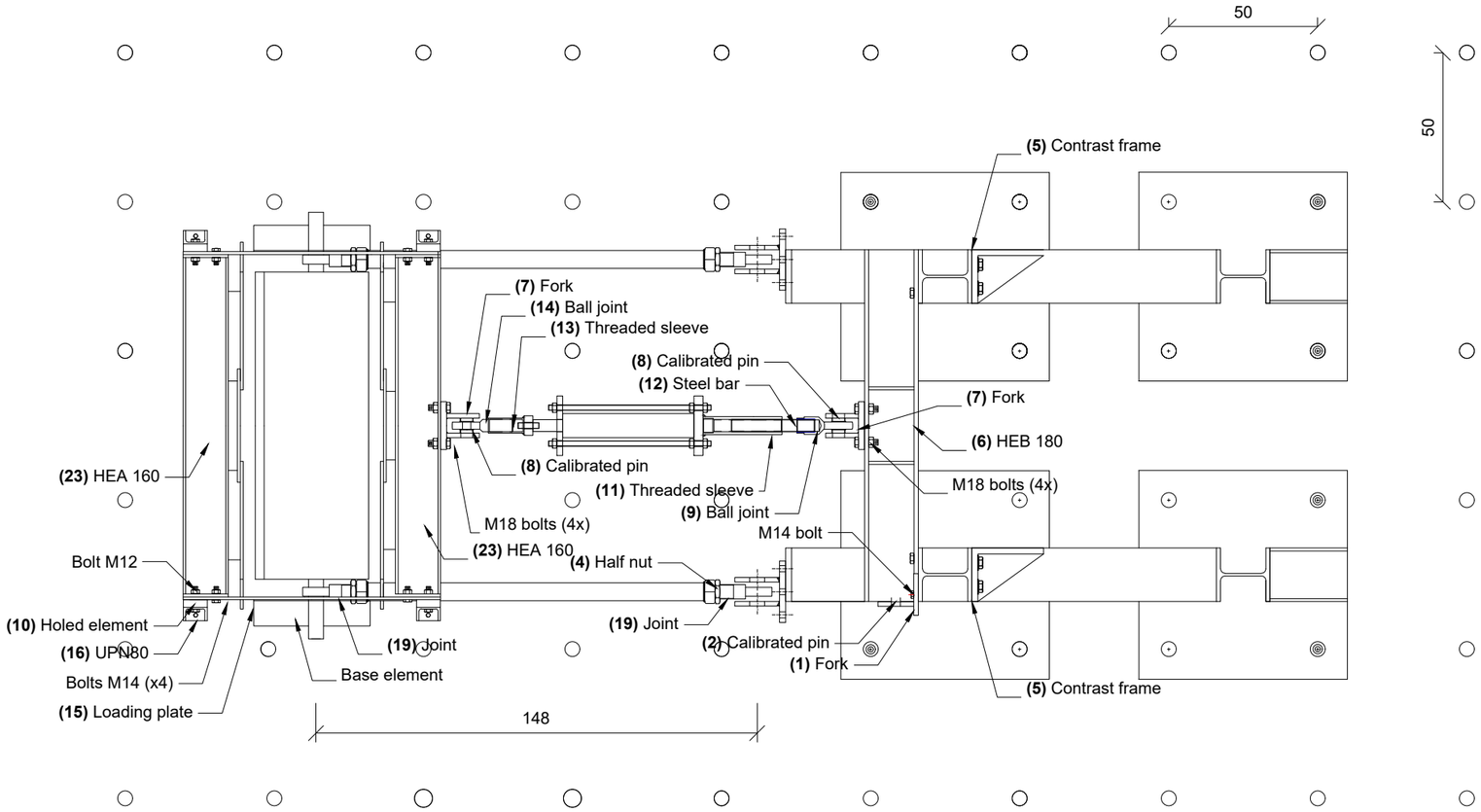

Interreg ITALIA-SLOVENIJA | CONSTRAIN

TAV. **B.3**

BENDING TESTS ON MASONRY WALLS
STEEL ELEMENTS DETAILS
Quotes in mm - Scale 1:5

(23) HEA 160 - steel 275 (2x)

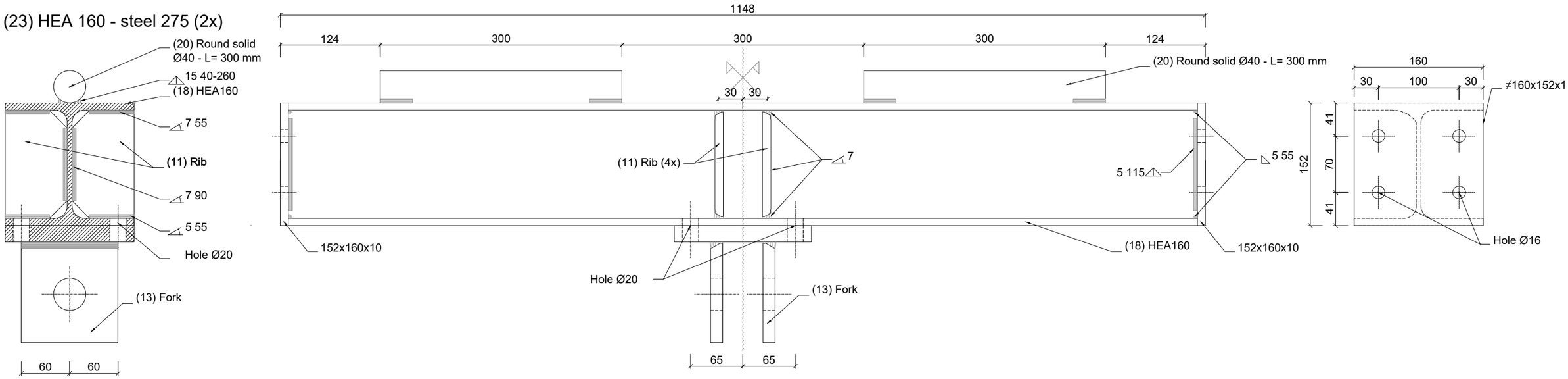

(15) LOADING PLATE with pins - steel S275 (2x)

Lateral view

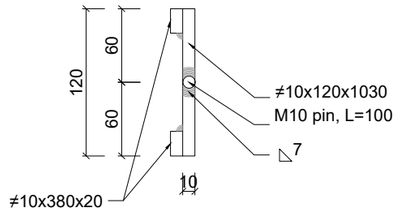

Front view

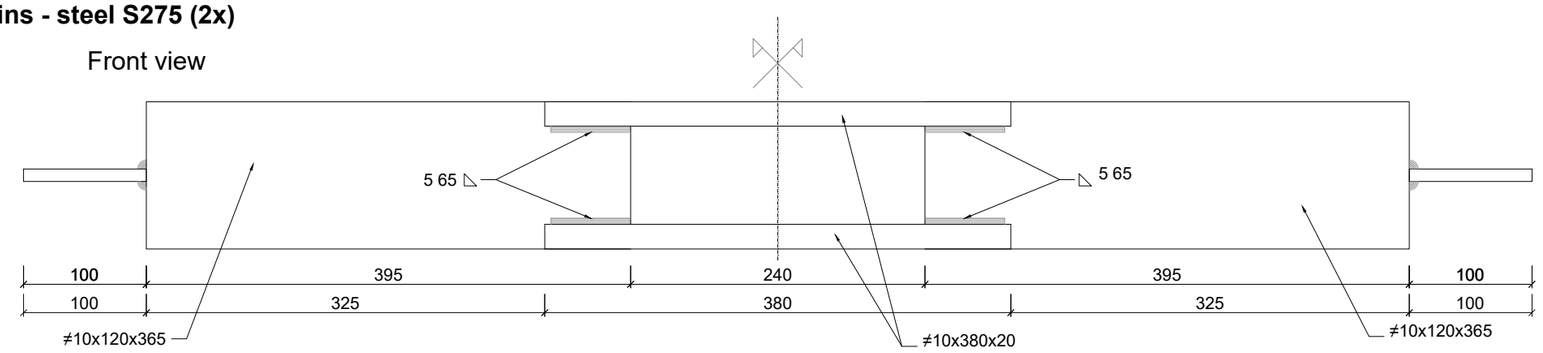

Top view

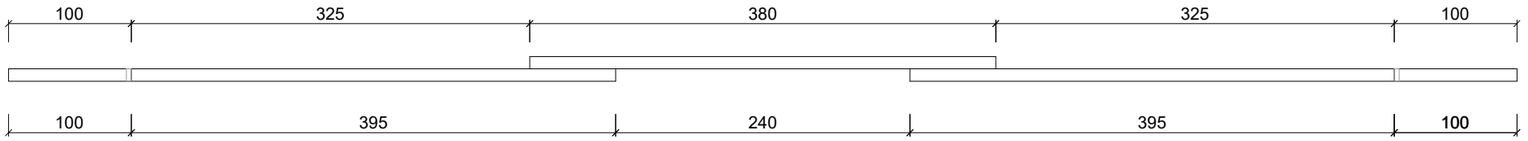

TAV.
B.4

BENDING TESTS ON MASONRY WALLS
STEEL ELEMENTS DETAILS

Quotes in cm - Scale 1:5

(7) FORK with Ø40 calibrated hole - steel S275 (2x)

Front view

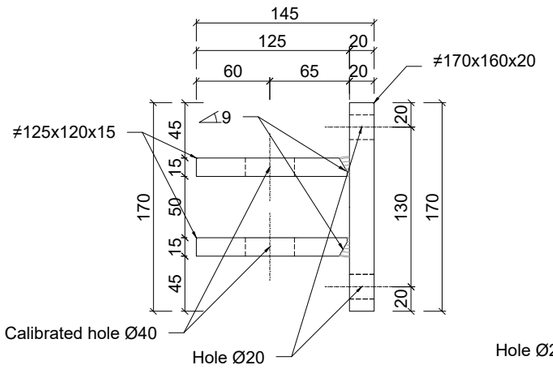

Plan view

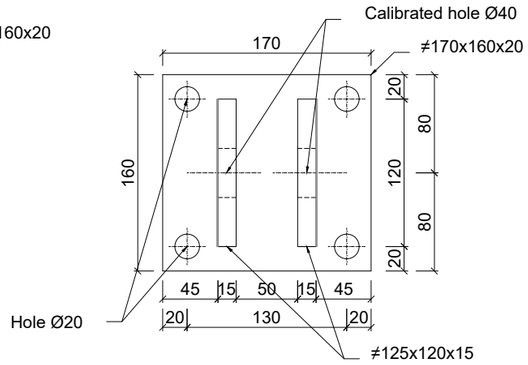

Lateral view

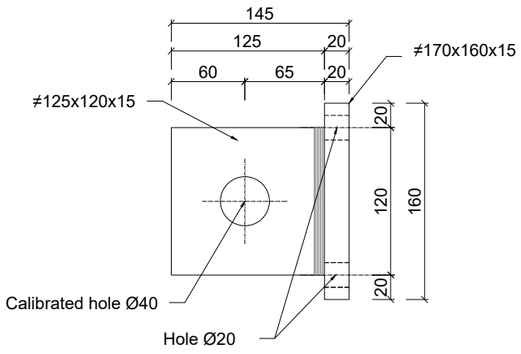

(17) FORK with Ø50 calibrated hole - steel S275 (2x)

Lateral view

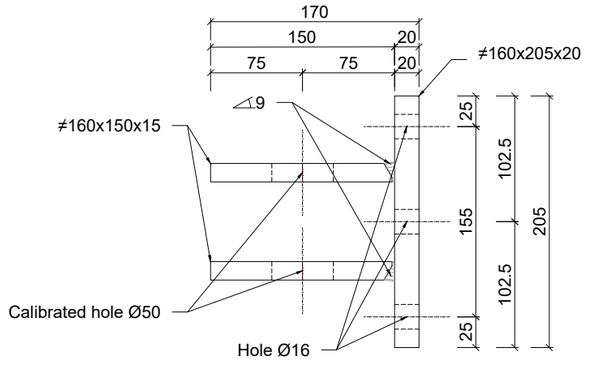

Plan view

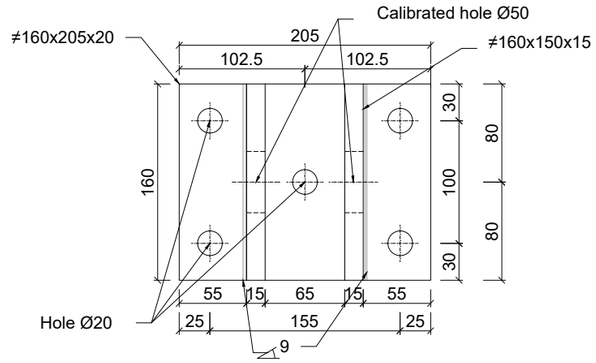

Lateral view

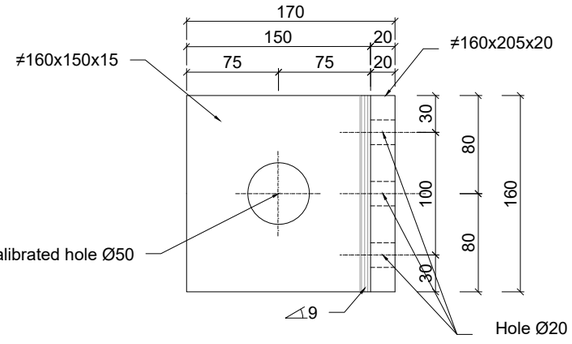

(4) Half nut - steel 8.8 (x4)

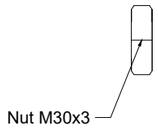

(20) Half nut - steel 8.8 (x4)

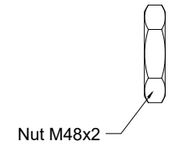

(11) THREADED SLEEVE - steel S275 (1x)

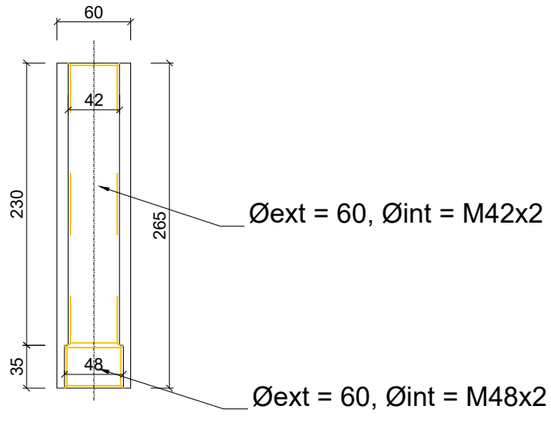

(19) HINGE JOINT MALE Ø50.5 steel S275 (4x)

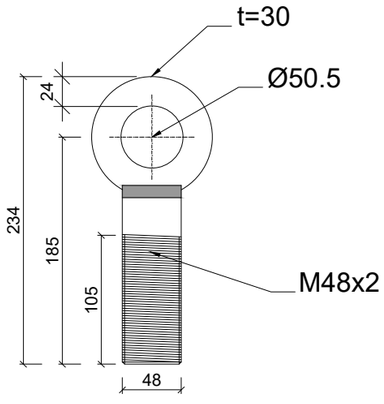

(29) HINGE JOINT MALE Ø40.5 steel S275 (2x)

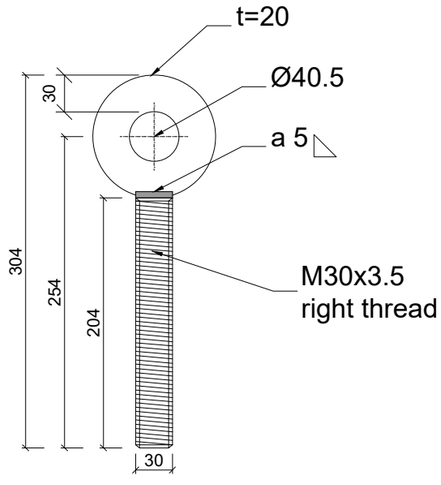

(22) BALL JOINT MALE Ø30 - steel S275 (2x)

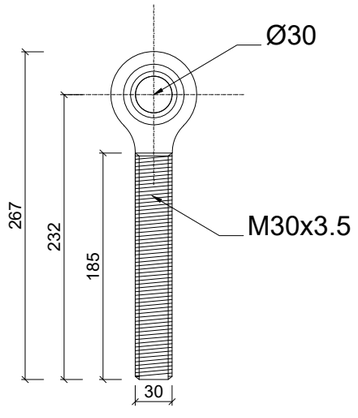

TAV.
B.5

BENDING TESTS ON MASONRY WALLS
STEEL ELEMENTS DETAILS

Quotes in cm - Scale 1:5

(1) FORK with Ø30 calibrated hole - steel S275 (2x)

Front view

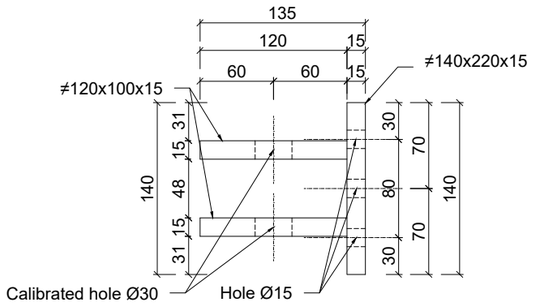

Plan view

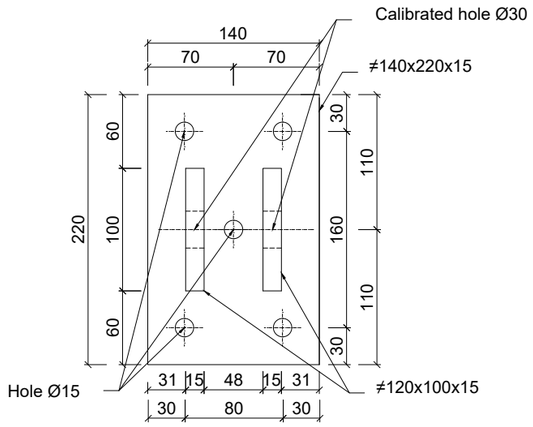

Lateral view

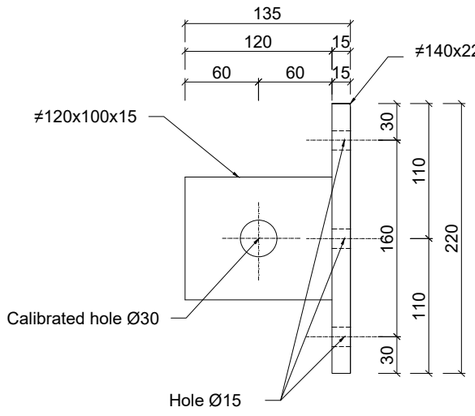

(2) CALIBRATED DOWEL PINS C40 steel (2x)

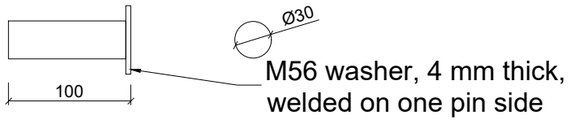

(8) CALIBRATED DOWEL PINS C40 steel (2x)

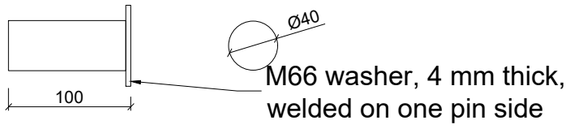

(10) Holed element - steel 275 (4x)

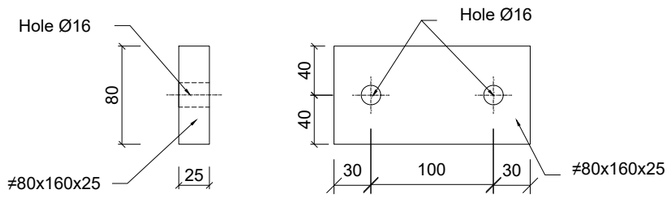

(18) CALIBRATED DOWEL PINS C40 steel (2x)

(27) Holed flange fork right - steel S275 (1x)

Front view

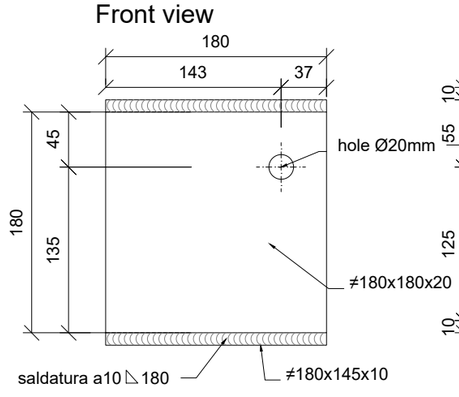

Lateral view

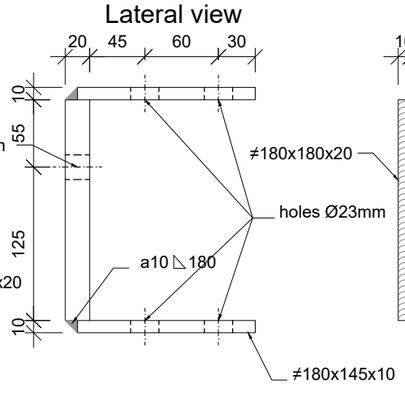

Plan view

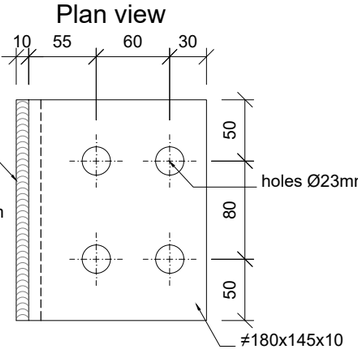

(27) Holed flange fork left - steel S275 (1x)

Front view

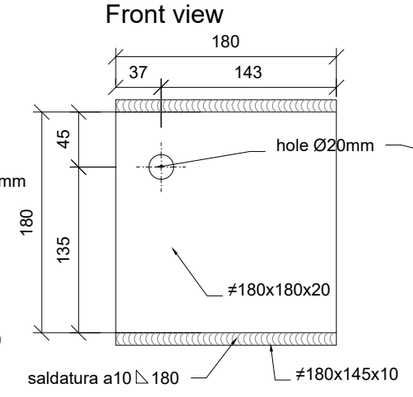

Lateral view

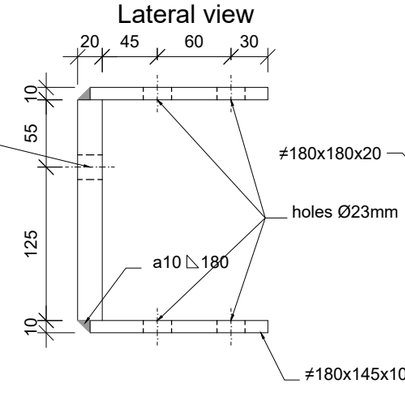

Plan view

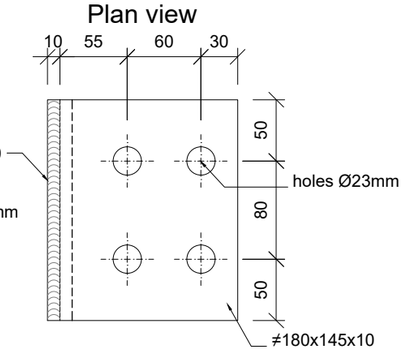

TAV.
B.6

BENDING TESTS ON MASONRY WALLS
STEEL ELEMENTS DETAILS

Quotes in cm - Scale 1:5

(6) HEB 180 - steel 275 (1x)

Back view

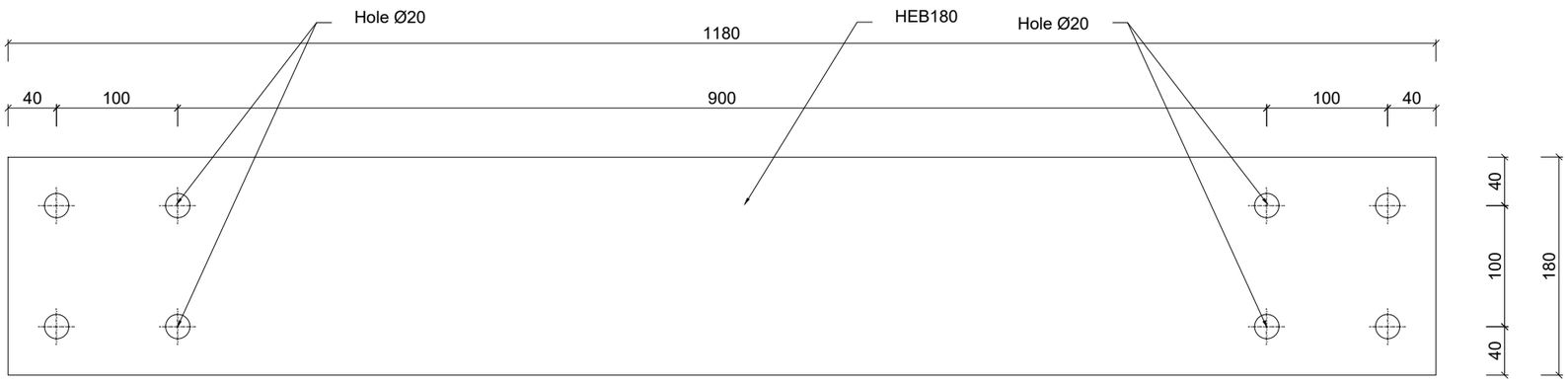

M20 threaded bars (8x) - Steel 8.8

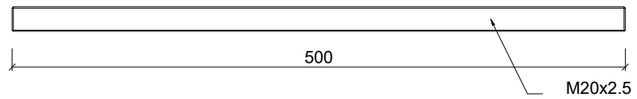

Top view

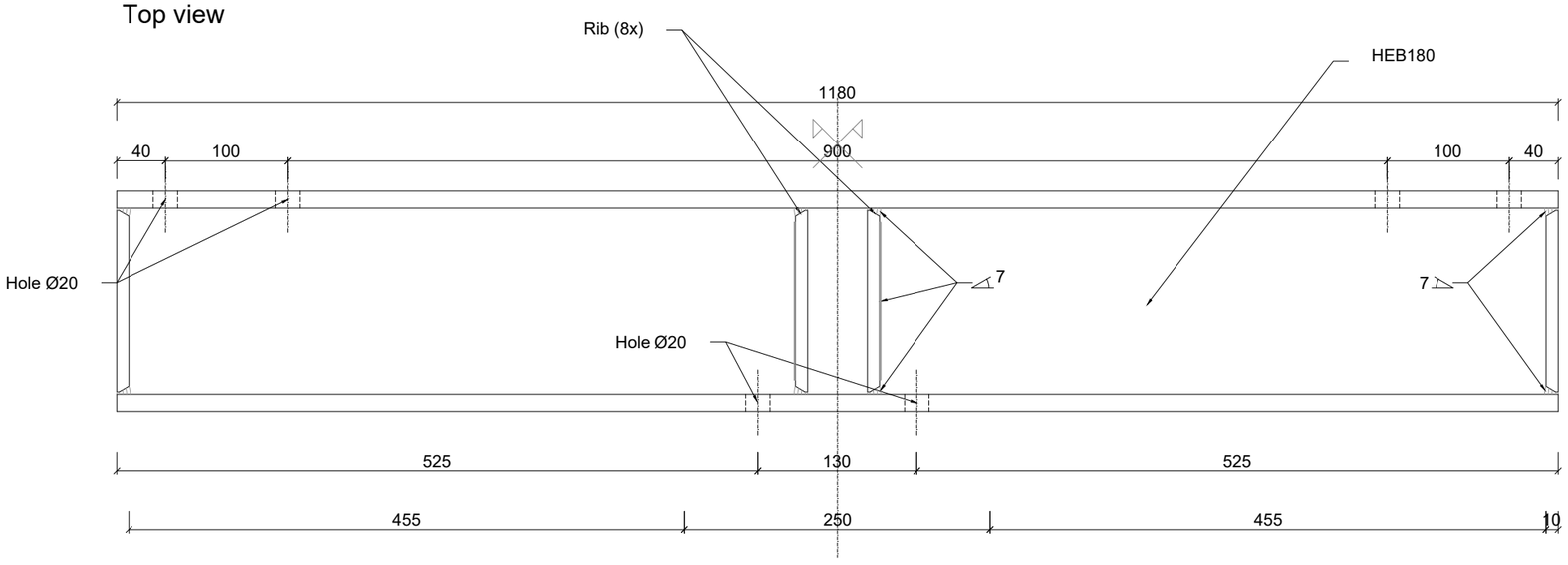

Lateral view

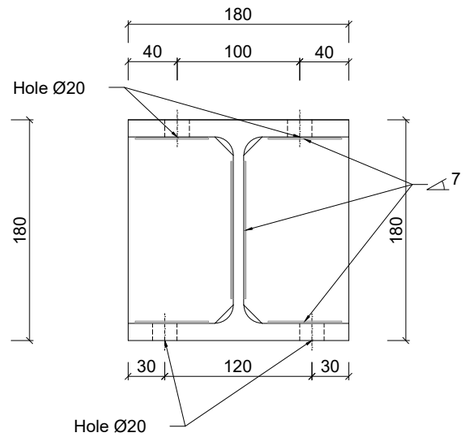

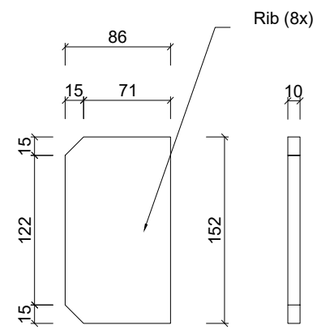

Steel tubular tensioners (8x)

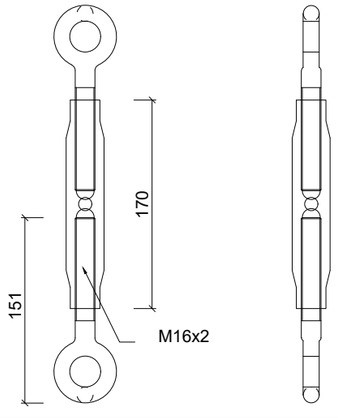

Frontal view

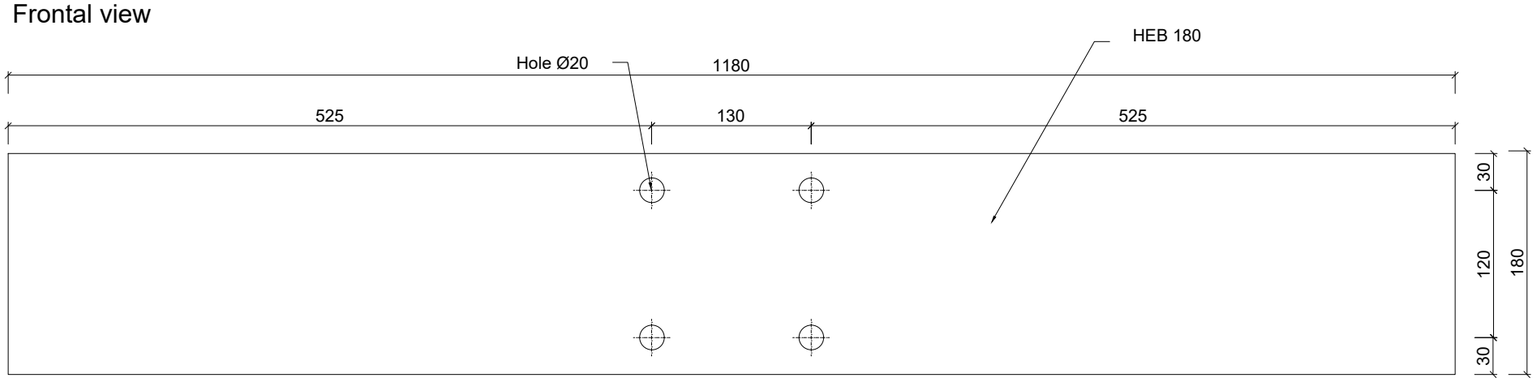

Interreg ITALIA-SLOVENIJA | CONSTRAIN

TAV. B.7

BENDING TESTS ON MASONRY WALLS
STEEL ELEMENTS DETAILS

Quotes in cm - Scale 1:5

(16) UPN80 - steel 275 (4x)

Frontal view

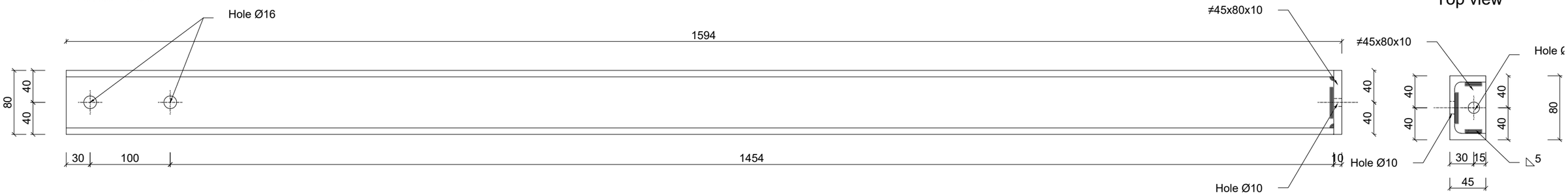

Top view

(21) Sleeve - S275 (x2)

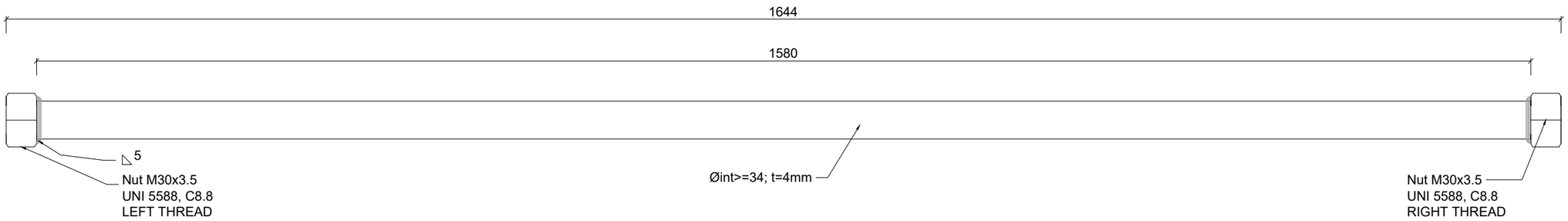

(25) Sleeve - S275 (x2)

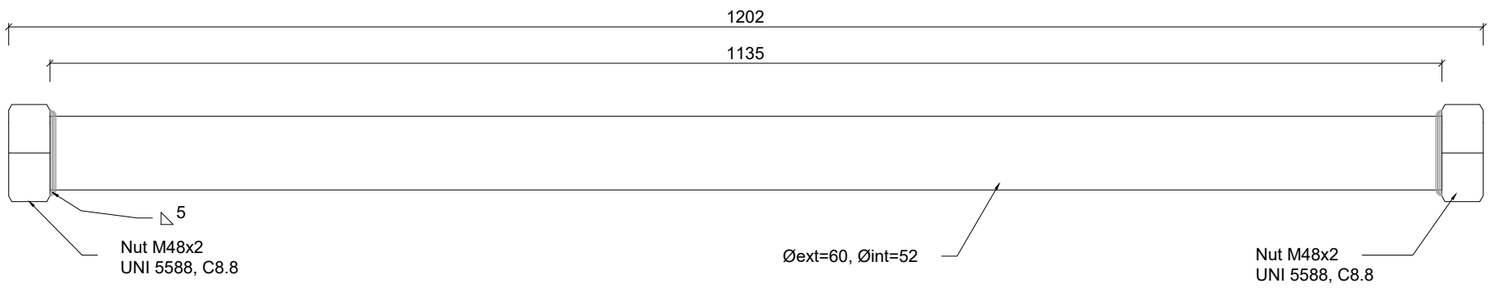

(12) THREADED BAR M42x2 steel steel 8.8 (1x)

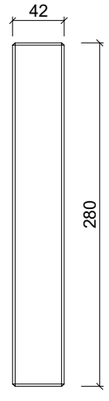

(24) CONNECTION PLATE - steel S275 (2x)

Lateral view

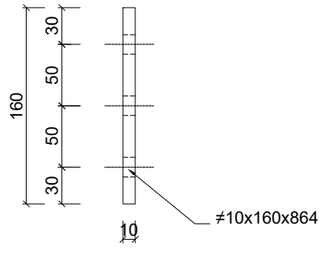

Front view

TAV.
B.8

BENDING TESTS ON MASONRY WALLS
STEEL ELEMENTS DETAILS
Quotes in cm - Scale 1:5

ACTUATOR Lateral view

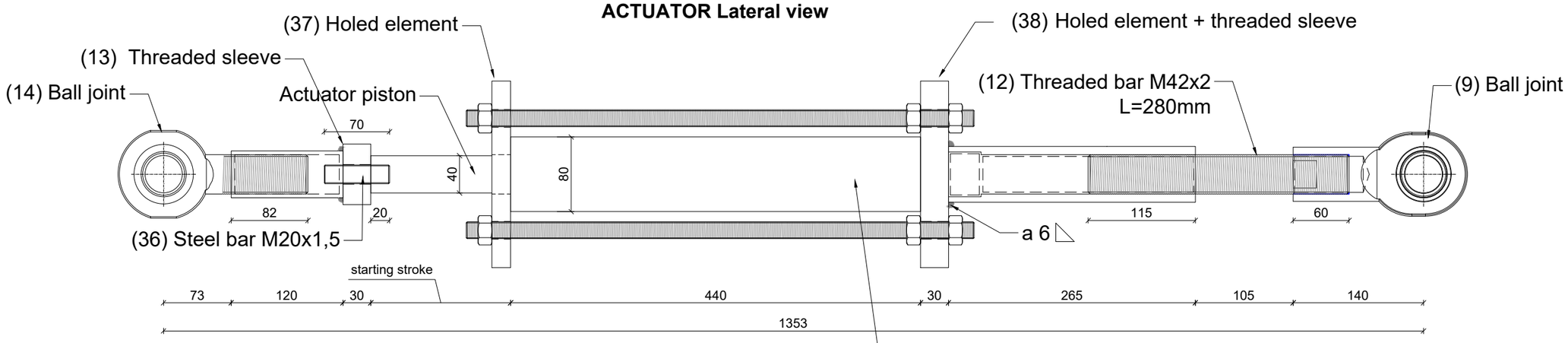

Actuator HYDRAFORE YG-20300S
Max stroke :300 mm
Capacity: push 198 kN , pull 110 kN
Oil capacity: push 848 cm³ , pull 471 cm³

(13) THREADED SLEEVE - steel S275 and C40 (1x)

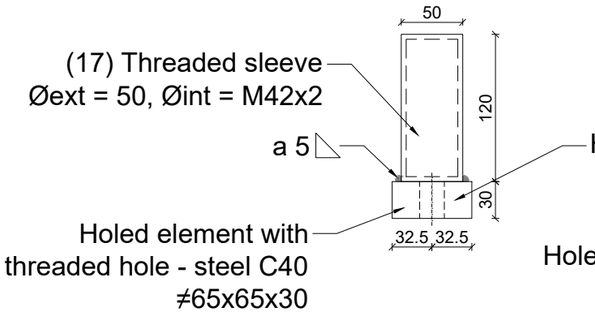

(36) STEEL BAR M20X1,5 - steel 8.8 (1x)

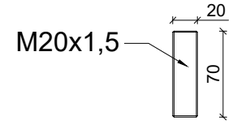

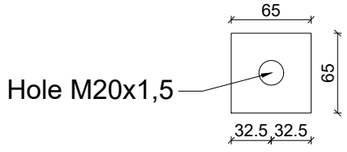

(37) HOLED ELEMENT - steel S275 (1x)

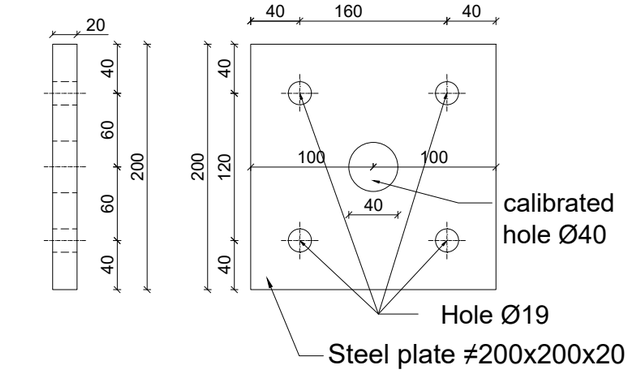

(38) HOLED ELEMENT + THREADED SLEEVE - steel S275 (1x)

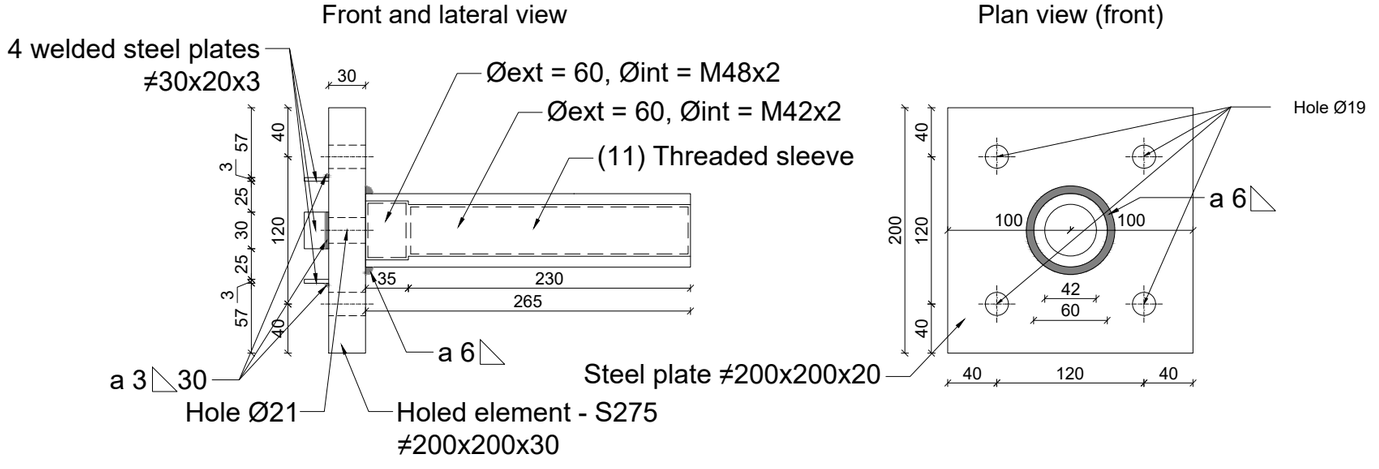

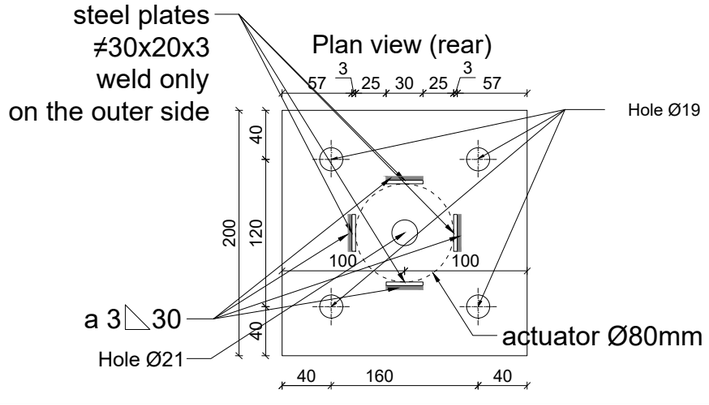

TAV.
S1

SHEAR-BENDING TESTS ON MASONRY SPANDRELS
SAMPLE CHARACTERISTICS
Quotes in cm - Scale 1:50

SOLID BRICK MASONRY - SINGLE LEAF (CRM on one side + Artificial Diatons)
S-B1

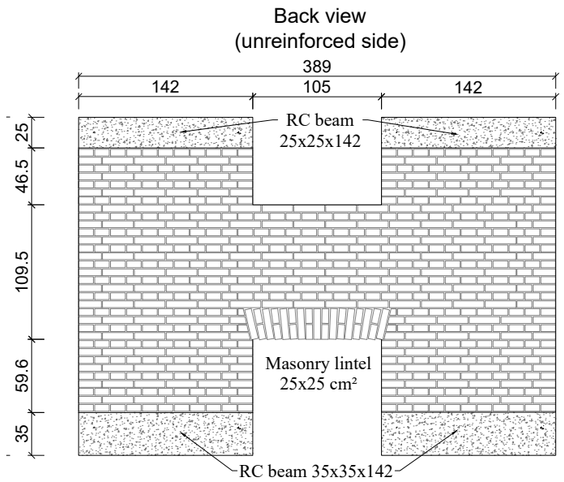

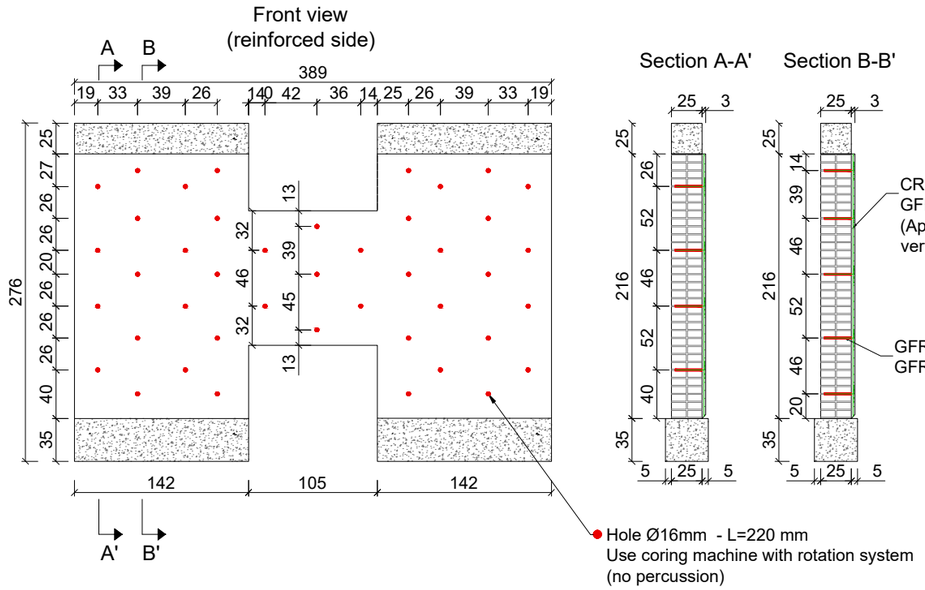

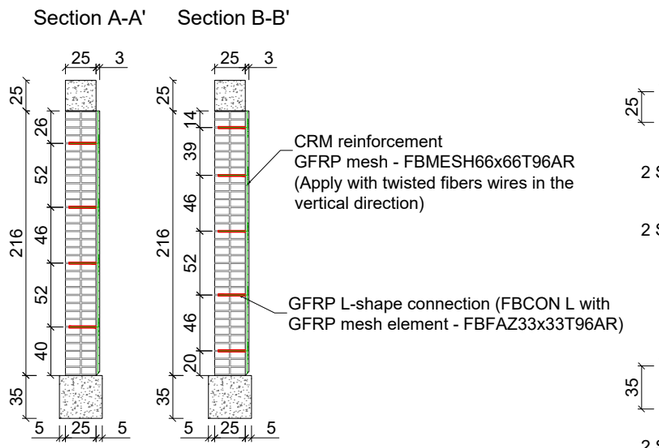

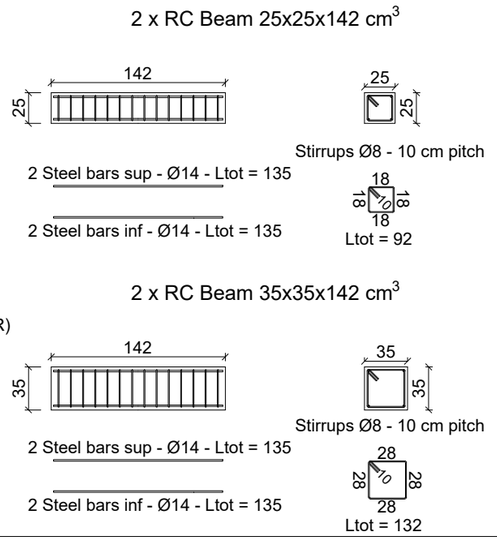

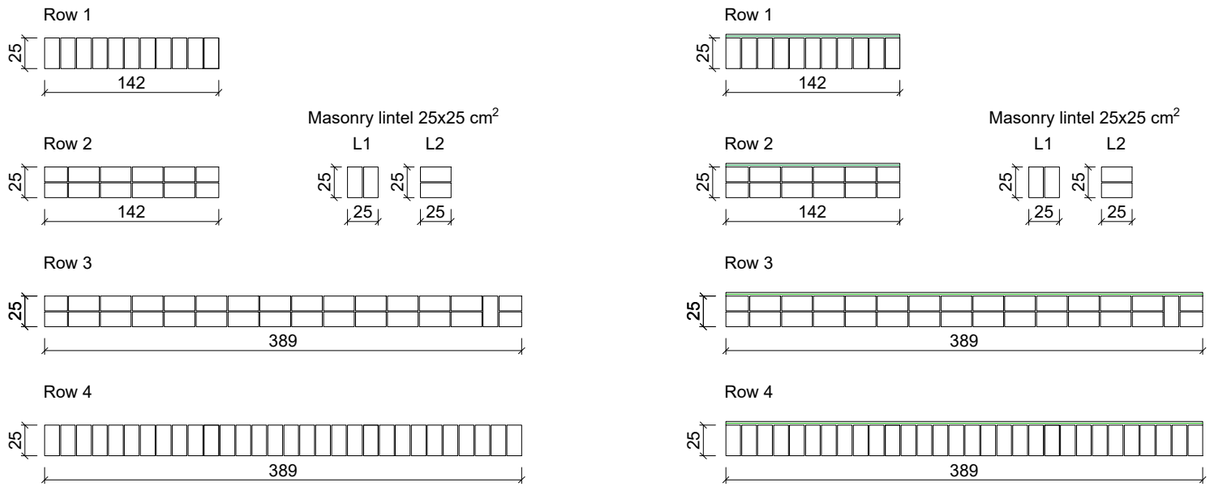

CRM reinforcement - Scale 1:25

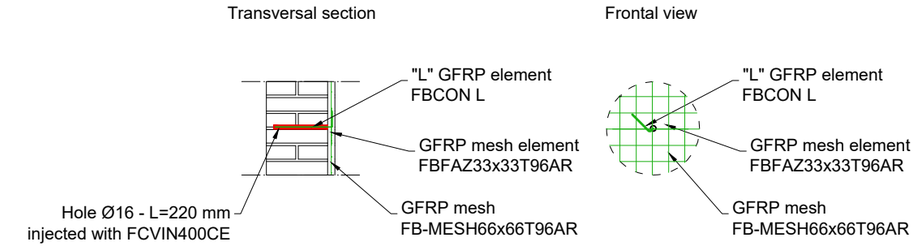

MATERIALS
For the masonry:
- Solid bricks UNI 5.5x12x25 "San Marco Rosso Vivo - Terreal"
- Hydraulic lime mortar: dosage lime-dry sand 1:5 (in volume)
  200 kg of lime and 1400 of kg dry sand for 1m³ of mortar
  Hydraulic lime "i.pro PLASTOCEM - Italcementi"
  Silica sand "Sabbia lavata 0/6 mm - Dal Zotto Srl"
  Add water so to obtain a plastic consistency for the mortar

NOTES:
Before installation, immerse the bricks in water till complete saturation (around 1 hour)
The mortar joints have a thickness of 1 cm

For the reinforcement:
- GFRP Mesh: FBMESH66x66T96AR (minimum overlapping lenght: 132 mm, placed at the half thickness of the mortar coating)
- GFRP local device: FBFAZ66x66T96AR
- GFRP L-shape connection: FBCON L 200x100 for solid brick masonry
  FCVIN400CE vinylester chemical anchor
- Mortar coating: FBNHL 15 MPa - natural lime mortar

SHEAR-BENDING TESTS ON MASONRY SPANDRELS (S)

TOT n° of sample type "S": 4
TOT n° of tests type "S": 8
PLACE OF CONSTRUCTION AND TESTING: Ljubljana University Laboratory

Masonry type	Leafs	Unreinforced	Retrofitted
Solid brick	Single	X	X(I)
	Double	X	X(II)
Stone	Double	X	X(II)
		X	X(III)

(I) CRM on one side, GFRP L-shape connectors
(II) CRM on one side + diatones
(III) CRM on both sides, GFRP L-shape passing-through connectors

TAV.
S2

SHEAR-BENDING TESTS ON MASONRY SPANDRELS
SAMPLE CHARACTERISTICS
Quotes in cm - Scale 1:50

SOLID BRICK MASONRY - DOUBLE LEAF (CRM on one side + Artificial Diatons)
S-B2

Back view
(unreinforced side)

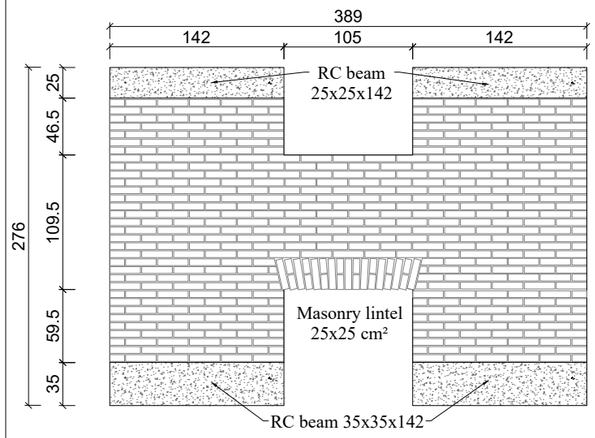

Front view
(reinforced side)

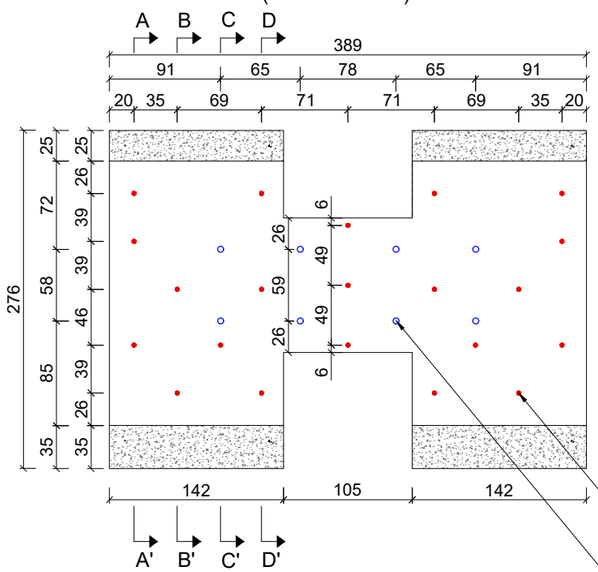

Section A-A'

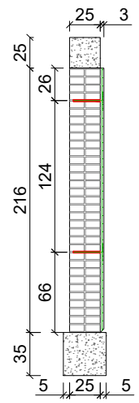

Section B-B'

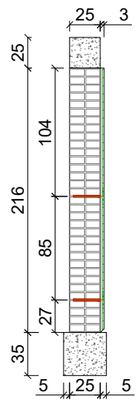

Section D-D'

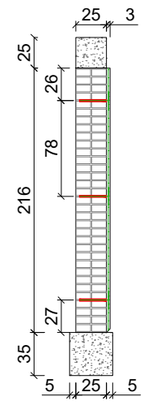

Section C-C'

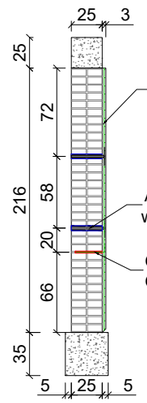

CRM reinforcement
GFRP mesh - FBMESH66x66T96AR
(Apply with twisted fibers wires in the vertical direction)

Artificial diaton (Steel bar AISI Ø16 with holed steel washer AISI Ø150)

GFRP L-shape connection (FBCON L with GFRP mesh element - FBFAZ33x33T96AR)

Hole Ø16mm - L=220 mm
Use coring machine with rotation system (no percussion)

Hole Ø50mm - L=250 mm (passing through)
Use coring machine with rotation system (no percussion)

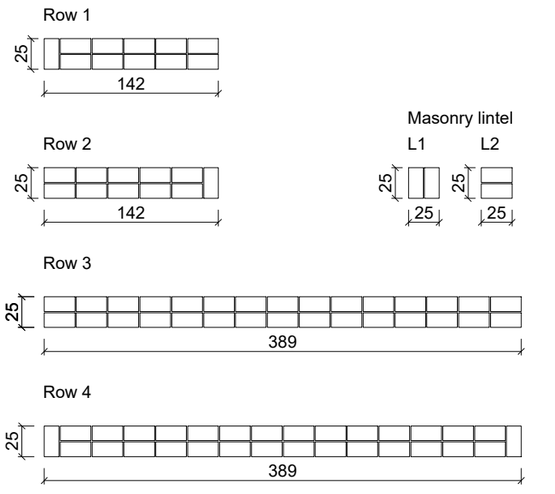

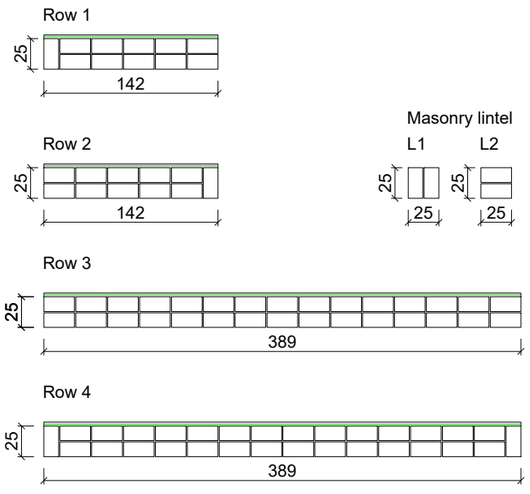

2 x RC Beam 25x25x142 cm³

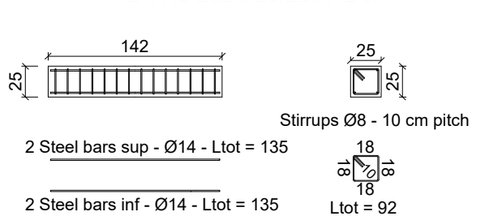

2 x RC Beam 35x35x142 cm³

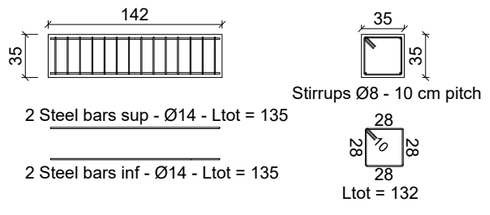

MATERIALS
- Solid bricks UNI 5.5x12x25 "San Marco Rosso Vivo - Terreal"
- Hydraulic lime mortar: dosage lime-dry sand 1:5 (in volume)
  200 kg of lime and 1400 of kg dry sand for 1m³ of mortar
  Hydraulic lime "i.pro PLASTOCEM - Italcementi"
  Silica sand "Sabbia lavata 0/6 mm - Dal Zotto Srl"
  Add water so to obtain a plastic consistency for the mortar

NOTES:
Before installation, immerse the bricks in water till complete saturation (around 1 hour)
The mortar joints have a thickness of 1 cm

For the reinforcement:
- GFRP Mesh: FBMESH66x66T96AR (minimum overlapping lenght: 132 mm, placed at the half thickness of the mortar coating)
- GFRP local device: FBFAZ66x66T96AR
- GFRP L-shape connection: FBCON L 200x100 for solid brick masonry
  FCVIN400CE vinylester chemical anchor
- Mortar coating: FBNHL 15 MPa - natural lime mortar
- Artificial diatones: steel bars AISI 304 (or 316) M16 l=350 mm for stone masonry, Struttura Tixo - TX 351 injection grout or equivalent cementitious based grout with inroganic grow and antishrink additives, minimum compressive strength 50 MPa
- Holed steel washer Ø150, AISI 304 (or 316) with central nut M16

For the RC beam:
- concrete C25/30 and steel B450C

CRM reinforcement - Scale 1:25

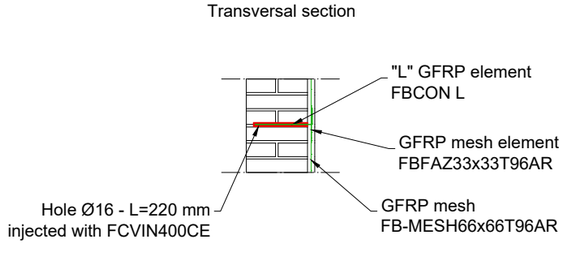

Artificial diaton - Scale 1:25

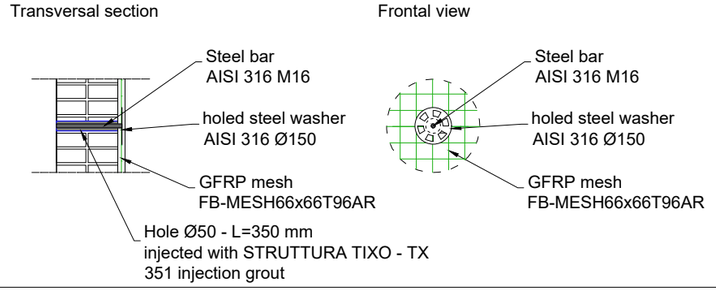

SHEAR-BENDING TESTS ON MASONRY SPANDRELS (S)

TOT n° of sample type "S": 4
TOT n° of tests type "S": 8
PLACE OF CONSTRUCTION AND TESTING: Ljubljana University Laboratory

Masonry type	Leafs	Unreinforced	Retrofitted
Solid brick	Single	X	X(I)
	Double	X	X(II)
Stone	Double	X	X(II)
		X	X(III)

(I) CRM on one side, GFRP L-shape connectors
(II) CRM on one side + diatones
(III) CRM on both sides, GFRP L-shape passing-through connectors

TAV.
S3

SHEAR-BENDING TESTS ON MASONRY SPANDRELS
SAMPLE CHARACTERISTICS
Quotes in cm - Scale 1:50

STONE MASONRY - DOUBLE LEAF (CRM on one side + Artificial Diatons)
S-R2-1

Back view
(unreinforced side)

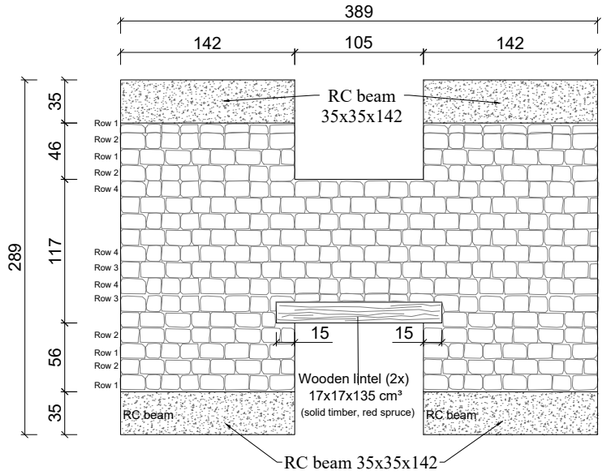

Front view
(reinforced side)

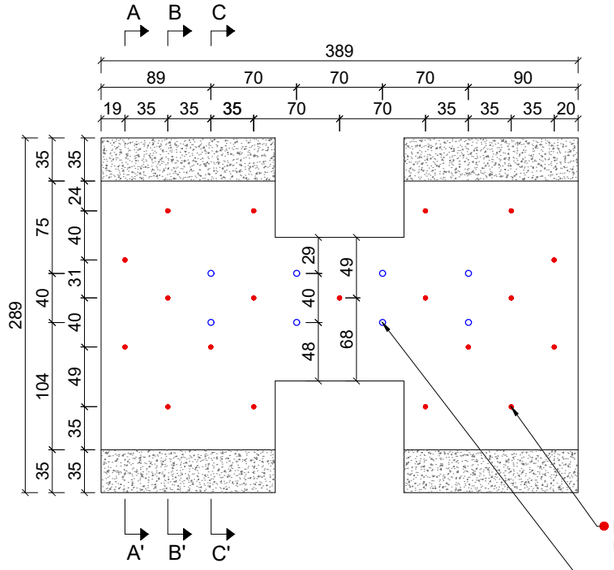

Section A-A'

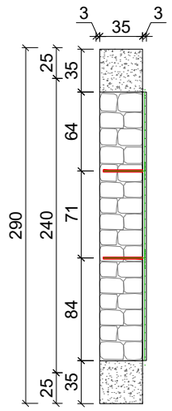

Section B-B'

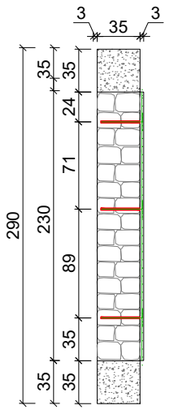

Section C-C'

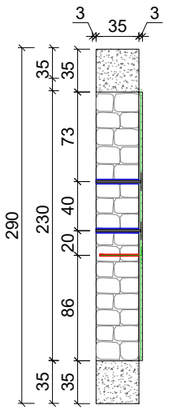

Hole Ø16mm - L=320 mm
Use coring machine with rotation system
(no percussion)

Hole Ø50mm - L=350 mm (passing through)
Use coring machine with rotation system (no percussion)

Row 1

Row 2

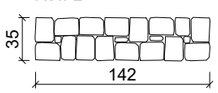

Wooden lintel

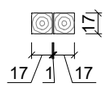

Row 3

Row 4

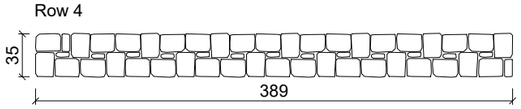

Row 1

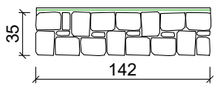

Row 2

Row 3

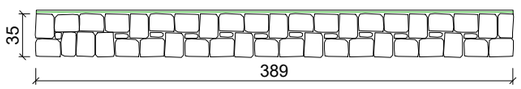

Row 4

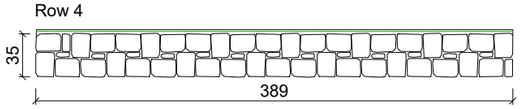

4 x RC Beam 35x35x142 cm³

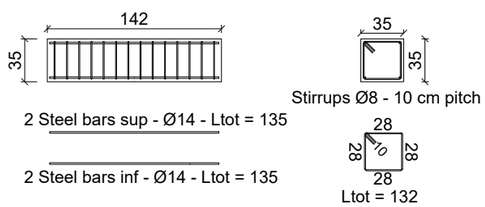

MATERIALS
- Stones: sandstone, roughly squared, mean dimensions 12x15x20 cm³
- Hydraulic lime mortar: dosage lime-dry sand 1:5 (in volume)
  200 kg of lime and 1400 of kg dry sand for 1m³ of mortar
  Hydraulic lime "i.pro PLASTOCEM - Italcementi"
  Silica sand "Sabbia lavata 0/6 mm - Dal Zotto Srl"
  Add water so to obtain a plastic consistency for the mortar

NOTES:
Before installation, clean thoroughly the stones with water.
The mortar joints have to be as thin as possible

For the reinforcement:
- GFRP Mesh: FBMESH66x66T96AR (minimum overlapping lenght: 132 mm, placed at the half thickness of the mortar coating)
- GFRP local device: FBFAZ66x66T96AR
- GFRP L-shape connection: FBCON L 300x100 for stone masonry
  FCVIN400CE vinylester chemical anchor
- Mortar coating: FBNHL 15 MPa - natural lime mortar
- Artificial diatones: steel bars AISI 304 (or 316) M16 l=350 mm for stone masonry, Struttura Tixo - TX 351 injection grout or equivalent cementitious based grout with inroganic grow and antishrink additives, minimum compressive strength 50 MPa
- Holed steel washer Ø150, AISI 304 (or 316) with central nut M16

For the RC beam:
- concrete C25/30 and steel B450C

CRM reinforcement - Scale 1:25

Transversal section

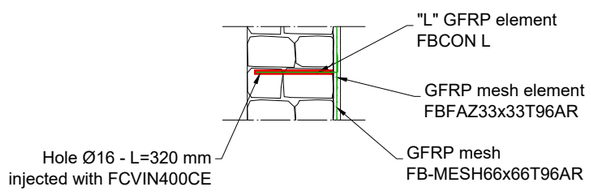

Frontal view

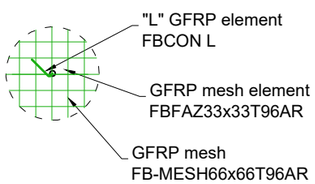

Artificial diaton - Scale 1:25

Transversal section

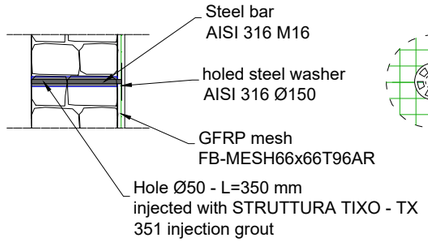

Frontal view

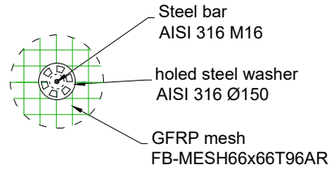

SHEAR-BENDING TESTS ON MASONRY SPANDRELS (S)

TOT n° of sample type "S": 4
TOT n° of tests type "S": 8
PLACE OF CONSTRUCTION AND TESTING: Ljubljana University Laboratory

Masonry type	Leafs	Unreinforced	Retrofitted
Solid brick	Single	X	X(I)
	Double	X	X(II)
Stone	Double	X	X(II)
		X	X(III)

(I) CRM on one side, GFRP L-shape connectors
(II) CRM on one side + diatones
(III) CRM on both sides, GFRP L-shape passing-through connectors

TAV.
S4

SHEAR-BENDING TESTS ON MASONRY SPANDRELS
SAMPLE CHARACTERISTICS

Quotes in cm - Scale 1:50

STONE MASONRY - DOUBLE LEAF (CRM on one side + Artificial Diatons)
S-R2-2

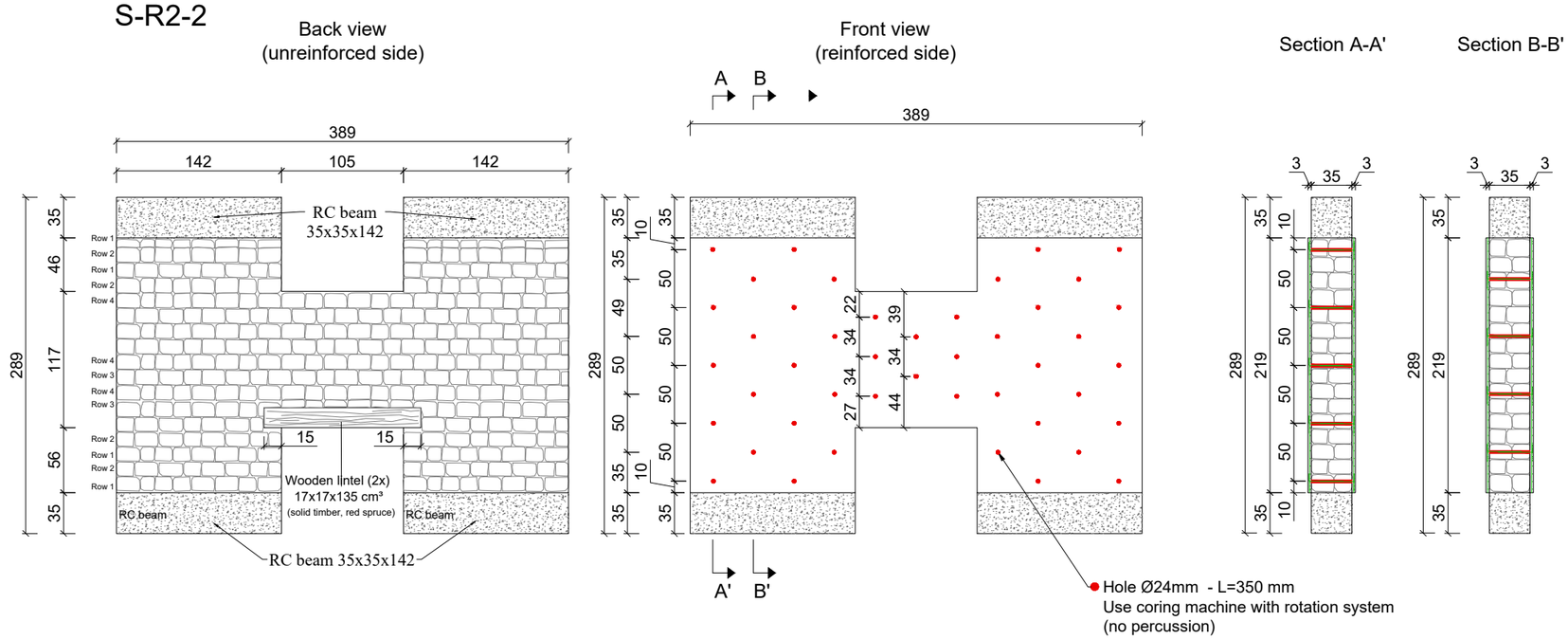

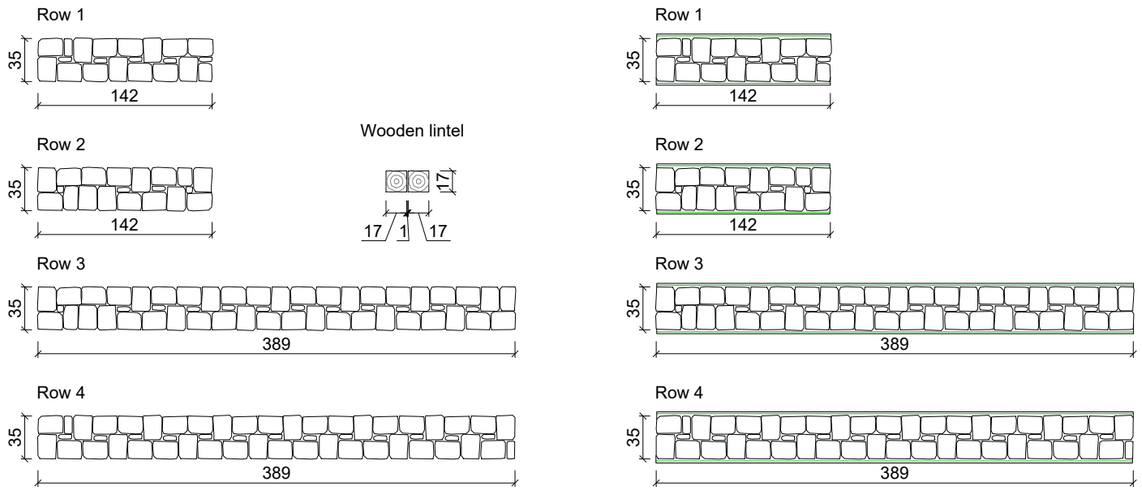

4 x RC Beam 35x35x142 cm³

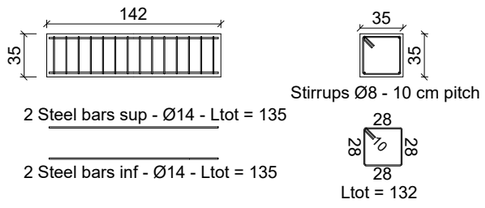

CRM reinforcement - Scale 1:25

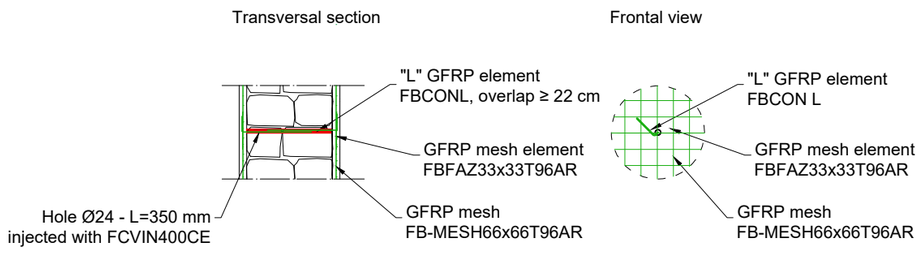

MATERIALS
- Stones: sandstone, roughly squared, mean dimensions 12x15x20 cm³
- Hydraulic lime mortar: dosage lime-dry sand 1:5 (in volume)
  200 kg of lime and 1400 of kg dry sand for 1m³ of mortar
  Hydraulic lime "i.pro PLASTOCEM - Italcementi"
  Silica sand "Sabbia lavata 0/6 mm - Dal Zotto Srl"
  Add water so to obtain a plastic consistency for the mortar

NOTES:
Before installation, clean thoroughly the stones with water.
The mortar joints have to be as thin as possible

For the reinforcement:
- GFRP Mesh: FBMESH66x66T96AR (minimum overlapping lenght: 132 mm, placed at the half thickness of the mortar coating)
- GFRP local device: FBFAZ66x66T96AR
- GFRP L-shape connection: FBCON L 300x100 for stone masonry
  FCVIN400CE vinylester chemical anchor
- Mortar coating: FBNHL 15 MPa - natural lime mortar

For the RC beam:
- concrete C25/30 and steel B450C

SHEAR-BENDING TESTS ON MASONRY SPANDRELS (S)

TOT n° of sample type "S": 4
TOT n° of tests type "S": 8
PLACE OF CONSTRUCTION AND TESTING: Ljubljana University Laboratory

Masonry type	Leafs	Unreinforced	Retrofitted
Solid brick	Single	X	X(I)
	Double	X	X(II)
Stone	Double	X	X(II)
		X	X(III)

(I) CRM on one side, GFRP L-shape connectors
(II) CRM on one side + diatones
(III) CRM on both sides, GFRP L-shape passing-through connectors

TAV.

T

BENDING TESTS ON TOP TIE MASONRY BEAMS
SAMPLE CHARACTERISTICS

Quotes in cm - Scale 1:50

SOLID BRICK MASONRY - SINGLE LEAF
T-B1

Frontal view

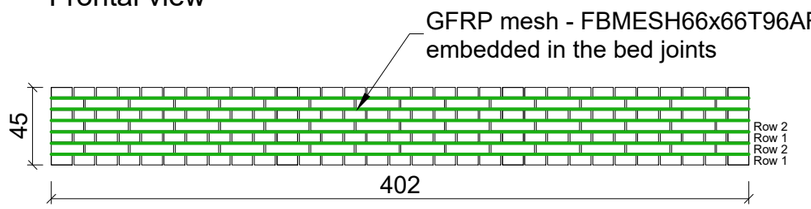

Lateral view

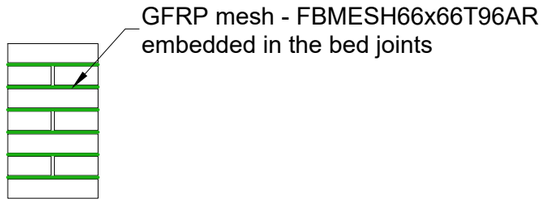

SCALE 1:25

Horizontal sections

Row 1

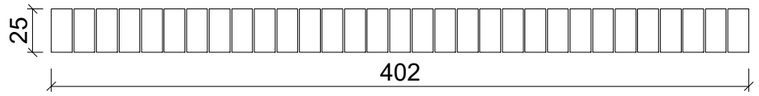

Row 2

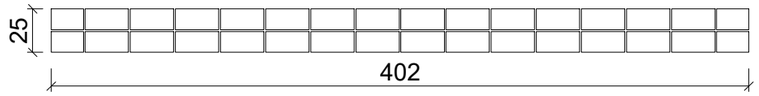

STONE MASONRY - DOUBLE LEAF
T-R2

Frontal view

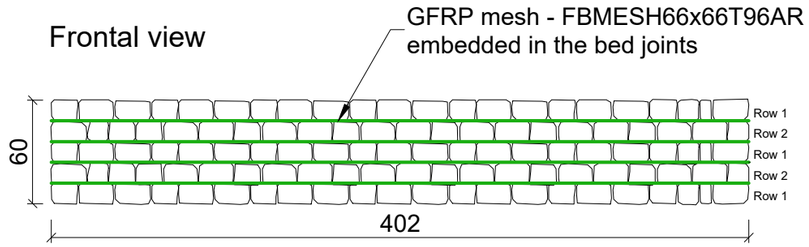

Lateral view

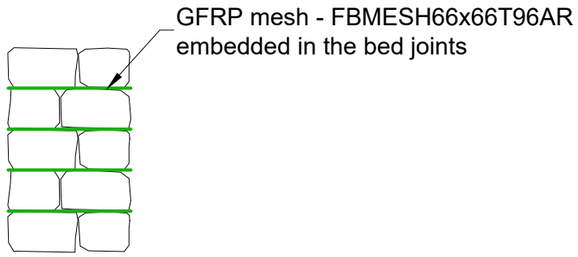

SCALE 1:25

Horizontal sections

Row 1

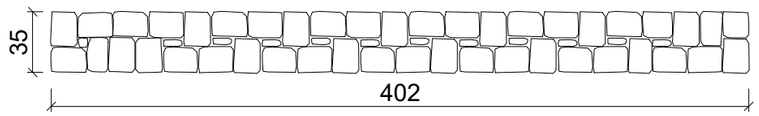

Row 2

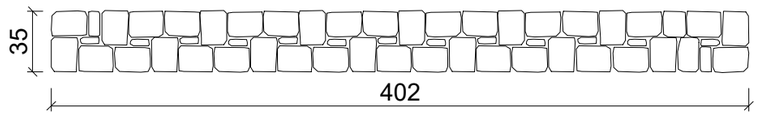

MATERIALS
- Solid bricks UNI 5.5x12x25 "San Marco Rosso Vivo - Terreal"
- Stones: sandstone, roughly squared, mean dimensions 12x15x20 cm³
- Hydraulic lime mortar: dosage lime-dry sand 1:5 (in volume)
  200 kg of lime and 1400 of kg dry sand for 1m³ of mortar
  Hydraulic lime "i.pro PLASTOCEM - Italcementi"
  Silica sand "Sabbia lavata 0/6 mm - Dal Zotto Srl"
  Add water so to obtain a plastic consistency for the mortar

NOTES:
Before installation, immerse the bricks in water until complete saturation /wet the stones with sprinkle water
In solid brick masonry, the mortar joints have a thickness of 1 cm
In stone masonry, the mortar joints have to be as thin as possible

BENDING TESTS ON TOP TIE MASONRY BEAMS (T)

TOT n° of sample type "T": 2
TOT n° of tests type "T": 2
PLACE OF CONSTRUCTION AND TESTING: Ljubljana University Laboratory

Masonry type	Leafs	Reinforced
Solid brick	Single	X(V)
Stone	Double	X(V)

(V) GFRP mesh embedded in bed joints (FBMESH T96 - 66x66 or 33x33)

Interreg ITALIA-SLOVENIJA | CONSTRAIN

TAV. C.1

BENDING TESTS ON MASONRY "C" WALLS
TEST SETUP: STONE WALL

Quotes in mm - Scale 1:20

Plan view

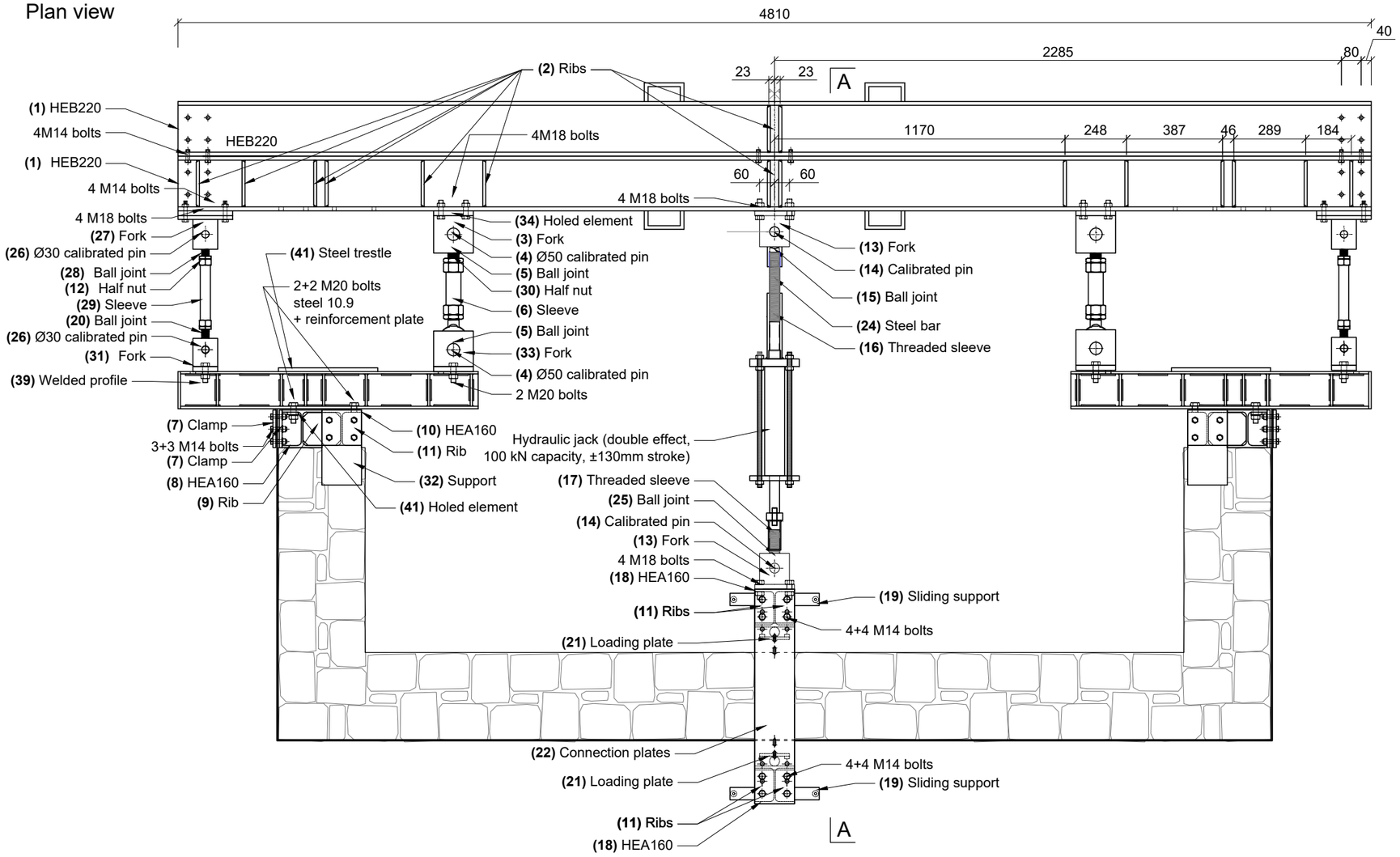

Lateral view
Scale 1:20

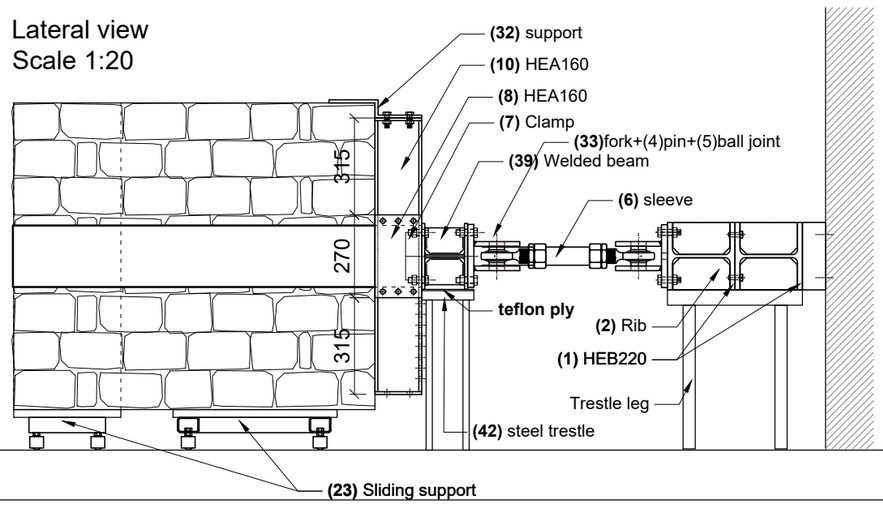

Section A-A

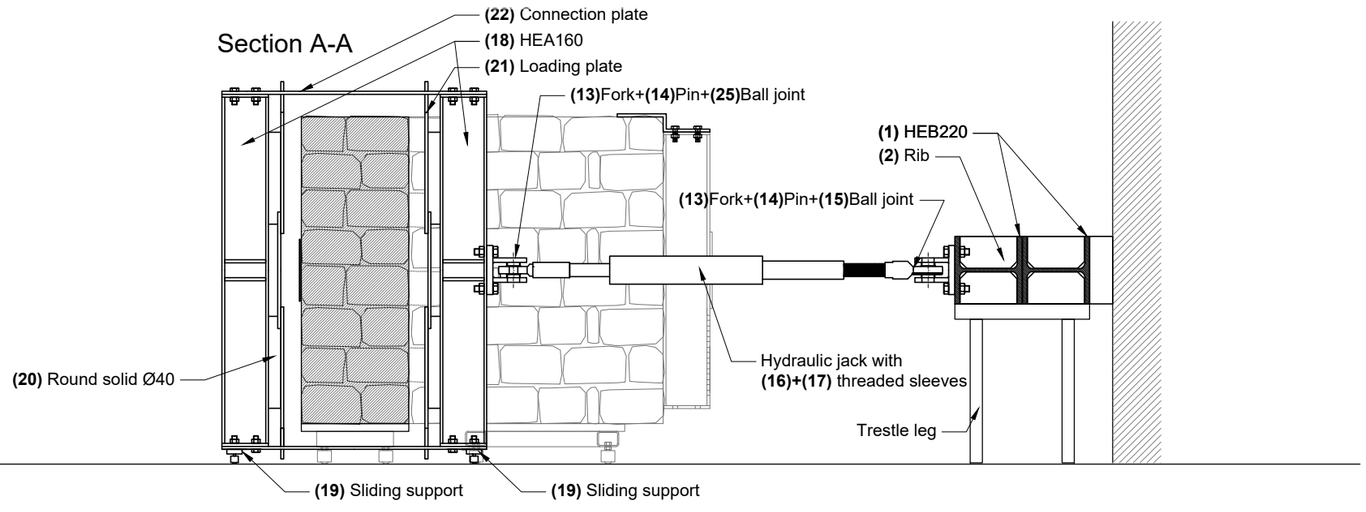

TAV.
C.2

BENDING TESTS ON MASONRY "C" WALLS
STEEL ELEMENTS DETAILS
27 April 2021 Quotes in mm - Scale 1:5

(33) FORK with Ø50 calibrated hole - steel S275 (2x)

Lateral view

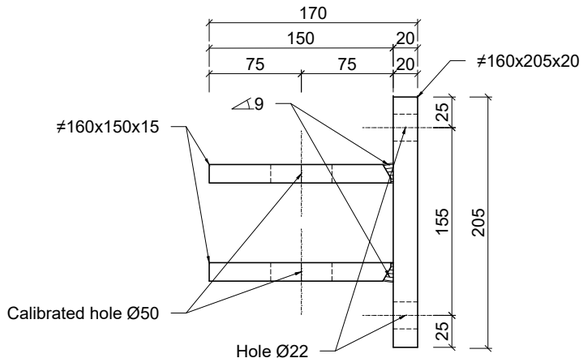

Plan view

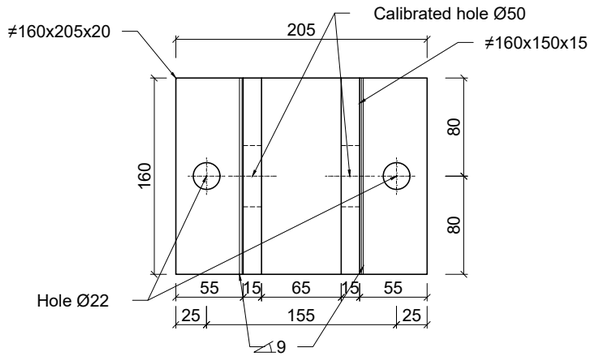

Lateral view

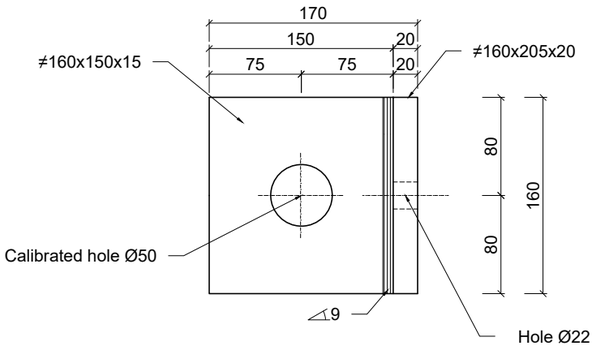

(31) FORK with Ø30 calibrated hole - steel S275 (2x)

Front view

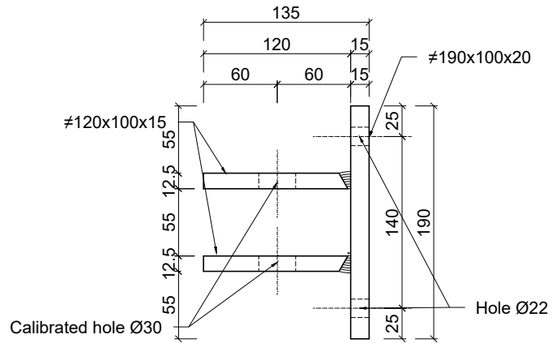

Plan view

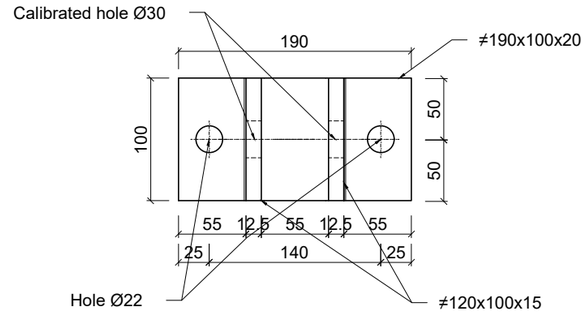

Lateral view

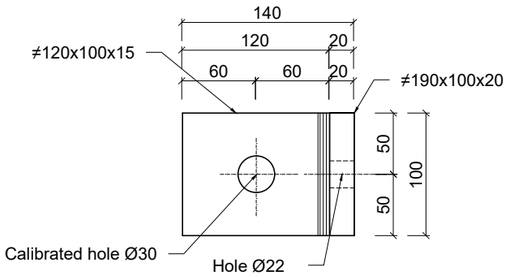

(32) Support - steel S275 (2x)

Front view

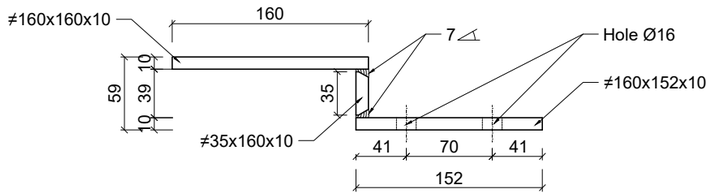

Top view

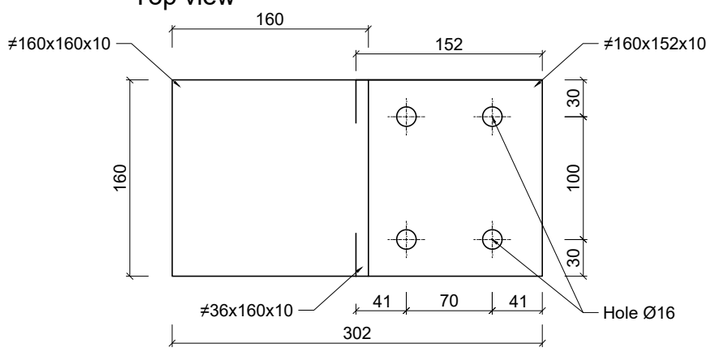

(19) SLIDING SUPPORT - steel S275 (2x)

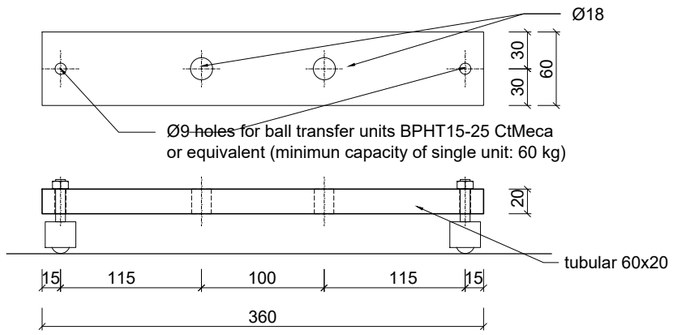

TAV.
C.3

BENDING TESTS ON MASONRY "C" WALLS
STEEL ELEMENTS DETAILS
14 September 2020 Quotes in mm - Scale 1:5

(2) RIB - steel S275 (12x)

Front view Lateral view

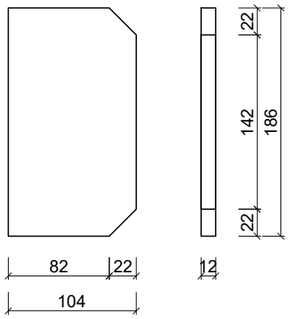

Welding details in (1)

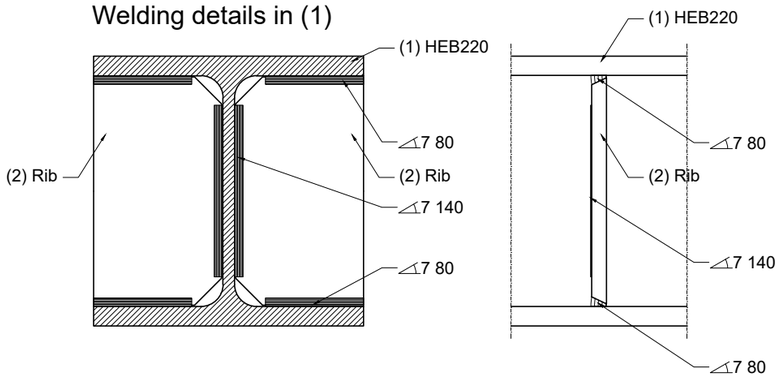

(11) RIB - steel S275 (4x)

Front view Lateral view

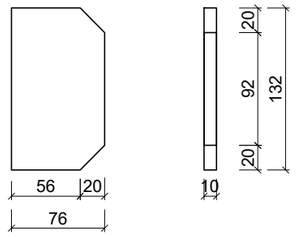

(9) RIB - steel S275 (2x)

Front view Lateral view

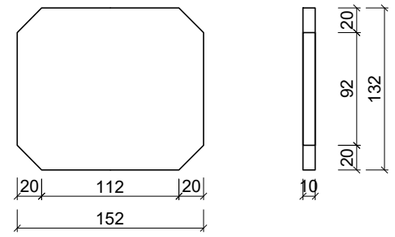

Position of holes, welded rib (9) and clamp (7) in (8)

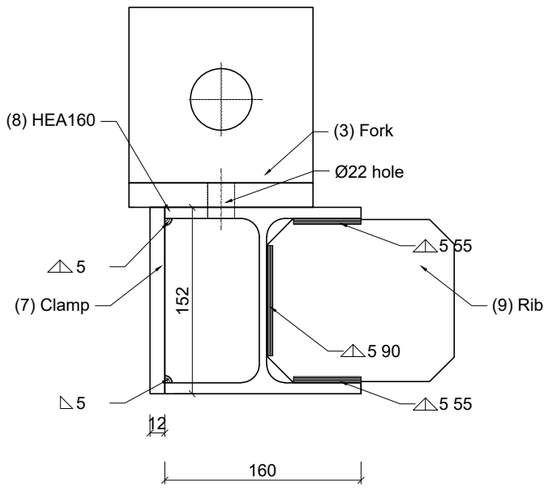

Position of holes and welded ribs (11) and (9) in (10)

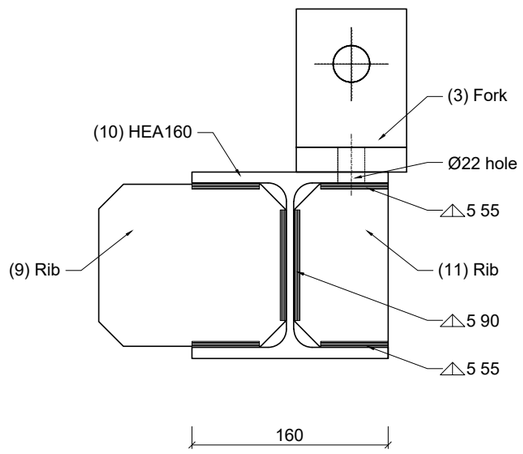

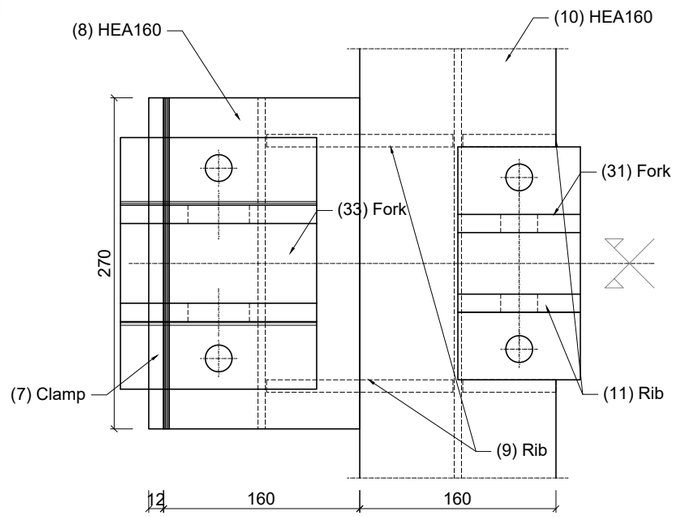

(22) CONNECTION PLATE - steel S275 (2x)

Lateral view

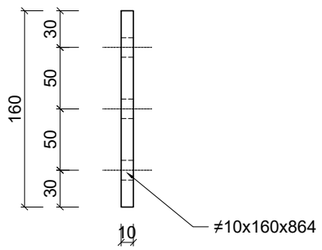

Front view

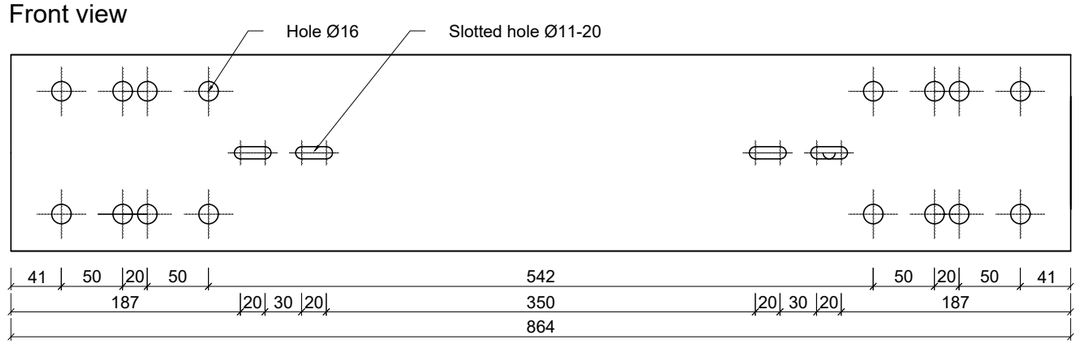

TAV.
C.4

BENDING TESTS ON MASONRY "C" WALLS
STEEL ELEMENTS DETAILS
14 September 2020 Quotes in mm - Scale 1:5

(21) LOADING PLATE with pins - steel S275 (2x)

Lateral view

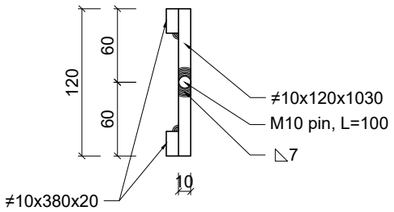

Front view

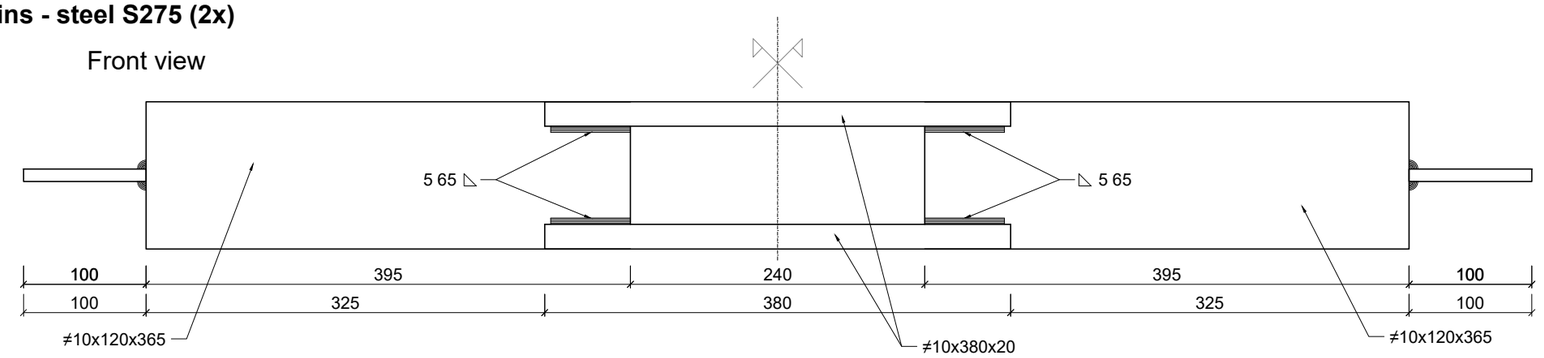

Top view

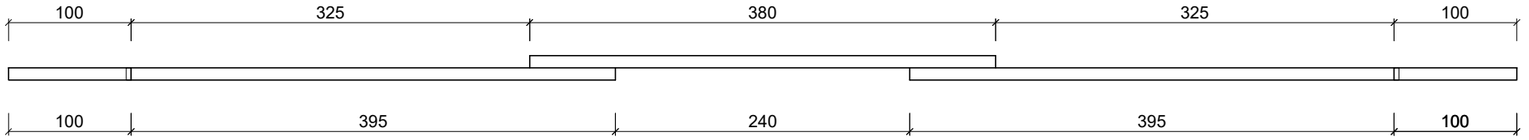

(18) HEA 160 - steel 275 (2x)

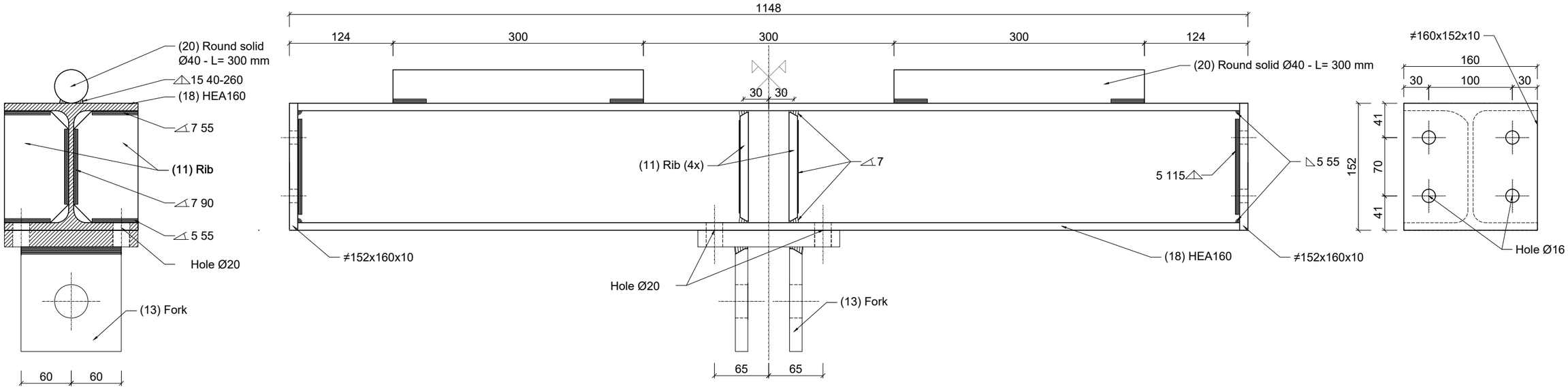

TAV.
C.5

BENDING TESTS ON MASONRY "C" WALLS
STEEL ELEMENTS DETAILS
14 September 2020 Quotes in mm - Scale 1:5

Position of holes and welded ribs (2) in (1)

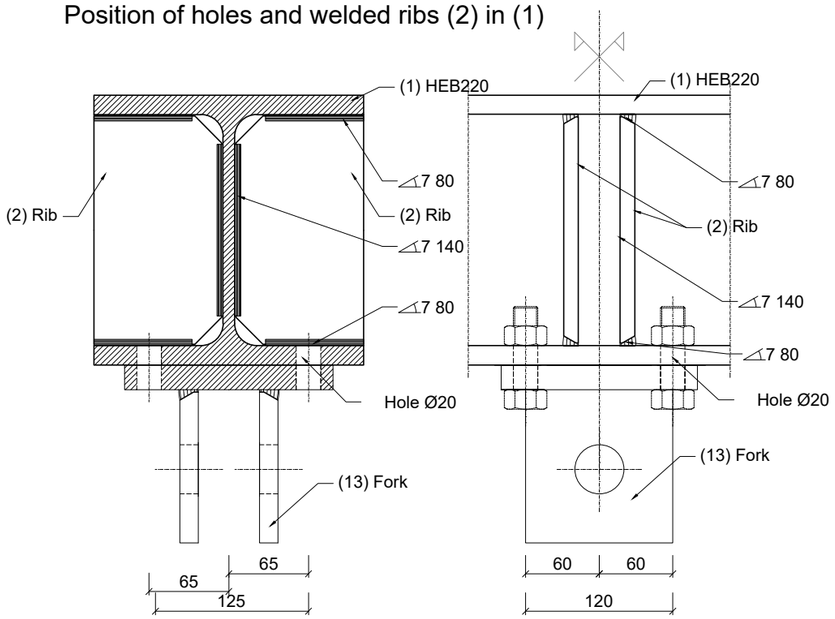

(4) CALIBRATED DOWEL PINS
C40 steel (4x)

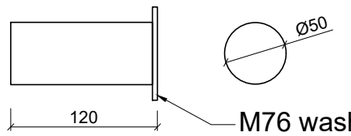

(12) Half nut - S275 (x4)

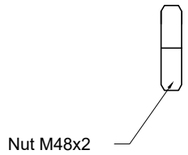

(7) CLAMP - S275 (4x)

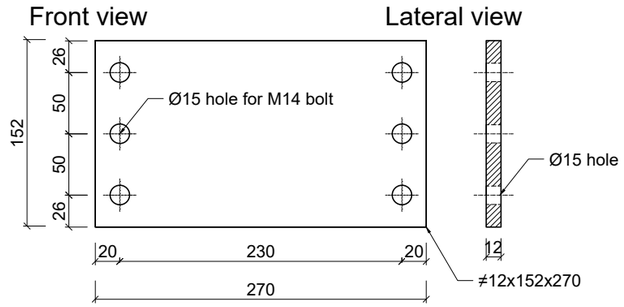

(30) Half nut - S275 (x4)

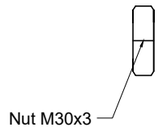

(23) SLIDING SUPPORT (12x) - S275

Front view

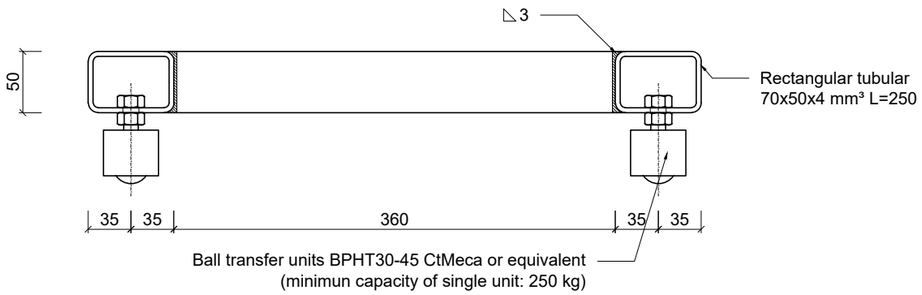

Plan view

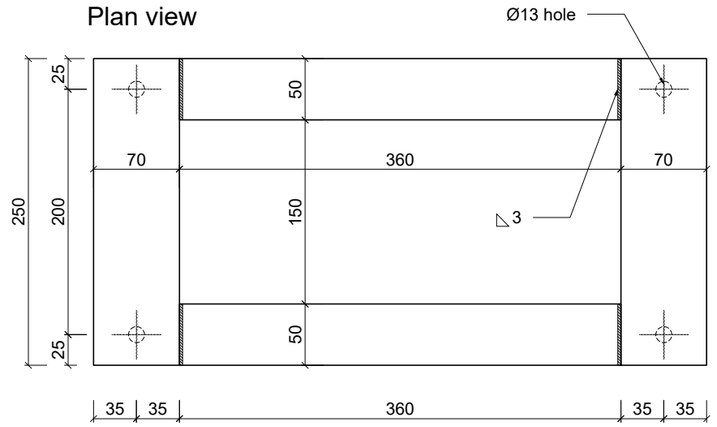

(25) BALL JOINT MALE Ø40 - steel S275 (1x)
(Type Garotti)

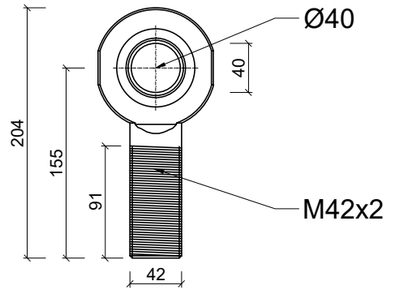

Interreg ITALIA-SLOVENIJA — CONSTRAIN

TAV. C.6

BENDING TESTS ON MASONRY "C" WALLS
STEEL ELEMENTS DETAILS

14 September 2020 Quotes in mm - Scale 1:5

(13) FORK with Ø40 calibrated hole - steel S275 (2x)

Front view

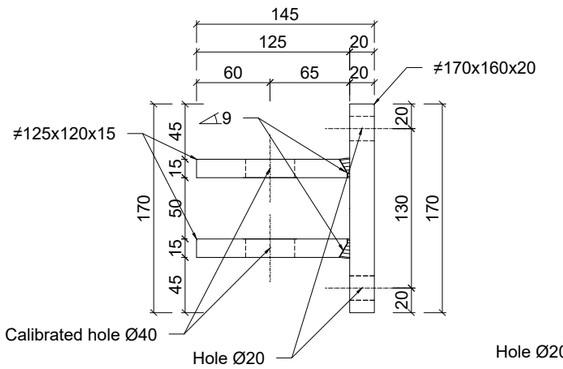

Plan view

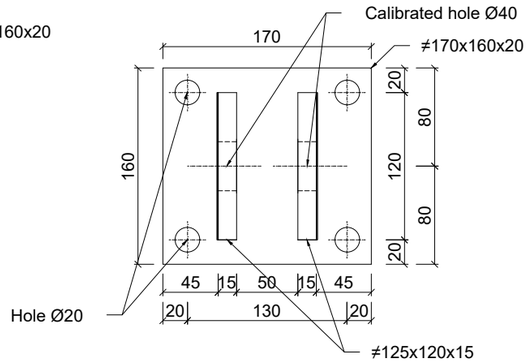

Lateral view

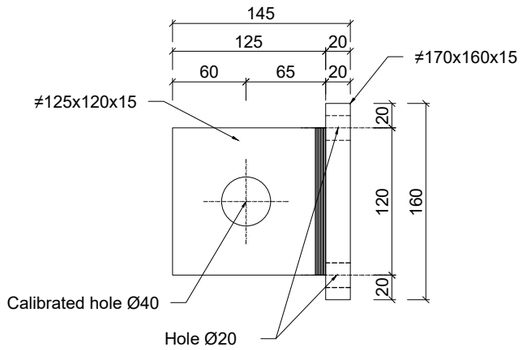

(27) FORK with Ø30 calibrated hole - steel S275 (2x)

Front view

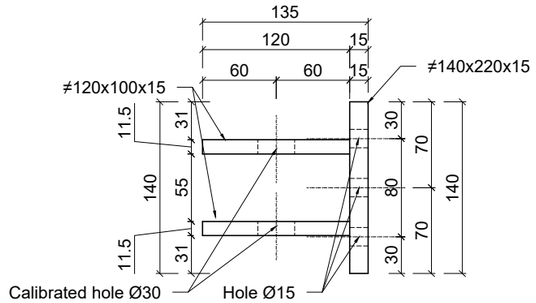

Plan view

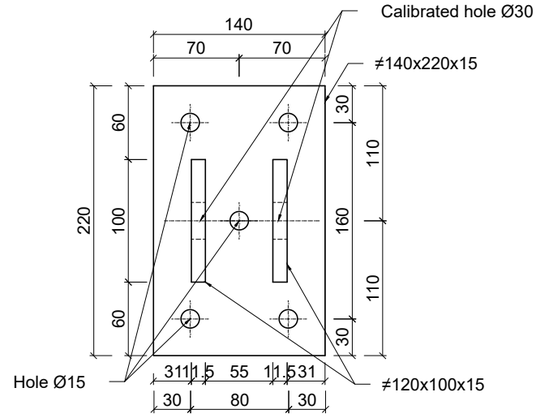

Lateral view

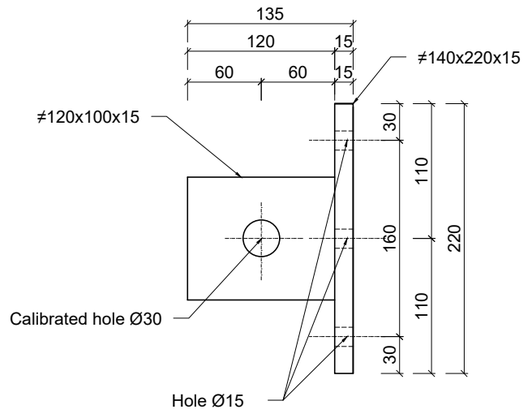

≠140x220x20

(3) FORK with Ø50 calibrated hole - steel S275 (2x)

Lateral view

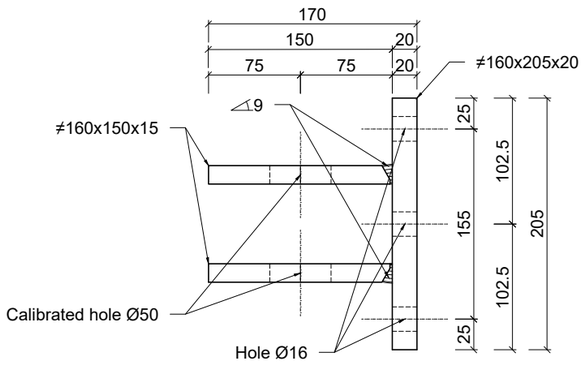

Plan view

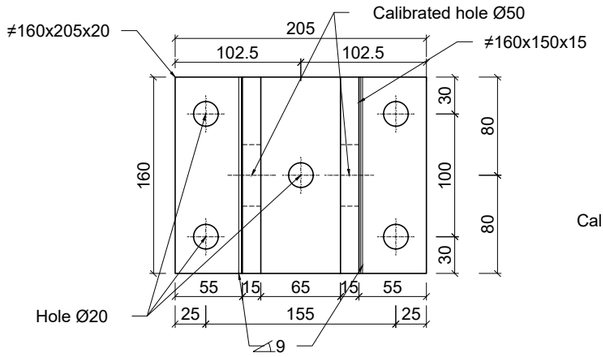

Lateral view

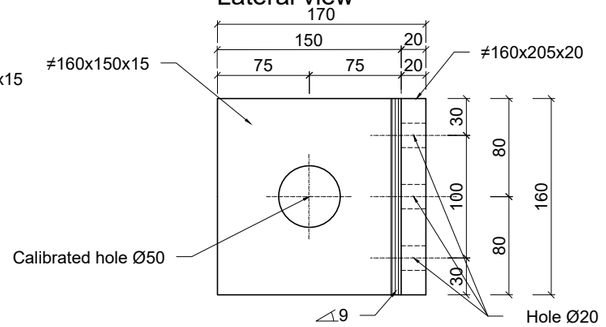

Position of holes in (1)

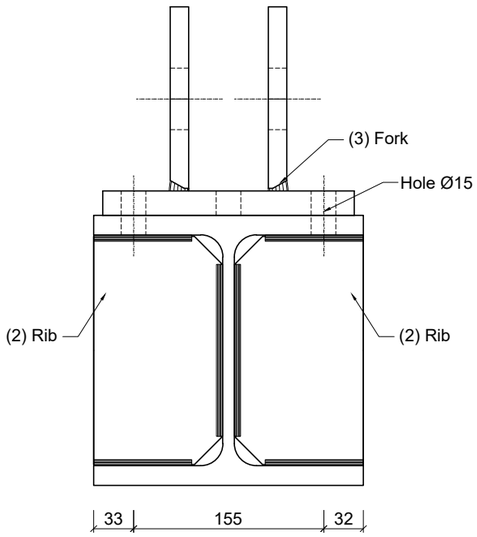

TAV.
C.7

BENDING TESTS ON MASONRY "C" WALLS
STEEL ELEMENTS DETAILS
09 February 2021 Quotes in mm - Scale 1:5

(14) CALIBRATED DOWEL PINS
C40 steel (2x)

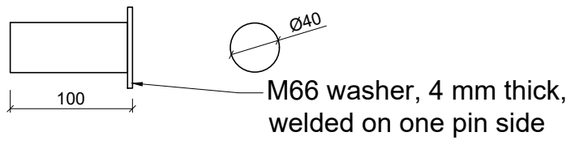

(29) THREADED SLEEVE - steel S275 (2x)
with end nuts

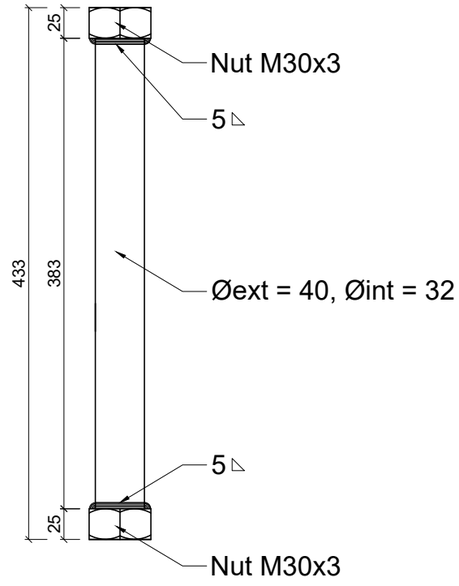

(26) CALIBRATED DOWEL PINS
C40 steel (4x)

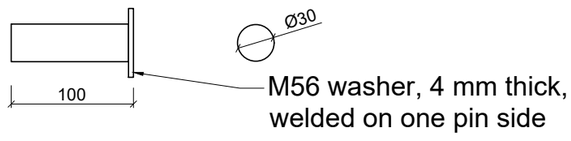

(5) BALL JOINT MALE Ø50 - steel S275 (4x)
(Type Garotti)

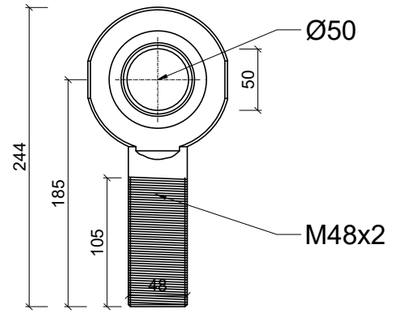

(15) BALL JOINT FEMALE Ø40 - steel S275 (1x)
(Type Garotti)

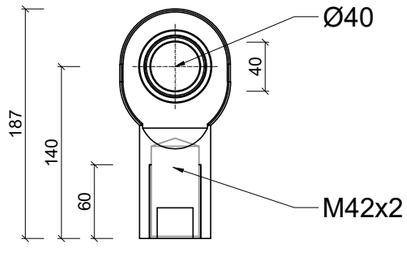

(28) BALL JOINT MALE Ø30 - steel S275 (2x)

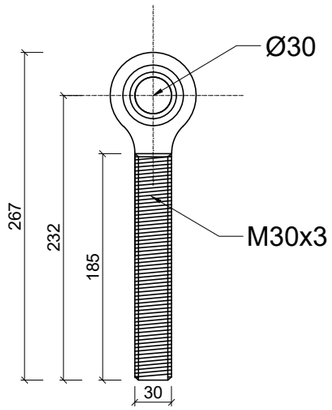

(6) THREADED SLEEVE - steel S275 (2x)
with end nuts

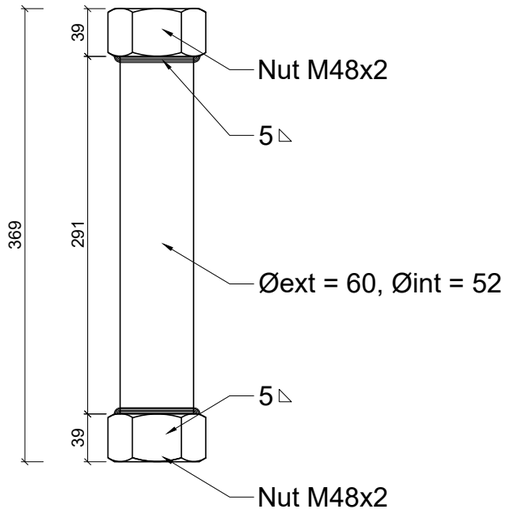

(24) STEEL BAR M42x2 - steel S275 (1x)

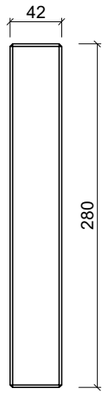

(16) THREADED SLEEVE - steel S275 (1x)

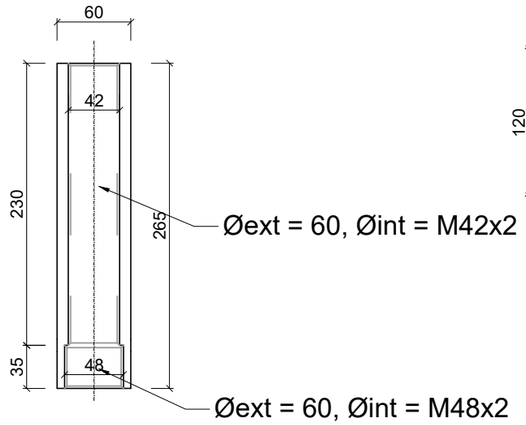

(17) THREADED SLEEVE - steel S275 (1x)

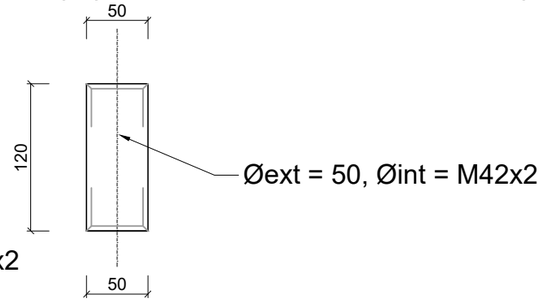

(34)Holed element - steel S275 (2x)

Plan view

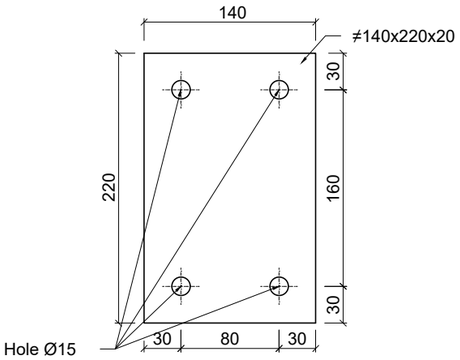

TAV.
C.8

BENDING TESTS ON MASONRY "C" WALLS
ALTERNATIVE ACTUATOR - STEEL ELEMENTS DETAILS
Quotes in mm - Scale 1:5

ACTUATOR Lateral view

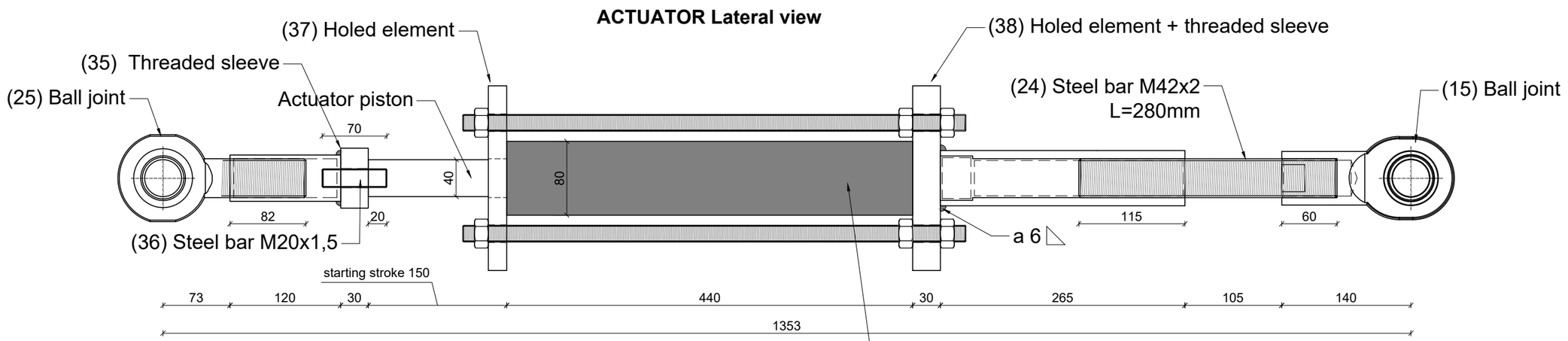

Actuator HYDRAFORE YG-20300S
Max stroke :300 mm
Capacity: push 198 kN , pull 110 kN
Oil capacity: push 848 cm³ , pull 471 cm³

(35) THREADED SLEEVE - steel S275 and C40 (1x)

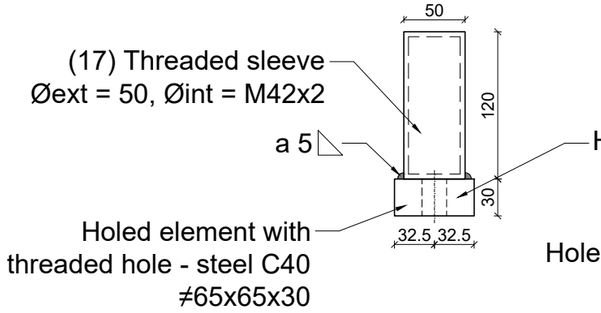

(36) STEEL BAR M20X1,5 - steel 8.8 (1x)

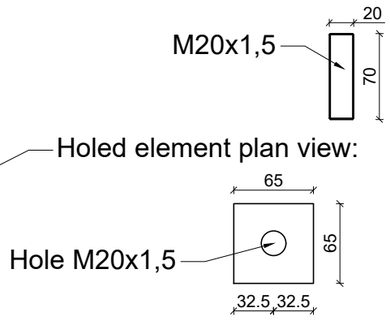

(38) HOLED ELEMENT + THREADED SLEEVE - steel S275 (1x)

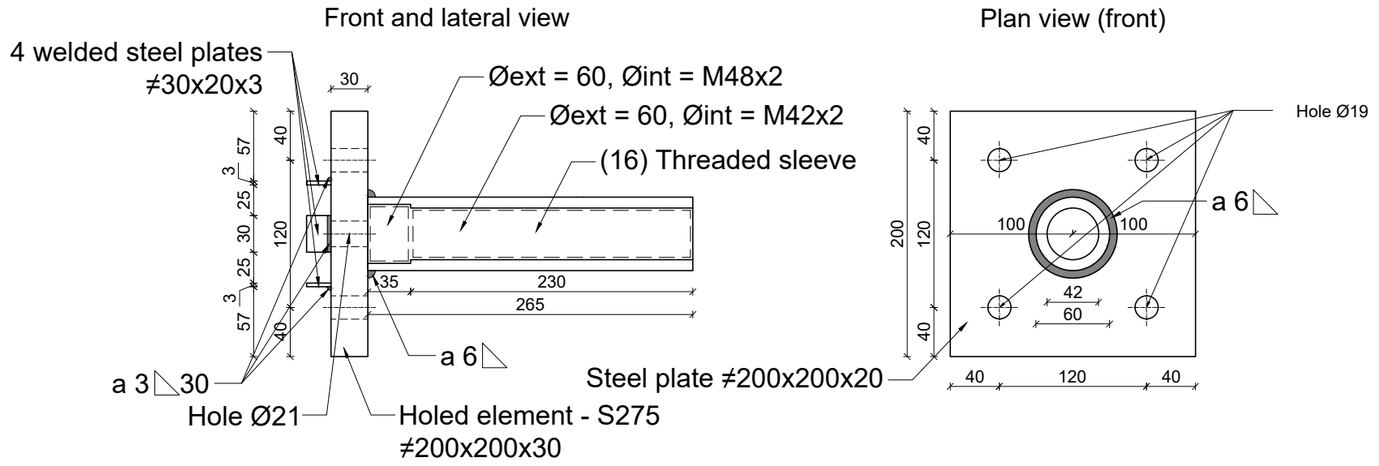

(37) HOLED ELEMENT - steel S275 (1x)

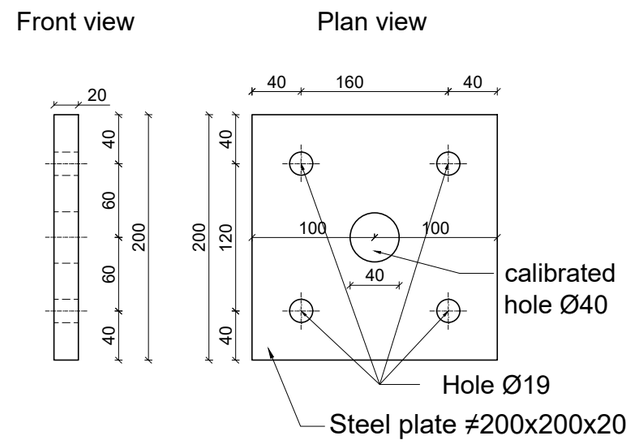

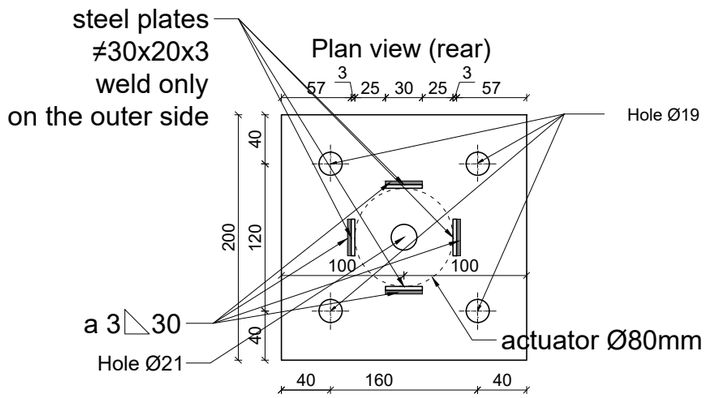

BENDING TESTS ON MASONRY "C" WALLS
MODIFICATIONS TO THE WALL CONSTRAINT - STEEL ELEMENTS DETAILS

Quotes in mm - Scale 1:5

(39) WELDED BEAM - steel S355 (2x)

Lateral view

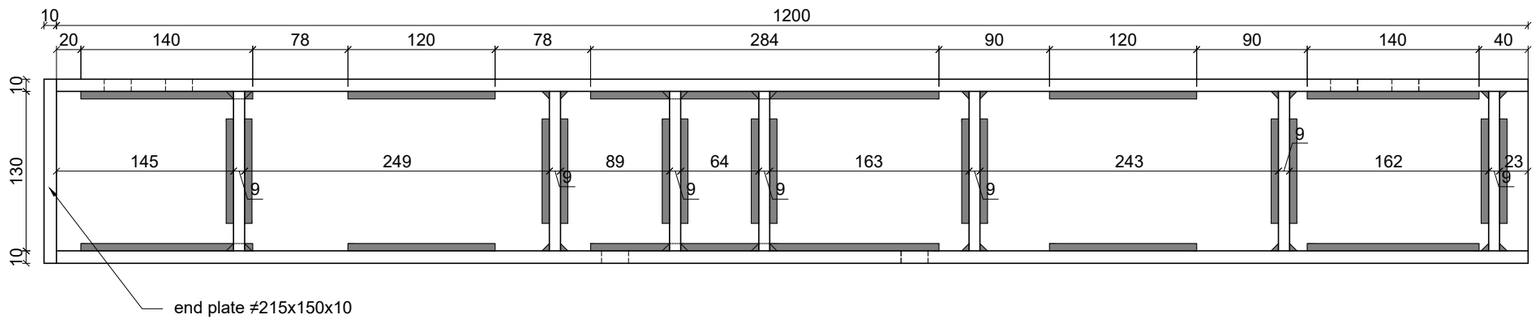

Front view

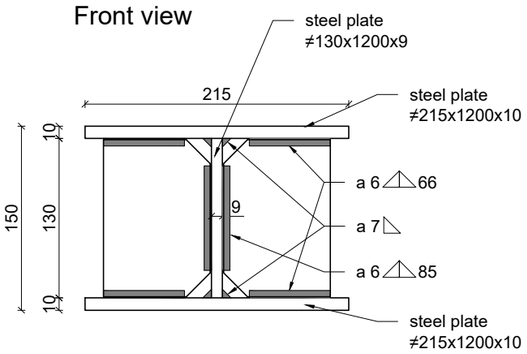

Plan view

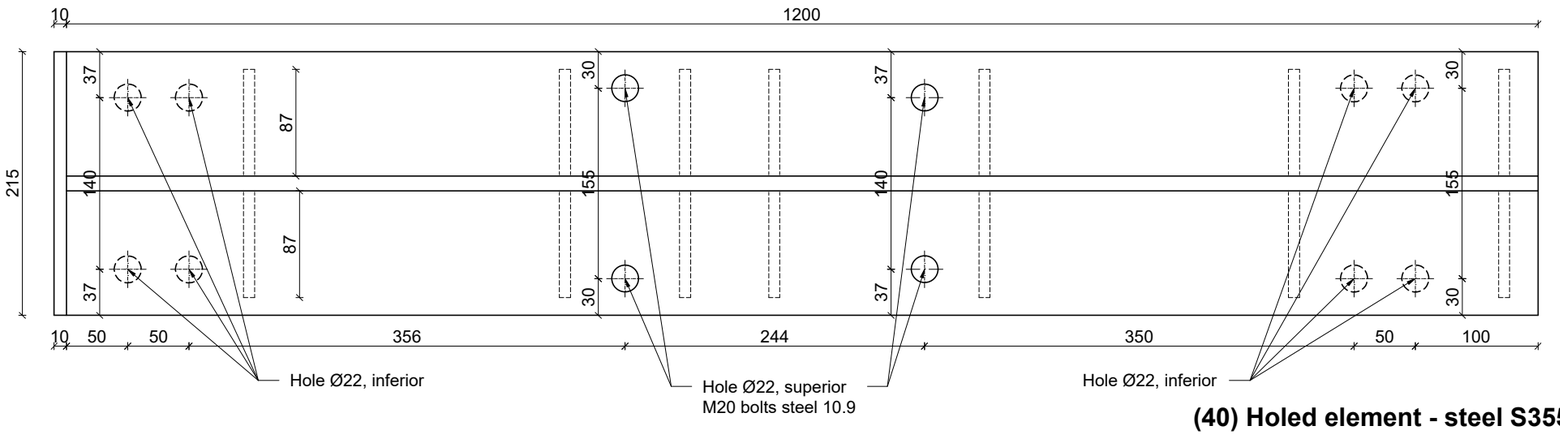

Stiffeners - steel S355 (28x)

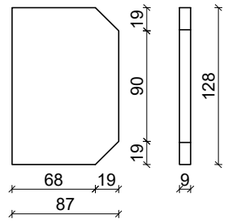

(29) THREADED SLEEVE steel S275 (2x) with end nuts

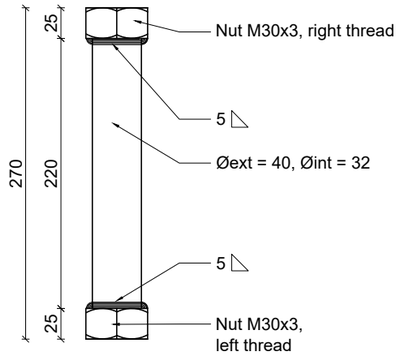

(10) Modifications to HEA 160 - steel S275 (2x)

Lateral view

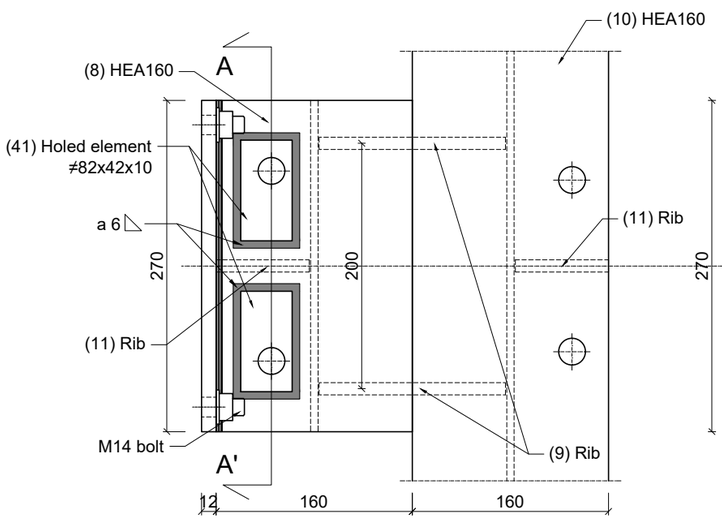

Section A-A'

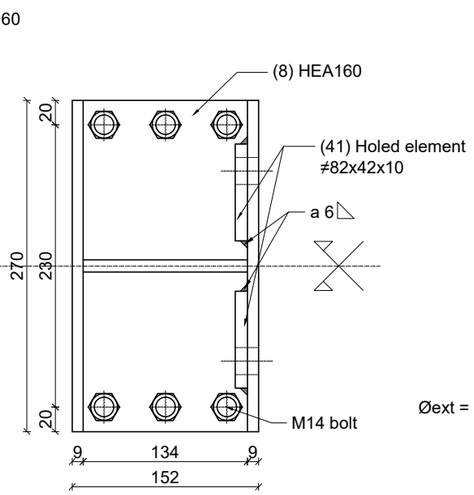

(40) Holed element - steel S355 (4x)

Front view Lateral view

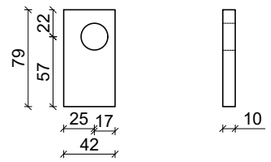

(6) THREADED SLEEVE - steel S275 (2x) with end nuts

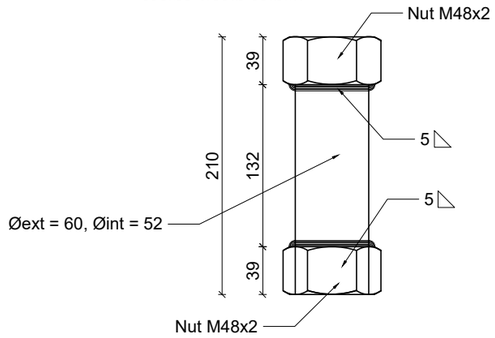

(41) Steel trestle for the welded beam (2x)

Scale 1:10

Plan view

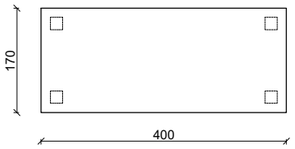

Front view

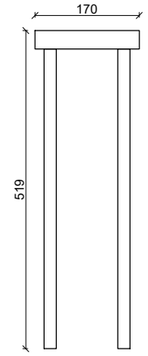

TAV.
C.10

BENDING TESTS ON MASONRY "C" WALLS
MODIFICATIONS TO THE WALL CONSTRAINT - STEEL ELEMENTS DETAILS

29 April 2021 Quotes in mm - Scale 1:10

Plan view - half beam
Scale 1:10

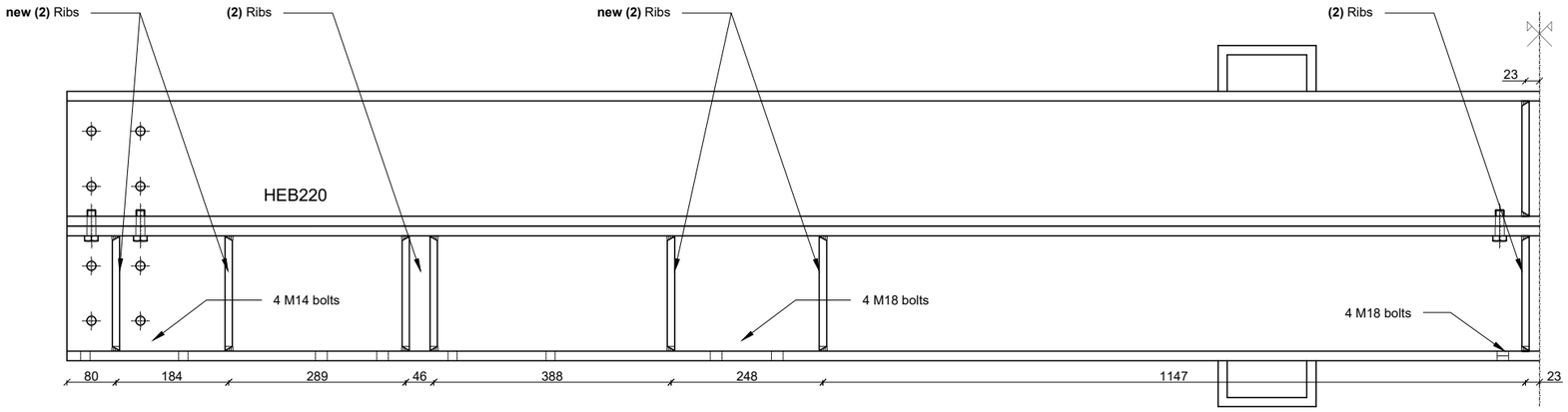

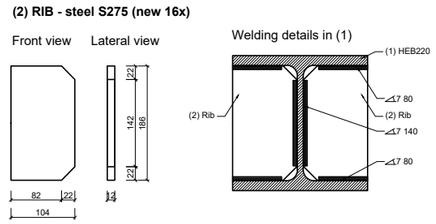

Front view - half beam
Scale 1:10

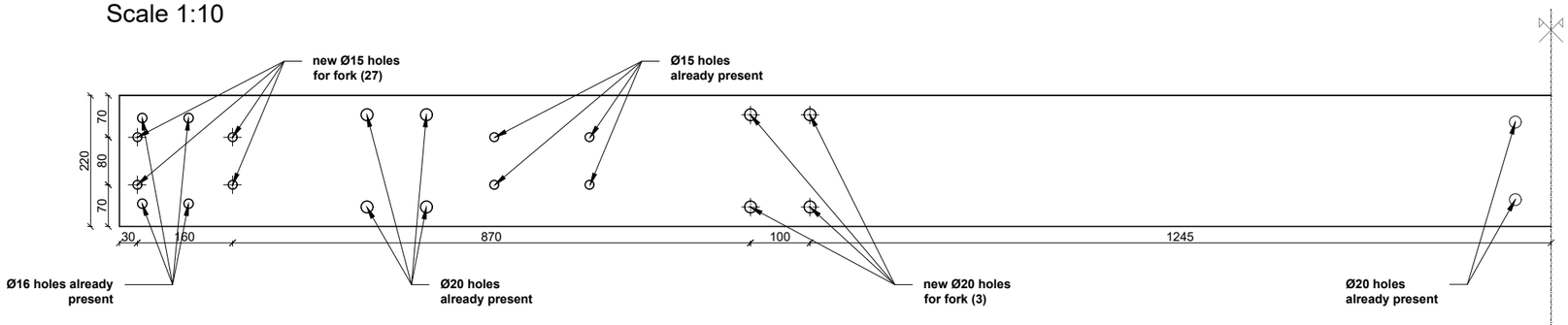

Lateral view
Scale 1:20

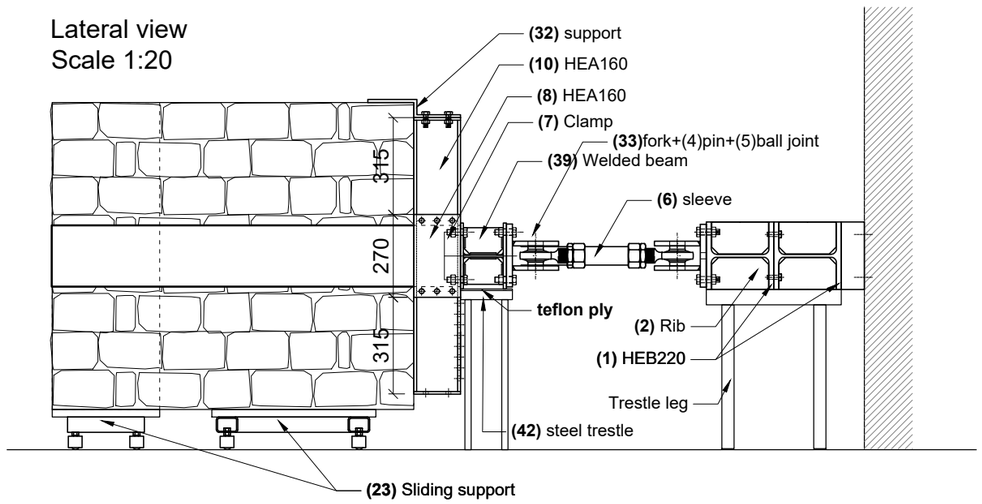

NEW ELEMENTS

(39) Welded beam - Steel S355 (2x)

(40) Holed element - Steel S355 (4x)

(41) Steel trestle (2x)

MODIFICATIONS TO THE HEB220 BEAM

Ø15 Holes (8X)
Ø20 Holes (8X)
Welding of (2) Ribs (16x) to the HEB220 beam

TAV.
PB1.1

PILOT BUILDING
FOUNDATION
Quotes in cm - Scale 1:50

RC foundation
Horizontal section
Scale 1:50

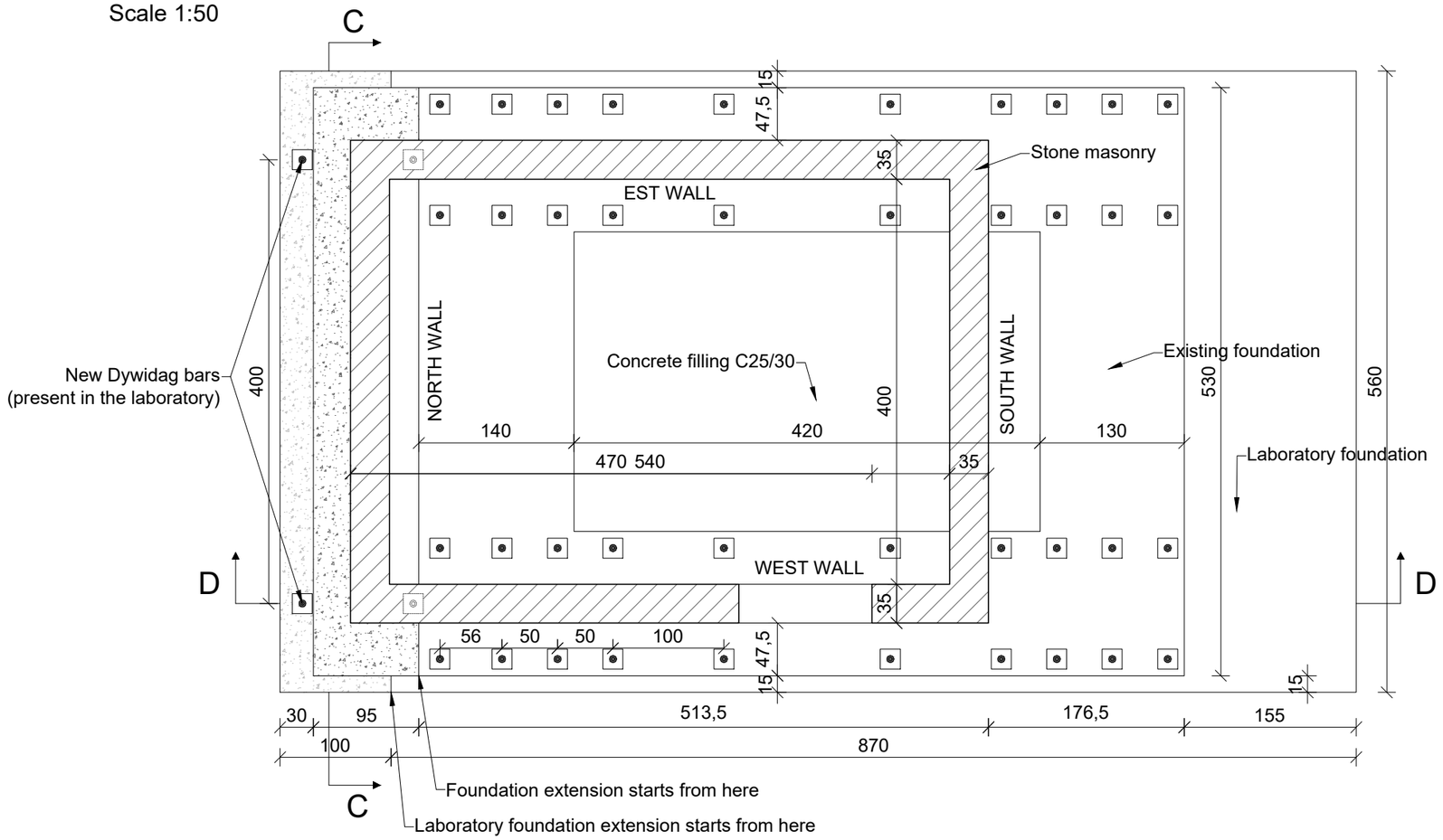

MATERIALS:
For the foundation (h=40cm):
Concrete C25/30
Steel B450C

For the laboratory foundation (h=80cm):
Concrete C30/37
Steel B450C

Before casting the concrete, protect the laboratory foundation and the two dywidag bars under the masonry with a bituminous sheet ply t=5 mm. With the same method protect the bottom of the PVC tubes as shown in the photo:

RC foundation
Section D-D
Scale 1:50

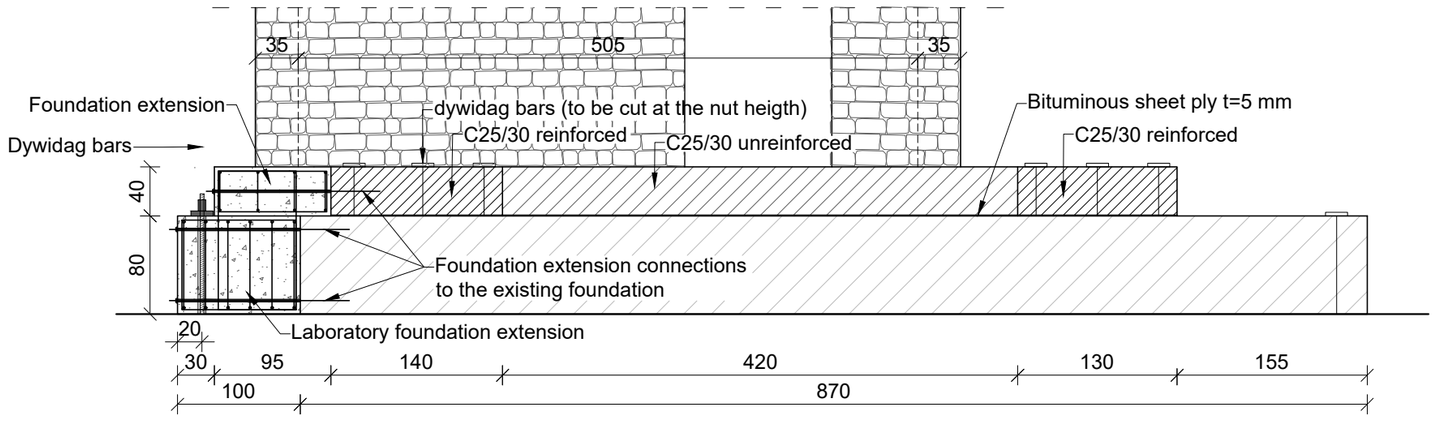

TAV.

PB1.2

PILOT BUILDING
FOUNDATION
Quotes in cm - Scale 1:50

Detail of the foundation extension
Section C-C
Scale 1:50

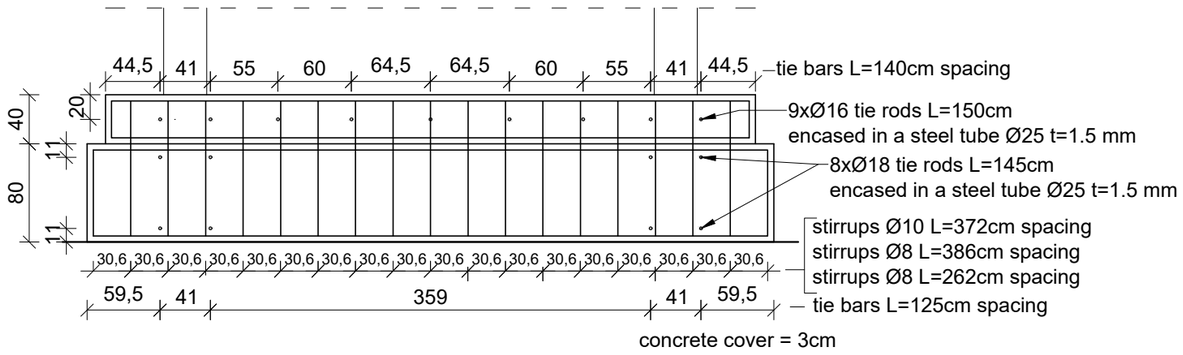

concrete cover = 3cm

Detail of the foundation extension
Section D-D
Scale 1:25

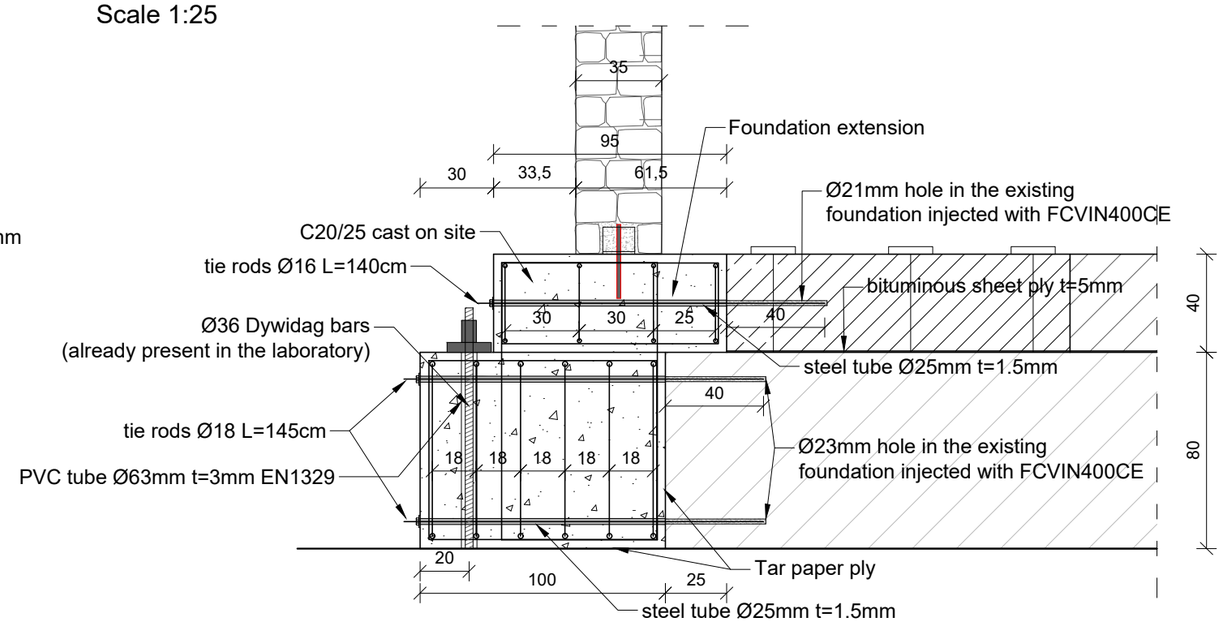

Bars for the building foundation

Longitudinal bars sup B450C Ø16/30 cm l=580 cm (4x)

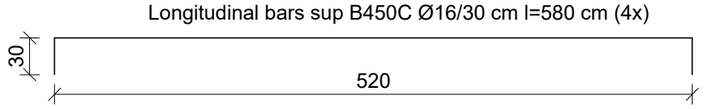

Longitudinal bars inf B450C Ø16/30 cm l=580 cm (4x)

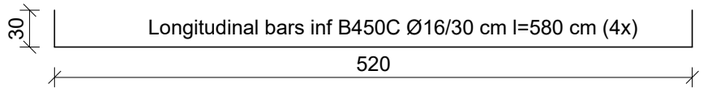

Bars for the laboratory foundation (80 cm)

Longitudinal bars sup B450C Ø20/18 cm l=640 cm (6x)

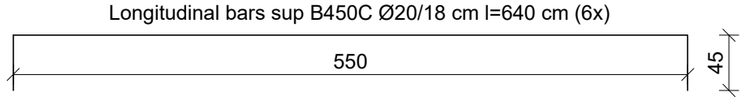

Longitudinal bars inf B450C Ø20/18 cm l=640 cm (6x)

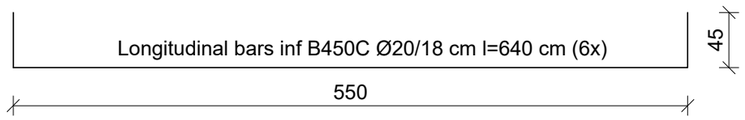

Detail of the tie rods
Scale 1:15, quotes in mm

Tie rod B450C Ø16 L=140cm with rhreaded end (9x)

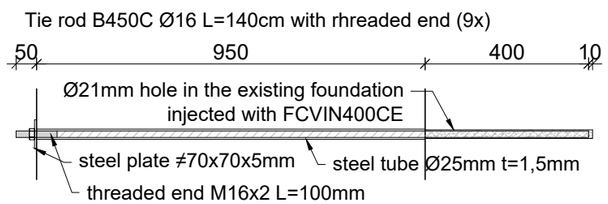

Tie rod B450C Ø18 L=145cm with rhreaded end (8x)

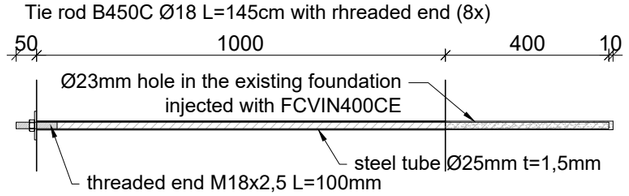

Stirrups B450C Ø8/30cm L=262 cm (17x)

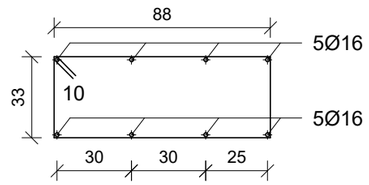

Stirrups B450C Ø8/30cm L=386 cm (17x)

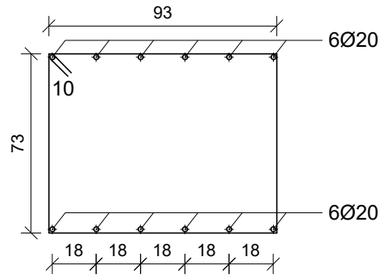

Stirrups B450C Ø10/30cm L372 mm (17x)

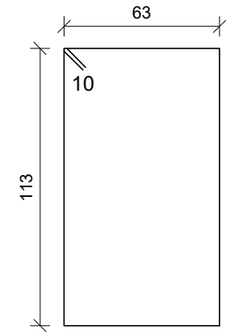

Detail of the plates
Scale 1:5, quotes in mm

Ø16 tie bar plates

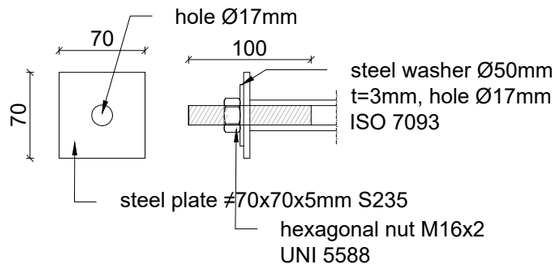

Ø18 tie bar plates

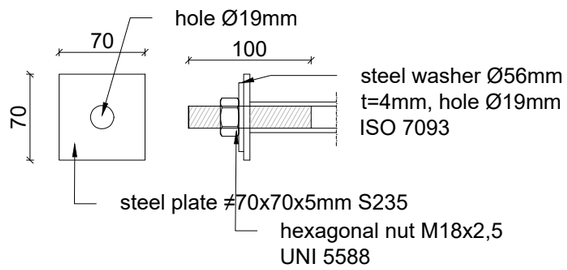

MATERIALS:

- For the foundation (h=40cm):
- Concrete C25/30
- Steel B450C

For the laboratory foundation (h=80cm):

- Concrete C25/30
- Steel B450C
- Tar paper / nylon ply to be installed at the interfaces between the existing foundation and the new extensions and on the bottom of the laboratory foundation extension
- PVC tubes EN1329 t=3mm: Øe=63mm L=1200mm (2x)
- Steel tubes Ø25mm t=1,5mm L=1000mm (8x) and L=950mm (9x)

Before casting the concrete, position the PVC tubes to create the 2 housings for the Ø36 mm dywidag bars and protect the horizontal tie rods with the steel tubes.

Tighten the tie rods until reaching a pre-tension of 40 kN for the Ø16 and 45kN for the Ø18 rods.

Interreg ITALIA-SLOVENIJA — CONSTRAIN

TAV.
PB1.3

PILOT BUILDING
FOUNDATION
Quotes in cm - Scale 1:50

Detail of the connection of stones to the foundation (first row of stones)
Plan view
Scale 1:50

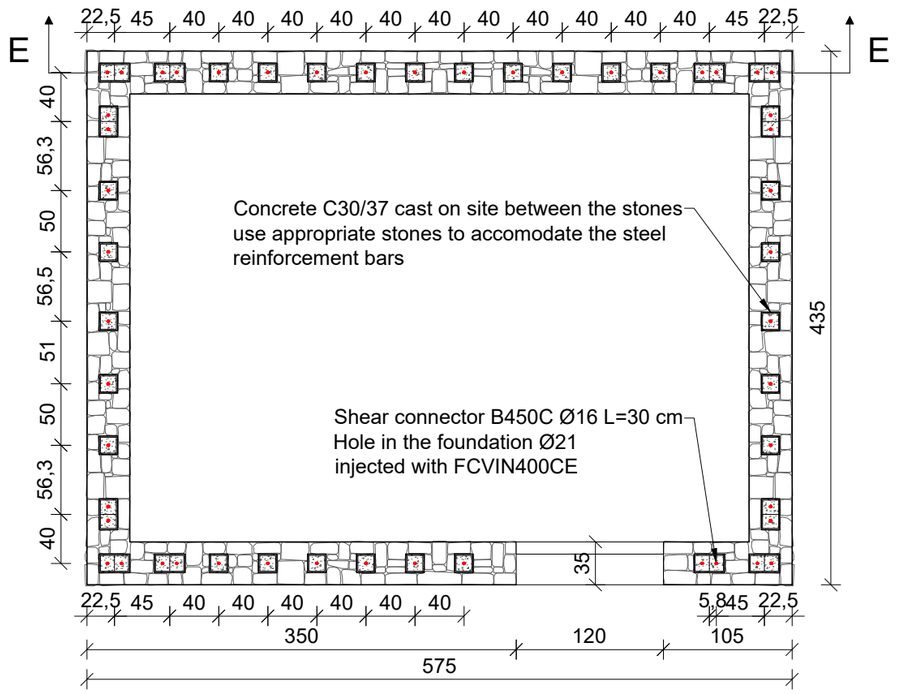

Detail of the connection of the stones to the foundation
Section E-E
Scale 1:50

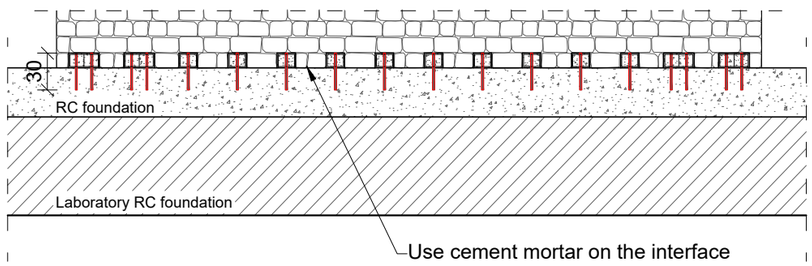

Detail of the first row concrete reinforcements
Scale 1:10

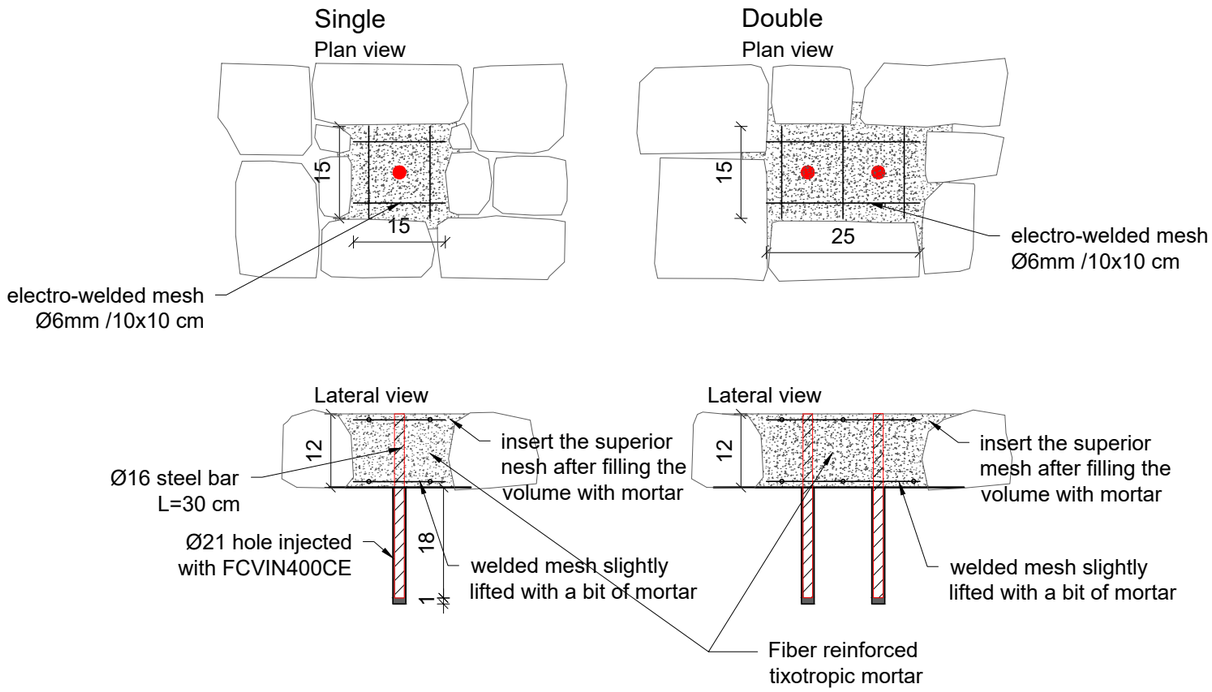

52x pieces of electro-welded mesh Ø6/10x10

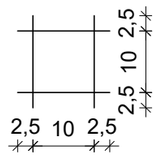

24x pieces of electro-welded mesh Ø6/10x10

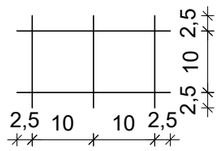

Detail of the connection of the stones to the foundation
(preparation of the surface)
Plan view
Scale 1:20

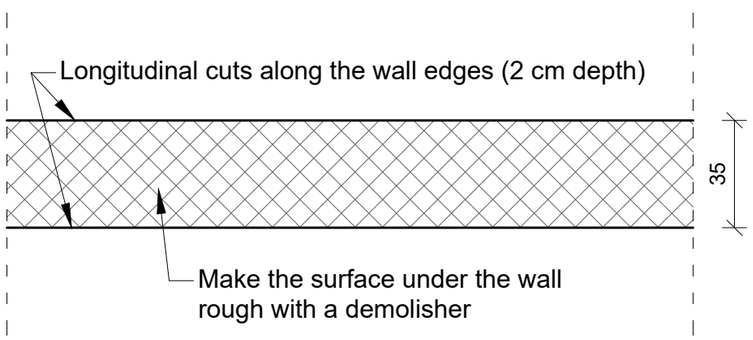

MATERIALS:
For the foundation (h=40cm):
Concrete C25/30

For the laboratory foundation (h=80cm):
Concrete C25/30

For the first row reinforcement:
Concrete C25/30
Steel B450C Ø16 L=30 cm
Before casting install the shear connectors

Use cement mortar on the interface between the first row of stones and the foundation and until half stone heigth (2.5 kg of cement per 25 kg of mortar)

TAV.
PB1

PILOT BUILDING
UNREINFORCED BUILDING - PLAN VIEWS
Quotes in cm - Scale 1:50

Ground Floor

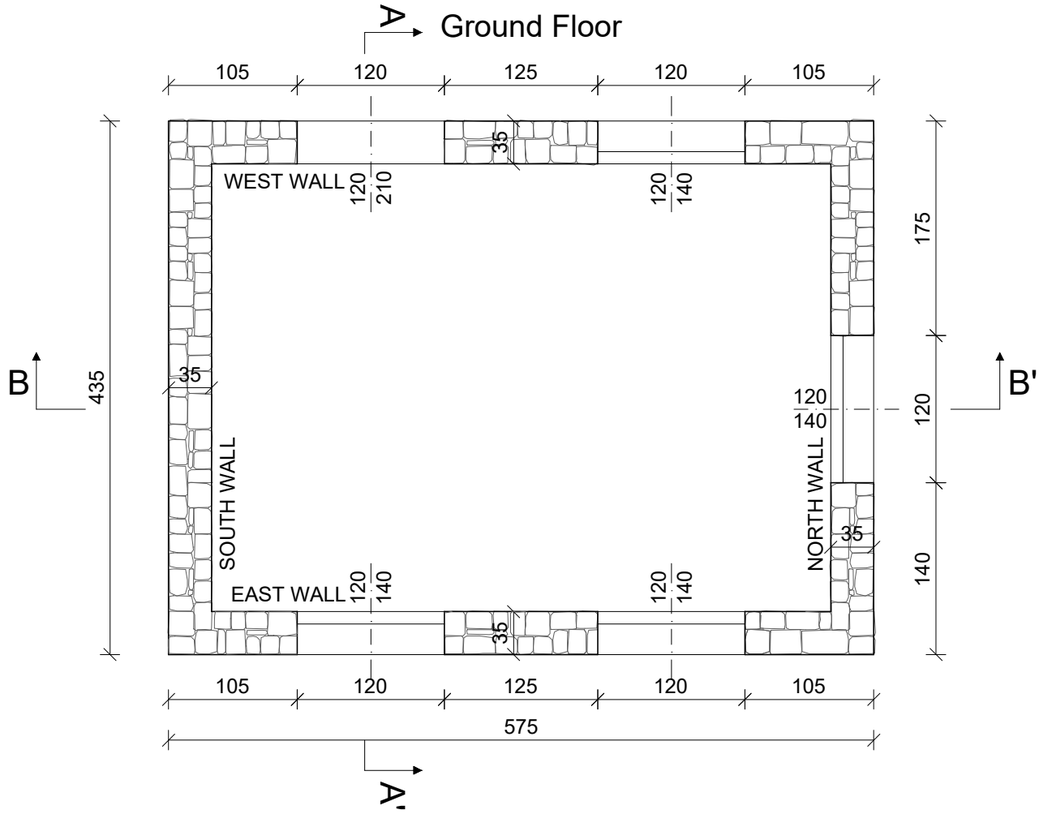

First Floor

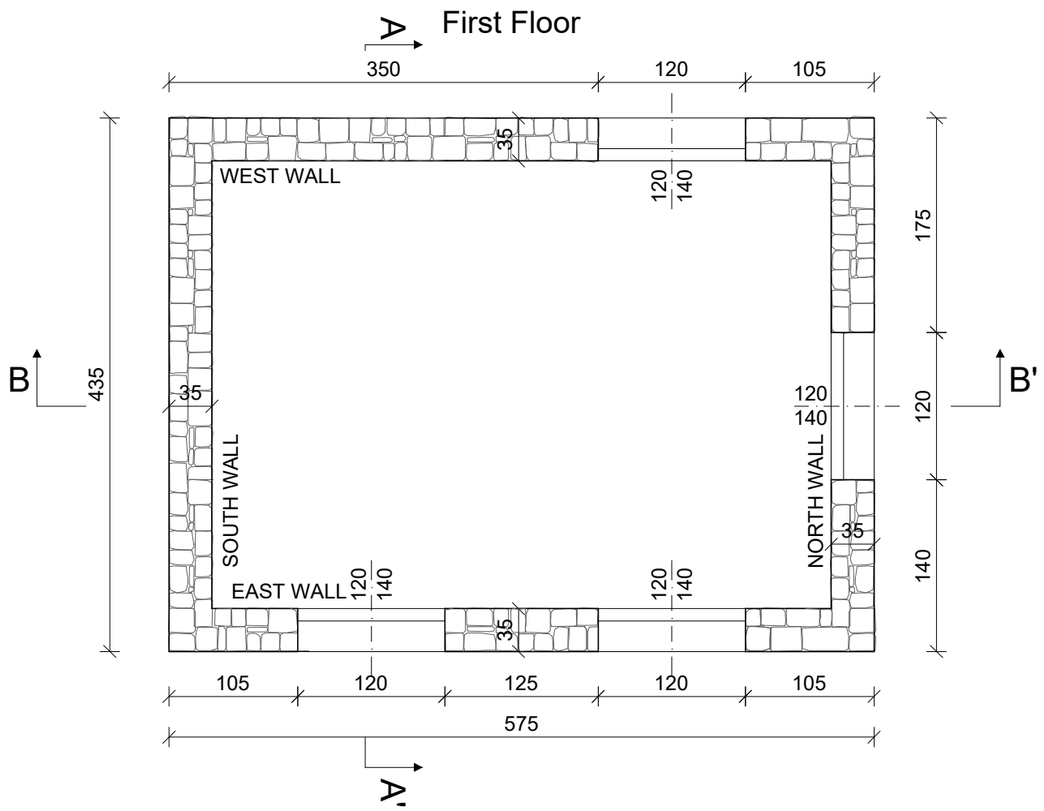

Detail of intermediate storey decking

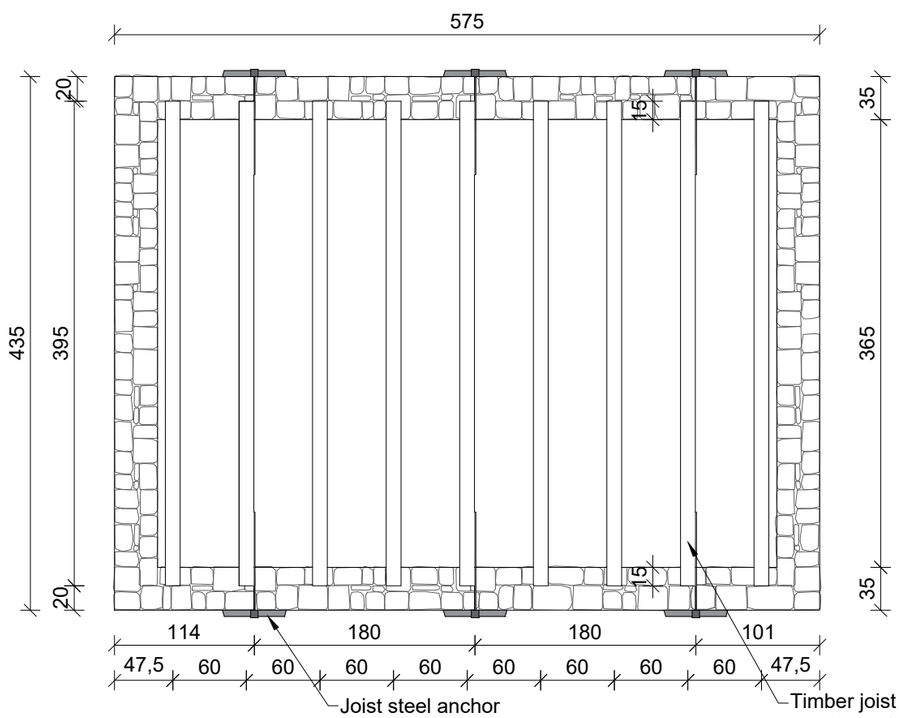

Detail of roof frame

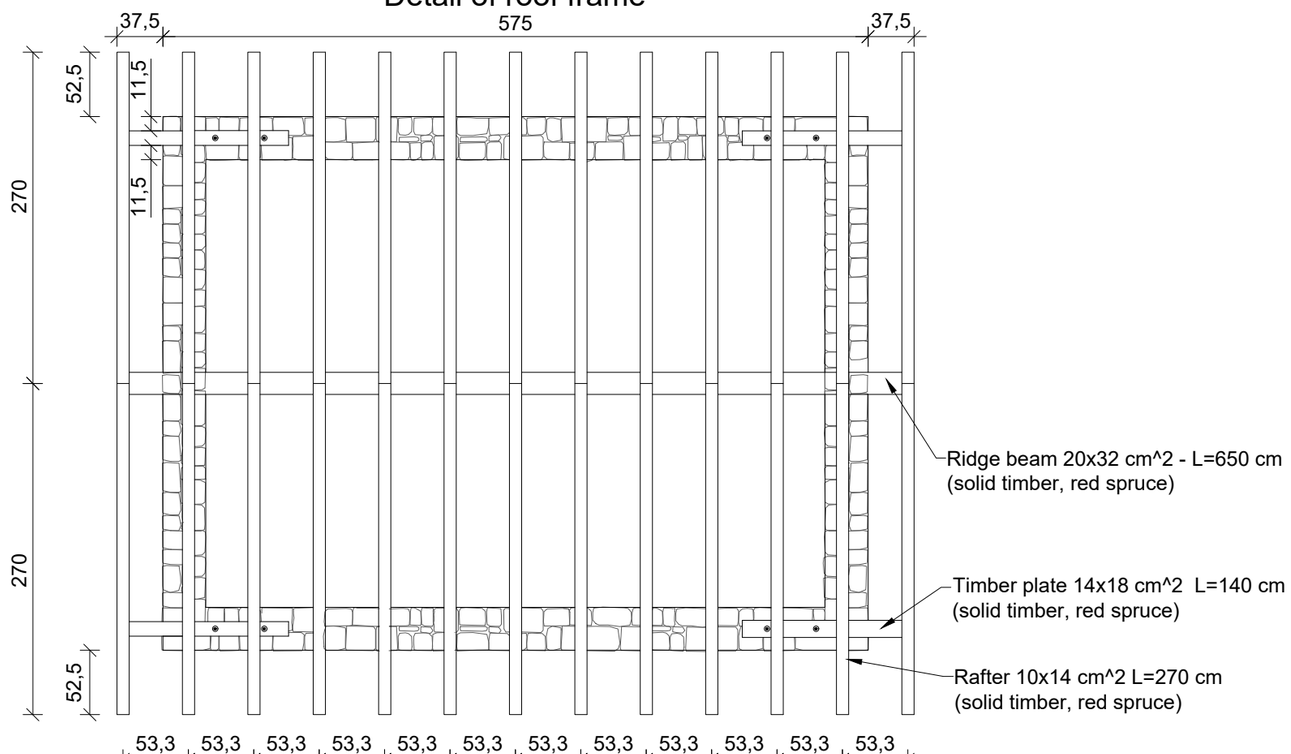

Interreg ITALIA-SLOVENIJA | CONSTRAIN

TAV.
PB2

PILOT BUILDING
UNREINFORCED BUILDING - SECTION VIEWS
Quotes in cm - Scale 1:50

SECTION A-A'

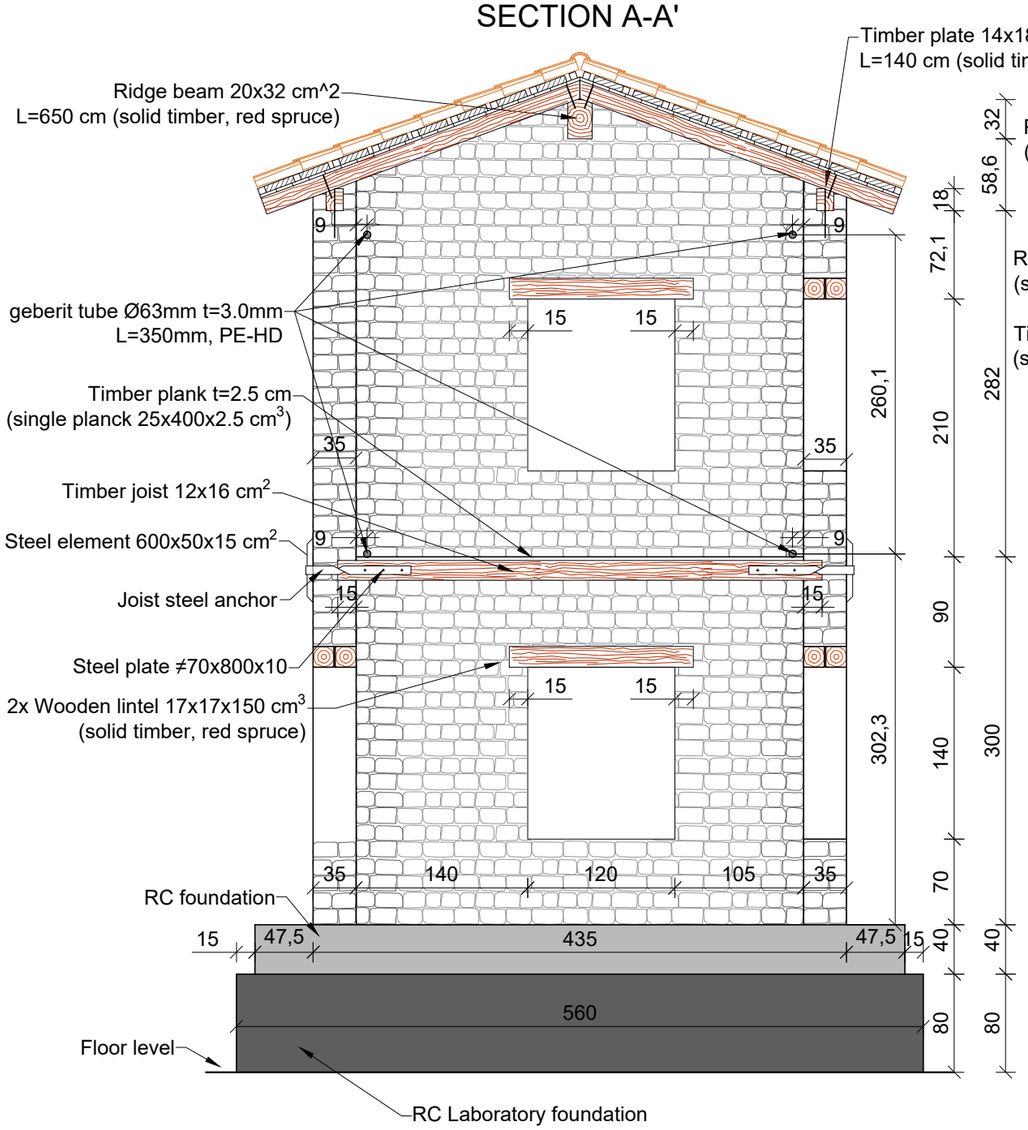

SECTION B-B'

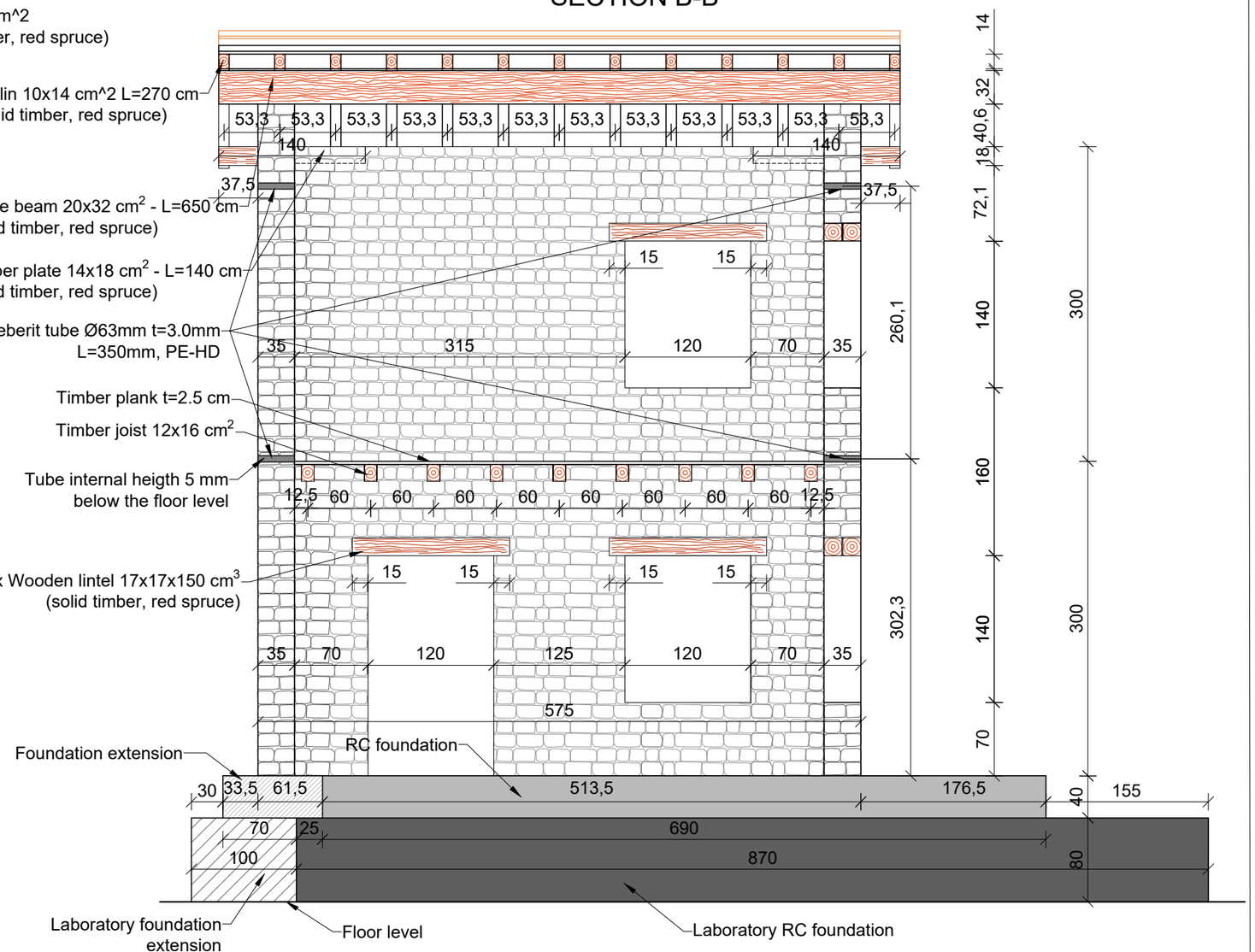

Detail of Joist steel anchor - Scale 1:10, quotes in mm

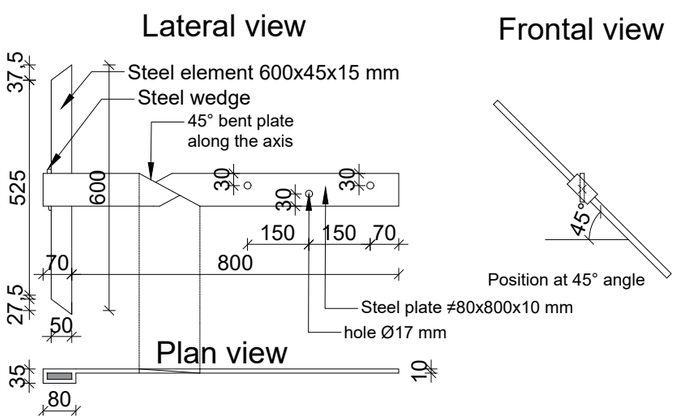

Steel wedge detail
Scale 1:5, quotes in mm

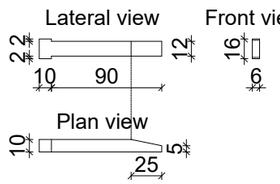

For fixing the joist steel anchor to the wooden beam, use UNI 704 C.L. 4.8 steel hexagonal head screws M16x100 for wood, with an ISO 7093 M16 steel washer. Use a pre-drilled hole Ø14mm for the threaded part and a Ø16mm hole for the smooth part.

MATERIALS
For the masonry:
- Stones: sandstone, roughly squared, mean dimensions 12x15x20 cm³
- Hydraulic lime mortar: dosage lime-dry sand 1:5 (in volume)
  200 kg of lime and 1400 of kg dry sand for 1m³ of mortar
  Hydraulic lime "i.pro PLASTOCEM - Italcementi"
  Silica sand "Sabbia lavata 0/6 mm - Dal Zotto Srl"
  Add water so to obtain a plastic consistency for the mortar

NOTES:
- Before installation wash the stones with water, the stones need to damp
- The mortar joints have to be as thin as possible

Interreg ITALIA-SLOVENIJA | CONSTRAIN

TAV.
PB3.1

PILOT BUILDING
UNREIFORCED BUILDING - FRONTAL VIEWS
Quotes in cm - Scale 1:50

West wall

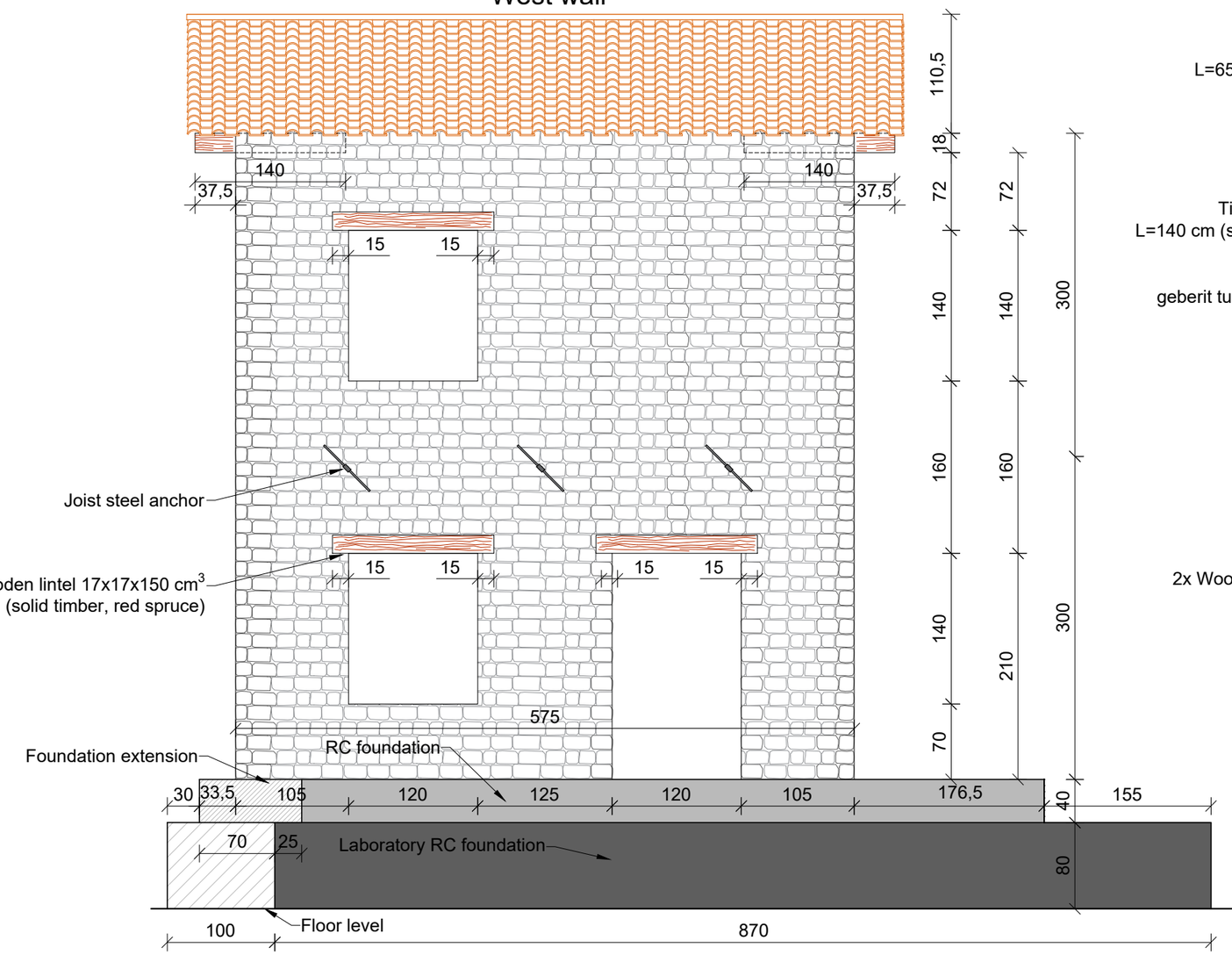

North wall

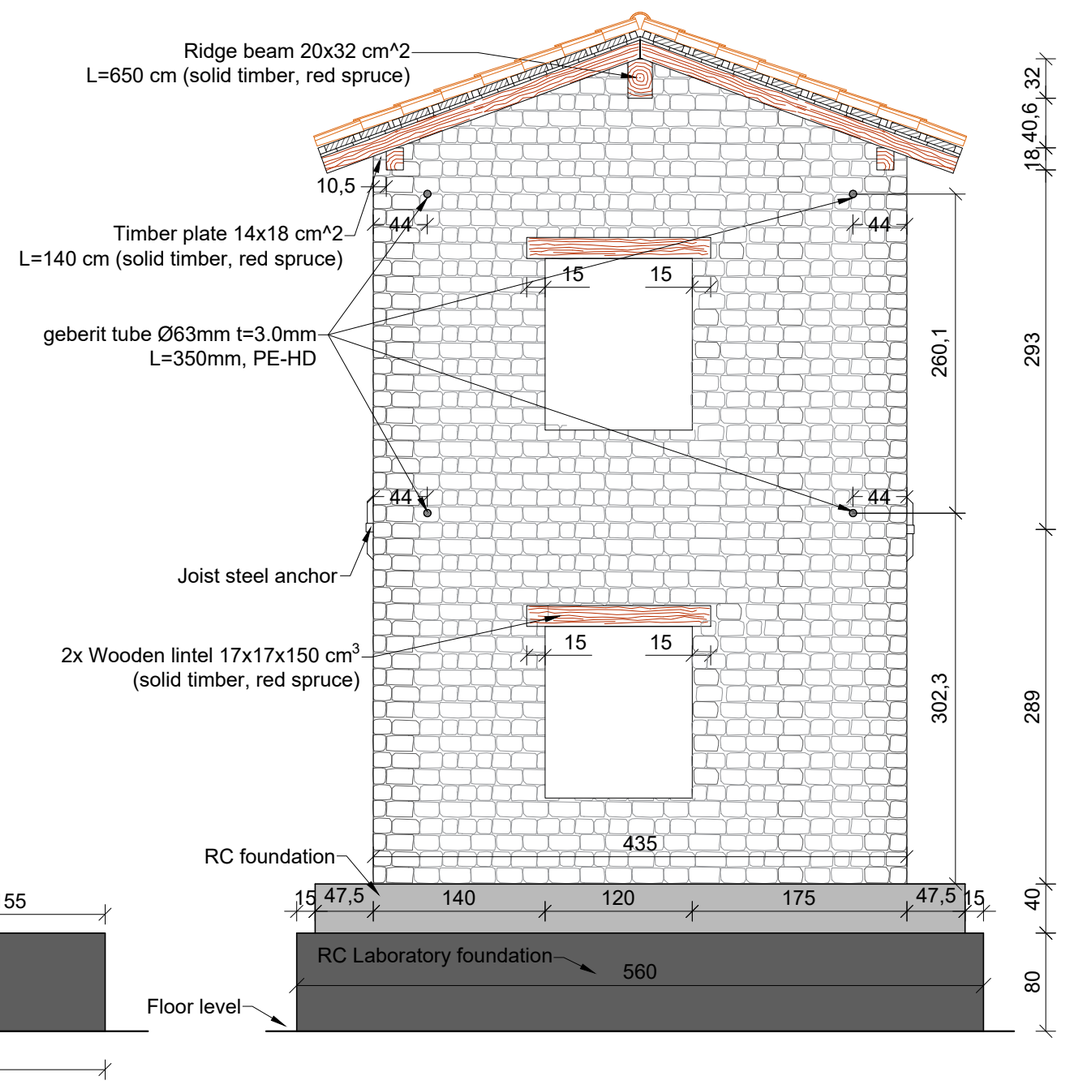

Detail of RC fundation

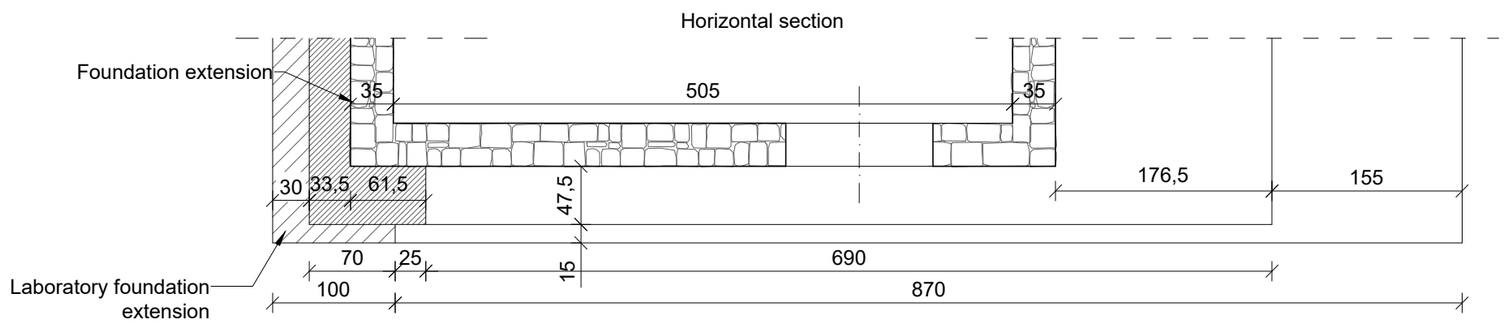

Detail of RC fundation

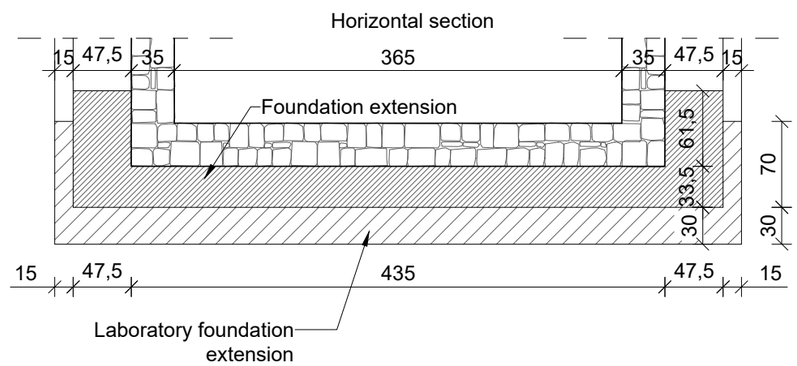

TAV.

PB3.2

PILOT BUILDING

UNREIFORCED BUILDING - FRONTAL VIEWS

Quotes in cm - Scale 1:50

East wall

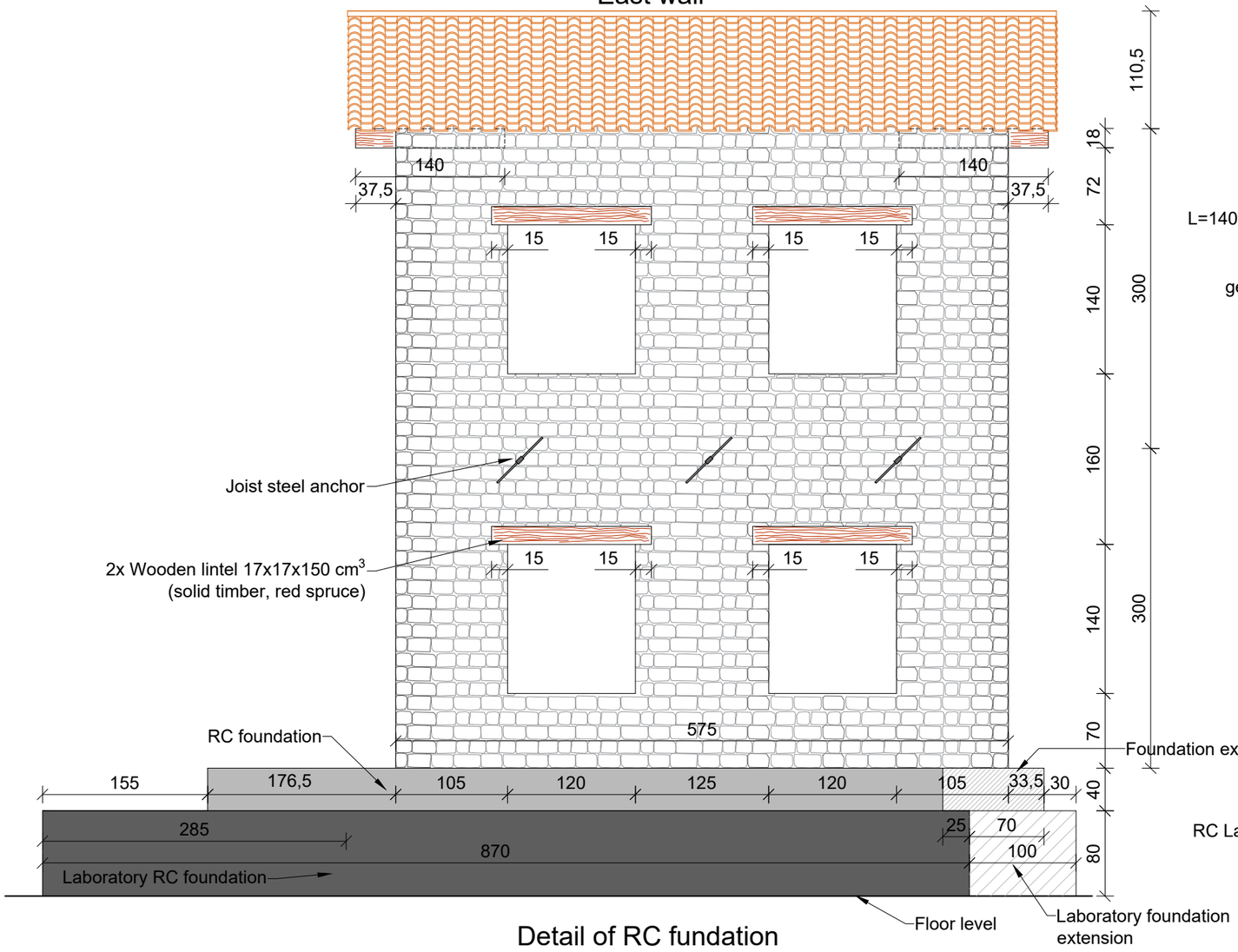

South wall

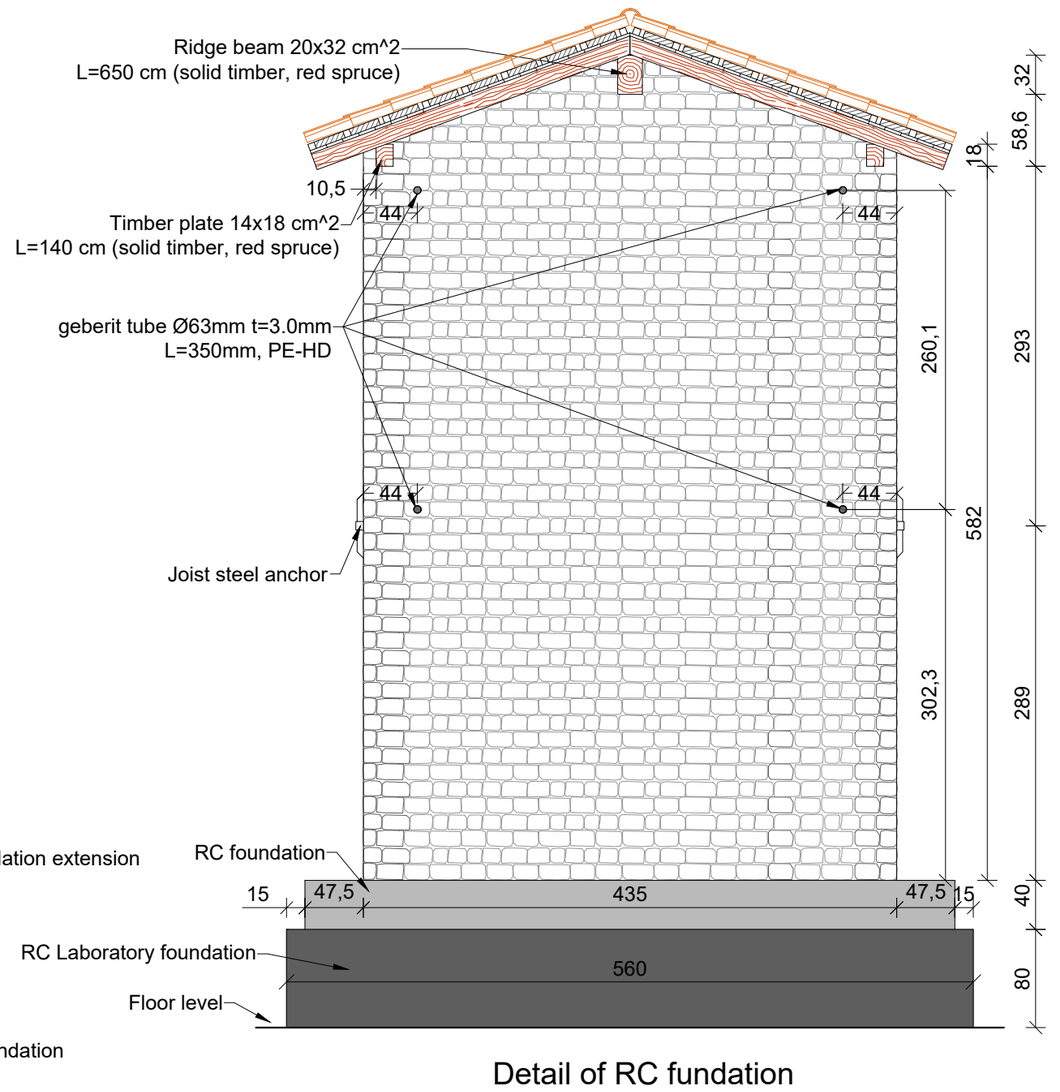

Detail of RC fundation

Horizontal section

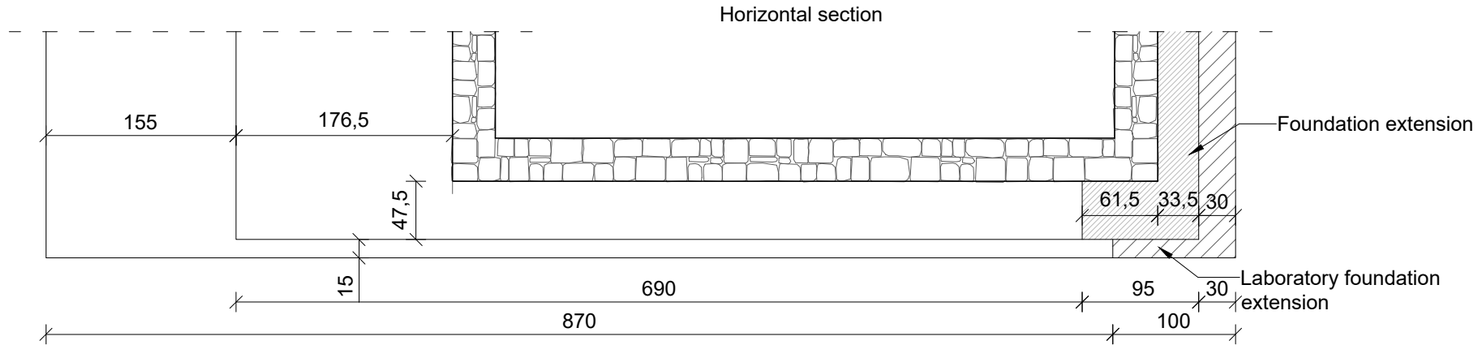

Detail of RC fundation

Horizontal section

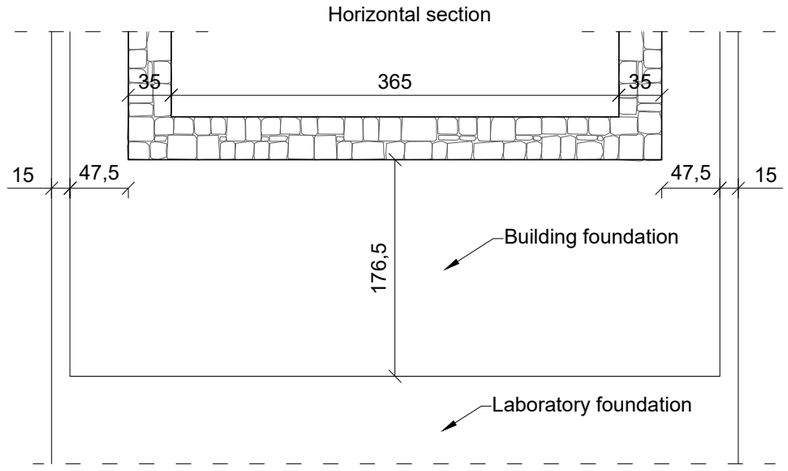

TAV.

PB3.3

PILOT BUILDING
UNREIFORCED BUILDING - ROOF DETAILS
Quotes in cm - Scale 1:50

Detail of roof frame - Scale 1:50

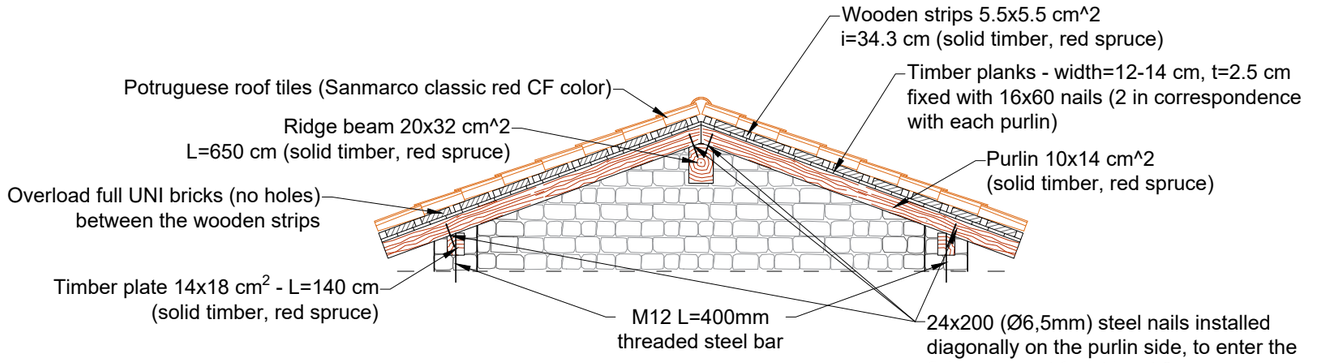

The purlins outside the timber plates are leant on the masonry wall and surrounded by the wall up to the purlin height.

Detail of the connection of the timber plate to the masonry - Scale 1:25

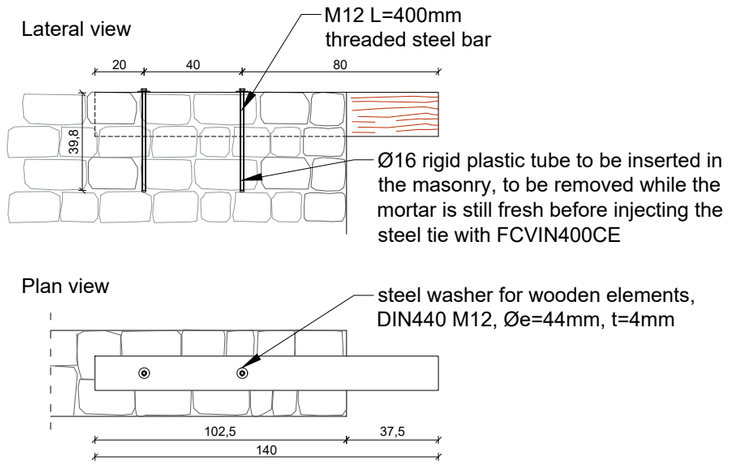

Detail of the overload on the roof - Scale 1:50

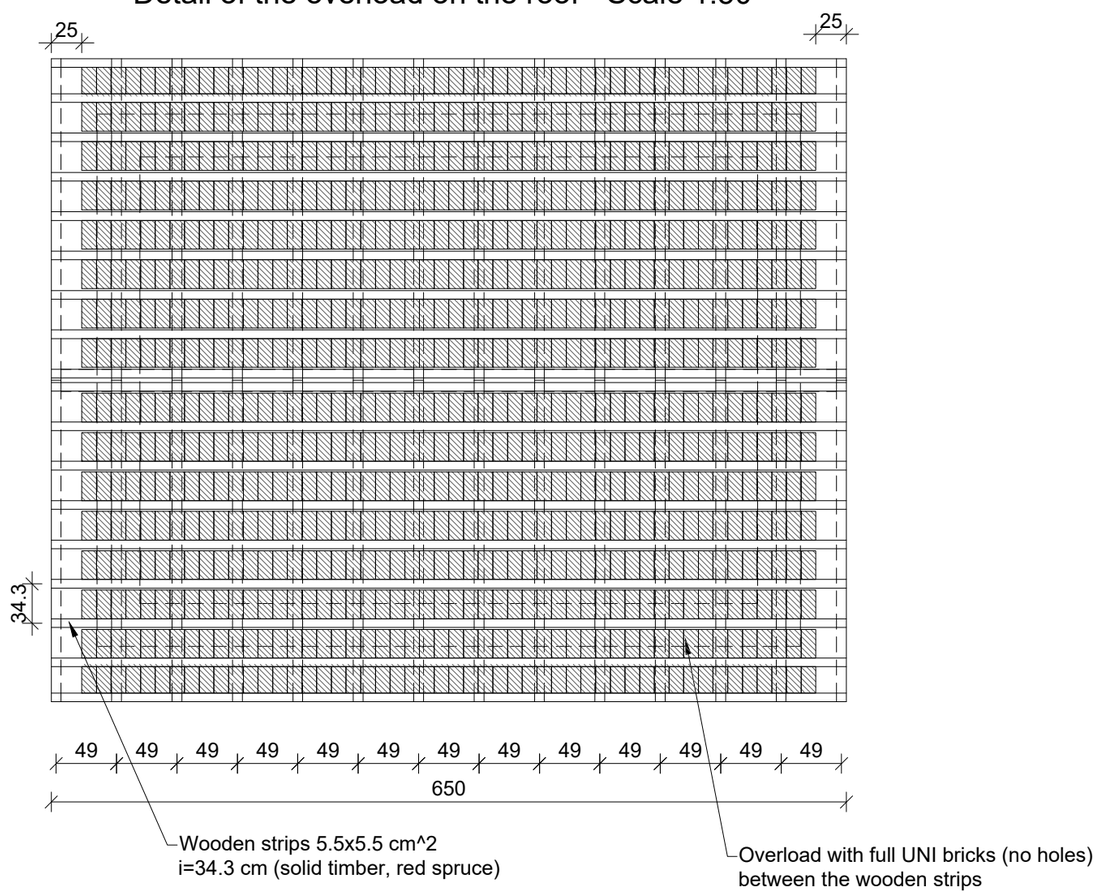

type Sanmarco

Tegola Portoghese

SCHEDA TECNICA | TECHNICAL SPECIFICATIONS

	Prod. Valenza		Prod. Castiglion Fiorentino	
	Tutti i colori	**Grey e Testa di moro**	**Tutti i colori**	**Rosata**
lunghezza / lenght	cm 41,0	cm 40,5	cm 40,9	cm 41,7
larghezza / width	cm 25,0	cm 25,0	cm 25,1	cm 25,7
pezzi al mq / pieces for sqm	14	14	14,5	13,6
peso unitario / unitary weight	Kg 3,1	Kg 3,1	Kg 2,9	Kg 2,9
peso al mq / weight for sqm	Kg 43,4	Kg 43,4	Kg 42,0	Kg 42,0
passo listelli / batten gauge	cm 34,3	cm 34,1	cm 34,6	cm 35,4
pezzi per mazzetta / pieces for bundle	6	6	6	6
pezzi per pallet / pieces for pallet	180 / 256*	180	180	180
garanzia / warranty	30 anni/years	30 anni/years	30 anni/years	30 anni/years
pendenza minima / minimum slope	> 30%	> 30%	> 30%	> 30%

TAV.
PB4

PILOT BUILDING
REINFORCED BUILDING - PLAN VIEWS
Quotes in cm - Scale 1:50

Ground Floor

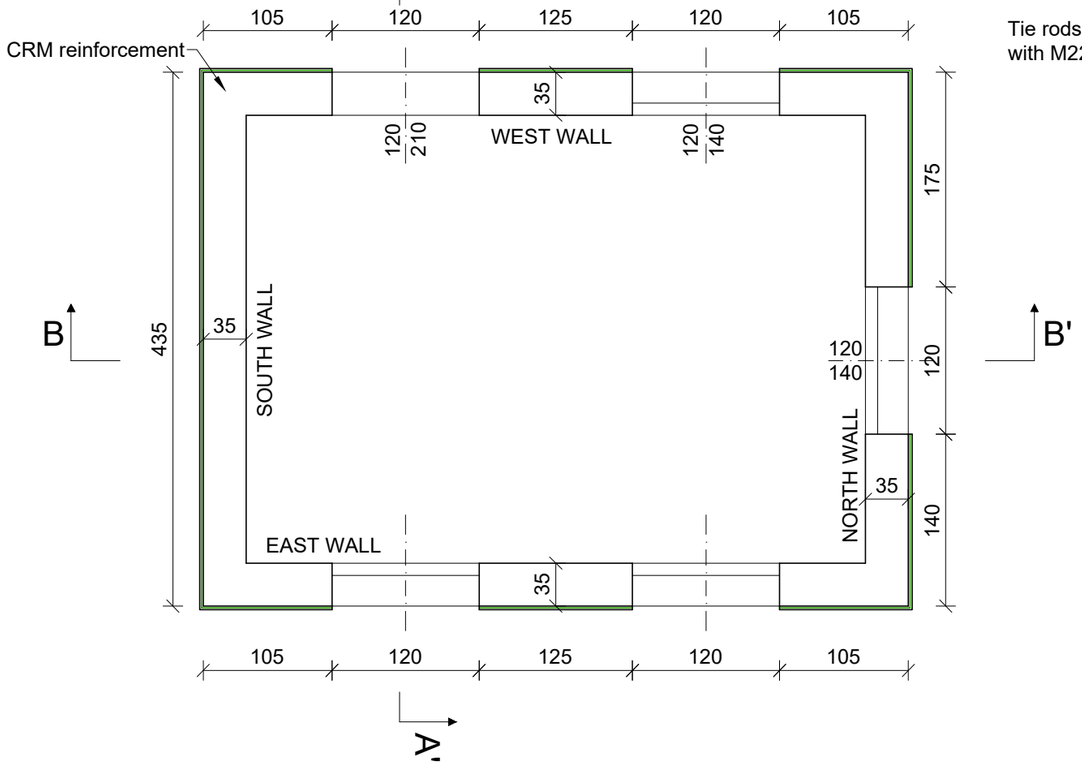

First Floor

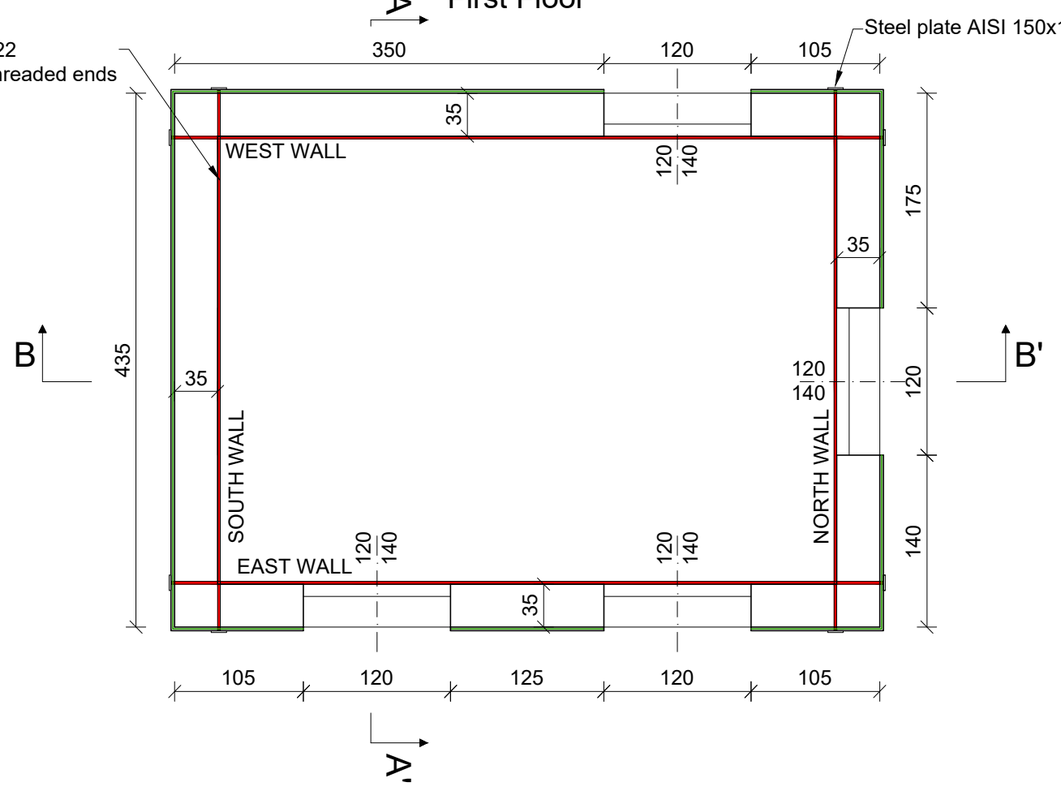

Detail of intermediate storey decking

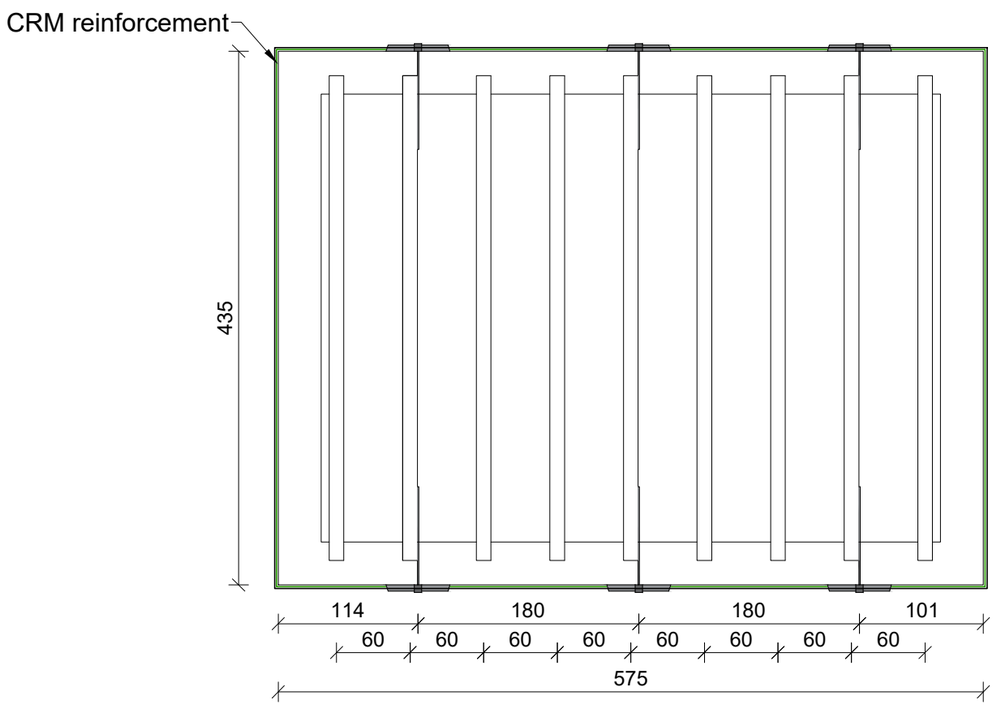

Detail of roof frame

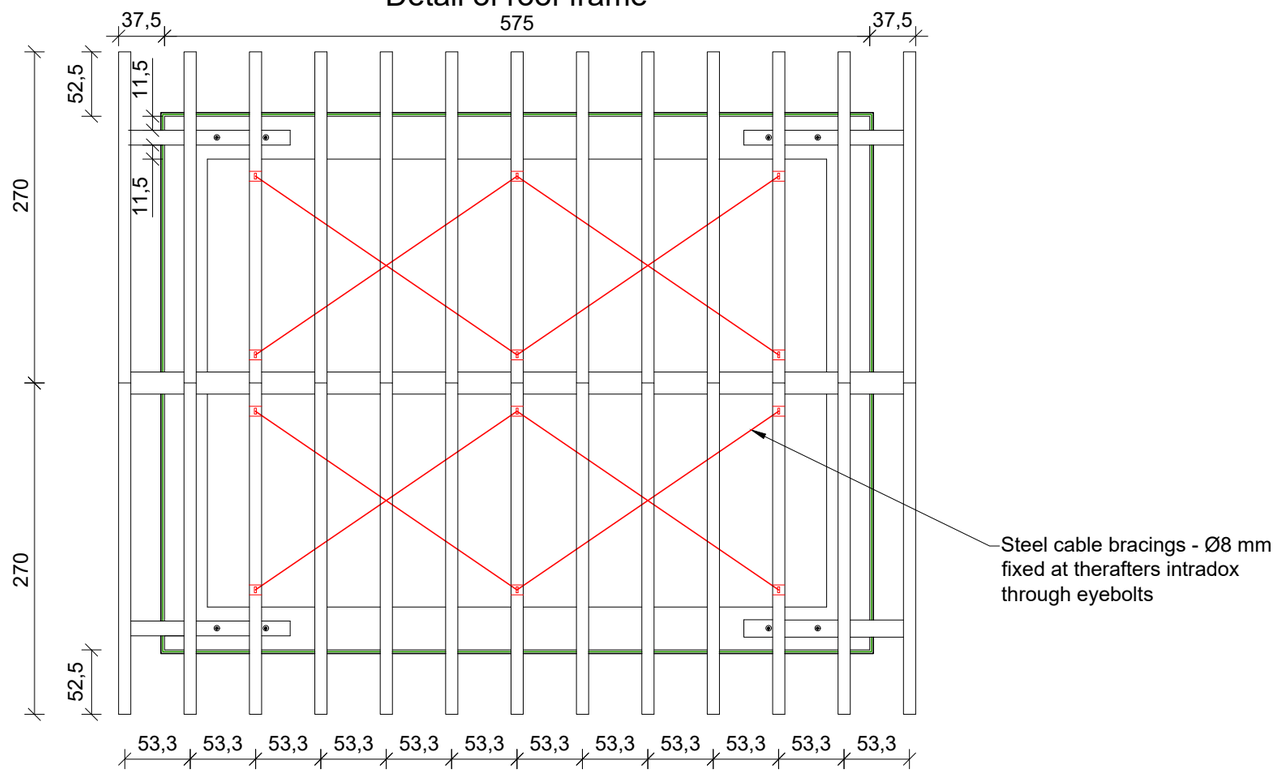

TAV.
PB5.1

PILOT BUILDING
REINFORCED BUILDING - REINFORCEMENT DETAIL
Quotes in cm - Scale 1:25

MATERIALS:
For the reinforcement:
- GFRP Mesh: FBMESH66x66T96AR (minimum overlapping lenght: 132 mm)
- GFRP local device: FBFAZ66x66T96AR (minimum overlapping lenght: 132 mm)
- GFRP L-shape connection: FBCON L 300x100 for stone masonry
  FCVIN400CE vinylester chemical anchor
- Mortar coating: FBNHL 15 MPa - natural lime mortar
- Artificial diatones: steel bars AISI 304 (or 316) M16 l=350 mm for stone masonry, Struttura Tixo - TX 351 injection grout or equivalent cementitious based grout with inroganic grow and antishrink additives, minimum compressive strength 50 MPa
- Holed steel washer Ø150, AISI 304 (or 316) with central nut M16
- Steel cable bracings - Ø8 mm fixed at the roof intradox through eyebolts
- Tie rods Ø22
- Ribbed steel plates AISI 150x150x15 mm^3
- Threaded steel bar AISI 316 - Ø8 - L=65 cm - pitch 3/m (injected in holes drilled in the RC beams for a minimum lenght 250 mm)

Detail of the corner - Scale 1:25

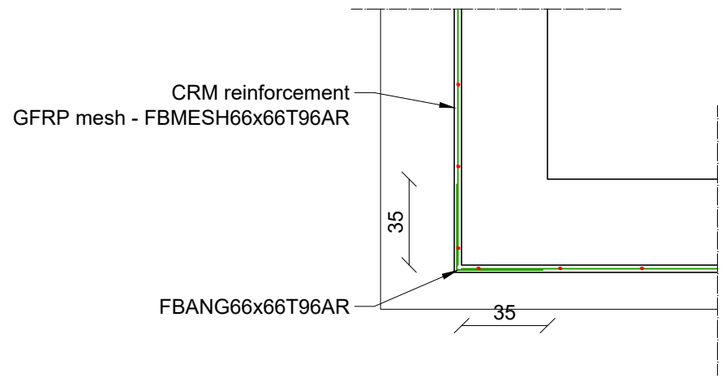

CRM reinforcement - Scale 1:25

Transversal section

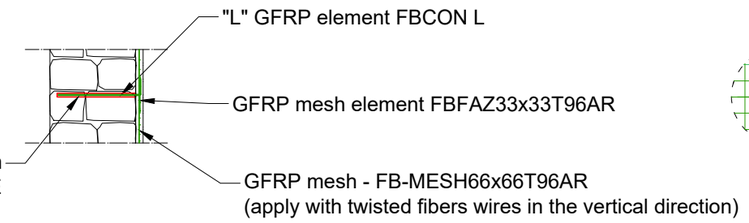

Frontal view

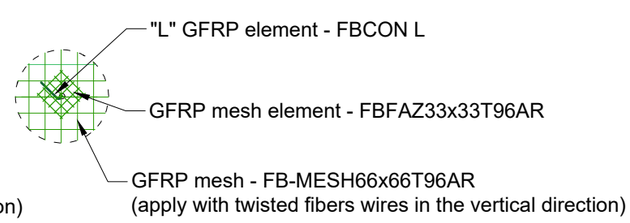

Detail of steel anchor - Scale 1:25

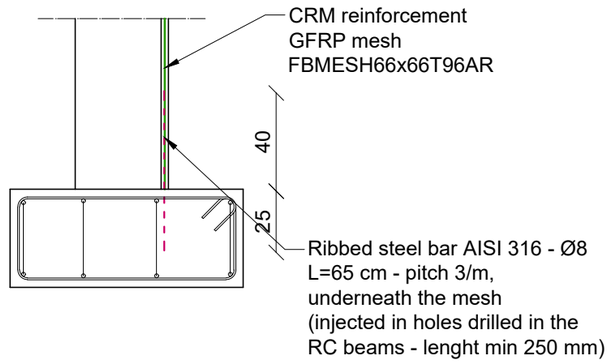

Artificial diaton - Scale 1:25

Transversal section

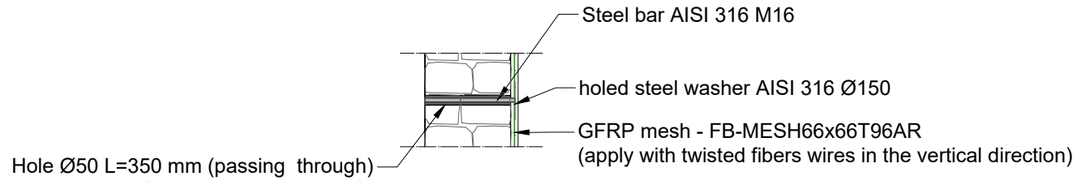

Frontal view

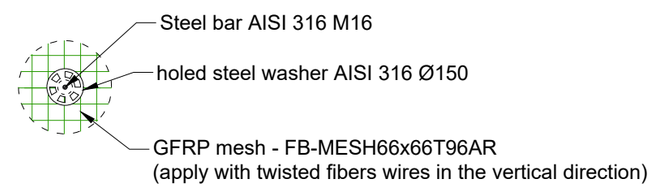

For installing the holed steel washers:
Scratch the steel surface on both sides of the washer with an angle grinder;

Holed steel washer
lateral view

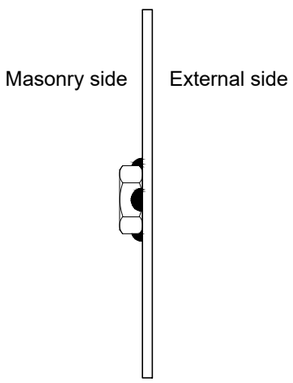

TAV.

PB5.2

PILOT BUILDING
REINFORCED BUILDING - REINFORCEMENT DETAIL
Quotes in cm - Scale 1:25

Steel fork with eye nuts at the base of the rafters (6x)
steel S275

Front view

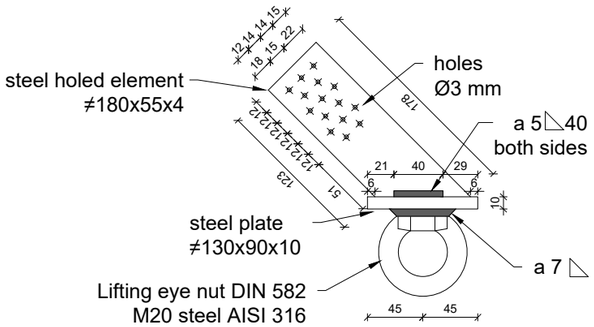

Rear view

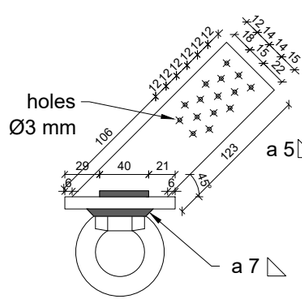

Lateral view

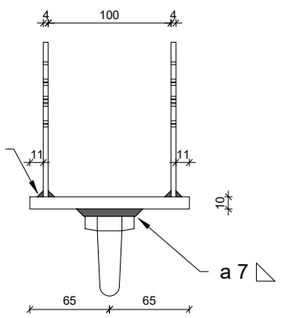

Steel fork with eye nuts at the top of the rafters (6x)
steel S275

Front view

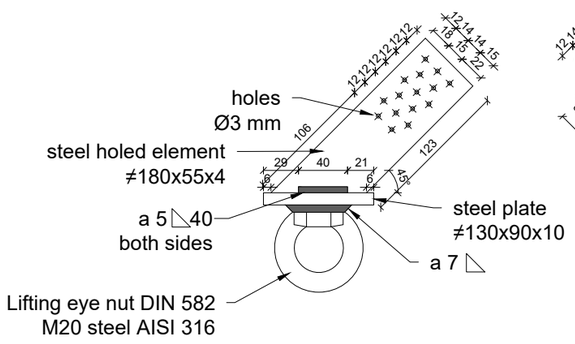

Rear view

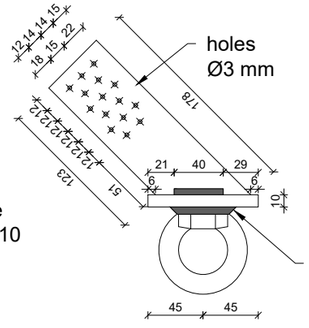

Lateral view

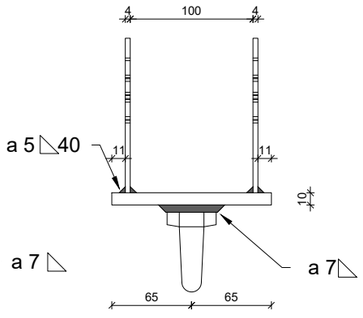

To fix the steel forks use steel nails 17x70 round section (Ø3.0 mm, L=70mm)
shot with a nail gun, 30 nails per element

Detail of the steel tie rods - Scale 1:25

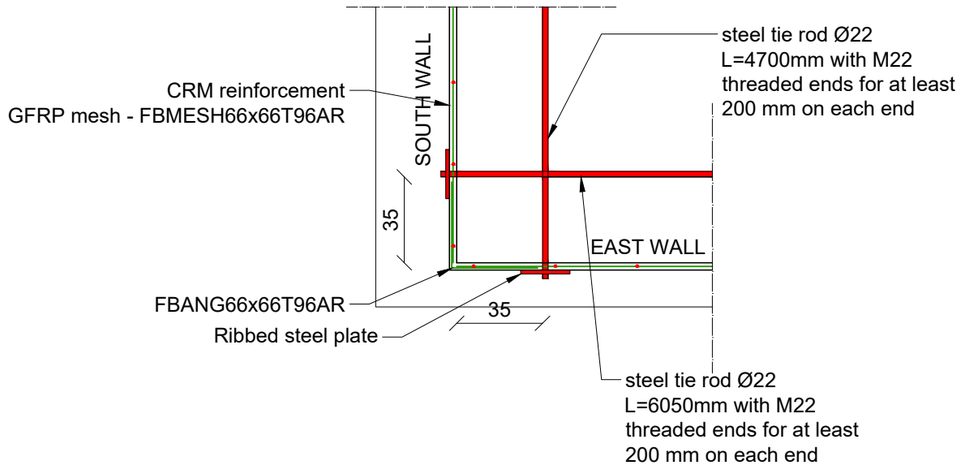

Commercial ribbed steel plate (8x)
steel S275

Front view

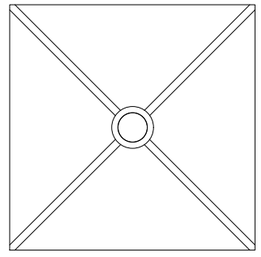

Lateral view

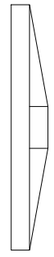

Approximate dimensions 150x150x15 mm

Interreg ITALIA-SLOVENIJA | CONSTRAIN

TAV.
PB6

PILOT BUILDING
REIFORCED BUILDING - SECTION VIEWS
Quotes in cm - Scale 1:50

SECTION A-A'

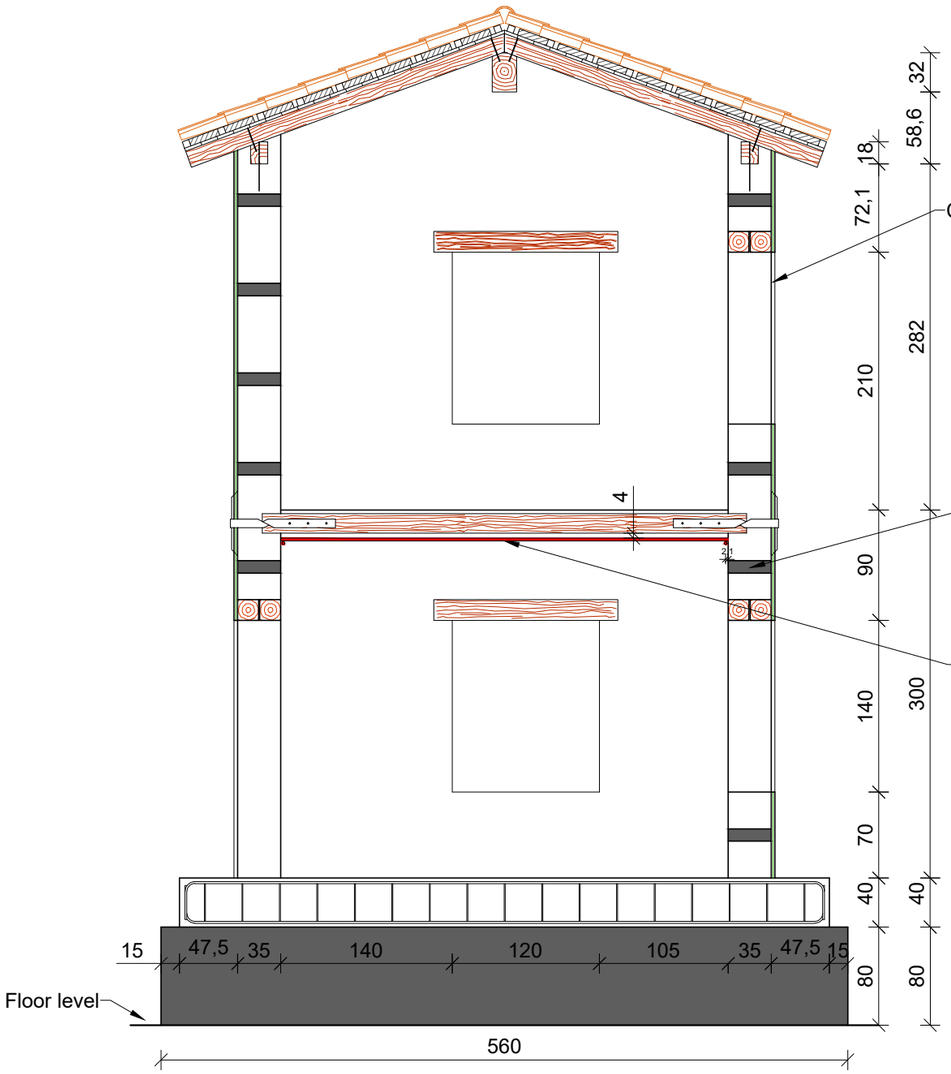

SECTION B-B'

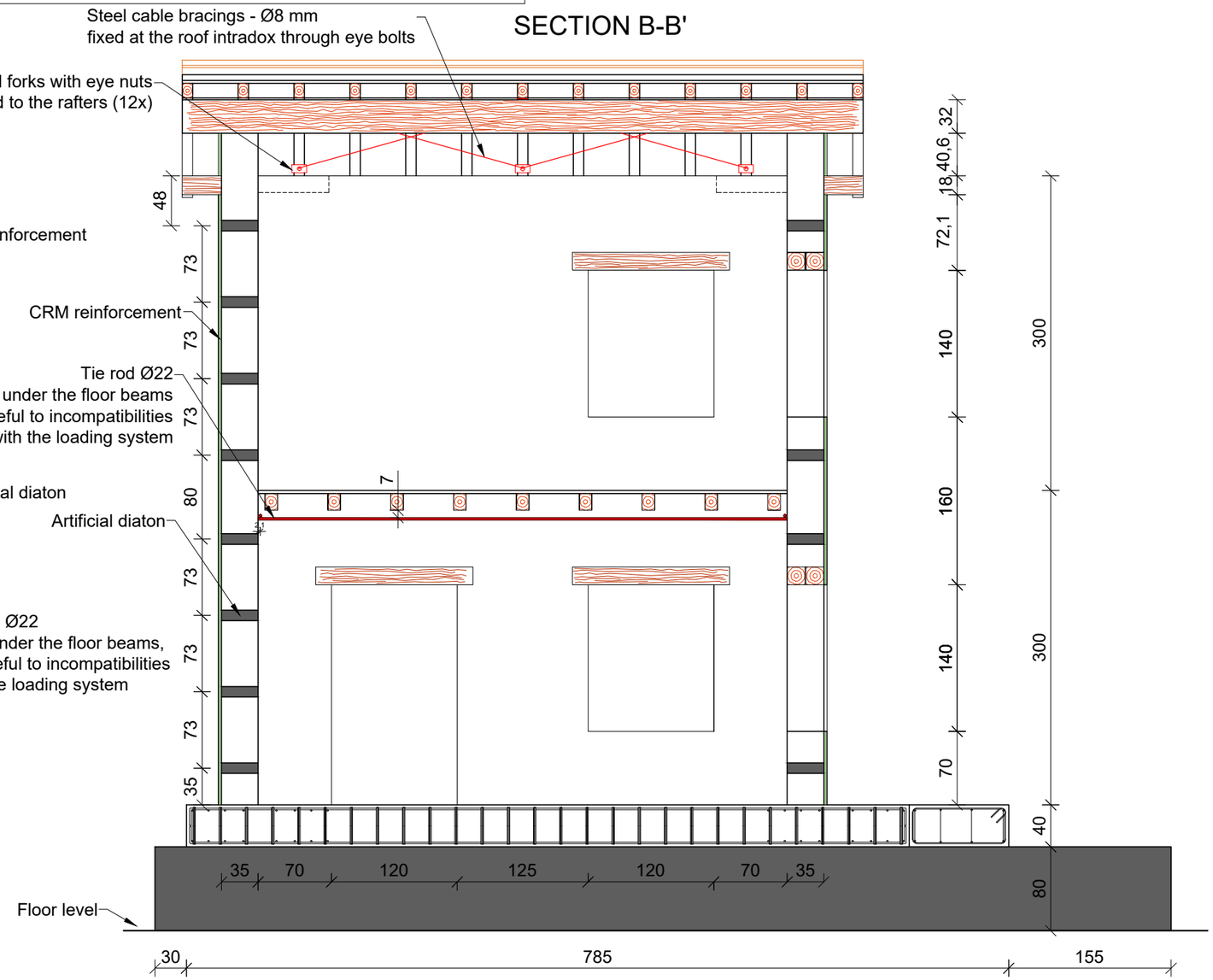

Detail of roof tyings - Scale 1:25

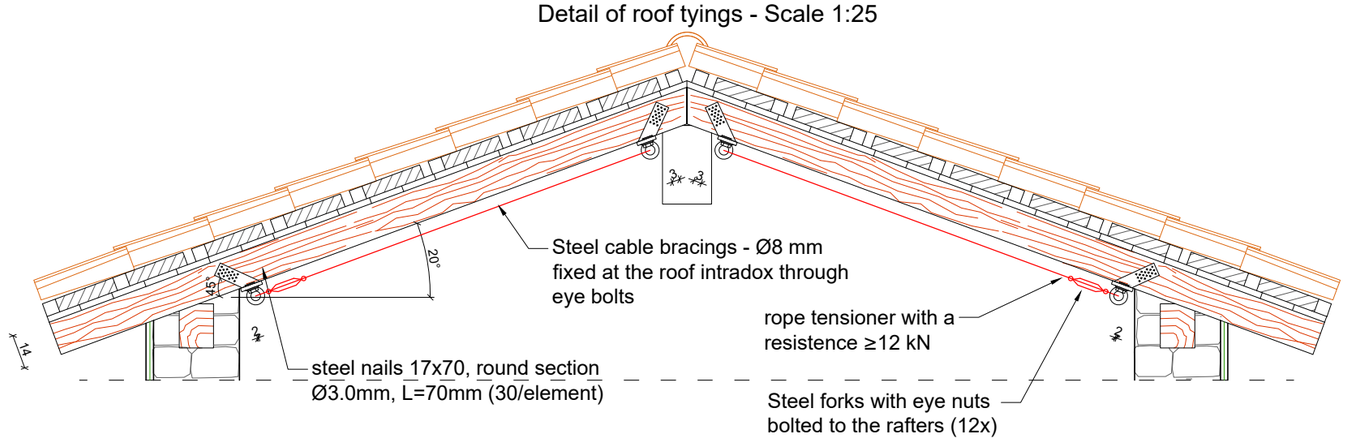

Interreg ITALIA-SLOVENIJA | CONSTRAIN

TAV.
PB7.1

PILOT BUILDING
REIFORCED BUILDING - FRONTAL VIEWS
Quotes in cm - Scale 1:50

West wall

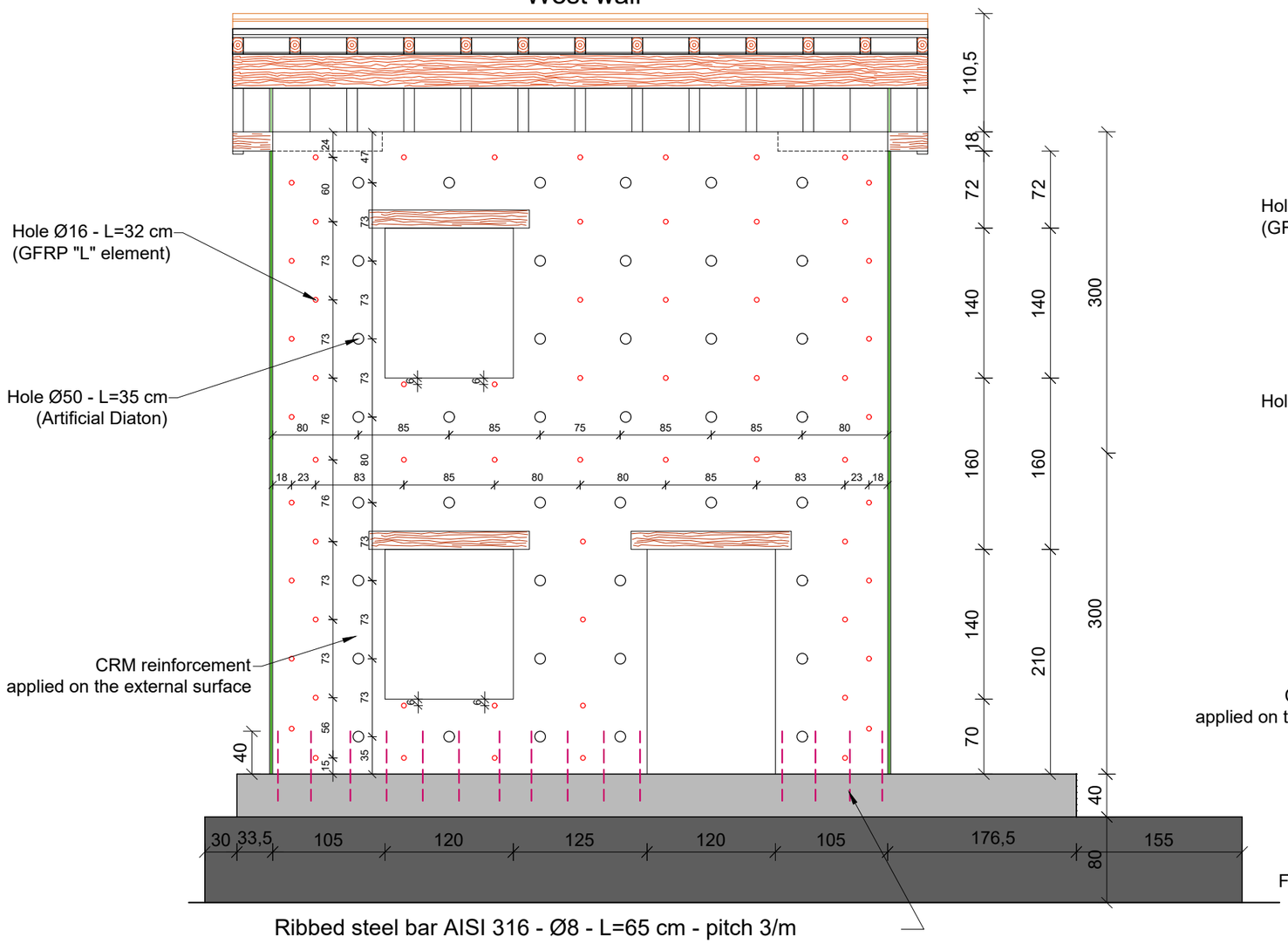

Ribbed steel bar AISI 316 - Ø8 - L=65 cm - pitch 3/m
(injected in holes drilled in the RC beams - lenght min 250 mm)

North wall

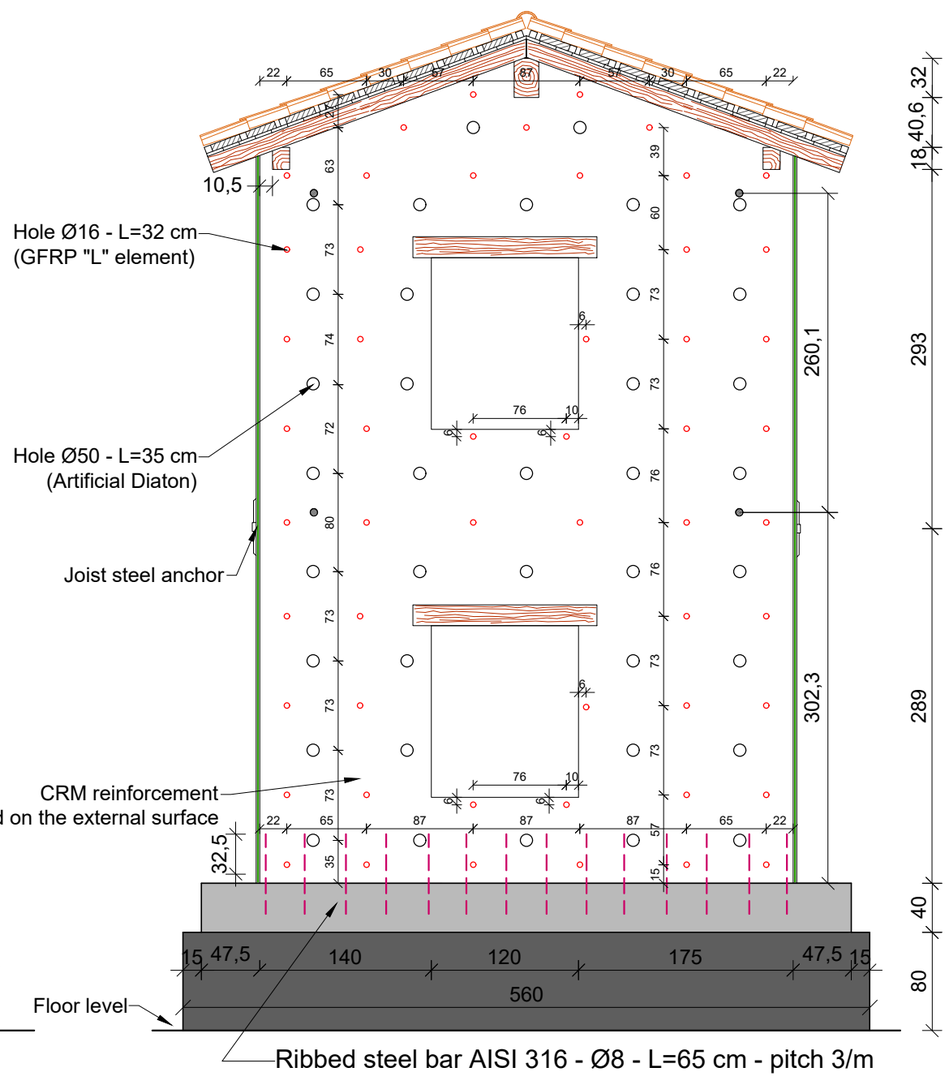

Ribbed steel bar AISI 316 - Ø8 - L=65 cm - pitch 3/m
(injected in holes drilled in the RC beams - lenght min 250 mm)

Detail of RC fundation

Horizontal section

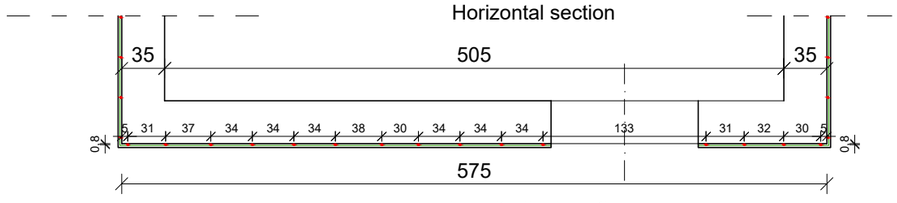

Longitudinal section

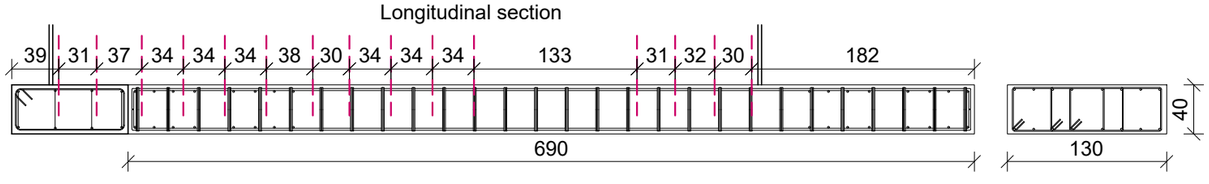

Detail of RC fundation

Horizontal section

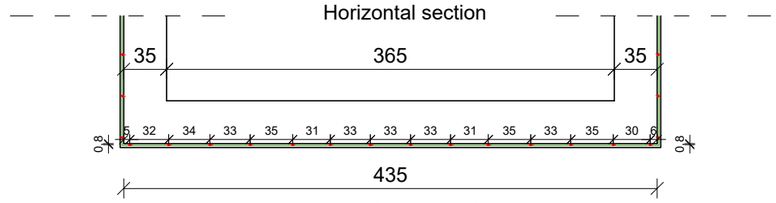

Longitudinal section

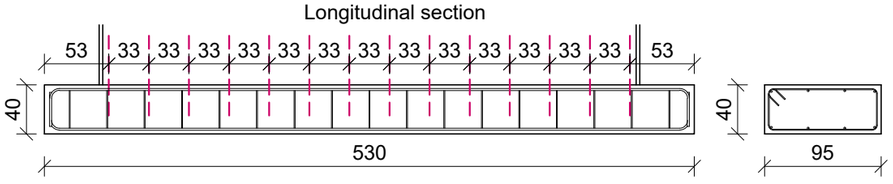

Interreg ITALIA-SLOVENIJA — CONSTRAIN

TAV.
PB7.2

PILOT BUILDING
REIFORCED BUILDING - FRONTAL VIEWS
Quotes in cm - Scale 1:50

East wall

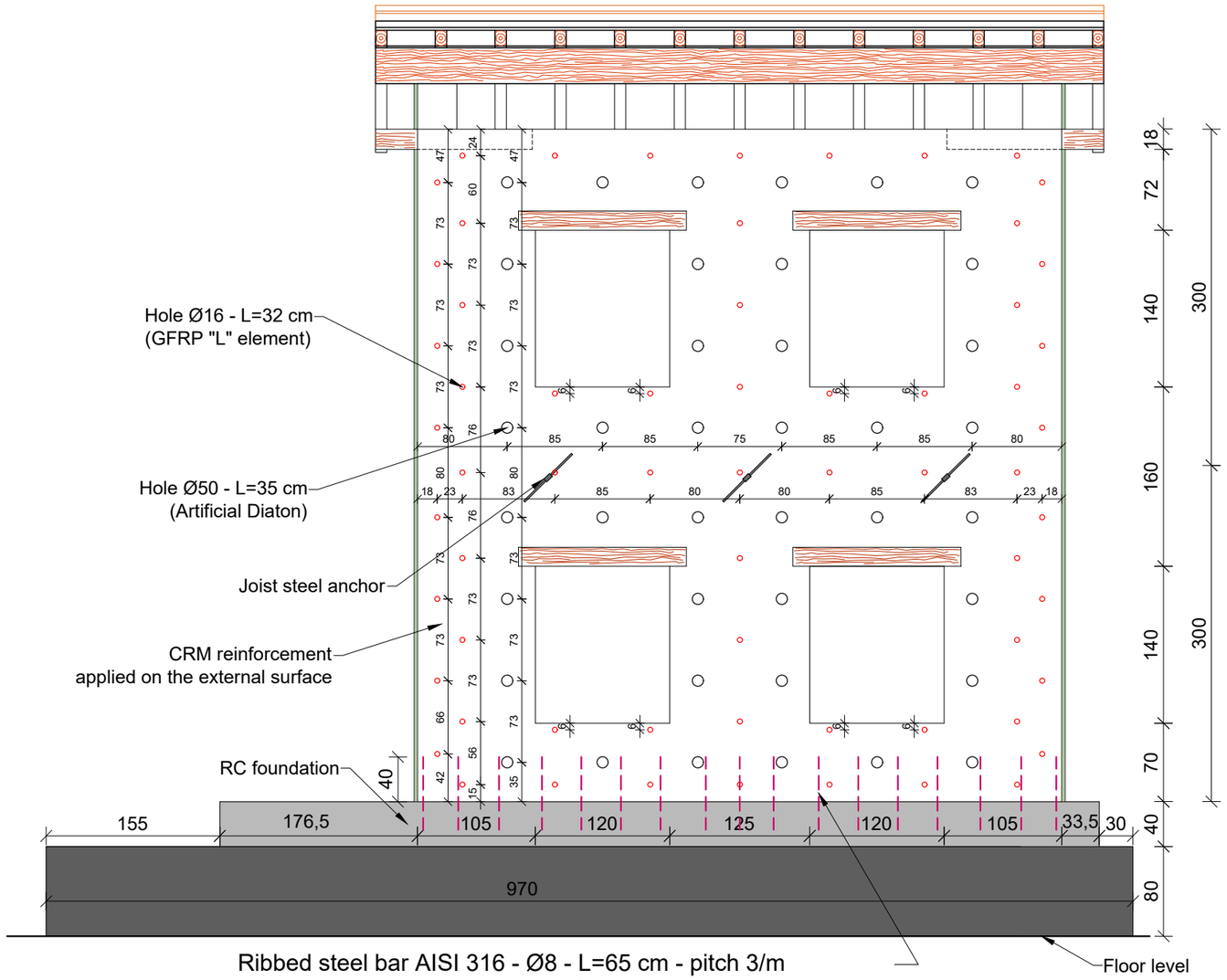

Ribbed steel bar AISI 316 - Ø8 - L=65 cm - pitch 3/m
(injected in holes drilled in the RC beams - lenght min 250 mm)

South wall

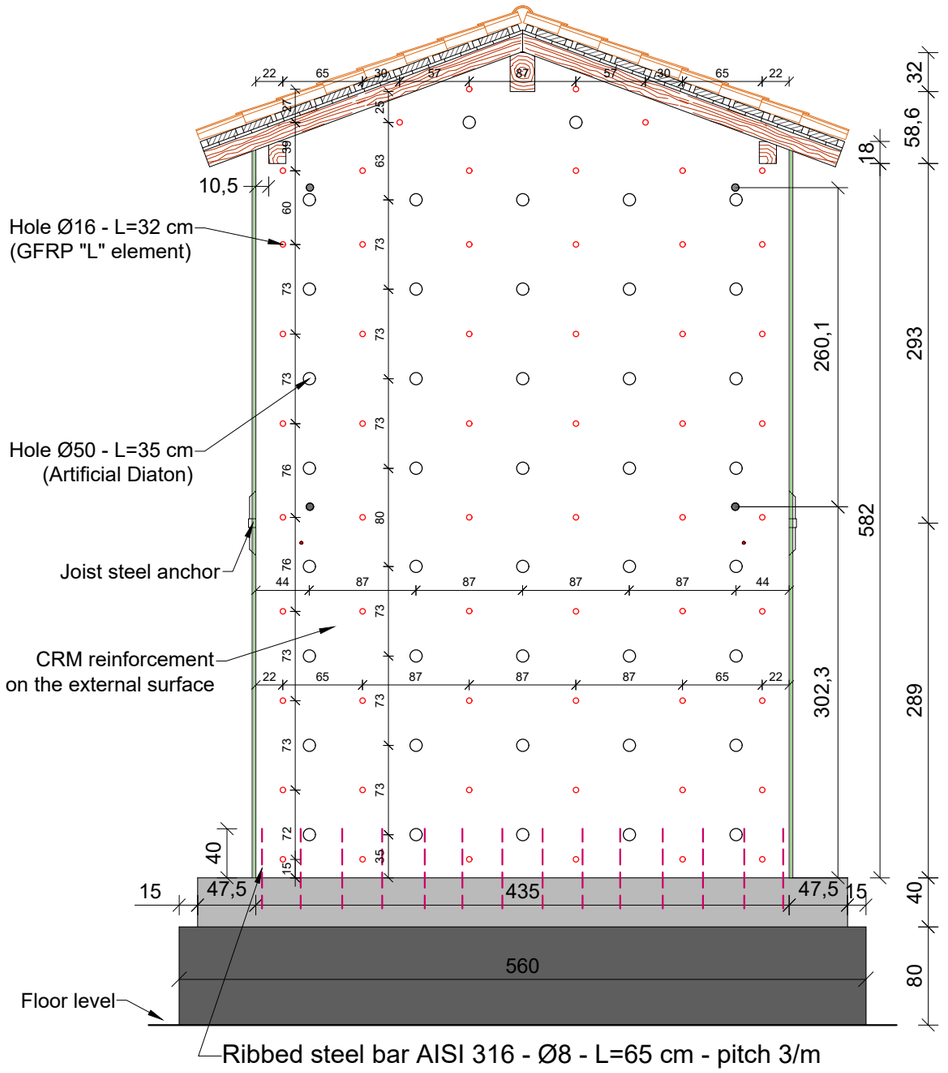

Ribbed steel bar AISI 316 - Ø8 - L=65 cm - pitch 3/m
(injected in holes drilled in the RC beams - lenght min 250 mm)

Detail of RC fundation

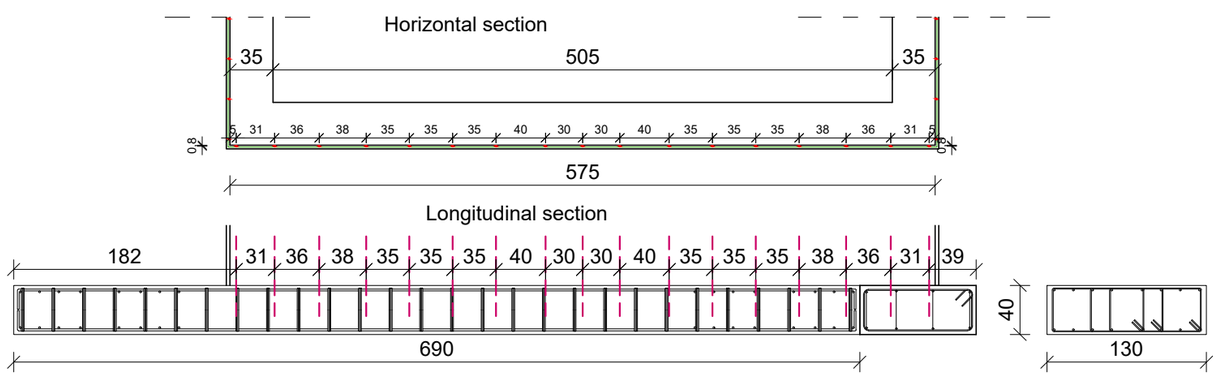

Detail of RC fundation

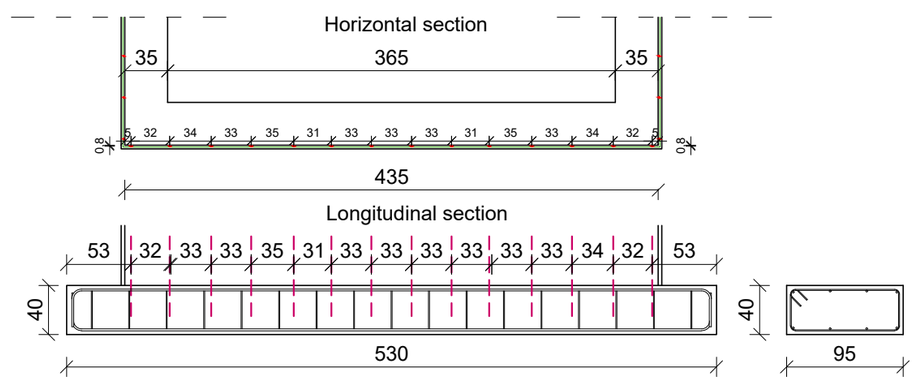

Testing apparatus: lateral view EAST wall

Scale 1:25

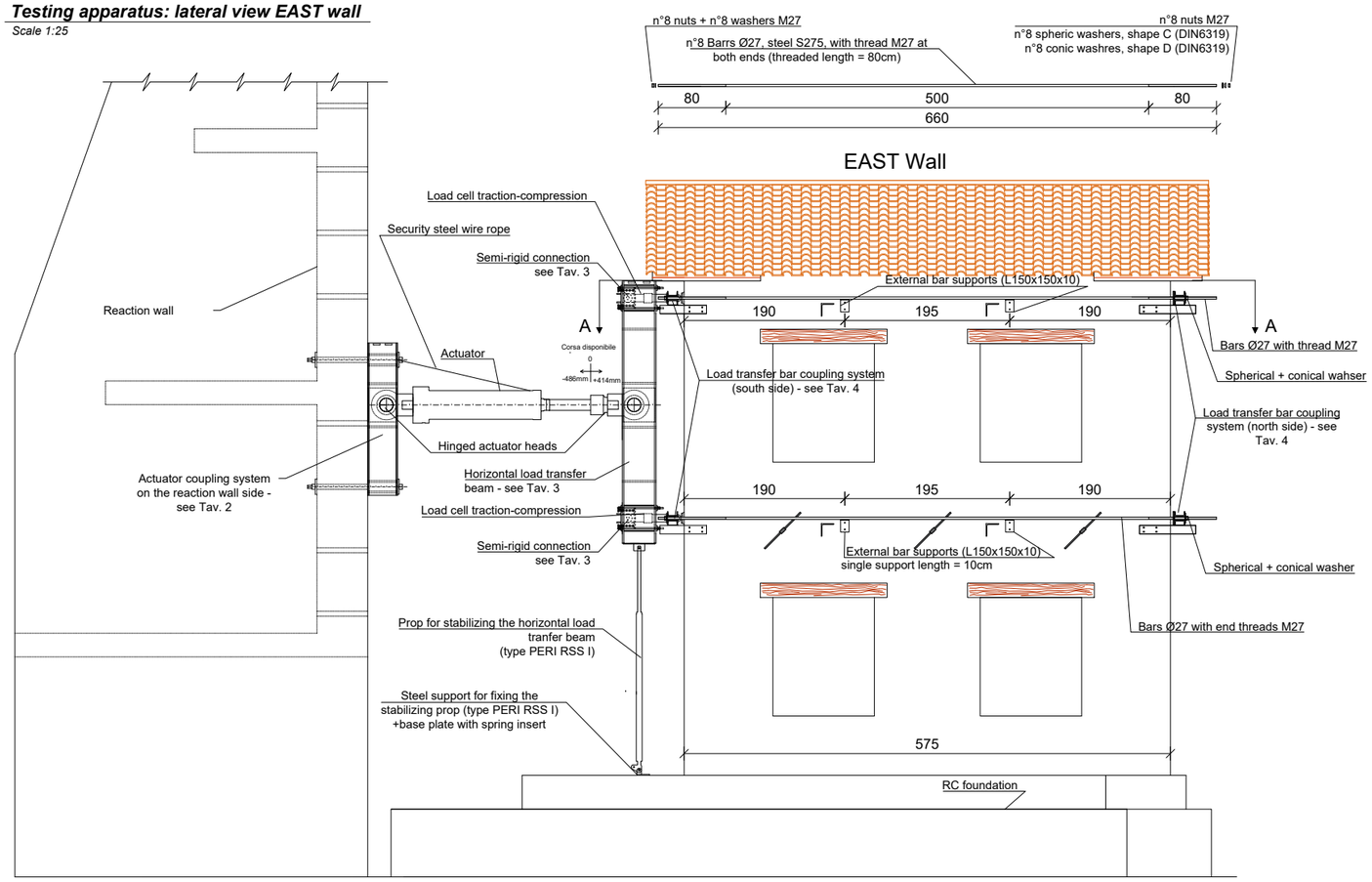

Testing apparatus: lateral viewSOUTH wall

Scale 1:25

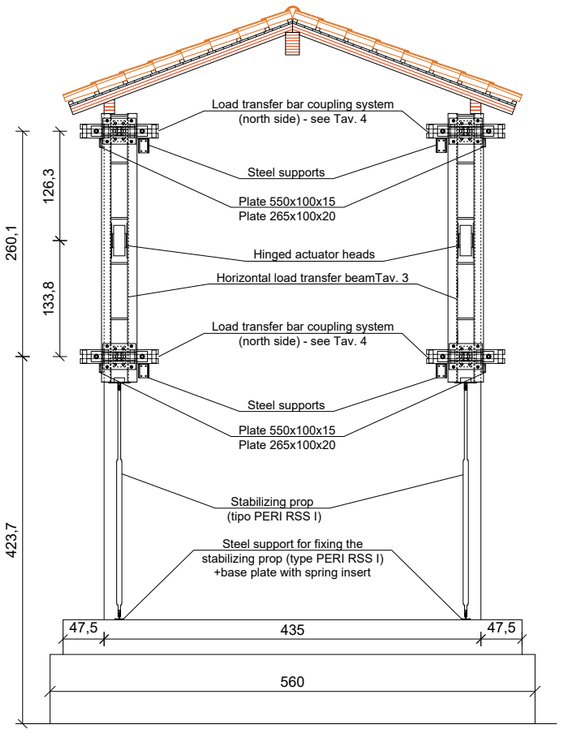

Steel supports (n°8)

Scale 1:5 - quotes in mm

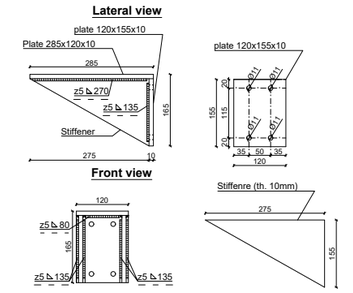

External bar supports (n°12)

Scale 1:5 - quotes in mm

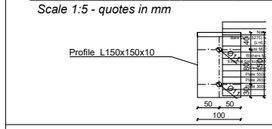

MATERIALS BILL		
Name	N°	Weight [kg]
Bars Ø27 (S275) with end threads (L=6,6m)	8	264,4
Nuts M27 - 8.8	8	-
Wahers M27 - 8.8	8	-
External bar supports (L150x150x10)	12	27,6
Steel supports	8	60,0
Plate 550x100x15	8	51,8
Plate 265x100x20	8	33,3
Plate 300x120x10	4	11,3
	TOT.	448.4

Testing apparatus: section A-A

Scale 1:25

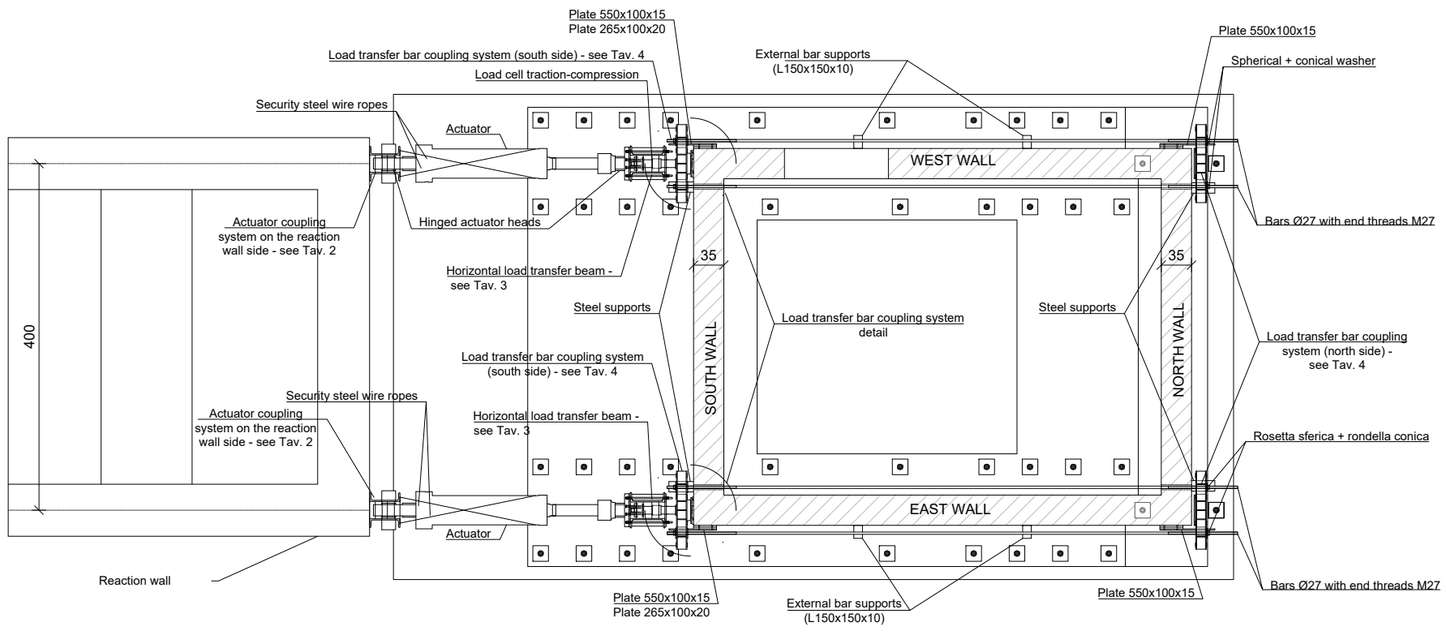

Detail of the load transfer bars coupling system (south side)

Scale 1:25 - quotes in mm

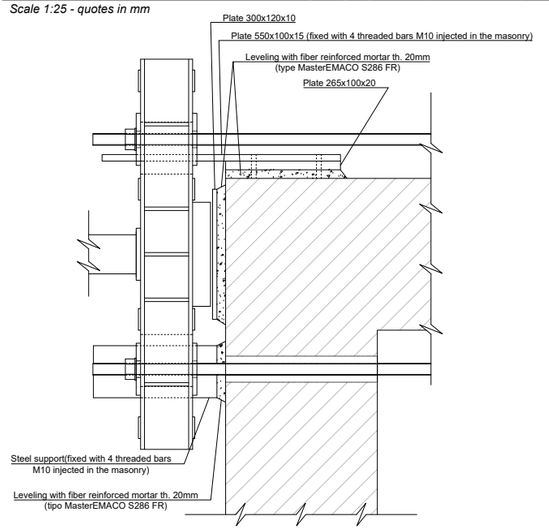

Plate 300x120x10 (n°4)

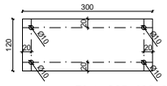

Plate 550x100x15 (n°8)

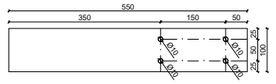

Plate 265x100x20 (n°8)

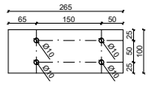

MATERIAL PRESCRIPTIONS

Steel S355 as per UNI EN 10025 - hot rolled products

- ULTIMATE TENSILE STRENGTH ftk>490MPa
- YIELDING STRENGTH fyk>355MPa

ANGULAR WELDING

All welding beads are executed with con electrodes type E52 with quality class 4B (UNI5132)

TYPUCAL WELDING BEADS

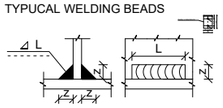

BOLTS - NUTS - WASHERS

- Bolts, nuts and washers according to point §11.3.4.6 of the D.M. 17/01/2018
- All bolts and the threaded bars are of high strength class 8.8 unless different specification in the drawings
- All bolts and the threaded bars must be got galvanized

Interreg ITALIA-SLOVENIJA — CONSTRAIN

Oggetto:

Loading system for the cyclic test on the stone masonry pilot building

TAV. PB8.1 — Testing apparatus assembly

Quotes in mm - Scale 1:25, 1:5, 1:2.5

Coupling system for the actuator to the reaction wall side (n°2): lateral view

Scale 1:5

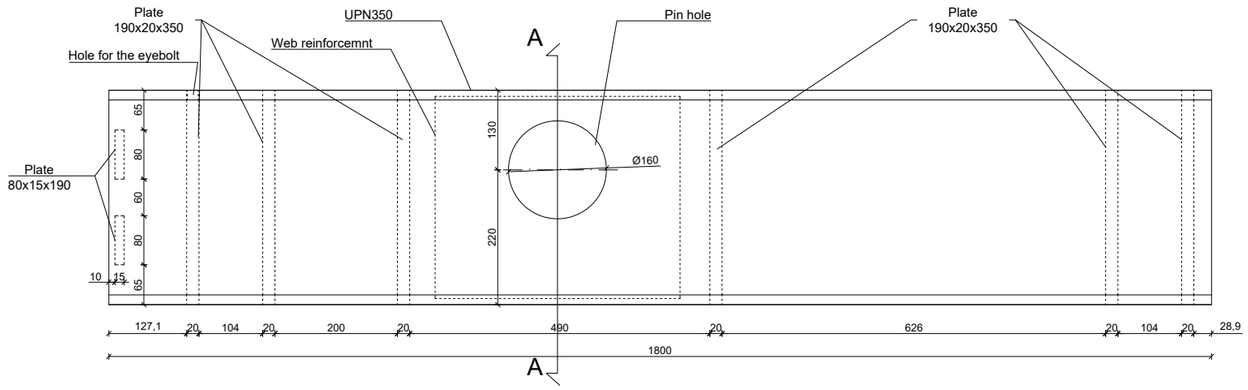

Section A-A

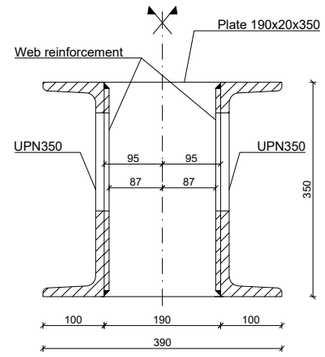

MATERIALS BILL		
Name	N°	Weight [kg]
Galvanized steel wire rope spiroide 1x19 - Ø8 (L=2,5m/ea.)	4	-
Mousqueton galvanized steel 120mm	8	-
Wire rope clamps Ø8	16	-
Tensioner 2 eyebolts DIN1480 - M20	4	-
Eyebolt DIN580-C15E-M16 with nut M16	4	-
UPN350 (L=1,8m)	4	336
Plate 190x20x350	12	93,7
Plate 80x15x190	4	7,2
Web reinforcement (plate 400x330x8)	4	28,1
	TOT.	465,2

Coupling system for the actuator to the reaction wall side: plan view (superior/inferior)

Scale 1:5

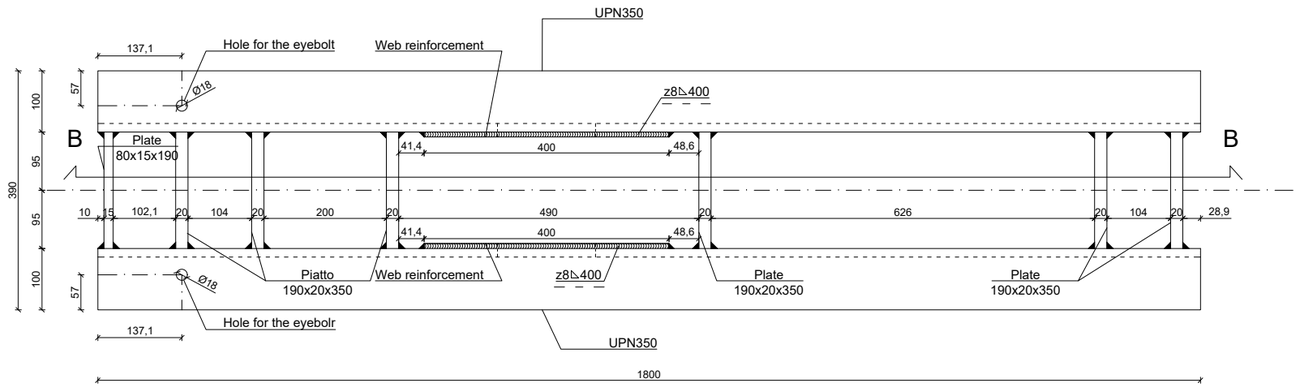

Web reinforcement (n°2)

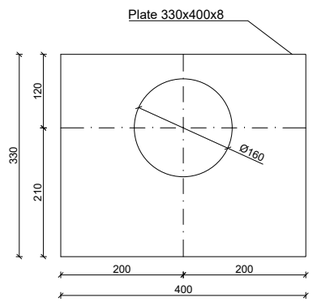

Section B-B

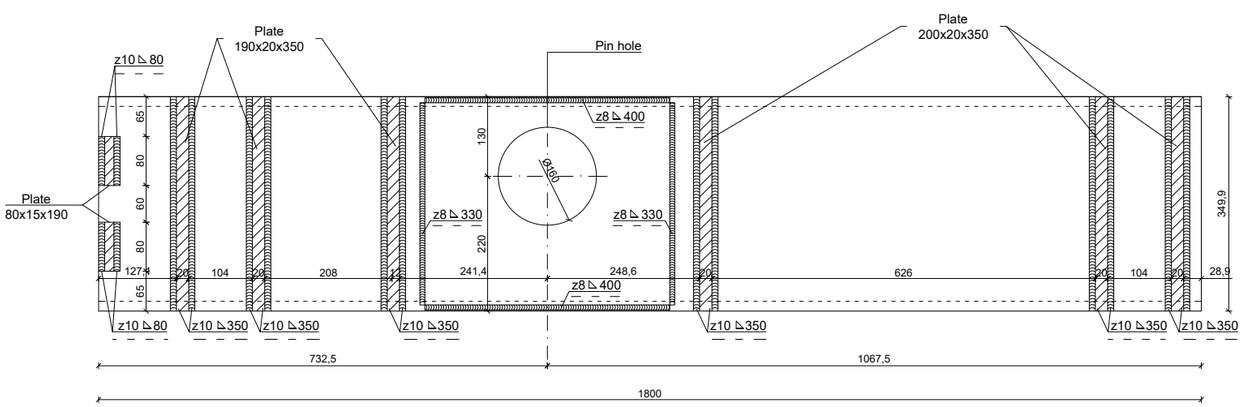

MATERIAL PRESCRIPTIONS

Steel S355 as per UNI EN 10025 - hot rolled products

- ULTIMATE TENSILE STRENGTH ftk>490MPa
- YIELDING STRENGTH fyk>355MPa

ANGULAR WELDING

All welding beads are executed with con electrodes type E52 with quality class 4B (UNI5132)

TYPUCAL WELDING BEADS

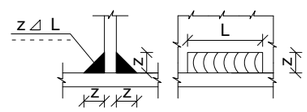

Interreg ITALIA-SLOVENIJA — CONSTRAIN

Oggetto:

Loading system for the cyclic test on the stone masonry pilot building

TAV. **PB8.2**

Coupling system betweenbetween the actuator and the reaction wall

Quotes in mm - Scale 1:5

Horizontal load transfer beam (n°2): lateral view

Scala 1:5

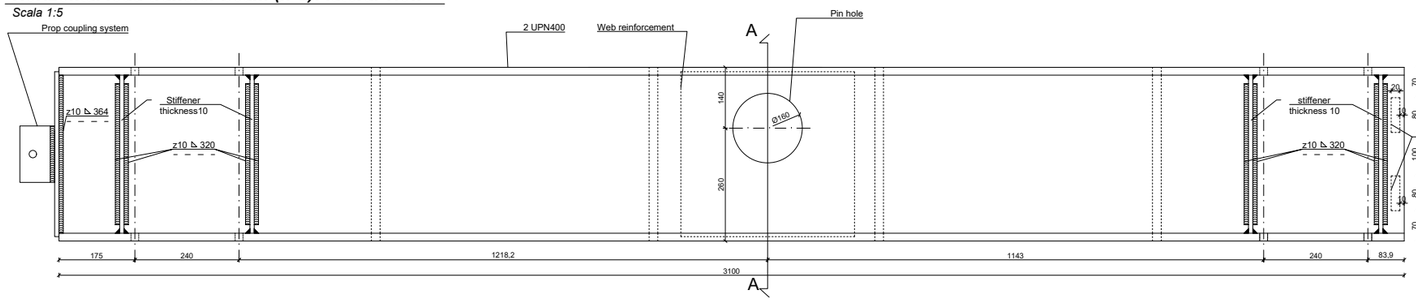

Section A-A

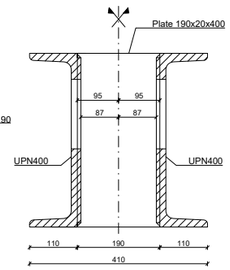

Horizontal load transfer beam: Plan view (superior/inferior)

Scale 1:5

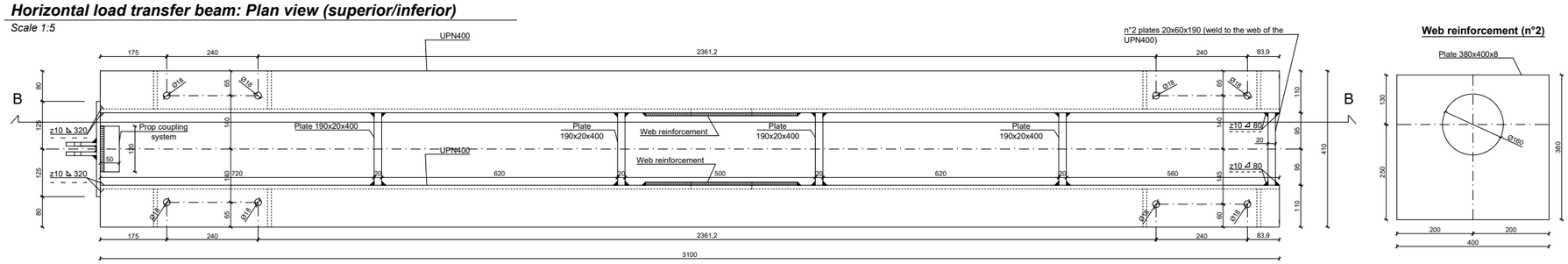

Web reinforcement (n°2)

Section C-C

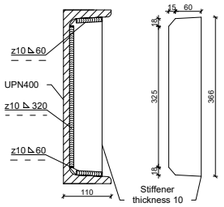

Section B-B

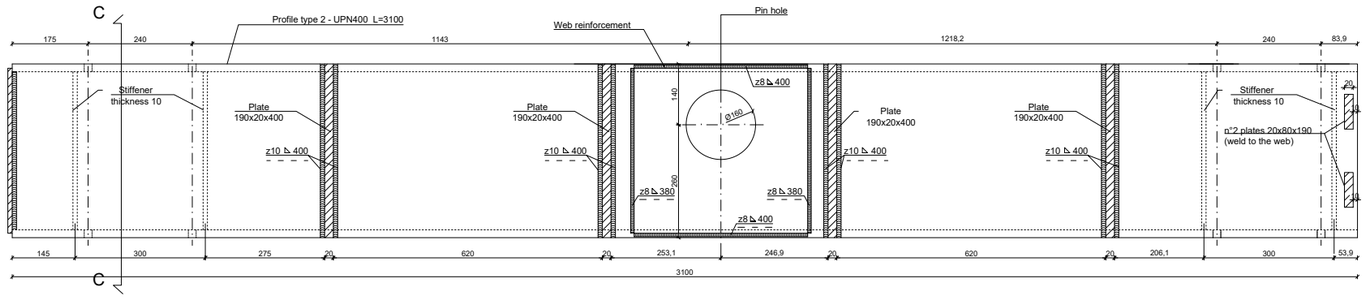

Horizontal load transfer beam (n°2): detail of the coupling system

Scala 1:10

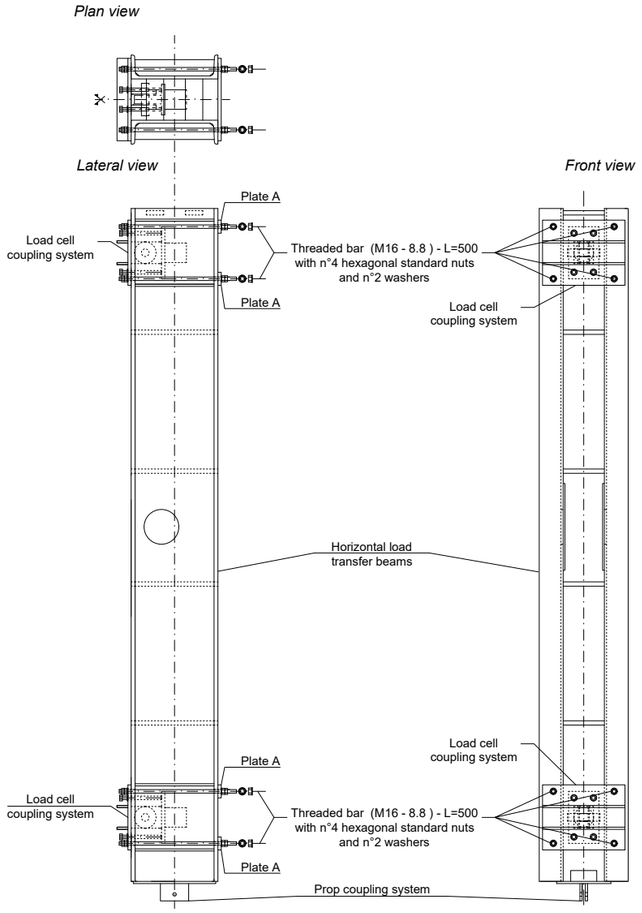

Prop coupling system (n°1/load transfer beam)

Scala 1:5

Plan view (superior)

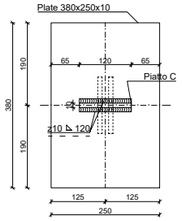

Plan view (inferior)

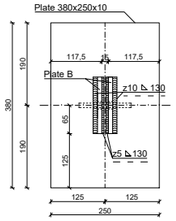

Plate B (n°2)

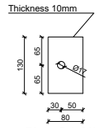

Plate C (n°1)

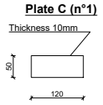

Plate A (n°4/load transfer beam)

Scale 1:5

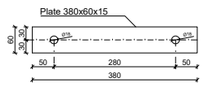

Load cell coupling system (n°2/load transfer beam)

Scala 1:5

Assembly

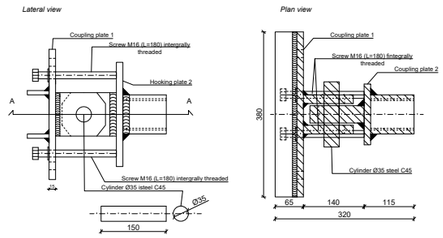

Coupling plate 1 (n°2)

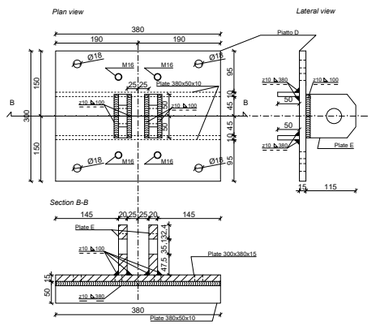

Coupling plate 2 (n°2)

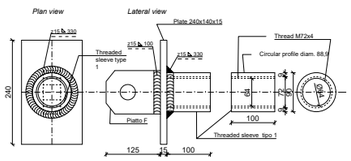

Plate E (n°2)

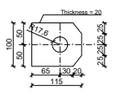

Plate D (n°1)

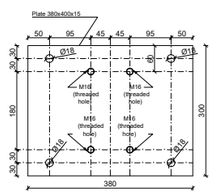

Plate F (n°1)

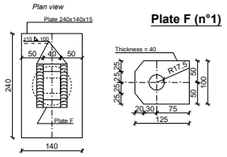

MATERIALS BILL		
Name	N°	Weight [kg]
UPN400 (L=3100)	4	890,7
Stiffeners	16	33,6
Plate 190x20x400	8	95,5
Plate 20x60x190	4	7,2
Web reinforcement (plate 400x380x8)	4	33,1
Plate 380x250x10	2	14,9
Plate 120x50x10	2	0,9
Plate 130x80x10	4	3,3
Plate D (380x400x15)	4	71,6
Plate E	8	13,1
Plate 380x50x10	8	11,9
Plate 240x140x15	4	15,8
Plate F	4	14,3
Threaded sleeve type 1 (L=100mm)	4	7,2
Ciclinder Ø35 - steel C45 (L=150mm)	4	4,5
Threaded bars M16 (L=500mm)	16	-
Bolt M16 totally threaded (L=180mm)	16	-
	TOT.	1217,7

MATERIAL PRESCRIPTIONS

Steel S355 as per UNI EN 10025 - hot rolled products

- ULTIMATE TENSILE STRENGTH ftk>490MPa
- YIELDING STRENGTH fyk>355MPa

ANGULAR WELDING

All welding beads are executed with con electrodes type E52 with quality class 4B (UNI5132)

TYPUCAL WELDING BEADS

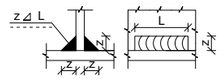

BOLTS - NUTS - WASHERS

- Bolts, nuts and washers according to point §11.3.4.6 of the D.M. 17/01/2018
- All bolts and the threaded bars are of high strength class 8.8 unless different specification in the drawings
- All bolts and the threaded bars must be got galvanized

Interreg ITALIA-SLOVENIJA — CONSTRAIN

Oggetto:

Loading system for the cyclic test on the stone masonry pilot building

TAV. PB8.3

Horizontal loads transfer beam and load cell coupling system

Quotes in mm - Scale 1:5

Load transfer bar coupling system - SOUTH side (n°4)

Scale 1:5

Profile type 3 - 2UPN120 (superior plan view)

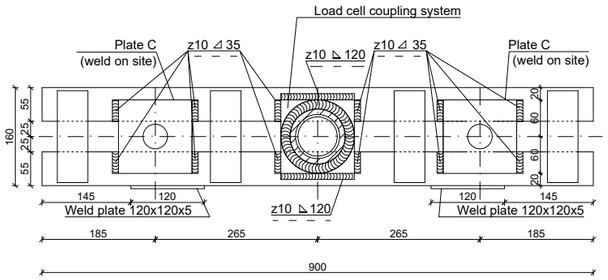

Profile type 3 - 2UPN120 (inferior plan view)

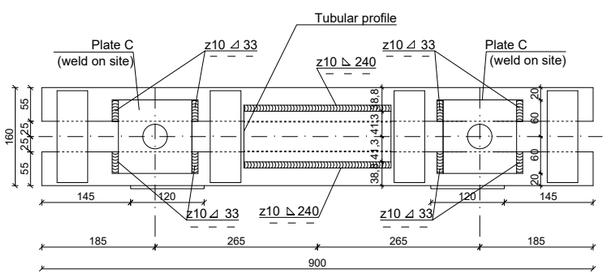

Lateral view

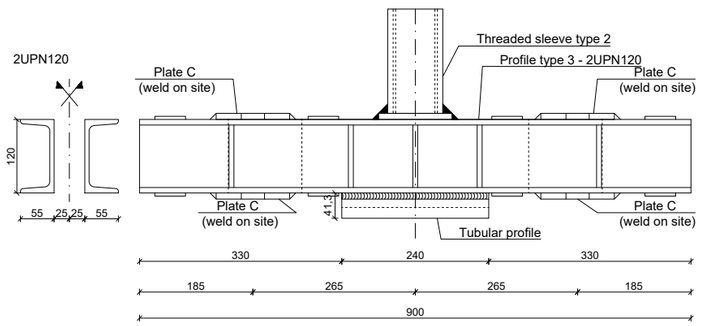

Threaded sleeve type 2 (n°1)

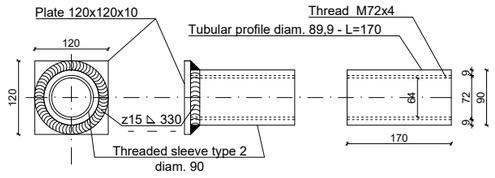

Plate C (n°4)

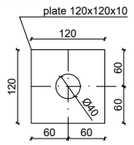

Tubular profile (n°1)

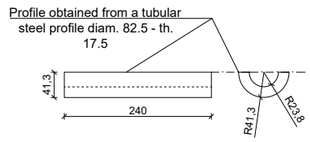

MATERIALS BILL		
Name	N°	Weight [kg]
Threaded sleeve type 2	4	12,2
Plate 120x120x10	4	4,5
Plate C (120x120x10)	24	27,1
Tubular profile	4	7,6
Plate 160x15x350	4	26,4
Plate 120x120x5	16	9,0
	TOT.	86,9

MATERIAL PRESCRIPTIONS

Steel S355 as per UNI EN 10025 - hot rolled products

- ULTIMATE TENSILE STRENGTH ftk>490MPa
- YIELDING STRENGTH fyk>355MPa

ANGULAR WELDING

All welding beads are executed with con electrodes type E52 with quality class 4B (UNI5132)

TYPUCAL WELDING BEADS

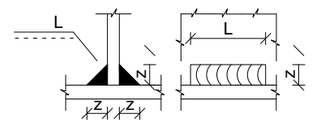

Load transfer bar coupling system - NORTH side (n°4)

Scale 1:5

Profile type 3 - 2UPN120 (superior plan view)

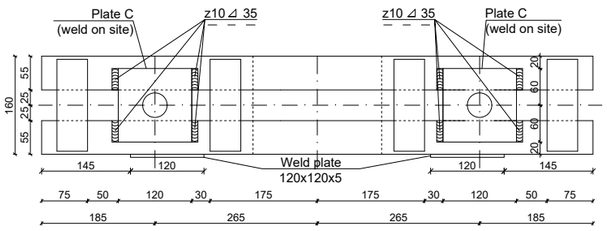

Profile type 4 - 2UPN120 (inferior plan view)

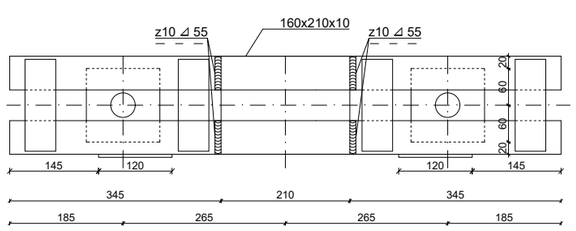

Lateral view

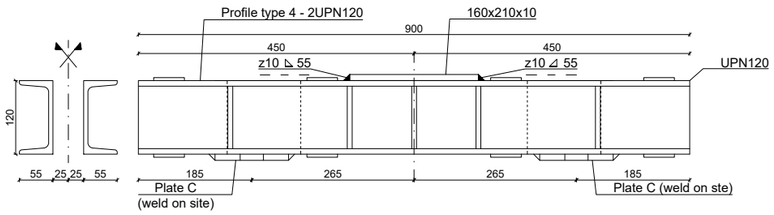

Plate C (n°2)

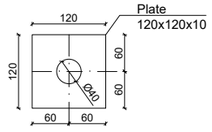

UNIONE EUROPEA
EVROPSKA UNIJA
Interreg
ITALIA-SLOVENIJA
CONSTRAIN

Oggetto:

Load transfer bar coupling system

TAV.

PB8.4

Testing apparatus assembly

Quotes in mm - Scale 1:5